

Development of Oligonucleotide Modified Substrates for the Selective Detection of Harmful Algal Bloom Causative Microalgae

A thesis submitted for fulfilment of the degree of
Doctor of Philosophy

Karen L. Bruce

BTech (Forensic & Analytical Chemistry), BSc (Honours)



Faculty of Science & Engineering
School of Chemical and Physical Sciences

September 2016

Declaration

'I certify that this thesis does not incorporate without acknowledgement any material previously submitted for a degree or diploma in any university; and that to the best of my knowledge and belief it does not contain any material previously published or written by another person except where due reference is made in the text.'

Karen L. Bruce

..... on

Acknowledgements

To thank everyone individually would be a thesis in itself. Everyone close to me has shared an important part in my completion of this research even if they didn't know it.

First and foremost I must thank my supervisor, Professor Claire Lenehan. Your patience and advice were invaluable. You helped me finally gain confidence in my research and writing. To my co-supervisors, Sophie Leterme and Amanda Ellis, thank you for your guidance on my publications. Extra thanks goes to Sophie for helping me with my transition to a biology cross-discipline project. Shout out to Jan who put up with all my dumb questions and helped me culture my algae samples. Even though I ended up killing it (whoops!), your assistance provided me with the confidence to work in the biology laboratory. Further thanks to the mighty Analytical Research group. Once we were only 5 students, now we are one giant super group. Thank you for listening to my repetitive presentations and providing me with great advice. I hope that at some stage I was able to provide the same in return. To all my office buddies, past and present, thanks for bringing bright attitudes and hilarious jokes to the daily routine. It definitely helped keep me sane during each stage of my PhD.

Massive shout out to some of my absolute favourites; Rachel, Leigh, Caitlyn, Gos and Lachlan. You all mean the absolute world to me. Every little thing you did to help me smile will never be forgotten. From the beautiful note left on my car windscreen, chocolates left on my desk after a bad day, crude jokes in the corridors, coffee/tea and chats and the loud "ooohs" in the hallway. Thank you for making this an experience I will never forget. Love you all!

A loving thank you to my amazing parents, Neil and Cathy. You both mean so much to me and I don't think I tell you this enough. Your unconditional love and support helped me to persevere and achieve this huge task. From the hugs, motivational chats and delicious roast dinners, every little bit helped. I am so lucky to be surrounded by such a loving family. Also a shout out to my four legged family, Mitsy moo and Tiger. You were both such a big part of my life. I could be having the worst day but one cuddle and all was perfect with the world again. You will never be forgotten.

To all my other extended friends outside of university. I know secretly you were all wondering what the hell I was doing still studying at university and questioning if I would actually ever finish. Well, I finally got there! Thanks for the weekends I will never forget! It was so fantastic being able to escape the stress of the week and just enjoy the weekend with you all. From crazy antics in town to relaxing nights in with beers and board games.

To Jack, the love of my life. Thank you so much for being by my side through it all. I know that sometimes I was an absolute stress head but no matter how grumpy I was, you still stayed right there by my side. You were the reason I was able to stop, take a breath and relax. You were also my reason to smile and laugh. Your unconditional love and support is the reason I was able to achieve this. I love you.

Summary

Harmful algal bloom (HAB) events have become more prevalent in the last few decades, with each event leading to the subsequent release of biotoxins. Bloom monitoring is essential to prevent detrimental damage to the environment and human health. Traditional methods using light microscopy can encounter difficulties in discriminating between toxic and non-toxic species of the same genus due to similarities in cellular morphology. Alternatively, specific, and highly discriminative detection can be achieved using oligonucleotide probes that are able to target variable regions found within the rRNA of HAB species. Detection of HABs using these specifically designed oligonucleotides provides a highly sensitive and selective route for monitoring microalgae bloom formations.

This thesis reports the covalent attachment of oligonucleotides to solid supports for model hybridisation with fluorescently labelled target oligonucleotide sequences specific to HAB species *Alexandrium catenella* in the aim to develop substrates for the sensitive, selective detection of HAB microalgae. Initial investigation into substrate compared PDMS and glass microscope slides for their performance in hybridisation experiments with the target sequence. Glass exhibited superior properties when compared to PDMS, with a higher sensitivity and improved stability of attachment during storage. PDMS modified surfaces were subject to hydrophobic recovery resulting in a re-arrangement of the surface, minimising oligonucleotides available on the surface over time for hybridisation.

Evaluation of the effect of surface chemistry used in attachment was also completed. Here, the amine functionalisation was compared to a thiolene attachment using a vinyl functionalised glass slide. The vinyl modification was able to effectively eliminate non-specific binding. Furthermore, the vinyl functionalised surface performed better with sensitivity and also demonstrated the potential for quantitative analysis required for future bloom monitoring when applied to natural seawater samples. Use of the vinyl functionalised glass slide allowed for the selective discrimination when hybridised with a non-complimentary target sequence. Vinyl functionalised surfaces were also able to be regenerated after one cycle, with only a loss of 0.7 % reactivity upon re-hybridisation.

In order to further improve sensitivities of the oligonucleotide modified surfaces, vinyl terminated nanoparticles were trialled as attachment substrates. Initial experiments using 1-dodecanethiol as a model reagent demonstrated the successful attachment using a thiolene photoinitiated reaction. Attachment densities were also calculated using ATR-FTIR with a 1000 molar excess addition of 1-dodecanethiol generating an attachment density of 10.6 ± 5.6 attachments.nm⁻². Issues with the reproducibility resulted in high variation between analysed samples. Alternatively, TGA was trialled to calculate theoretical attachment densities resulting in 2.4 attachments.nm⁻². Attachment of thiol modified oligonucleotides was also tested as a proof of concept, but was unsuccessful as shifting the reaction to an aqueous solution resulted in aggregation of the hydrophobic vinyl terminated nanoparticles. Investigation into alternative ethanol solutions resulted in false positive signals from blank nanoparticle aggregations formed upon drying.

In summary, the use of thiolene attached oligonucleotides to glass surfaces provides a highly sensitive, selective surface for the detection of *A. catenella* target sequences in model hybridisation experiments. Future application of these surfaces on natural seawater samples would be required to determine if it is effective in the presence of other nucleic acids. Future use of vinyl terminated nanoparticles for oligonucleotide attachment requires more optimisation to prevent aggregation in solution which inhibits the reaction.

Publications

Resulting publications produced during this research include the following:

Karen L. Bruce, Amanda V. Ellis, Sophie C. Leterme, Dmitriy A. Khodakov and Claire E. Lenehan

Detection of harmful algal bloom causing microalgae using covalently immobilised capture oligonucleotide probes on glass and poly (dimethylsiloxane) surfaces

Proceedings of SPIE Micro/Nano Materials, Devices and Systems, Vol. 8923 (2013)

Karen L. Bruce, Sophie C. Leterme, Amanda V. Ellis and Claire E. Lenehan

Approaches for the detection of harmful algal blooms using oligonucleotide interactions

Analytical and Bioanalytical Chemistry, Vol 407 (1), 2015, pp. 95-116

Dedicated to

Jack Gardner

For your continued love and support during all the highs and lows.

Thank you for believing in me.

Contents

Declaration	i
Acknowledgements	ii
Summary	iv
Publications	vi
Contents	viii
Figures	xii
Tables	xvi
Equations	xvii
List of Acronyms	xix
1. Introduction	1
1.1 Harmful algal blooms	2
1.1.1 Nucleic Acid Amplification Based Detection.....	5
1.1.1.1 Real-time PCR Applications.....	5
1.1.1.2 Nucleic Acid Sequence Based Amplification (NASBA) Assays.....	7
1.1.1.3 Loop-mediated isothermal amplification	11
1.1.2 Fluorescence in situ hybridisation (FISH).....	18
1.1.3 Sandwich Hybridisation Assay (SHA)	27
1.1.3.1 Nuclease Protection Assay Sandwich Hybridisation (NPA-SH)	38
1.2 Strategies for the covalent immobilisation of oligonucleotides to solid supports	41
1.2.1 Amine silanised surfaces for oligonucleotide attachment	42
1.2.2 Thiol based chemistry for oligonucleotide attachment.....	44
1.3 Silica nanoparticle substrates for oligonucleotide attachment	46
1.3.1 Silica nanoparticle synthesis	46
1.3.2 Silica nanoparticle functionalisation.....	48

1.3.3 Methods for oligonucleotide attachment to silica nanoparticles	49
1.4 Conclusion and Project Premise	50
2. Substrate selection for the covalent attachment of amine modified oligonucleotides.....	51
2.1 Introduction.....	52
2.2 Scope of study.....	54
2.3 Experimental.....	55
2.3.1 Materials	55
2.3.2 APTES covalent modification strategy for PDMS and glass substrates	55
2.3.2.1 PDMS substrate	55
2.3.2.2 Glass substrate.....	56
2.3.3 Surface hybridisation experiments for amine modified PDMS and glass substrates.....	57
2.3.4 Water contact angle measurements of glass substrates modified using the APTES silanisation method	58
2.4 Results and Discussion	59
2.4.1 Surface characterisation of APTES silanisation strategies	59
2.4.2 Oligonucleotide attachment to APTES silanised glass substrates	60
2.4.3 Hybridisation performance - A direct comparison of APTES modified glass and PDMS.....	70
2.4.4 APTES modified PDMS and glass surface stability	71
2.5 Conclusions.....	76
3. An investigation into covalent strategies for the immobilisation of oligonucleotides to glass substrates.....	77
3.1 Introduction.....	78
3.2 Scope of study.....	81
3.3 Experimental.....	82
3.3.1 Materials	82

3.3.2 APTES covalent modification strategy for glass slides.....	82
3.3.3 VTES covalent modification strategy for glass slides.....	83
3.3.4 Hybridisation experiments for amine and vinyl modified substrates	84
3.3.5 Surface regeneration	85
3.3.6 Water contact angle measurements of glass substrates modified using the VTES silanisation method	86
3.4 Results and Discussion	87
3.4.1 Surface characterisation of VTES silanisation strategies	87
3.4.2 Oligonucleotide attachment to VTES silanised glass substrates	88
3.4.3 Selectivity comparison between VTES and APTES modified glass substrates	96
3.4.4 Direct comparison of APTES and VTES modified glass hybridisation performance	97
3.4.5 Regeneration capacity of VTES modified glass substrates	99
3.4.5.1 Effect on de-hybridisation time on the complete removal of Cy5 labelled ACat Seq using VTES modified glass substrates.....	101
3.4.5.2 Effect on de-hybridisation temperature on the complete removal of Cy5 labelled ACat Seq using VTES modified glass substrates	102
3.5 Conclusions.....	105
4. Covalent attachment of oligonucleotides to vinyl terminated silica nanoparticles	106
4.1 Introduction.....	107
4.2 Scope of study.....	109
4.3 Experimental.....	110
4.3.1 Materials	110
4.3.2 Synthesis of vinyl terminated nanoparticles.....	110
4.3.3 Preparation of calibration samples to determine attachment density of 1-dodecanethiol.....	111
4.3.4 Covalent attachment of 1-dodecanethiol to vinyl terminated nanoparticles	112

4.3.4.1 Molar excesses of 1-dodecanethiol used for attachment density calculations	112
4.3.5 Thermogravimetric analysis of reacted nanoparticles	114
4.3.6 Attachment of SH-ACat probe to vinyl terminated nanoparticles	115
4.3.7 Hybridisation experiments for VTES silica nanoparticle oligonucleotide modified substrates	116
4.4 Results and Discussion	117
4.4.1 Nanoparticle synthesis and characterization.....	117
4.4.2 Vinyl terminated nanoparticle model experiment	122
4.4.3 Oligonucleotide attachment optimisation for vinyl nanoparticles.....	133
4.5 Conclusions.....	137
5. Conclusions and Future Work	138
5.1 Conclusions.....	139
5.2 Future work	141
5.2.1 Oligonucleotide attachment to glass and PDMS surfaces	141
5.2.2 Oligonucleotide attachment to nanoparticles.....	142
5.2.3 Application of surfaces for the selective detection of <i>A. catenella</i>	143
6. Appendix.....	144
7. References	153

Figures

Figure 1:	Detection methods used for RT-PCR.....	5
Figure 2:	Diagrammatic representation of the NASBA process	9
Figure 3:	Process of LAMP amplification.....	13
Figure 4:	Diagrammatic representation of the steps required for FISH analysis	18
Figure 5:	Diagrammatic representation of the SHA process.....	28
Figure 6:	Process of the Nuclease Protection Assay coupled to the SHA	38
Figure 7:	Diagrammatic representation of electrochemiluminescent detection using NPA-SH	40
Figure 8:	Silanisation chemistry used to generate organofunctional surfaces for oligonucleotide attachment. Adapted from [107].....	41
Figure 9:	Oligonucleotide attachment to amine silanised substrates	43
Figure 10:	Attachment strategies for the immobilisation of oligonucleotides to thiol functionalised surfaces	45
Figure 11:	Sol-gel process for silica nanoparticle synthesis	47
Figure 12:	Reversed micelles in a water-in-oil system for silica nanoparticle synthesis	47
Figure 13:	Reaction schematic for the APTES modification	57
Figure 14:	Effect of initial oxidation method on the final hybridisation with Cy5 labelled ACat Seq for glass surfaces	61
Figure 15:	Modification of oxidised glass surface to amine functionalised surface using 2 %(v/v) APTES.....	63
Figure 16:	Effect of APTES silanisation time on the final hybridisation efficiency of the modified glass surface	63
Figure 17:	Modification of APTES silanised glass with 10 mM PDITC cross-linker.....	64
Figure 18:	Effect of PDITC reaction time on the final hybridisation efficiency of the modified glass surface	65
Figure 19:	Attachment of the amine modified oligonucleotide (NH ₂ -Probe) to the PDITC modified glass slide.....	66
Figure 20:	Effect of NH ₂ -probe attachment time on the final hybridisation efficiency of the modified glass surface	67

Figure 21: Hybridisation of the oligonucleotide (blue) modified glass slide with Cy5 labelled ACat Seq (red)	68
Figure 22: Effect of hybridisation time on the final hybridisation efficiency of the modified glass surface	69
Figure 23: Obtainable fluorescence intensities using the PDMS and glass substrates.....	71
Figure 24: Comparison of PDMS and glass surface stability after initial oligonucleotide attachment	72
Figure 25: Comparison of PDMS and glass surface stability after hybridisation of the attached oligonucleotides	74
Figure 26: Thiol modified oligonucleotide attachment strategies.....	79
Figure 27: General overview of a photoinitiated thiol-ene reaction	80
Figure 28: Schematic and optimised conditions for the attachment of oligonucleotide probes to glass substrates	83
Figure 29: Hypothesised interactions between the oligonucleotides and two silanised glass substrates	88
Figure 30: Effect of VTES silanisation time on the final hybridisation efficiency of the modified glass surface	90
Figure 31: Effect of irradiation time on SH-probe thiolene attachment to vinyl modified glass slide surfaces.....	92
Figure 32: Effect of hybridisation time on the final signal: background ratio of the VTES modified region.....	94
Figure 33: Selectivity of the APTES and VTES modified glass surfaces for complimentary and non-complimentary target sequences.....	96
Figure 34: Standard curve for target ACat Seq generated using the APTES (red) and VTES (blue) modified glass surfaces	98
Figure 35: Regeneration capacity of the VTES modified glass surface for 120 min at 80 °C	100
Figure 36: Effect of de-hybridisation time on the complete removal of hybridised Cy5 labelled target sequence	101
Figure 37: Regeneration capacity of the VTES modified glass surface after de-hybridisation for 10 min at 80 °C.....	102
Figure 38: Effect of de-hybridisation temperature (°C) on the complete removal of hybridised Cy5 labelled target sequence.....	103

Figure 39: Regeneration capacity of the VTES modified glass surface after de-hybridisation for 10 min at 60 °C.....	104
Figure 40: Dithiol attachment of thiol modified oligonucleotides to MPTS silanised silica nanoparticles	107
Figure 41: Simplified nanoparticle synthesis diagram for VTES.....	110
Figure 42: Schematic for the attachment of thiol-modified oligonucleotides to vinyl nanoparticles	116
Figure 43: SEM images of synthesised vinyl terminated silica nanoparticles (average diameter 354.0 ± 29.7 nm)	117
Figure 44: BET isotherm of the synthesised vinyl terminated silica nanoparticles.....	118
Figure 45: ATR-FTIR of neat vinyl terminated nanoparticles	120
Figure 46: ATR-FTIR spectra of the trial attachment of 1-dodecanethiol with vinyl terminated nanoparticles	123
Figure 47: Calibration curve generated using the ratio of $\nu_{\text{asymm}}(\text{CH}_2)$ vibration at 2920 cm^{-1} relative to the $\nu(\text{C}=\text{C})$ stretch vibration at 1602 cm^{-1}	124
Figure 48: ATR-FTIR spectra of varying molar excesses of 1-dodecanethiol reacted with vinyl nanoparticles.....	125
Figure 49: SEM of unquenched vinyl terminated nanoparticles showing modified structure compared to clean vinyl nanoparticles in Figure 43	128
Figure 50: ATR-FTIR spectra of 1-dodecanethiol attachment replicates to vinyl nanoparticles (n=5).....	129
Figure 51: Orientation of samples under UV light source.....	130
Figure 52: Effect of molar excess of 1-dodecanethiol (A) and mass of benzophenone (B) on reproducibility of calculated attachment densities.....	130
Figure 53: Resulting TGA plots of blank, unreacted vinyl nanoparticles (black) and vinyl nanoparticles reacted with 1-dodecanethiol (blue and red).....	132
Figure 54: Nanoparticle interactions in different percentage compositions of ethanol	134
Figure 55: Confocal microscope imaging of blank vinyl terminated nanoparticles (A) and Cy5 ACat Seq hybridised nanoparticles (B).....	135
Figure 56: Confocal image of YO-PRO-1 treated hybridised nanoparticles	136
Figure 57: Effect of fluorescence intensity degradation under different storage conditions	145

Figure 58: Use of 0.1 M sodium phosphate buffer (pH 8.0) for the de-hybridisation of Cy5 labelled target sequence.....	146
Figure 59: Use of 1x SSC buffer (pH 7.0) for the de-hybridisation of Cy5 labelled target sequence	147
Figure 60: Comparison between the use of ν (C=C) and ν (Si-O-Si) as an internal standard reference peak for determining attachment density of 1-dodecanethiol	150
Figure 61: Cy5 labelled target sequence adsorbed to cleaned, bare amine functionalised nanoparticles shown as blue.....	152
Figure 62: Growth curve for <i>A. catenella</i> cultured in f/2 medium (blue) and GSe medium (red)	152

Tables

Table 1:	Overview of NASBA used in HAB detection	16
Table 2:	Overview of methodology used for FISH analysis of HAB species	22
Table 3:	Overview of methodology used for the SHA of HAB species.....	30
Table 4:	Oligonucleotides used in the substrate selection study	55
Table 5:	Step-wise WCA measurements for the APTES modified PDMS (using optimised conditions [151]) and glass substrates (n=3).....	59
Table 6:	Final conditions of the APTES modified PDMS and glass substrates	70
Table 7:	Oligonucleotide sequences used for attachment to APTES and VTES functionalised glass slides.....	82
Table 8:	Resulting step-wise WCA measurements for the VTES modified glass substrates (n= 3)	87
Table 9:	Final reaction conditions for the APTES and VTES modification compared to the Escorihuela <i>et al.</i> conditions [113]	95
Table 10:	Correlation of functional groups based on spectra in Figure 45.....	121
Table 11:	Effect of reaction solvent on 1-dodecanethiol attachment to cleaned and unquenched nanoparticles	127
Table 12:	Resulting Ratio of $\nu_{\text{asymm}}(\text{CH}_2)$ to $\nu(\text{C}=\text{C})$ and subsequent attachment densities for 1000:1 molar excess (n = 5)	129

Equations

Equation 1: Calculation of the signal: background ratio for the fluorescence microscope images	85
Equation 2: Number of nanoparticles available for reaction (3 mL, 5 mg.mL ⁻¹ stock solution)	113
Equation 3: Total available surface area (nm ²) per reaction.....	113
Equation 4: Number of attachments possible for 1:1 stoichiometry	113
Equation 5: Molar equivalent of 1-dodecanethiol (mol) from attachment number using 1:1 stoichiometry	114
Equation 6: Molar amount of 1-dodecanethiol (mol) required for a 10 molar excess attachment	114
Equation 7: Volume of 1-dodecanethiol (mL) required for a 10 molar excess attachment	114
Equation 8: Mass (g) of 1-dodecanethiol based on the TGA average mass loss (%) .	115
Equation 9: TGA calculated attachment density of 1-dodecanethiol (attachments.nm ⁻²).....	115
Equation 10: Mass (g) per nanoparticle	118
Equation 11: Surface area (nm ²) per nanoparticle calculated from BET isotherm	119
Equation 12: Theoretical surface area (nm ²) based on a radius of 175 nm.....	119
Equation 13: Normalisation of the ν_{asymm} (CH ₂) stretch at 2920 cm ⁻¹	123
Equation 14: Number of moles of 1-dodecanethiol (mol) present based on the calibration curve (Figure 47).....	125
Equation 15: Attachments per nm ² of 1-dodecanethiol attached to the vinyl terminated nanoparticles	126
Equation 16: Calculated working for the number of nanoparticles available for reaction	148
Equation 17: Calculated working for the total available surface area (nm ²) per reaction	148
Equation 18: Calculated working for the number of attachments possible for 1:1 stoichiometry	148
Equation 19: Calculated working for the molar equivalent of 1-dodecanethiol (mol) from attachment number using 1:1 stoichiometry	149

Equation 20: Calculated working for the molar amount of 1-dodecanethiol (mol) required for a 10 molar excess attachment	149
Equation 21: Calculated working for the volume of 1-dodecanethiol (mL) required for a 10 molar excess attachment.....	149
Equation 22: Calculated working for the mass (g) of 1-dodecanethiol based on the TGA average mass loss (%)	151
Equation 23: Calculated working for the TGA calculated attachment density of 1-dodecanethiol (attachments.nm ⁻²)	151

List of Acronyms

6-FAM	6-carboxy fluorescein
ABTS	2,2'-azino-bis(3-ethylbenzthiazoline-6-sulfonic acid)
AMV	Avian myeloblastosis virus
APTES	3-aminopropyltriethoxysilane
APTMS	3-aminopropyltrimethoxysilane
ASP	Amnesic shellfish poisoning
ATR-FTIR	Attenuated total reflection Fourier transform infrared spectroscopy
AZP	Azaspiracid
BET	Brunauer-Emmet-Teller
BSA	Bovine serum albumin
cELISA	Competitive enzyme-linked immunosorbent assay
DABCYL	4-((4-(dimethylamino)phenyl)azo)benzoic Acid
DETA	Trimethoxysilylpropyl diethylenetriamine
DIG	Digoxigenin
DMF	Dimethylformaldehyde
DNA	Deoxyribonucleic acid
DPI	Dual polarisation interferometry
DSP	Diarrhetic shellfish poisoning
EDA	N-(2-aminoethyl)-3-aminopropyltrimethoxysilane
EDC	1-ethyl-3-(3-dimethylaminopropyl)-carbodiimide
ELISA	Enzyme-linked immunosorbent assay
FISH	Fluorescence <i>in situ</i> hybridisation
HAB	Harmful algal bloom
HRP	Horseradish peroxidase
IC-NASBA	Internal control nucleic acid sequence based amplification
IC-RNA	Internal control ribonucleic acid
LAMP	Loop-mediated isothermal amplification
LM	Light microscopy
LOD	Limit of detection
LSU	Large subunit
MPTS	3-mercaptopropyl trimethoxysilane

mRNA	Messenger RNA
NASBA	Nucleic acid sequence based amplification
NPA	Nuclease protection assay
NSP	Neurotoxic shellfish poisoning
PCR	Polymerase chain reaction
PDITC	P-phenylene diisothiocyanate
PDMS	Poly(dimethylsiloxane)
PEG	Polyethylene glycol
PEGMA	Polyethylene glycol methacrylate
POD	Peroxidase
qPCR	Quantitative polymerase chain reaction
rDNA	Ribosomal deoxyribonucleic acid
RNA	Ribonucleic acid
rRNA	Ribosomal RNA
RTFQ-PCR	Real-time fluorescence quantitative PCR
RT-LAMP	Real-time LAMP
RT-PCR	Real-time PCR
SA	Succinic anhydride
SDS	Sodium dodecyl sulfate
SEM	Scanning electron microscopy
SHA	Sandwich hybridisation assay
SMPB	Succinimidyl 4-(maleimidophenyl)butyrate
SSC	Saline sodium citrate
TCEP	Tris(2-carboxyethyl) phosphine hydrochloride
TEOS	Tetraethyl orthosilicate
T_m	Melting temperature
TMB	3,3',5,5'-tetramethylbenzidine
TTP	Time to positivity
VTES	Vinyltriethoxysilane
VTMS	Vinyltrimethoxysilane
WC	Whole cell hybridisation
WCA	Water contact angle

1

Introduction

This chapter introduces the concept of oligonucleotide based strategies for the molecular detection of harmful algal blooms.

1.1 Harmful algal blooms

The term 'harmful algal bloom' (HAB) refers to a rapid proliferation of algal cells in an aquatic environment with harmful consequences. This may be due to the production of biotoxins or the accumulated biomass altering the ecosystem in a harmful manner [1]. In some cases, the number of cells may increase to such an extent that they discolour the water, such as in those of 'red tides'. Globally, HABs have become more prevalent over the last few decades and the number of toxins and toxic species has increased [2]. Most coastal countries are now threatened by HAB formations which were unheard of several decades ago. The cause of the expansion is still not thoroughly understood however there are claims that environmental impacts as well as human impacts may be to blame [1]. This increased prevalence has in-turn impacted on local economies due to sea life mortality and cessation of seafood trade as many of the organisms are unfit for consumption. Bioaccumulation of biotoxins in shellfish and filter feeding bivalves can result in poisoning of higher organisms through the consumption of contaminated shellfish [3]. These can have a range of side effects and are classified as paralytic (PSP), amnesic (ASP), diarrhetic (DSP), neurotoxic (NSP) and azaspiracid (AZP) shellfish poisoning, and are potentially lethal [4-6]. With the exception of ASP (where diatoms are the biotoxin source), all of the poisonous biotoxins result from a type of algae known as dinoflagellates. The most commonly encountered of these include organisms from the *Karenia*, *Alexandrium* and *Pseudo-nitzschia* genus [7].

The average duration of HABs, during the bloom stage, and their geographic spread has increased over the past few decades. A number of factors have been hypothesised to be linked to this increase in proliferation, but the underlying causes are not well understood. This could be due to improved detection strategies, however current consensus is that the increase in global population has led to increased nutrient pollution resulting in excessive algal growth [8, 9]. The increased geographic spread of species has been linked to the release of ballast water from ships and through natural water movement such as currents and storms [1, 10]. Alternately, it has been suggested that increased fishing could be affecting the food chain leading to an unbalanced relationship between organisms that feed on the algae to control growth [8].

Given the increase in HABs over the last few decades there has been a significant research effort towards methods for monitoring the levels of such species in the environment. The development of improved detection methods provides a greater understanding of HAB

lifecycles, leading to improved strategies for HAB prevention and/or control. Currently, monitoring strategies include i) satellite monitoring of ocean colour [11, 12], ii) analysis for the presence of exuded biotoxins [2, 13, 14] and iii) localised monitoring of cellular densities of the causative organisms [15, 16].

Remote sensing using satellite monitoring typically concentrates on the detection of ocean spectral changes resulting from a bloom. This approach can be complicated by atmospheric conditions and the presence of coloured dissolved organic matter and suspended solids. For further information on this approach the reader is referred to extensive reviews by Blondeau-Patissier *et al.* [17] and Moisan *et al.* [18]. Biotoxin analysis generally focuses on either the determination of the toxin concentration in bivalves such as mussels, or the concentration in the waterway [2, 13]. Detection is typically achieved through liquid chromatography with either mass spectrometry [19-21] or fluorescence detection [22-25]. Generally, these methods require time consuming extraction and pre-concentration sample preparation steps [26]. Examples include passive sampling devices and solid phase adsorption toxin tracking for water sampling [14, 27]. Whilst important for monitoring the potential toxic effects during and post bloom, this approach can be expensive and the time delay between sampling and analysis can limit monitoring in the initial stages of a bloom [28, 29].

Monitoring of cell densities can be achieved manually using light microscopy (LM). This approach has the advantage of being able to determine cell density during a bloom while also identifying the causative species. However, in some cases, species identification is difficult due to the similar morphologies of toxic and non-toxic species of the same genus [30]. Additionally, as many species are motile, fixation of the cells must occur prior to LM. This process can compromise the structural integrity of the cell, further complicating species identification. Whilst useful for identifying causative species, LM is labour intensive and time consuming, and is unsuitable for rapid at-site monitoring of bloom events [31].

An alternative method for the detection of HAB species was demonstrated by Scholin *et al.* who was able to target the species cellular genome. Here, the research reported a variable region within the LSU rRNA of toxic and non-toxic *Pseudo-nitzschia* diatom species which could be targeted for detection [32]. Further work found that variable regions in the LSU rRNA were present in other HAB microalgae species [33-35]. These offer an ideal alternative target for a species specific detection approach that can be

rapid, automated and indicative of cell numbers [32]. As a result, research employing specifically chosen single strand oligonucleotide sequences that are able to hybridise with variable regions within the HAB genetic material has received much attention. Developed methods based on this technique include nucleic acid amplification techniques such as real-time PCR (RT-PCR) and nucleic acid sequence based amplification (NASBA) as well as oligonucleotide based detection via fluorescence *in situ* hybridisation (FISH) assays and sandwich hybridisation assays (SHA). These are reviewed within Sections 1.1.1 to 1.1.3.

1.1.1 Nucleic Acid Amplification Based Detection

An alternative to targeting rRNA directly within the cell is to target DNA with the aid of amplification based techniques. Typically, this has been done using real-time polymerase chain reaction (RT-PCR), nucleic acid sequence based amplification (NASBA) and loop-mediated isothermal amplification (LAMP).

1.1.1.1 Real-time PCR Applications

RT-PCR (also called quantitative PCR, qPCR) is a modified PCR technique whereby amplified DNA is detected in real-time as the amplification reaction progresses. Detection of amplification is achieved through the use of fluorescent materials such as a) TaqMan probe, b) molecular beacon and c) an intercalating dye such as SYBR green (refer to Figure 1). The fluorescence intensity of the signal increases with increasing cycle of the PCR until a cycle detection threshold (C_t) is reached. The C_t can then be used to calculate the concentration of genetic material in a sample based on the inverse relationship between C_t and initial concentration of genetic material [36]. Production of a standard curve allows for the quantification of genetic material present [37].

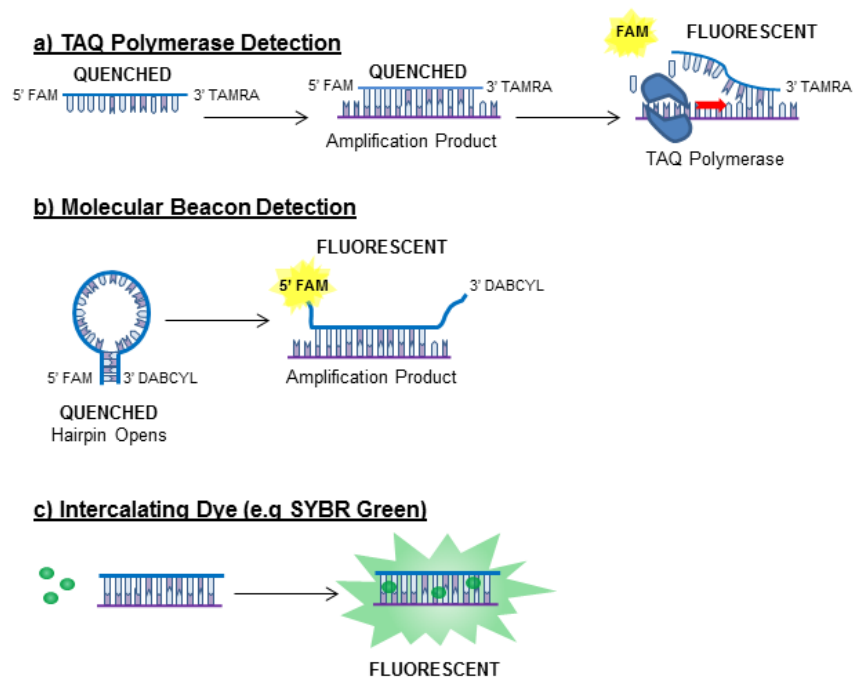


Figure 1: Detection methods used for RT-PCR

a) TaqMan probes with TAQ Polymerase, b) Molecular beacon detection and c) the use of an intercalating dye like SYBR Green

Although RT-PCR has been applied to clinical and environmental diagnostics for some time, application of this methodology towards HAB detection is relatively new. This section focuses on recent developments (2013 onwards) in RT-PCR for HAB detection, for a comprehensive review of RT-PCR applications for the detection of causative HAB prior to 2013 the reader is referred to Antonella and Luca (2013) [37]. The expanse of this RT-PCR research has been significant with a number of methods being reported for dinoflagellate, diatom, Raphidophyceae, Haptophyceae, Pelagophyceae and Cyanophyceae [37]. Applications directed at the detection of *Alexandrium* species such as *A. catenella* [38-42], *A. minutum* [26, 43], *A. fundyense* [44, 45], *A. taylori* [40] and *A. tamarense* [38, 39, 46] have been thoroughly reported. Similarly, RT-PCR methods were developed for dinoflagellate species *Dinophysis acuta* and *D. acuminata* [47]. Recent outbreaks of *Pseudo-nitzschia* in the US have propelled the development of RT-PCR methods being developed for *P. australis*, *P. pungens*, *P. delicatissima*, *P. calliantha*, *P. multistriata* [48, 49] and *P. multiseriata* [50]. Raphidophyceae such as within the genus *Chatonella* have also been applied to RT-PCR [51]. This includes *C. verrucolosa* [52, 53], *C. antiqua* [52], *C. ovata* [52] and *C. subsala* [52, 53].

A method for Raphidophyceae species *F. japonica* was also developed [52]. Haptophyceae are less researched however a number of methods have been developed for *Prymnesium parvum* using both SYBR green intercalating dyes (Figure 1C) [54, 55] and molecular probes (Figure 1B) [56]. Cyanobacteria HAB species have also been researched with a detailed review being published recently looking into the RT-PCR application for the species monitoring [57].

C. polykrikoides detection using RT-PCR methods on both natural seawater and cultured samples has also been reported [58]. This study demonstrated how the application of RT-PCR can be used to look at the variation on a sub-species level, most likely caused by ecological factors and cellular adaptations. Sub-species variable regions in the LSU rRNA were identified for *C. polykrikoides* with no observable cross reactivity with alternate HAB species. Reaction efficiencies of 91 % were reported and melting point analysis found only the target region was successfully amplified. A decrease in reaction efficiency was observed however when analysing natural seawater samples. This was most likely due to the presence of inhibitors such as mucopolysaccharides, phenolic compounds, humic acids and heavy metals. The inhibition was overcome by a simple ten-fold sample dilution prior to analysis [58].

RT-PCR method development for eight species in the genera *Karenia*, *Gymnodinium*, *Karlodinium* and *Takayama* has also been recently reported [59]. The optimised assays were highly specific and sensitivity was reported to be below one cell in all cases. The method was successfully applied to a bloom event in New Zealand with *Gymnodinium catenatum* being recorded at 3 cells.L⁻¹, well below the detection limit of LM, reported as 100 cells.L⁻¹ in this case.

Further extension of RT-PCR was recently reported by Zhang *et al.* for the detection of dinoflagellate species *P. donghaiense* [60]. This method allowed for the quantification of cell numbers based on a correlation with resulting plasmid copy numbers. A detection sensitivity of 3.45 cells was achieved when using the designed amplification primers [60].

RT-PCR is one of the most widely utilised nucleic acid methods for HAB detection. The use of specifically designed primers facilitates selective amplification of target sequences allows the detection of very low concentrations of target DNA. Quantitation of HAB causative species in natural seawater samples has been subject to some problems. Importantly, PCR inhibitors such as polyphenols and plant materials can reduce the efficiency of the RT-PCR process and reduce or even prevent the overall amplification of target sequences. This can make detection almost impossible in some cases [61]. Consequently, elimination of PCR inhibitors is essential in order to obtain the highest accuracy results and can be overcome by modifications to nucleic acid extraction and purification. Digital RT-PCR, which utilises dilute samples, may overcome the inhibition of molecules making it a good alternative [62]. Additionally, the requirement for amplification typically limits the analysis of samples to a laboratory environment. Optimising the conditions into a hand-held device would potentially allow for direct bloom tracking in the field. Direct correlations to cell numbers from the RNA concentration will also allow for direct tracking of bloom formation. Recently there has been an increase in popularity of isothermal nucleic acid methods such as NASBA and LAMP. These do not require the use of thermo-cyclers for amplification and subsequent detection and have demonstrated an increase in sensitivity of the analysis.

1.1.1.2 Nucleic Acid Sequence Based Amplification (NASBA) Assays

NASBA is an isothermal reaction used to amplify specific variable regions of target mRNA within the lysate of a cell with the aid of specific primers. There are two phases involved with NASBA amplifications, a linear phase followed by an amplification phase (Figure 2). In the linear phase a specific forward primer (Primer 1) anneals to the complimentary

sequence present in the RNA sample. Avian myeloblastosis virus (AMV) reverse transcriptase is then added to the reaction mixture and extends the 3' end of the primer. This, in turn, produces a DNA strand complementary to the RNA. Treatment with RNase H then removes the RNA from the duplex leaving single stranded cDNA. The reverse primer (Primer 2) then anneals to the complementary 5' region of cDNA and produces the complementary DNA strand with the help of reverse transcriptase. Treatment with T7 RNA polymerase then produces the complementary antisense RNA strand (to the original target RNA) from these templates [63].

The amplification phase follows the linear phase with the second primer once again annealing to the complementary antisense RNA strand. Reverse transcriptase then produces the complementary DNA strand in the form of another RNA: DNA duplex. RNase H is then removes the antisense RNA leaving the template DNA. The first primer is then reacted with the DNA producing a DNA: DNA duplex. RNA polymerase is then reacted to produce the complementary RNA. The cycle then continues leading to the overall amplification of target RNA (Figure 2) [63].

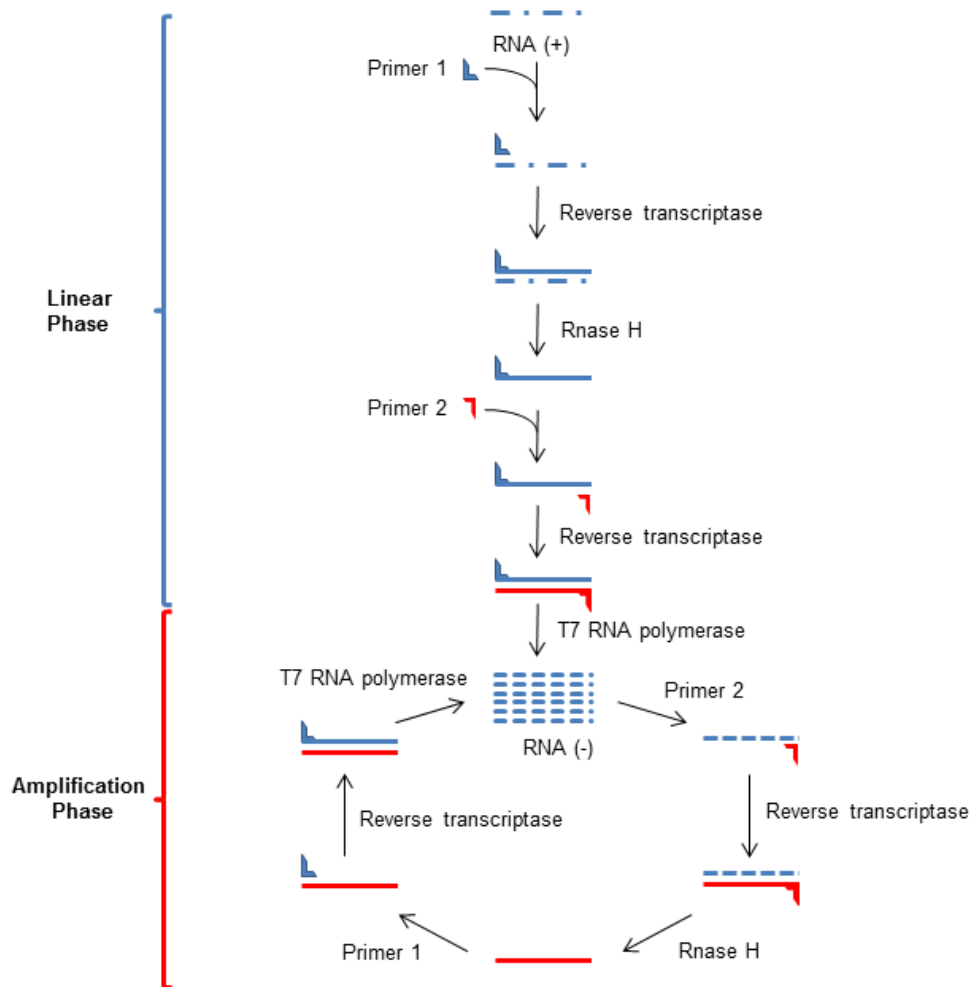


Figure 2: Diagrammatic representation of the NASBA process
Including the Non-Cyclic and Cyclic phases

Real time detection with a molecular beacon labelled with 6-carboxy fluorescein (6-FAM) at the 5' end and a DABCYL quencher at the 3' end allows for quantitation of initial target RNA. When no target RNA is present, the molecular beacon remains quenched by the DABCYL in a hairpin formation (refer to Figure 1b). However, in the presence of complimentary target RNA, the molecular beacon hybridises to the RNA separating the quencher and 6-FAM resulting in a detectable fluorescent signal. Time to positivity (TTP), or the time taken for the fluorescent signal to reach exponential growth, can then be measured and used to quantify the initial concentration of target RNA in the sample. This is done by producing standard curves generated using known cell numbers and their subsequent TTP values. Table 1 outlines the reports of the use of NASBA for HAB detection, some of which are highlighted below.

In 2004, Casper *et al.* reported the first use of NASBA for the detection of *K. brevis*. They recorded an estimated sensitivity to one cell based on the detectable 1.0 fg of *in vitro* transcript; however no data was given on these results. The method was highly selective when analysing closely related organisms as no non-target organisms were positively identified. A 10 fold excess of closely related cellular *rbcL* mRNA did not inhibit the assays results. Ten alternative *K. brevis* strains were all positively identified using the designed primers. Alternative *Karenia sp.* however was not tested as there was limited sequencing data at the current time of publication. Environmental samples were also re-analysed with the NASBA assay and compared to results previously attained by the Florida Fish and Wildlife Conservation Commission (FWC) with 72 % of events showing a good level of agreement between the NASBA and LM cell counts [64]. The calculated concentration using NASBA was stated as being limited by the accuracy of the standard curve. Using the TTP for the standard curve data can result in variations due to the three different enzymes displaying different kinetics and hence reacting at different rates [64].

To overcome the issues surrounding the use of the TTP standard curve, internal control RNA (IC-RNA) was introduced by the same research group in 2005 [65]. This aided in the quantification of the genetic material. This IC-RNA has a sequence that is the same as the target RNA but with a different attached fluorophore. A ratio of IC-RNA TTP values and the target RNA TTP values can then be taken to minimise the errors associated with the three enzymes and standard curve. As such, both accuracy and precision of the NASBA assay were improved for the quantification of cell numbers in a sample. Internal control NASBA showed magnitude of predictions ranging from 59 % to 740 % whereas the TTP standard curve ranged from 6 % to 3820 %. It was noted that the main associated errors were at low cellular concentrations. Compared to one another, the variance with the IC-RNA was much lower. For example, a cell number of 1000 was reading 677 ± 209 cells for the TTP standard curve and 920 ± 118 cells for the IC-RNA method. At lower cell numbers of 1, TTP results predicted 58 ± 143 cells whereas the IC-RNA method predicted 3 ± 2.5 cells [65].

The same research group aimed to simplify the internal control NASBA (IC-NASBA) assay for in field analysis in 2007 [66]. Here an extraction protocol and portable hand-held NASBA device was developed for the detection of *K. brevis*. The protocol developed by the RNeasy Mini Kit was altered so that instead of centrifugation, the solutions could be pushed through the spin columns with a flow of air. A *t*-test of the linear plot of the counts

obtained from the modified in field RNeasy Mini Kit versus the direct extraction showed no significant difference from 1.0 ($p > 0.05$). The hand held NASBA cell predictions were compared to LM cell counts with a good level of agreement. In most cases the bloom classifications were similar with very little variance and a paired sample *t*-test suggested that there was no significant difference between the NASBA and LM cell counts ($p > 0.05$) [66].

The research was extended to include *K. mikimotoi* in 2010 by the same research group but not using the hand held device discussed previously [67]. Using IC-NASBA, a theoretical detection limit of 1250 cells.L⁻¹ was calculated based on a 250 mL sample size which is reasonable when monitoring high cell concentrations in a bloom. When tested with closely related *K. brevis* no variation in cell number was observed suggesting the technique is also highly selective. Cell count comparisons showed a linear relationship between values obtained using the same NASBA method and LM cell counts [67].

With the aid of an internal control oligonucleotide, quantification of HAB causative organisms using NASBA has improved significantly. Unlike PCR based techniques, NASBA is an isothermal process by which the reaction can occur without the need of expensive equipment. The method offers high sensitivity and selectivity with the use of two specifically designed primers. The method has also been successfully automated using a hand-held NASBA device which will allow for research and analysis in the field. As RNA is the target material, potential degradation of the sample needs to be taken into account as discussed previously. Any degradation of the sample prior to analysis can severely alter the final bloom results, potentially underestimating the concentrations present. The use of a hand-held NASBA device and direct in field analysis could potentially overcome this issue. As different enzymes are also used in this analysis, the kinetics of each needs to be thoroughly understood as each may be different and subsequently affect the standard curve. This has been shown to be significantly improved however with the use of IC-NASBA making it a good alternative.

1.1.1.3 Loop-mediated isothermal amplification

Loop-mediated isothermal amplification (LAMP) has been introduced more recently as a method of HAB detection. This rapid procedure has been reported to increase the sensitivity of regular PCR by up to 100-fold [68]. Nucleic acid amplification occurs in three stages; an initial step, cycling amplification step and elongation step (Figure 3) [69]. Unlike NASBA and RT-PCR, LAMP utilises four specifically designed primers in the amplification

process. Two inner and two outer primers are able to recognize 6 regions of the target DNA strand. As amplification of the target DNA only occurs when all six regions are present, the process is highly specific. Other advantages of LAMP include the low costs involved in amplification as it all occurs at isothermal temperatures [69]. The exact method has been described in detail elsewhere [70]. Briefly, during the non-cyclic steps a DNA strand with two loops at the 5' and 3' end is formed with the aid of a forward inner primer (FIP), a forward outer primer (F3), a backward inner primer (BIP) and a backward outer primer (B3) [71]. In the cyclic amplification the loops allow for a strand displacement DNA synthesis in the form of inverted repeats of the target sequence within a single strand during elongation [69].

The first example of LAMP being used for the detection of six HAB species within the genus *Alexandrium* wasn't until 2008, 8 years after its initial development [72]. In this study, a comparison between LAMP and PCR sensitivity was conducted. It was found that the sensitivity of LAMP was 10-fold higher than that demonstrated using PCR.

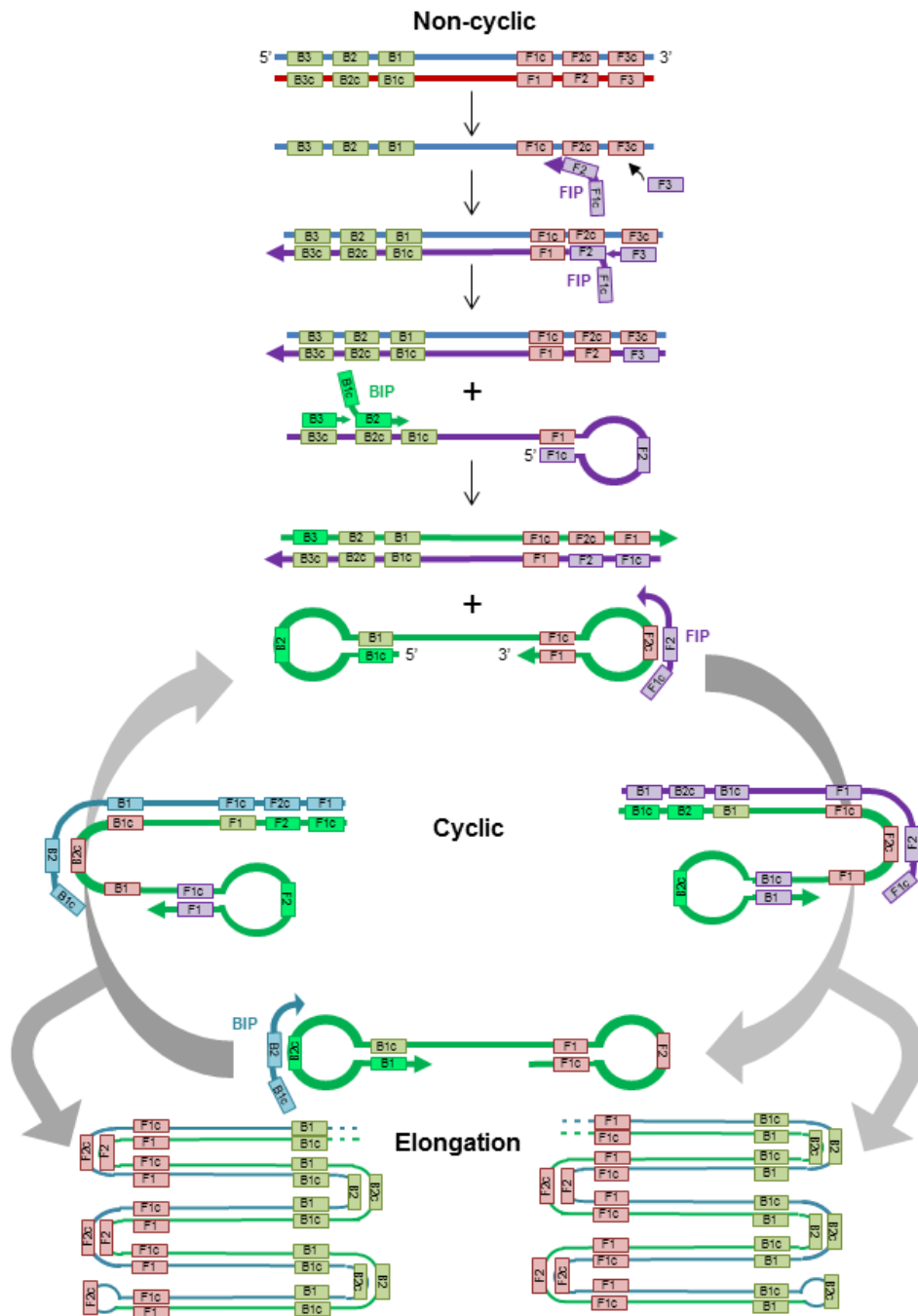


Figure 3: Process of LAMP amplification

Three main steps: non-cyclic reaction and formation of dual looped DNA strand, cyclic amplification and elongation leading to strand displacement DNA synthesis.

A. catenella and *A. tamarensis* identification using LAMP was possible within 25 min of amplification using both cultured and natural seawater samples [73]. Detection limits were not stated in this research and instead a 5 cell and single cell (≈ 5 ng) amplification

was completed in the presence of > 10 ng of non-target *Alexandrium* species DNA. The fluorescence intensity seemed unaffected by the non-target DNA with the fluorescence exhibited being the same as that expected for 5 ng of target DNA. In a continuation of the study, alternative DNA extraction methods to the TE buffer-boiling, which was found to not extract DNA of the closely related *Alexandrium* species [73], was trialled [74]. Extraction using a TE buffer, CTAB buffer, 0.5 % Chelex buffer and 5 % Chelex buffer demonstrated that the two Chelex buffer systems were able to provide the highest amplification success (100 %) in both species. Limits of detection in this case were not reported as with the previous research.

LAMP has also been used to track *A. tamarensis* resting cysts in sediment core samples in Funka Bay, Japan [75]. Primers specific to *A. tamarensis* and *A. catenella* were used to determine if either species were present in the sample. 91.9 % of the isolated cysts were found to be *A. tamarensis* with no *A. catenella* detection suggesting there were little to no cysts of this species in Funka Bay.

A LAMP method for the identification of *K. mikimotoi* was developed and compared to previously used PCR [68]. Four specific primers were developed as before and upon comparison with PCR, a 100-fold increase in sensitivity was observed for LAMP. The detection limit reported for this species was approximately 6 pg of DNA (cell number not specified); lower than the previously recorded limits for *A. minutum*. High selectivity was also observed with no amplification occurring with alternate HAB species of varying genus using the same four primers.

Another comparison between the use of LAMP and real-time fluorescence quantitative PCR (RTFQ-PCR) was also conducted for the detection of *P. minimum* [76]. The sensitivity of LAMP was also found to be 10-fold higher in LAMP than conventional PCR. The detection limit for LAMP however was higher at 36 pg of DNA compared to RTFQ-PCR which had a recorded detection limit of 10 pg of DNA. These limits of detection were also higher than some previously discussed methods for alternative species suggesting further optimisation is still necessary. LAMP was determined to be a more applicable method for detecting samples with high throughput in the field compared to RTFQ-PCR which is restricted to analysis in the laboratory.

Reverse transcription-coupled LAMP (RT-LAMP) has also been introduced for the detection of *P. donghaiense* [77]. Compared to the previously discussed LAMP, RT-LAMP

allows RNA to be targeted in a sample with the initial production of cDNA before amplification. A detection limit of $0.6 \text{ cells.mL}^{-1}$ (0.4 ng) was achieved using the specifically designed primers developed in this study. As was shown for LAMP, RT-LAMP was able to provide a visible detection of amplification making it a practical option for the detection of this HAB species.

Overall, LAMP has a lot of potential for the detection of HAB formations. The use of four designed primers makes the procedure extremely selective. The reaction also occurs in a single tube with no need for expensive equipment, such as the thermal cycler required for PCR [72]. Detection limits when compared to PCR are also much lower making the technique suitable for low cell number analysis during the initial stages of a HAB. The issues with DNA extraction do need to be thoroughly assessed prior to using this method for detection however as some cells require more treatment than others. Very careful consideration on the primer sequences must also be taken into account to provide the best selectivity possible for the targeted species.

Table 1: Overview of NASBA used in HAB detection

Authors	Species Identified	Sample	Extraction protocol	Forward (1) Primer Sequence (5'-3')	Reverse (2) Primer Sequence (5'-3')	Molecular Beacon Sequence (5'-3')
		Cultured				
Casper <i>et al.</i> [64]	<i>K. brevis</i>	Medium and temperature not specified, 12 h:12 h light:dark cycle Natural seawater Coastal Florida, US	RNeasy Mini Kit (Qiagen) or Absolutely RNA Microprep kit (Stratagene)	ACGTTATTGGGTCTGTGTA	AATTCTAATACGACTCACT ATAGGGAGAAGGTACACA CTTTCGTAAACTA	[6-FAM]- CGATCGCTTAGTCTCGGG TTATTTTTTCGATCG- [DABCYL]
Patterson <i>et al.</i> [65] ^a	<i>K. brevis</i>	Cultured Medium not specified, 24 °C, light:dark cycle not specified	RLT lysis buffer (Qiagen) followed by RNeasy spin column (Qiagen) purification	ACGTTATTGGGTCTGTGTA	AATTCTAATACGACTCACT ATAGGGAGAAGGTACACA CTTTCGTAAACTA	[6-FAM]- CGATCGCTTAGTCTCGGG TTATTTTTTCGATCG- [DABCYL]

Authors	Species Identified	Sample	Extraction protocol	Forward (1) Primer Sequence (5'-3')	Reverse (2) Primer Sequence (5'-3')	Molecular Beacon Sequence (5'-3')
Casper <i>et al.</i> and Smith <i>et al.</i> [66, 78] ^a	<i>K. brevis</i>	Cultured Medium not specified, 24 °C, 12 h:12 h light:dark cycle	RNeasy Mini Spin Kit (Qiagen) or field extraction protocol (refer to [78])	ACGTTATTGGGTCTGTGTA	AATTCTAATACGACTCACT ATAGGGAGAAGGTACACA CTTTCGTAAACTA	[6-FAM]- CGATCGCTTAGTCTCGGG TTATTTTTTCGATCG- [DABCYL]
Ulrich <i>et al.</i> [67] ^b	<i>K. mikimotoi</i>	Cultured L1 medium, 22 °C, 12 h:12 h light:dark cycle Natural seawater Coastal Florida, US	RNeasy Mini Kit (Qiagen)	AACCTAAAATGATTAAG GA	AATTCTAATACGACTCACT ATAGGGAGGAGACCCATT CTTGCGAAAAATAA	[6-FAM]- CGATCGAACAACTAAACA TGATTTTTCGATCG- [DABCYL]

^a IC-RNA molecular beacon used [6-ROX]CGATCGTGGCTGCTTATGGTGACAATCGATCG-[DABCYL] for *K. brevis*

^b IC-RNA molecular beacon used [6-ROX]-CATGCGTGGCTGCTTATGGTGACAATCGCATG-[DABCYL] for *K. mikimotoi*

1.1.2 Fluorescence in situ hybridisation (FISH)

Fluorescence *in situ* hybridisation (FISH), also referred to as whole cell hybridisation (WC), was first reported in the 1970's. However, it was almost 25 years before this technique was first applied to HAB detection [79-81]. A schematic diagram illustrating the FISH process is shown in Figure 4. FISH utilises a fluorescently labelled oligonucleotide capture probe that is complimentary to the variable region in cellular RNA or DNA of the target organism. RNA is the most commonly targeted substrate, with only one report targeting cellular DNA [82]. Typically, cells are immobilised with a fixative followed by hybridisation with labelled oligonucleotide probes. In this process, the probe crosses the cell membrane into the cell where it hybridises with the target intracellular rRNA. The sample is subsequently washed to remove unbound oligonucleotide strands and the resulting fluorescence intensity monitored using epifluorescence microscopy or flow cytometry [30, 83, 84]. Table 2 outlines the reports of the use of FISH for HAB detection, some of which are highlighted below.

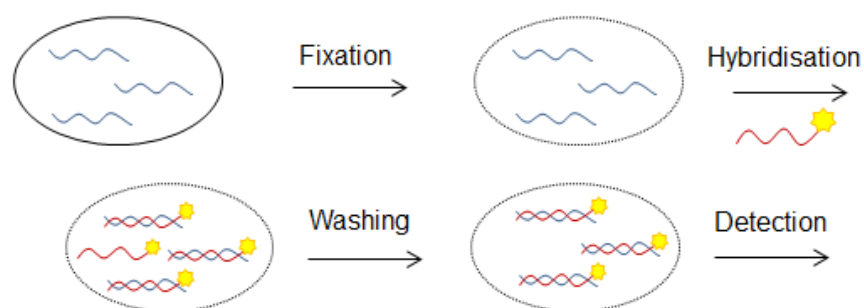


Figure 4: Diagrammatic representation of the steps required for FISH analysis

After identifying variable regions in the LSU rRNA of *Pseudo-nitzschia* diatoms [32], Scholin *et al.* [30] developed a fluorescein labelled oligonucleotide probe specific to *P. australis* (aus-D1, Table 2) and tested its sensitivity and cross reactivity using FISH. The aus-D1 capture probe demonstrated high selectivity with no observable cross reactivity for alternative *Pseudo-nitzschia* species such as *P. pungens*, *P. multiseriata*, *P. delicatissima*, *P. pseudodelicatissima*, *P. fraudulenta*, *P. heimii* and *P. americana*. They observed an improved and more uniform fluorescence response when an ethanol/saline fixative was used instead of the traditional formalin and aldehyde-type fixatives. This milder fixative reduced the exudation of cellular contents upon fixation thus minimising background fluorescence [30]. They continued this work and developed fluorescently

labelled oligonucleotide probes for an additional eight cultured *Pseudo-nitzschia* species (Table 2). Of the fifteen oligonucleotide sequences tested, eight provided species specific identification, however detection limits and cross reactivity were comparative only to the positive and negative control probes. Quantitative assessment of the method performance was not undertaken [34]. Subsequent work by this group focused on improving the assays via the incorporation of a vacuum manifold in order to increase the overall quantitative cell recovery and allow for potential automation using robotic processing [83, 84]. Collected samples were subjected to an initial ethanol/saline fixation prior to vacuum filtration onto a 13 mm Isopore membrane (Millipore). Hybridisation with fluorescein labelled oligonucleotide capture probes at 45 °C followed. Washing with hybridisation buffer removed all non-hybridised oligonucleotides. The authors also noted that antifade treatment with SlowFade® prior to fluorescence microscopy extended the fluorescence signal lifetime by preventing photobleaching [85].

In 2000 Miller and Scholin extended this work, demonstrating simultaneous detection of two different HAB species, *P. multiseriis* and *P. pungens*, by utilising a fluorescein labelled oligonucleotide probe for *P. pungens* and a Texas Red labelled oligonucleotide probe for *P. multiseriis* [86]. Stability trials undertaken during this study also showed that ethanol/saline fixed cells integrity was not compromised after 6 weeks for cultured cells and 4 to 6 weeks for natural seawater samples. After this time there was a rapid reduction in the reactivity of intracellular material and resulting fluorescence response [86].

A vacuum manifold sample collection system previously developed by Scholin and colleagues [84] allowed for preparation of both FISH and scanning electron microscopy (SEM) samples on the same apparatus. Initially FISH was used to identify the species present based on the variable rRNA region within the target cell. Subsequent SEM imaging confirmed the results based on morphological features of the same cells [84]. The level of cell density that can be effectively analysed via this FISH method is in the range of 1250-2500 cells.L⁻¹, which is well below the minimum cell concentration present in a bloom [84].

Other *Pseudo-nitzschia* species such as *P. australis*, *P. multiseriis*, *P. pseudodelicatissima* and *P. pungens* were compared to those found using the SHA technique (reviewed in Section 1.1.3). A good correlation between FISH and SHA results was observed making both methods an effective tool for tracking bloom formations [87]. No observable variations between the cell growth stage and signal intensity were observed during the

different stages of *Pseudo-nitzschia* species cell growth suggesting that the amount of genetic material in the cell is independent of cell growth [87].

Species specific identification of *Alexandrium* dinoflagellates, *A. tamarensis*, *A. catenella* and *A. affine* using oligonucleotide capture probes Atm1, Act1 and Aaf1, (Table 2) respectively was achieved using FISH in cultured samples [88-90]. No cross reactivity between the oligonucleotide probes and non-target species was reported. In contrast to *Pseudo-nitzschia* diatom species [30] the use of a paraformaldehyde fixative in place of ethanol/saline provided the greatest level of uniform fluorescence across the cells [89]. Furthermore, the hybridisation time for the *Alexandrium* assays were typically 5 min, in contrast to the 1-4 h used for the *Pseudo-nitzschia* diatom species reported previously [89].

Application of FISH to natural seawater samples from Japan confirmed the presence of *A. tamarensis* and *A. catenella*. The results obtained allowed for quantitative, rapid and precise detection of the two species [89]. Multiple organic solvents have also been tested on *A. tamarensis* and *A. catenella* species with the aim of decolourising fixed natural seawater samples. Treatment with 80 % acetone prior to hybridisation was found to significantly reduce background autofluorescence [88]. A quantitative spike study showed a 92.5 ± 2.1 % recovery of *A. tamarensis* using the Atm1 probe and a 94.1 ± 1.0 % recovery of *A. catenella* using the Act1 probe [90]. Two oligonucleotide probes with different fluorescent labels, previously shown by Miller and Scholin [86], was trialled for the *Alexandrium* species with a rhodamine labelled Atm1 probe selective for *A. tamarensis* and a FITC-labelled Act1 probe selective for *A. catenella*. The two fluorochromes were able to identify the two species, however high levels of autofluorescence interfered with the overall identification of *A. tamarensis* [90].

The use of FISH to detect *K. brevis* was first reported in 2005 [91]. Initial PCR sequencing of the species allowed for a series of test oligonucleotide capture probes to be developed and tested. Kprobe-7 (Table 2) provided the highest level of fluorescent labelling for formalin fixed cells when compared to the alternative probes tested. This oligonucleotide probe demonstrated high selectivity for *K. brevis* when mixed with a range of dinoflagellate, diatom and raphidophyte taxa. Kprobe-7 was mixed with stored samples from a 2001 bloom to determine if *K. brevis* was the causative species. Successful identification of this species followed giving rise to a potential method for tracking bloom formation [34, 91].

PCR sequencing resulted in the development of specific oligonucleotide probes for *C. polykrikoides* (Table 2). These were tested on cultured samples of *C. polykrikoides* along with isolates from Korean and Hong Kong waters [92]. Of the probes tested, Cp-C4 provided the greatest probe reactivity towards *C. polykrikoides*. No cross reactivity with alternative dinoflagellate, diatom or raphidophyte species was observed for the positively labelled isolates [92]. However, isolates of the same species from North America showed no hybridisation with any of the developed probes. This is most likely due to the slight difference in the genetic sequence for this isolate [92].

A FISH detection method was also developed for *H. akashiwo*, another HAB causative species. Here, both the rRNA and rDNA were targeted using different probes specific to each. The rRNA probe successfully labelled the cytoplasmic rRNA with 80 % of the target being detected and the rDNA probe successfully labelled the nucleic material only in the nucleus with 70 % of the target being identified. When tested with eight other species, no cross reactivity was observed [82].

Overall, FISH provides a quick and easy method for the detection of HAB cells in cultured and natural seawater samples. As RNA can be targeted with oligonucleotide probes *in situ*, without the need for complex extraction and sample preparation, the method is non-destructive of the sample. This allows the analyst to confirm species identity whilst keeping the cell intact for cell morphology studies. Unfortunately, FISH is typically restricted by high background fluorescence from material present within a natural seawater sample. This can obscure labelled cells making quantification difficult and time consuming. Furthermore, cellular integrity must also be closely considered during the fixation step as cell rupture can lead to a loss of target RNA and result in difficulties in both identification and cell studies. Cell counting via fluorescence microscopy is also time consuming, but can be overcome by using automated methods such as flow cytometry.

Table 2: Overview of methodology used for FISH analysis of HAB species

Authors	Species Identified	Probe Name	Oligonucleotide capture probe sequence (5'-3')	Sample	Hybridisation conditions	Detection
Miller <i>et al.</i> [34]	<i>P. australis</i>	auD1	AAATGACTCACTCCACCAGG	Cultured Maintained in f/2 enriched seawater medium, 13 °C, 10 h:14 h light:dark cycle	3 h at 45-55 °C	SEM and epifluorescence microscopy
	<i>P. australis</i>	auD1a	ATGACTCACTCCACCA			
	<i>P. pungens</i>	puD1	ATGACTCACTTTACCA			
	<i>P. pungens</i>	puD2	AAGTCCACAGCGCCCAGGCC			
	<i>P. pungens</i>	puD2a	TCCACAGCGCCCAGG			
	<i>P. multiseriis</i>	muD1	ATGACTCACTCTGCCA			
	<i>P. multiseriis</i> / <i>P. pseudodelicatissima</i>	muD2	AAGCCCACAGCGCCCAAGCC			
	<i>P. multiseriis</i> / <i>P. pseudodelicatissima</i>	muD2a	CCCACAGCCCAAG			
	<i>P. heimii</i>	heD1	CCATGACTCATTCTAACCAGA			
	<i>P. heimii</i>	heD2-1	CAAGGGAAATATGAACATA			
	<i>P. heimii</i>	heD2-2	TATCCACAGCGCCCACA			
	<i>P. heimii</i> / <i>P. fraudulenta</i> / <i>P. delicatissima</i>	frD1	AAAGACTCATTCTAACCAGG			
	<i>P. delicatissima</i>	deD1	AGACTCACTCTACCA			
	<i>P. americana</i>	amD1	ATGACTCATTCAGCCA			
	<i>P. fraudulenta</i> / <i>P. delicatissima</i>	amD3	ATATCCAACCACTGTTA			

Authors	Species Identified	Probe Name	Oligonucleotide capture probe sequence (5'-3')	Sample	Hybridisation conditions	Detection
Miller <i>et al.</i> [84]	<i>A. tamarense</i>	NA1	AGTGCAACTCCCACCA	Natural seawater Santa Cruz, California	1-2 h at 45 °C	SEM and epifluorescence microscopy
	<i>P. australis</i>	auD1	AAATGACTCACTCCACCAGG			
	<i>P. pungens</i>	puD1	ATGACTCACTTTACCA			
	<i>P. multiseriis</i>	muD1	ATGACTCACTCTGCCA			
	<i>P. multiseriis / P. pseudodelicatissima</i>	muD2	AAGCCCACAGCGCCCAAGCC			
	<i>P. heimii</i>	heD2-2	TATCCACAGCGCCCACA			
	<i>P. fraudulenta</i>	frD1	AAAGACTCATTCTACCAGG			
	<i>P. delicatissima</i>	deD1	AGACTCACTCTACCA			
	<i>Nitzschia americana</i>	amD1	ATGACTCATTGAGCCA			
Scholin <i>et al.</i> [30]	<i>P. australis</i>	aus-D1	AAATGACTCACTCCACCAGG	Cultured Maintained in f/2 enriched seawater medium, 15 °C, 12 h:12 h light:dark cycle	3-4 h at 42 °C	Epifluorescence microscopy

Authors	Species Identified	Probe Name	Oligonucleotide capture probe sequence (5'-3')	Sample	Hybridisation conditions	Detection
Scholin <i>et al.</i> [83]	<i>P. australis</i>	aus-D1	AAATGACTCACTCCACCAGG	Natural seawater Monterey Harbor, California	1 h at 45 °C	Epifluorescence microscopy
Scholin <i>et al.</i> [87]	<i>P. australis</i>	auD1S	AAATGACTCACTCCACCAGGCGG	Natural seawater Monterey Bay and Santa Cruz, California	1-2 h at 45 °C	SEM and epifluorescence microscopy
	<i>P. pungens</i>	puD1S	TGACTCACTTTACCAGGCGG			
	<i>P. multiseriis</i>	muD1S	AAATGACTCACTCTGCCAGG			
	<i>P. multiseriis / P. pseudodelicatissima</i>	muD2S	AGCCACAGCGCCCAAGCCA			
Miller <i>et al.</i> [86]	<i>P. australis</i>	auD1	AAATGACTCACTCCACCAGG	Natural seawater Monterey Bay and Santa Cruz, California	1 h at 45 °C	Epifluorescence microscopy
	<i>P. pungens</i>	puD1	ATGACTCACTTTACCA			
	<i>P. multiseriis</i>	muD1	ATGACTCACTCTGCCA			
Sako <i>et al.</i> [89]	<i>A. tamarensis</i>	Atm1	ACACCCACAGCCCAAAGCTC	Cultured Maintained in SWIlm medium, 15 °C, 14 h:10 h light:dark cycle	5 min at 40 °C	Epifluorescence microscopy and flow cytometry
	<i>A. catenella</i>	Act1	GCACTTGACAGCCAAAACCCA			
	<i>A. affine</i>	Aaf1	GCACCCACAAATCAAAACCTA			

Authors	Species Identified	Probe Name	Oligonucleotide capture probe sequence (5'-3')	Sample	Hybridisation conditions	Detection
Ayers <i>et al.</i> [31]	<i>P. australis</i>	auD1	AAATGACTCACTCCACCAGG	Cultured	n.d	Epifluorescence microscopy
Hosoi-Tanabe <i>et al.</i> [88]	<i>A. tamarense</i>	Atm1	ACACCCACAGCCCAAAGCTC	Natural seawater Kure Bay, Tokuyama Bay and Kitsuki Bay, Japan	5 min at 40 °C	Epifluorescence microscopy
	<i>A. catenella</i>	Act1	GCACTTGCAGCCAAAACCCA			
Mikulski <i>et al.</i> [91]	<i>K. brevis</i> / <i>K. mikimotoi</i>	Kbprobe-4	AAGATTGCAAGCAAGCAC	Natural seawater Gulf of Mexico, USA	1.5 h at 45 °C	Epifluorescence microscopy and flow cytometry
		Kbprobe-5	TCCTGGCACTAGCAACCT			
	<i>K. brevis</i>	Kbprobe-7	GCTGGTGCAGATATCCCAG			
Hosoi-Tanabe <i>et al.</i> [90]	<i>A. tamarense</i>	Atm1	CACCCACAGCCCAAAGCTC	Natural seawater Tokuyama Bay and Kitsuki Bay, Japan	5 min at 40 °C	Epifluorescence microscopy and flow cytometry
	<i>A. catenella</i>	Act1	GCACTTGCAGCCAAAACCCA			

Authors	Species Identified	Probe Name	Oligonucleotide capture probe sequence (5'-3')	Sample	Hybridisation conditions	Detection
Chen <i>et al.</i> [82]	<i>H. akashiwo</i>	HS-lsu	CAGCATACCCGAGAGAGGAAC	Cultured Maintained in f/2 or f/2 + Si medium, 20-22 °C, 12 h:12 h light:dark cycle	30 min at 45 °C	Epifluorescence microscopy
		HS-its	CAGATTGGAGGTTGTTTGGG			
Mikulski <i>et al.</i> [92] ^a	<i>C. polykrikoides</i>	Cp-C1	GCCCAAGCAACTCGCACAT (*)	Cultured Maintained in f/2 medium/ L1 medium, 15 °C/ 25 °C/ 20 °C, 16 h:8 h light:dark cycle based on strain	1.5 h at 45 °C	Epifluorescence microscopy
		Cp-C2	GCGCATGGGTTTGCAGCCC (**)			
		Cp-C4	CTCGCAATTGATCAGTCGGT (***)			
		Cp-C5	GGTCTCAAACACGTATTTA (*)			

^a +, ** and *** refer to level of fluorescence observed towards *C. polykrikoides* using the respective probes

1.1.3 Sandwich Hybridisation Assay (SHA)

The sandwich hybridisation assay (SHA) is another common method for the detection of HABs. Unlike FISH, which targets whole cells, SHA comprises of a two-step hybridisation of lysed cellular material. Two specific oligonucleotide probes, one for capture and the other to provide a signal, are employed as outlined in Figure 5 [30]. The lysed sample is introduced to biotinylated capture probes, usually bound to a coated streptavidin surface on the base of a microwell or bead surface [30, 87]. Following the tethering of the target sequence to the capture probe, a secondary hybridisation event follows with a specifically labelled signal probe. This probe can be labelled with fluorescein, biotin or digoxigenin (DIG). Once hybridised, a reaction with the corresponding antibody conjugated to horseradish peroxidase (HRP) follows. Depending on the substrate used in the next step, a colourimetric or electrochemical response can be recorded and used in subsequent cell quantitation [83, 93, 94].

Fluorescein signal probes are most commonly used in the SHA detection of HAB species [35, 87, 92, 93, 95-99]. This requires a reaction post-hybridisation with anti-fluorescein HRP conjugates followed by a reaction with a commercially available 3,3',5,5'-tetramethylbenzidine (TMB) or 2,2'-azino-bis(3-ethylbenzthiazoline-6-sulfonic acid) (ABTS) HRP substrate solution. A detectable colourimetric response follows that is proportional to the level of HRP reactivity in the system. Biotin labelled signal probes also provide a colourimetric response when reacted with anti-biotin HRP conjugates followed by reaction with the corresponding commercially available HRP conjugate (details not specified) [30, 83]. Electrochemical responses can be obtained by using DIG labelled signal probes that can react with anti-DIG HRP conjugates and a hydrogen peroxide substrate. The resulting reduction of the hydrogen peroxide with HRP generates a change in signal [94]. A simplified detection of utilising a Cy3 labelled signal probe and recording the subsequent fluorescence response has also been published in literature [100].

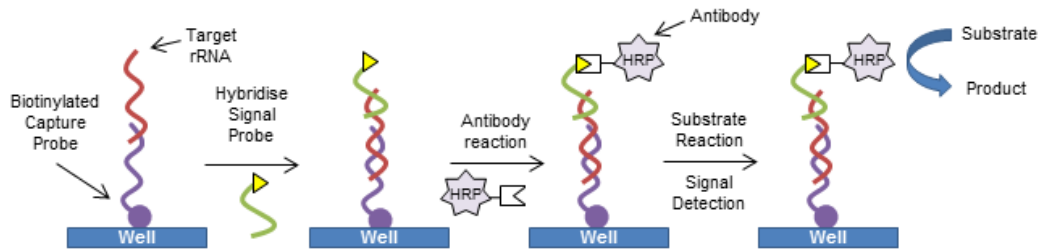


Figure 5: Diagrammatic representation of the SHA process

Both the capture probe (purple) and signal probe (green) bind to specifically chosen complimentary regions within the target rRNA (red). This approach has the advantages of no purification steps prior to exposing the lysate to the capture probe, and that the amplification of the genetic RNA occurs naturally within the cell eliminating the need for PCR, prior to detection [93, 98]. Caution must be taken though, as lysed RNA is sensitive to degradation when in contact with ribonucleases (RNase) [98]. Table 3 outlines the reports of the use of SHA for HAB detection, some of which are highlighted below.

The use of SHA for the detection of HABs was first reported in 1996 for the detection of *P. australis* in cultured samples [30]. Here, oligonucleotide capture probes were adsorbed onto a nylon bead which was added to crude lysates. As SHA undergoes two hybridisation events with two specific oligonucleotide probes, the selectivity is further enhanced when compared to the alternative FISH detection discussed previously. *P. australis* specific oligonucleotide sequences exhibited a high level of selectivity when compared to other species present in the *Pseudo-nitzschia* genus such as *P. pungens*, *P. multiseriata*, *P. fraudulenta*, *P. heimii* and *P. delicatissima*.

Semi-automation of the SHA procedure was also trialled and compared to results from light microscopy (LM) and FISH for the detection of *P. australis* [83]. The SHA method was reported to be several times faster than the FISH method with quantifiable results obtained using a standard curve [83]. Field samples from Monterey Harbour, California were tested with naturally occurring particulate organic matter and organisms, such as other diatoms and zooplankton, present not affecting SHA hybridisation efficiency [83]. To evaluate how the growth phase influences levels of nucleic cellular material, samples were collected at different growth stages and analysed using the semi-automated SHA method [87]. Cellular rRNA concentrations were found to remain stable throughout the different growth stages. This is an important factor as some other species, such as

A. catenella [99], have demonstrated fluctuating concentrations of rRNA at different growth stages, skewing cellular concentrations based on that SHA analysis [87].

Further quantification of *F. japonica* and *H. akashiwo* by SHA was also achieved using a standard curve. Initially, FISH (discussed in Section 1.1.2) was used to test the specificity of the designed oligonucleotide probes. Once developed, the probes (outlined in Table 3) were introduced to SHA. Overall the SHA method was rapid, easy and more affordable when compared to FISH and LM [35]. This approach was applied to the detection of *H. akashiwo* in natural seawater samples from Puget Sound and Hood Canal, USA [95]. Here, the fixation step was omitted as the cells were found to rupture upon treatment with Lugol. Instead cells were lysed immediately with the lysate and stored at -70 °C until analysis. Higher cell densities resulted in difficulties in quantitation, with this being overcome by serial dilution of the cellular samples [95]. Similarly, natural seawater samples from the Californian coast between 2001 and 2002 were examined by SHA for the presence of *H. akashiwo* [96]. In this case, SHA results resulted in a good agreement with the end-point polymerase chain reaction (PCR) assay on samples collected during a bloom event along Monterey Bay and San Francisco Bay, California. Using LM, positive identification of *H. akashiwo* was difficult due to cellular rupture upon fixation. The SHA and PCR methods however, were able to positively identify the species making it an alternative approach for the rapid screening of fragile HAB organisms [96].

Later in 2005, SHA was developed for the validation of *F. japonica* and *H. akashiwo* in New Zealand [31]. This method was found to underestimate cell densities for *F. japonica* but was comparable to counts from LM with *H. akashiwo*. The cause for underestimation was due to samples being collected during late stationary phase meaning the level of target rRNA may have been limited. During bloom collapse it was also noted that there was an increase in rRNA levels most likely due to cell rupture upon death leading to overestimation of cell concentration using SHA. Based on the results of this study, international accreditation was awarded for the developed SHA method by the International Accreditation New Zealand (IANZ; ISO 17025) [31].

Table 3: Overview of methodology used for the SHA of HAB species

Author.	Species Identified	Capture oligonucleotide probe sequence (5'-3')	Signal oligonucleotide probe sequence (5'-3')	Sample	Detection
Scholin <i>et al.</i> [30]	<i>P. australis</i>	AAATGACTCACTCCACCAGGCGG	CTCTTTAACTCTCTTTTCAAAG TTCTTTGCATC	Cultured Maintained in f/2 enriched seawater medium, 15 °C, 12 h:12 h light:dark cycle	Photographed beads after colour development
Scholin <i>et al.</i> [83]	<i>P. australis</i>	AAATGACTCACTCCACCAGGCGG	CTCTTTAACTCTCTTTTCAAAG TTCTTTGCATC	Cultured Maintained in f/2 medium, 13 °C, 10 h:14 h light:dark cycle Natural seawater Monterey Harbour, California	Photographed beads after colour development

Author.	Species Identified	Capture oligonucleotide probe sequence (5'-3')	Signal oligonucleotide probe sequence (5'-3')	Sample	Detection
Scholin et al. [87]	<i>P. australis</i>	AAATGACTCACTCCACCAGGCGG		Cultured Maintained in f/2 medium, 13 °C, 10 h:14 h light:dark cycle	Plate reader: 655 nm then 450 nm after 10 % H ₂ SO ₄ treatment
	<i>P. pumgens</i>	TGACTCACTTTACCAGGCGG			
	<i>P. multiseriis</i>	AAATGACTCACTCTGCCAGG	CTCTTTAACTCTCTTTTCAAAG		
	<i>P. pseudo-delicatissima</i>		TTCTTTGCATC		
	and <i>P. multiseriis</i>	AGCCACAGCGCCCAAGCCA			
Tyrrell et al. [95]	<i>H. akashiwo</i>	ACCACGACTGAGCACGCACCTTT	CCGCTTCACTCGCCGTTACTA G	Natural seawater Puget Sound and Hood Canal, USA	Plate reader: 655 nm then 450 nm after 10 % H ₂ SO ₄ treatment

Author.	Species Identified	Capture oligonucleotide probe sequence (5'-3')	Signal oligonucleotide probe sequence (5'-3')	Sample	Detection
O'Halloran <i>et al.</i> [96]	<i>H. akashiwo</i>	ACCACGACTGAGCACGCACCTTT	CCGCTTCACTCGCCGTTACTA G	<p>Cultured</p> <p>Maintained in f/2 medium, 15 °C, 12 h:12 h light:dark cycle</p> <p>Natural seawater</p> <p>Monterey Bay and Berkeley Pier, California</p>	<p>Plate reader: 655 nm then 450 nm after 10 % H₂SO₄ treatment</p>
Tyrrell <i>et al.</i> [35]	<i>H. akashiwo</i>	ACCACGACTGAGCACGCACCTTT	CCGCTTCACTCGCCGTTACTA G	<p>Cultured</p> <p>Maintained in f/2 medium, 20 °C, 12 h:12 h light:dark cycle</p>	<p>Plate reader: 655 nm then 450 nm after 10 % H₂SO₄ treatment</p>
	<i>F. japonica</i>	CGGCTGGACACGCTTCTGTAG			

Author.	Species Identified	Capture oligonucleotide probe sequence (5'-3')	Signal oligonucleotide probe sequence (5'-3')	Sample	Detection
	<i>H. akashiwo</i>	n.d	n.d	Cultured	
Ayers <i>et al.</i> [31]	<i>F. japonica</i>	n.d	n.d	Natural seawater Bay of Plenty and Marlborough Sounds, NZ	Plate reader: 655 nm then 450 nm after 10 % H ₂ SO ₄ treatment
	<i>P. australis</i>	AAATGACTCACTCCACCAGGCGG	CTCTTTAACTCTCTTTTCAAAG TTCTTTGCATC		
Anderson <i>et al.</i> and Ahn <i>et al.</i> [100, 101]	<i>A. fundyense</i>	GCAAGTGCAACTCCCACCA	TTCAAAGTCCTTTTCATATTTCC	Cultured	Fluorescence measured as light intensity per bead
	<i>A. ostensfeldii</i>	GTGGACGCAACAATCTCACCA	TTCAAAGTCCTTTTCATATTTCC	Maintained in f/2 medium, 15 °C, 14 h:10 h light:dark cycle	
	<i>P. australis</i>	AAATGACTCACTCCACCAGGCGG	CTCTTTAACTCTCTTTTCAAAG TTCTTTGCATC		
Diercks <i>et al.</i> [97]	<i>A. minutum</i>	GAAGTCAGGTTTGGATGC	TAATGACCACAACCCTTCC	Cultured Maintained in multiple media, 15-22 °C, 14 h:10 h light:dark cycle	Varian Cary 4000 UV-Vis Spectrometer

Author.	Species Identified	Capture oligonucleotide probe sequence (5'-3')	Signal oligonucleotide probe sequence (5'-3')	Sample	Detection
Metfies <i>et al.</i> [94] ^a	<i>A. ostenfeldii</i>	CAACCCTTCCAATAGTCAGGT	GAATCACCAAGGTTCCAAGCA G	Cultured Maintained in K-medium, 15 °C, 14 h:10 h light:dark cycle	Electrochemical signal recorded for 10 s at -150 mV
Zhen <i>et al.</i> [99] ^b	<i>A. catenella</i>	ATTTGGCACAGCCTGAGCATTAT C	ACAACCTGCACTTGACTGTGTG GTGTG	Cultured Maintained in f/2 medium, 22- 25 °C, 12 h:12 h light:dark cycle Natural seawater Old Stoneman Beach, Qingdao, China	Plate reader 450 nm/630 nm ratio recorded after 2 M H ₂ SO ₄ treatment
Zhen <i>et al.</i> [98] ^c	<i>Phaeocystis globosa</i>	GGATTGGAGGGTGTTCGTTTCG	GCACCTTACGGGAAACTAAA GTCTTTG	Cultured Maintained in f/2 medium, 22- 25 °C, 12 h:12 h light:dark cycle Natural seawater Luxun Park, Qingdao, China	Plate reader 450 nm/630 nm ratio recorded after 2 M H ₂ SO ₄ treatment

Author.	Species Identified	Capture oligonucleotide probe sequence (5'-3')	Signal oligonucleotide probe sequence (5'-3')	Sample	Detection
Zhu <i>et al.</i> [102] ^e	<i>P. minimum</i>	ACAGTCCGCAAATGAGTTCTGCC	n.d	Cultured Maintained in f/2 medium, 22 °C, 12 h:12 h light:dark cycle Natural seawater East China Sea, China	ECL detection at 1.0 V, 1.0 mA measured in counts per second (CPS)
		AAGGCTATTCCTCACCCTAGACGAGCTACCATGA			
Cai <i>et al.</i> [93] ^d	<i>P. minimum</i>	TCATGGTAGCTCGTCTACGGGTG A	GGCAGAACTCATTGCGGACT GT	Cultured Maintained in f/2 medium, 22- 25 °C, 12 h:12 h light:dark cycle	Plate reader 450 nm/630 nm ratio recorded after 2 M H ₂ SO ₄ treatment
	<i>P. micans</i>	ATCGAGGAAAACCTCCAGGGACAT G	GGGTGGGTGAATGTGCCTGG T		

^a A helper probe was also used in this study (5'-GCATATGACTACTGGCAGGATC-3')

^b Nuclease protection probe also used for NPA-SH for *P. minimum* (5'-ACAGTCCGCAAATGAGTTCTGCCAAGGCTATTCCTCACCCTAGACGAGCTACCATGA-3') and *P. micans* (5'-ACCAGGCACATTCACCCACCCAGGGGTAGGCTACCATGTCCCTGGAGTTTTCTCGAT-3')

^c Nuclease protection probe also used for NPA-SH (5'-CAAAGACTTTAGTTTCCCGTAAGGTGCTGAAGAGGTCGAAACGAACACCCTCCAATCC-3')

^d Nuclease protection probe also used for NPA-SH (5'-CACACCACACAGTCAAGTGAGTTGTGCTTTCAAGATAAATGCTCAGGCTGTGCCAAAT-3')

^e Nuclease protection probe also used for NPA-SH (5'-ACAGTCCGCAAATGAGTTCTGCCAAGGCTATTCCTCACCCTAGACGAGCTACCATGA-3')

Automated SHA has been applied to natural seawater samples of *C. polykrikoides* with a recorded limit of detection (LOD) of 115 ± 53 cells.mL⁻¹. Cell concentrations below the LOD were still able to be detected but were not accurately quantifiable. The authors reported that in Korea HAB warning systems recognise 1000 cells.mL⁻¹ as a “red tide alert” cellular concentration. The LOD resulting from this SHA method was found to lie below these warning cellular concentrations making the LOD acceptable for bloom monitoring [92].

Alternative electrochemical detection was trialled in an SHA format for the detection of *A. ostenfeldii*. As stated previously, the electrochemical response was generated using a DIG labelled signal probe which reacts with an anti-DIG-HRP conjugate. Hydrogen peroxide was then added as the HRP substrate creating an electrochemical response. Hybridisation steps occurred on the streptavidin coated working electrode allowing for the detection [94]. Fragmentation of RNA was introduced in this research to maximise the sensitivity of the capture probe to the target sequence during the first hybridisation event. A “helper” oligonucleotide was also introduced which was able to successfully reduce the formation of secondary rRNA structures in solution. Both of these changes to the SHA methodology were able to increase the measured signal 6.3 times which correlated to an estimated detection limit of ≈ 16 ng.μL⁻¹ for the optimised conditions which was previously estimated at 100 ng.μL⁻¹ for the standard conditions [94]. Electrochemical detection SHA has also been applied for the detection of thirteen HAB causative microalgae species [103]. The assay resulted in the highly selective discrimination of each species using the described probes. A limit of detection of 1.8 nM was reported for synthetic target sequences and 143 cells for extracted cellular RNA [103].

More recently, SHA detection has been moved to an alternative fibre optic microarray as opposed to the normal microplate format for the detection of *P. australis*, *A. fundyense* and *A. ostenfeldii*. Here, oligonucleotides were attached to microspheres which were then introduced to fibre optic wells. The method of attachment of the capture probe to the microsphere surface was not specified. The lysate was then introduced to the microspheres, left to hybridise with the surface followed by a secondary hybridisation with the signal probe. A resulting epifluorescence signal was measured using the optic fibre as well as direct image analysis. Samples were prepared by the serial dilution of known cell concentrations ranging from 5 and 5000 cells.mL⁻¹ for the three species. As

such, cell concentrations were not recorded as the volume prior to filtration was dependant on the dilution of the initial culture. Detection limits of 5-10 cells.sample⁻¹ was obtained for *A. fundyense* and *P. australis* however detection limits for *A. ostenfeldii* were higher at 50 cells.sample⁻¹. Non-target species did not interfere with the signal produced making it possible to undergo SHA with no prior RNA purification. The platform also displayed high stability of the tethered capture probe making it possible to use multiple times with no loss in reactivity [101].

The fibre optic microarrays reaction conditions were optimised further in 2006 by the same research group [100]. Attachment of the oligonucleotides was achieved by initial activation with cyanuric chloride followed by attachment to amine modified microspheres. Surface characterisation and attachment density of the oligonucleotide probes to the microspheres were not reported. The method optimisation led to a detection limit of 5 cells.sample⁻¹ for all 3 species tested [100]. This is a significant improvement for *A. ostenfeldii* which previously only demonstrated a detection limit of 50 cells.sample⁻¹ [101]. Multiplexed arrays were also trialled and found to be successful and highly selective for individual HAB causative species independent of the sample matrix [100].

The SHA method was also simplified with the aid of a PCR ELISA DIG Detection Kit for *A. minutum*. Hybridisation buffer, conjugate dilution buffer, substrate buffer, anti-DIG-POD, washing tablets and ABTS tablets were utilised in the reaction. A standard curve was also produced taking into account the RNA content per μL instead of cell density (cells.mL⁻¹ or cells.L⁻¹). This allowed for the amount of RNA per cell to be calculated as 0.028 ± 0.003 ng. Both spiked culture samples and field samples were tested with the positive identification of *A. minutum* using the specific oligonucleotide capture and signal probe [97].

By targeting nucleic material in crude cell lysates SHA provides improved quantitation of HAB cells than FISH. This is due to the ability to minimise background fluorescence as well as removing the requirement for cell counting. Importantly, the stepwise approach of detection allows for automation of the procedure. The use of two probes targeting one sequence is also able to increase the selectivity of the process with careful oligonucleotide sequence design. Natural amplification of RNA within the cell also negates the need for expensive amplification techniques prior to analysis. RNA stability however is a cause for concern due to its sensitivity to degradation by RNase. In order to prevent any loss of material samples should be analysed or stored in stability buffers to maintain integrity.

Analysis is further complicated as the RNA content within HAB cells are influenced by the different growth phases, meaning concentrations can fluctuate over time. This could potentially be overcome by analysing whole cell samples to observe the potential growth phase of your collected sample.

1.1.3.1 Nuclease Protection Assay Sandwich Hybridisation (NPA-SH)

More recently, a nuclease protection assay (NPA) prior to sandwich hybridisation was introduced to increase sensitivity and selectivity of analysis. Specific NPA probes are selected that are complementary to the target sequence in the algal rRNA. After hybridisation with the NPA probes, a treatment with S1 nuclease is used to remove non-target single stranded RNA and mismatched probes leaving only perfectly matched sequences stoichiometrically (refer to Figure 6). The remaining NPA oligonucleotide probe is used for the subsequent detection, not the RNA usually targeted, making it more stable than previously completing the SHA with less stable RNA [93].

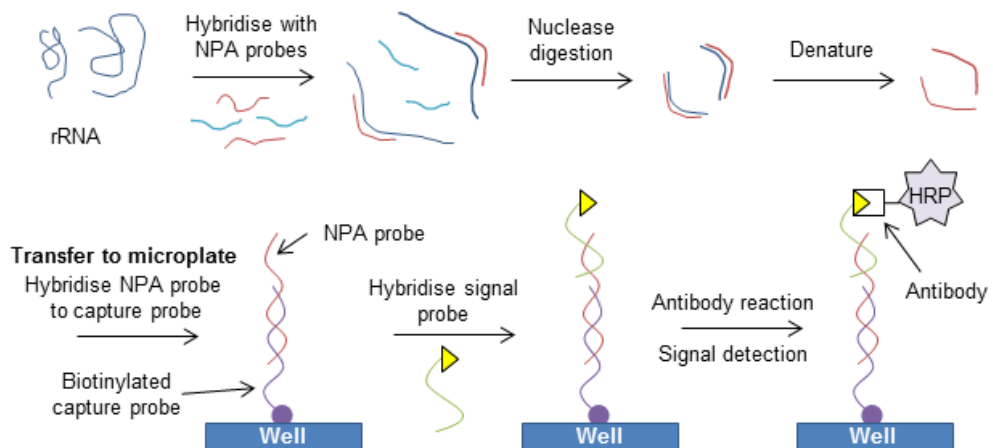


Figure 6: Process of the Nuclease Protection Assay coupled to the SHA

NPA-SH was first applied in 2006 for the detection of *P. minimum* and *P. micans* in both cultured and natural seawater samples. The use of NPA-SH provided an increased level of sensitivity compared to previous SHA methods. When the cell counts were compared to that of LM, a good level of agreement was found between both results. The sensitivity of the NPA-SH was found to be 15 cells.mL^{-1} for *P. minimum* and only 1 cell.mL^{-1} for *P. micans*. This proved that the NPA-SH could successfully detect low cell numbers of these two HAB species [93].

NPA-SH was also applied to the detection of cultured and natural seawater samples of *Phaeocystis globose*. Using this method a detection limit of 18 cells.mL^{-1} was possible.

Good agreement was seen between LM results as with previous methods and field samples displayed no interferences when in contact with biotic and abiotic material in the sample matrix [98]. More recently, NPA-SH has been applied for the rapid detection of *C. polykrikoides* [104]. Suh *et al.* [104] designed specific probe sequences for the sensitive and selective identification of cultured and natural seawater samples. Comparison with results obtained by LM demonstrated that a good correlation between manual counting and NPA-SH was possible [104].

NPA-SH has also been applied to *A. catenella* and *A. tamarensis*. Comparison with alternative testing method, competitive enzyme-linked immunosorbent assay (cELISA), was conducted each with their own advantages and disadvantages. NPA-SH analysis was unable to discriminate between the two closely related *Alexandrium* species but the cELISA was. NPA-SH overestimated cell concentrations in some cases when compared to LM and cELISA, most likely due to the varying genetic concentrations at different stages of cellular growth. cELISA and LM were unable to track these changes as the analysis was not based on concentrations of genetic material. The lowest obtainable detection for the NPA-SH method was determined to be 0.47 cells.mL⁻¹ [99].

Electrochemiluminescent detection was trialled for the NPA-SH detection of *P. minimum* in an attempt to further improve sensitivity. Extracted lysates were introduced to the NPA probe as before, however the NPA probe is labelled with biotin at one end and Ru(bpy)₃²⁺ at the other. rRNA then hybridised with the NPA probe followed by a S1 nuclease digestion (Figure 7). The strands are then denatured leaving the NPA oligonucleotide probes to bind via a streptavidin-biotin interaction onto magnetic modified beads. The probes can then be concentrated to a working electrode using a magnet allowing for a subsequent electron transfer reaction at the Ru(bpy)₃²⁺ in the presence of tripropylamine and detectable photon release after relaxation of the excited Ru(bpy)₃^{2+*}. This photon is measured at 610 nm after being passed through a photomultiplier tube. This alternative detection strategy was able to increase sensitivity with a detection range of 0.4 pmol to 4 nmol of rRNA [102].

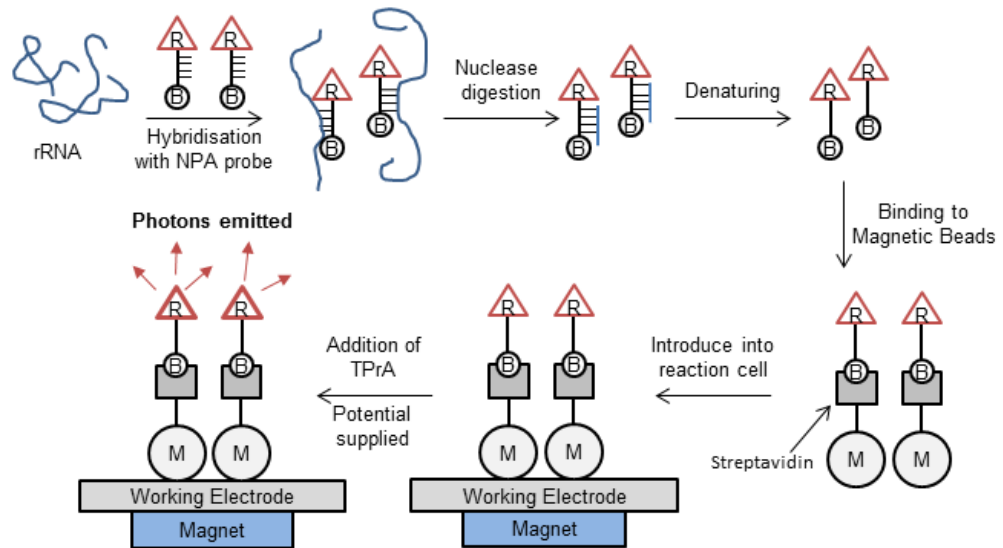


Figure 7: Diagrammatic representation of electrochemiluminescent detection using NPA-SH

B is biotin, R is the $Ru(bpy)_3^{2+}$ complex and M is the magnetic bead platform

The NPH-SH offers significant improvements over conventional SHA. The use of a NPA probe for detection (DNA oligonucleotide) minimises any effects of degradation of RNA by RNase. The sensitivity of this method is also acceptable for a bloom event, with the lowest obtainable detection limits being well below the cell concentrations expected during a bloom. Despite this advantage, variation in RNA concentrations during the different growth phases of the cell still needs to be investigated. Optimisation of probe sequences as well as experimental conditions is also essential to obtain the best sensitivity and selectivity for the target organism.

1.2 Strategies for the covalent immobilisation of oligonucleotides to solid supports

As discussed in Section 1.1.3, SHA can be used as a method for the sensitive and selective detection of HAB causative microalgae. In SHA, attachment of oligonucleotide probes to substrates is achieved using a non-covalent approach. This results in oligonucleotide positioning close to the surface, thus sterically hindering hybridisation with target oligonucleotides. Covalent attachment of oligonucleotides overcomes these problems as it allows for the incorporation of chemical spacers to increase distance from the surface, minimising steric hindrance [105, 106].

Silica surfaces require initial functionalisation to generate a reactive surface to facilitate oligonucleotide attachment. This is commonly achieved using a one-pot silanisation reaction with organofunctional alkoxysilanes. Here, the alkoxysilane reacts with hydroxyl groups on the surface of the silica substrates (Figure 8). This is achieved via the initial hydrolysis of the Si-OR bonds on the organofunctional alkoxysilane to form reactive Si-OH groups (Figure 8A), followed by subsequent condensation with the silanol groups present on the silica surface, forming Si-O-Si bridges for covalent attachment (Figure 8B) [107]. The R group of the alkoxysilane then acts as the reactive surface for oligonucleotide probe attachment. Due to the large number of commercially available organofunctional alkoxysilanes, many functionalised substrates can be generated [108].

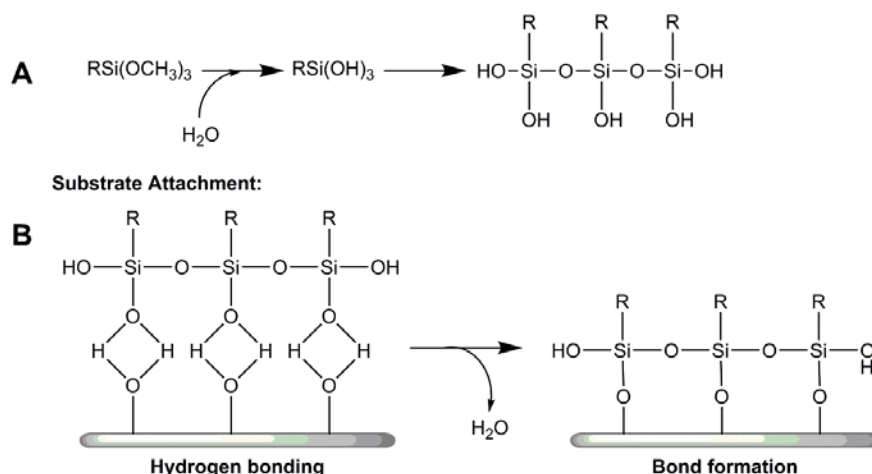


Figure 8: Silanisation chemistry used to generate organofunctional surfaces for oligonucleotide attachment. Adapted from [107]
The R group can be any alkyl, aryl or organofunctional group

Amine alkoxysilanes such as 3-aminopropyltriethoxysilane (APTES) [109], 3-aminopropyltrimethoxysilane (APTMS) [110], N-(2-aminoethyl)-3-aminopropyltrimethoxysilane (EDA) [106], p-aminophenyl-trimethoxysilane [109] and trimethoxysilylpropyldiethylenetriamine (DETA) [106] are commonly reported silanisation agents used for the covalent attachment of biomolecules. Alternative functionalities can be prepared using alkoxysilanes with terminal epoxides such as 3'-glycidoxy propyltrimethoxysilane [111], thiols such as 3-mercaptopropyl trimethoxysilane (MPTS) [112] and vinyl groups allyltrimethoxysilane (VTMS) [113]. Reported strategies for covalent attachment of oligonucleotides to these functionalised surfaces include attachment via amine [106, 109, 110, 114], epoxide [111, 115], thiol [112] and vinyl moieties [113]. Attachment to amine and thiol functionalised surfaces are relatively common and discussed in Sections 1.2.1 to 1.2.2.

1.2.1 Amine silanised surfaces for oligonucleotide attachment

Oligonucleotide attachment to amine modified substrates can be achieved by the formation of i) an amide linkage [109] ii) a thiourea bond [110] or iii) a thioether bond via a heterobifunctional cross-linker [106] (see Figure 9). The amide attachment is formed via a direct reaction between the amine functionalised surface and carboxylate modified oligonucleotides. This described method does not require the use of a cross-linker meaning the attachment is possible in a simple two-step reaction. Alternatively, attachment to the amine surface via a thiourea [110] or thioether [106] bond requires a three-step reaction. In these cases (Figure 9B and C), a cross-linker is used to facilitate attachment of amine and thiol modified oligonucleotides [106, 110] resulting in an increased distance of the oligonucleotide probe from the surface and the potential for improved hybridisation efficiency [106, 110].

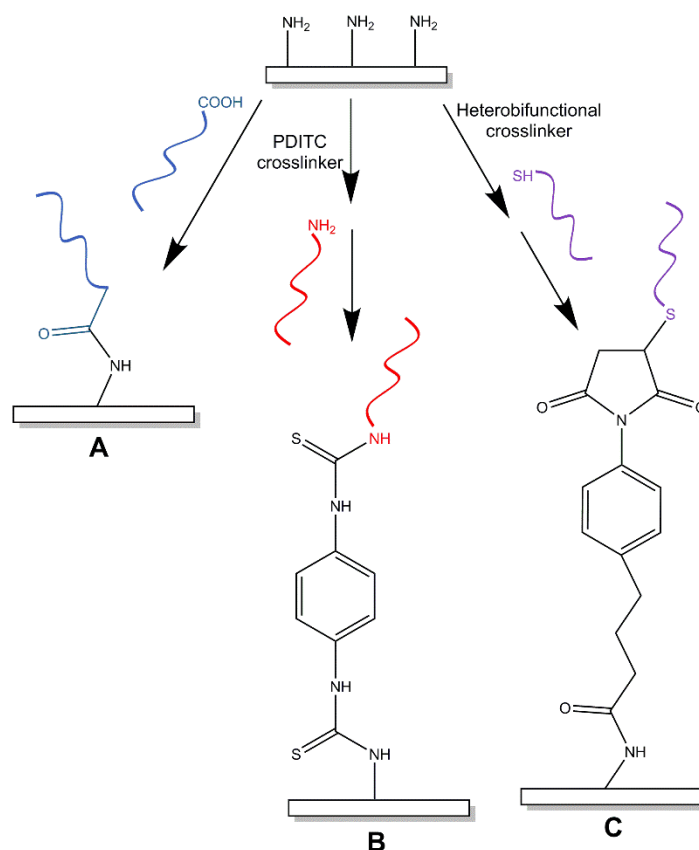


Figure 9: Oligonucleotide attachment to amine silanised substrates
Attachment of the oligonucleotides achieved by the formation of A) an amide linkage, B) a thiourea linkage and C) a thioether linkage

Direct attachment of oligonucleotide probes is typically achieved via amide linkages. For example, Joos *et al.* reported a method for the amide attachment of oligonucleotides using the strategy outlined in Figure 9A. This simple one step reaction led to 90 % of the total attached oligonucleotides being available for hybridisation [109]. Further improvement in attachment of oligonucleotides was achieved through the introduction of a carboiimide-mediated attachment. This method introduced 1-ethyl-3-(3-dimethylaminopropyl)-carboiimide (EDC) during amide attachment, effectively reducing side reactions, thus increasing oligonucleotide attachment densities. Using this strategy, 95 % of oligonucleotides were covalently immobilised at the 5' end and available for hybridisation [114].

Alternatively, direct attachment of oligonucleotide probes to amine substrates has also been accomplished using diazotization chemistry for attachment [116], however this chemistry has its drawbacks. Here, a diazonium salt present on the surface reacts with the aromatic rings within nucleic acid bases (adenine, cytosine and guanine) for covalent

attachment [116]. A two-fold increase in sensitivity was possible when using this method compared to attachment on commercially available Corning (aminosilane) and polylysine slides. Modification was difficult however with diazotization of p-aminophenyl trimethoxysilane (ATMS) only occurring at low temperatures (4 °C) due to instability of the diazonium salts [116].

Addition of a cross-linker during oligonucleotide attachment is commonly used as a mode to increase the distance of oligonucleotides from the surface, minimising steric effects and promoting hybridisation [110, 117]. Amine functionalised substrates are used as a tethering point for p-phenylene diisothiocyanate (PDITC) as a cross-linker which allows for the subsequent covalent attachment of both amine and thiol modified oligonucleotides [118]. Other cross-linkers have also been developed, including the use of aldehyde functionalised dendrimers which can effectively increase overall loading capacity of the oligonucleotide at the surface [119]. Using these dendrimers, a highly sensitive (detection limit estimated as 0.1 pM) and stable (3-5 months at room temperature) surface was generated for the detection of fluorescently labelled target sequences [119]. Heterobifunctional cross-linkers have also been applied for oligonucleotide attachment to amine functionalised substrates. For example, succinimidyl 4-(maleimidophenyl)butyrate (SMPB) was used for the attachment of thiol modified oligonucleotides with the amine surface reacting with the succinimide ester moiety of SMPB and the thiolated DNA with the maleimide [106] (Figure 9C). Use of this method resulted in a significant improvement in attachment densities when compared to PDITC cross-linker [110] and simple epoxy silane [111] attachment methods [106].

1.2.2 Thiol based chemistry for oligonucleotide attachment

Thiol functionalised glass surfaces are commonly prepared using MPTS. Use of these functionalised surfaces have been reported for the attachment of thiol modified oligonucleotides via a disulphide bond as shown in Figure 10A [112]. The resulting thiol/disulphide exchange reaction is highly specific with minimal side reactions resulting in the direct attachment of the oligonucleotide to the surface [120, 121]. Using this simple, one-step method an approximate attachment density of 0.3 oligonucleotides.mm⁻² was achieved by Rogers *et al.* [112]. The oligonucleotide arrays also exhibited high stability with them remaining stable for up to 4 weeks when stored in dry, cold (4 °C) conditions [112].

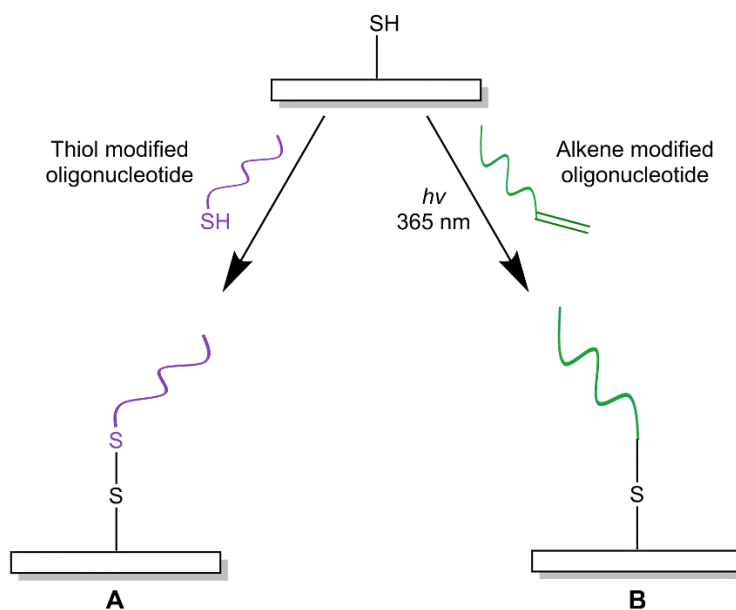


Figure 10: Attachment strategies for the immobilisation of oligonucleotides to thiol functionalised surfaces

Thiol-ene click chemistry has also been applied for the attachment of oligonucleotides to thiol functionalised glass surfaces using the method shown in Figure 10B [113]. Thiol-ene click chemistry is advantageous for biomolecule attachment as it can be performed in aqueous systems, using mild conditions [122]. Attachment of the oligonucleotides occurs via the formation of a thioether bond generated through a photoinitiated reaction. Here, a free radical intermediate is generated at the thiol surface which reacts with the alkene terminated oligonucleotide resulting in attachment [123]. This method has been previously described by Escorihuela *et al.* (2014) [113] using the functionalisation of silicon-based wafers and subsequent attachment by irradiation at 365 nm. A reported attachment density of 6 pmol.cm^{-2} ($3.61 \times 10^{12} \text{ oligonucleotides.mm}^{-2}$) was recorded [113], which is significantly higher than the $0.3 \text{ oligonucleotides.mm}^{-2}$ reported for the dithiol attachment [112].

1.3 Silica nanoparticle substrates for oligonucleotide attachment

It has been reported that the use of nanoparticles for oligonucleotide attachment is advantageous as a higher surface area is available for attachment compared to planar substrates [124]. Silica nanoparticles are popular for use in biological and biomedical applications due to their biocompatibility and low toxicity [125, 126]. In addition, the synthesis of silica nanoparticles is also scalable allowing for the careful control specifications such as size, porosity and shape [125]. The modification of silica nanoparticle surfaces is achieved using organofunctional alkoxy silanes in a similar manner to that discussed in Section 1.2 for the modification of flat silica surfaces. The versatility of this method allows for a broad range of modifications to be implemented for the attachment of oligonucleotides.

1.3.1 Silica nanoparticle synthesis

One common method for the preparation of silica nanoparticles is the Stöber synthesis which generates nanoparticles using a sol-gel process [127]. This method, allows for the production of monodispersed silica nanoparticles ranging from 50 nm to 2 μm [128]. The synthetic reaction requires an alkoxy silane, such as tetraethyl orthosilicate (TEOS), water, alcohol and ammonium which acts as a catalyst for the reaction [129]. The chemical process of nanoparticle formation, using TEOS as an example, is shown in Figure 11. Initially the ethoxy groups within TEOS undergo hydrolysis in water, substituting the ethoxy groups with hydroxyl groups [130]. The additional ammonium acts as a basic catalyst, promoting the attachment of the hydroxyl anions on the hydrolysed TEOS allowing for rapid subsequent condensation when in alcohol solution [130]. Here, the intermediate reacts with ethoxy groups of other hydrolysed TEOS molecules, forming connective Si-O-Si bonds and promoting nanoparticle nucleation and growth [130].

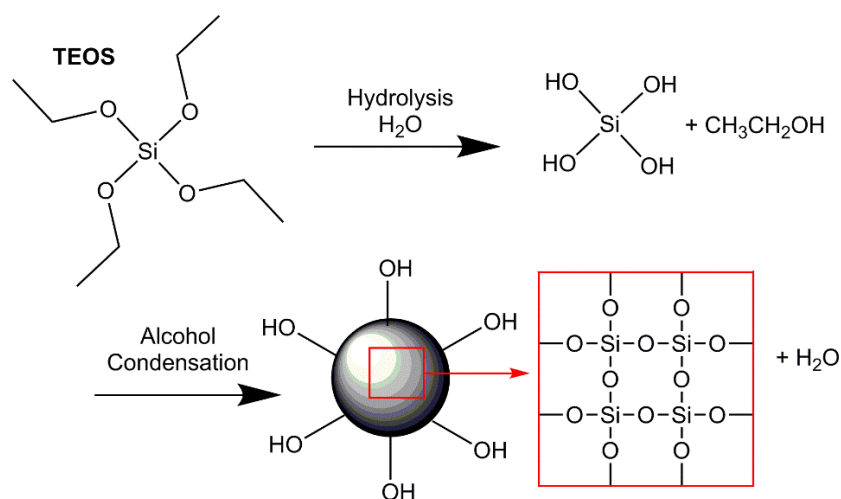


Figure 11: Sol-gel process for silica nanoparticle synthesis

Initial hydrolysis in basic catalysed conditions followed by condensation to form the nanoparticle structure

Alternatively, a microemulsion method can be used for silica nanoparticle synthesis based on hydrolysis and subsequent condensation. Use of this method allows for doping of the nanoparticle with fluorescent dyes for biomedical imaging [131] as well as the careful control of nanoparticle size. Microemulsion utilises a surfactant within a water-oil emulsion for the generation of nanoparticles. During reversed microemulsion synthesis, water droplets are formed within reversed micelles formed by the added surfactant [132] as shown in Figure 12. After alkoxy silane addition, polymerisation occurs within the water droplet resulting in the formation of silica nanoparticles with the aid of an ammonium catalyst [132]. The main disadvantage of this microemulsion synthesis when compared to the Stöber method is that the high concentrations of surfactant used in the synthesis need to be removed using extensive washing before use [133, 134].

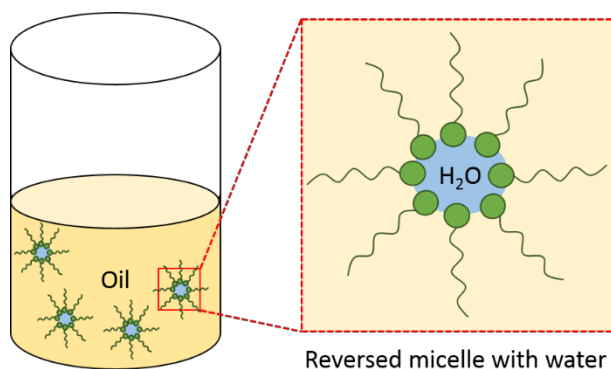


Figure 12: Reversed micelles in a water-in-oil system for silica nanoparticle synthesis

1.3.2 Silica nanoparticle functionalisation

The functionalisation of silica nanoparticles is achieved using the same silane chemistry discussed in Section 1.2 for planar silica surfaces. This modification strategy is highly versatile with a large variety of alkoxy silane molecules available allowing for use in extensive applications. Functionalisation of the surface can occur either using a co-condensation reaction or by post synthesis functionalisation. In both cases, alkoxy silane attachment is achieved by a polycondensation reaction generating Si-O-Si bridges with the surface silanol groups on the TEOS nanoparticle [135]. Co-condensation allows for nanoparticle functionalisation during synthesis based on the addition of alkoxy silane during nucleation and growth. Most co-condensation reactions require the use of a surfactant, such as described in the microemulsion synthesis, to create a nanoparticle template. Alternatively, post-synthesis functionalisation of nanoparticles requires the grafting of alkoxy silanes to synthesised silica nanoparticle surfaces as a secondary reaction [136]. Commonly reported alkoxy silanes for silica nanoparticle functionalisation include the use of polyethylene glycol (PEG)-silanes and APTES [135].

Modification of silica nanoparticles using PEG allows for the generation of a protective polymer layer over the surface, promoting stabilisation of nanoparticles in solution [137, 138]. This method is commonly used in biomedical applications of nanoparticles as it is approved by the FDA and significantly improves stability in biological matrices such as blood [139]. Attachment of PEG methacrylate (PEGMA) to nanoparticles for use in polymer nanocomposites has also been reported [140]. This method requires an initial silanisation with vinyltriethoxysilane (VTES) followed by a secondary reaction with PEGMA attachment using UV-photopolymerization [140]. The PEGMA functionalisation increases nanoparticle hydrophobicity resulting in improved dispersion of nanoparticles within polymer composites, allowing for further improvement of polymer mechanical performance [140].

Amine functionalised nanoparticles have been reported for applications ranging from gene delivery to the synthesis of silica-polypeptide composite particles as initiators in polymerisation reactions [141]. Amine functionalised nanoparticles have also been previously applied to enzyme immobilisation. Tethering the enzymes to these solid supports allowed for subsequent re-use, reducing costs associated with analysis [142].

1.3.3 Methods for oligonucleotide attachment to silica nanoparticles

Although modified nanoparticles are commonly used for a variety of biological applications, their use as a substrate for the attachment of oligonucleotides for hybridisation experiments still remains a relatively new concept. Currently, there are only two reported methods for the attachment of oligonucleotides to silica nanoparticles for hybridisation based detection, one using a thiol modified silica nanoparticle [143] and the other using a zirconium phosphate modification for attachment [124].

Attachment of thiol modified oligonucleotides to thiol functionalised nanoparticles via a dithiol bond has been reported by Hilliard *et al.* [143]. Silica nanoparticles were prepared using a water-in-oil microemulsion followed by a post-synthesis functionalisation with MPTS to create a reactive thiol surface. Maximum attachment of the probe was achieved after an 18 h incubation however attachment densities were not recorded. These oligonucleotide attachment times are significantly higher than similar attachments to planar substrates (2 h) [112] due to the greater surface area available for attachment. Stability of the oligonucleotide nanoparticles was tested demonstrating a significant 25 % loss of attached probe after 24 h indicating that modified nanoparticles have an optimal lifetime of only 1 day in storage.

More recently, amide attachment of amine modified oligonucleotides to zirconium phosphate functionalised nanoparticles was achieved via a reaction with imidazole in the presence of N-ethyl-N'-(3-dimethylaminopropyl) carbodiimide (EDC) [124]. Here nanoparticles were prepared using a sequential addition synthesis. Functionalisation of TEOS generated nanoparticles was achieved in a two-step reaction; initially using zirconium chloride followed by phosphoric acid to generate the zirconium phosphate functionality. Compared to the dithiol attachment [143] which required an 18 h incubation, this method exhibited optimal probe attachment after only a 5 h incubation. Using this method an attachment density of $12.49 \pm 1.1 \text{ pmol.cm}^{-2}$ and a detection limit of $1.22 \times 10^{-9} \text{ M}$ was reported.

Currently, oligonucleotide attachment to nanoparticles has not been reported for the sensitive detection of HABs. Based on the attachment chemistries attained by Rao *et al.* [124], if successful, attachment of oligonucleotides to three dimensional nanoparticle substrates would be able to effectively increase sensitivity of oligonucleotide platforms.

1.4 Conclusion and Project Premise

The detection of HAB formations in the early stages requires a truly sensitive and selective platform. Oligonucleotide modified substrates have shown promise using SHA formats, but there is limited research on the use of covalently attached oligonucleotides for HAB detection. Use of covalently modified oligonucleotide surfaces would allow for a stable and potentially re-usable surface to be prepared for the pre-concentration of target nucleic acids in solution. Control of oligonucleotide distance from the surface is also possible using chemical spacers, promoting hybridisation and further improving sensitivity. Furthermore, the use of high surface area nanoparticles for the selective detection of HAB causative microalgae may also increase achievable sensitivities. Oligonucleotide attachment to nanoparticles has only been trialled twice using model hybridisation experiments. Neither of these reported methods have been applied to the detection of natural seawater samples, such as oligonucleotide attachment to nanoparticles for HAB detection.

The aims of this research are:

1. To evaluate PDMS and glass substrates for covalent oligonucleotide attachment
2. To evaluate the effect of amine and thiol based attachment chemistries on the sensitivity and selectivity of oligonucleotide modified surfaces
3. To prepare oligonucleotide modified silica nanoparticles in an effort to further improve sensitivity

2

Substrate selection for the covalent attachment of amine modified oligonucleotides

This chapter compares poly(dimethylsiloxane) (PDMS) and glass slides substrates for the attachment of amine modified oligonucleotides using an APTES silanisation modification strategy. Results discussed include:

- *The use of APTES modification chemistry for the immobilisation of oligonucleotides to glass and PDMS surfaces*
- *An evaluation of the sensitivity of the oligonucleotide modified PDMS and glass surfaces for hybridisation with target oligonucleotide sequences*
- *A comparison of oligonucleotide stability, when covalently bound and hybridised, to PDMS and glass substrates*

2.1 Introduction

Monitoring HAB formations is essential to improve both public and environmental safety prior to and during a bloom event [144]. As discussed in Chapter 1, a number of methods have been developed to monitor cellular growth both prior to and during a bloom. Light microscopy (LM) is commonly used as a visual identification tool, with the cellular morphology allowing for discrimination between toxic and non-toxic microalgae [145]. This method is both difficult and time consuming, especially when dealing with species from the same genus as they can share similar morphological features [30]. Alternatively, species specific identification can be accomplished using molecular methods, such as the use of specifically designed oligonucleotide probes. These probes target variable regions of rRNA found within cells of different species of microalgae, allowing for selective discrimination [32-35]. Chapter 1 describes a range of methods that use oligonucleotide probes for detection, including FISH, SHA, NASBA, RT-PCR and LAMP. The use of immobilised oligonucleotides to solid supports has been limited to SHA however, with all others being completed in solution. Here, a biotin-streptavidin non-covalent interaction is used to tether oligonucleotides to the surface. This attachment, although strong and reproducible, can result in low hybridisation efficiencies due to steric hindrance from the probes at close proximity to the surface [146]. Covalent attachment strategies provide greater control of the surface modification, allowing for the addition of chemical spacers between oligonucleotide and substrate, overcoming these steric issues [105].

Solid support selection is very important when preparing oligonucleotide modified surfaces. The support must have a low background fluorescence and exhibit minimal non-specific adsorption of target molecules [147, 148]. Reproducibility of attachment is improved if the selected surface is flat and homogeneous [147-149]. When attaching oligonucleotides to a solid support, careful consideration into surface attachment chemistry needs to be taken. For example, the chemistry should be such that the attached oligonucleotides are distanced from the surface in order to minimise steric hindrance effects that ultimately limit hybridisation with target material [148, 150]. This can be achieved by a vast array of modification chemistries, allowing for a versatile suite of oligonucleotide attachment methods and substrates [148, 150].

One potential substrate that has been reported as a versatile surface for the covalent attachment of oligonucleotides is poly(dimethylsiloxane) (PDMS) [151]. In a study by Khodakov *et al.*, PDMS substrate were silanised using APTES, followed by treatment with

PDITC cross-linker and subsequent attachment of 5'-amine modified oligonucleotide probes [151]. PDMS is biocompatible, chemically inert, optically transparent and has low manufacturing costs associated with fabrication, making it a suitable substrate for the sensitive detection of nucleic acids [152]. However, the surface hydrophobicity of PDMS can be problematic. PDMS needs to be oxidised to create reactive surface silanol groups for silanization modifications. This hydrophilic modification creates a thermodynamically unstable surface that undergoes hydrophobic recovery [153]. Furthermore, the viscoelastic properties of PDMS leads to surface rearrangement resulting in a decrease in reactive sites available at the surface over time [153].

Glass surfaces are another popular substrate for microarray fabrication. The surface has exposed silanol groups, and does not suffer from hydrophobic recovery effects seen with PDMS [112, 154-158]. Glass surfaces also have low background fluorescence, high chemical stability, are rigid and flat with a range of established attachment chemistries [119, 148, 149]. These include modification with amine, epoxide, carboxylic acid, and aldehyde functionalities [148, 149, 159, 160].

2.2 Scope of study

PDMS [161, 162] and glass microscope slides [112, 118, 119] have both been reported as suitable substrates for the covalent attachment of oligonucleotides. This chapter examines the effect of the tethering substrate (glass versus PDMS) on the final hybridisation performance of covalently attached oligonucleotides.

Initially, reaction conditions were investigated for the alternative glass substrate including the effect of: reaction time with APTES and PDITC and probe attachment time on the hybridisation performance of the oligonucleotide modified surface. By doing this, both the PDMS and glass substrates were compared for viability for oligonucleotide attachment and subsequent hybridisation with target oligonucleotides. Stability studies were also completed for the PDMS and glass surfaces to determine if storage influences the hybridisation performance over time.

2.3 Experimental

2.3.1 Materials

Unless otherwise specified, all chemicals and reagents were of analytical grade and used as supplied. APTES and PDITC were purchased from Sigma-Aldrich, Australia. Ethanol (96 %), pyridine and dimethylformaldehyde (DMF) were purchased from Chem-Supply, Australia. All oligonucleotides were purchased from Integrated DNA Technologies (USA) with sequences shown in Table 4.

Table 4: Oligonucleotides used in the substrate selection study
Including the 5' amine modification for covalent attachment at the PDMS and glass surfaces and Cy5 modification for subsequent detection

Oligonucleotide Name	5' Modification	Sequence (5'-3')
NH ₂ -probe	Amine	GCACTTGCAGCCAAAACCCA
ACat Seq.*	Cy5	TGGGTTTTGGCTGCAAGTGC

* ACat Seq complimentary to the NH₂-probe sequence

PDMS was prepared using a PDMS Sylgard 184 (Dow Coming Corporation, USA) two component kit containing a pre-polymer base agent and cross-linker curing agent. Livingstone Premium Microscope pathology grade glass slides (76.2 mm x 25.4 mm, Australia) were used for the glass surface experiments. 0.1 M phosphate buffer (94.7 mM monosodium phosphate, 5.3 mM disodium phosphate, pH 8.0) was used to dilute the NH₂-probe oligonucleotide prior to attachment. A 1x saline sodium citrate (SSC) buffer (150 mM sodium chloride, 15 mM trisodium citrate, pH 7.0) was used for ACat Seq dilution and hybridisation experiments.

2.3.2 APTES covalent modification strategy for PDMS and glass substrates

2.3.2.1 PDMS substrate

PDMS was prepared with the two component Sylgard 184 kit by mixing a 10:1 ratio of base agent to cross-linker curing agent, as per Khodakov *et al.* [151]. The mixture was degassed under vacuum and poured onto a silicon wafer followed by curing on a hotplate at 120 °C for 1 h. Once cured, the PDMS was peeled off the wafer and stored until needed

at room temperature, in the dark. Prior to use, PDMS was cut to size using a scalpel and cleaned by ultrasonication in isopropanol (Merck Pty. Ltd, Australia).

PDMS surfaces were modified based on the schematic shown in Figure 13. Initially, the PDMS surfaces were oxidised using plasma oxidation at 0.2 Torr (O_2) for 40 s at 18 W. The resulting oxidised surface was immediately introduced into a solution of APTES (2 %v/v in ethanol) and allowed to react for 20 min at room temperature. The surfaces were subsequently removed and washed with ethanol, air dried then baked for 20 min at 100 °C. The APTES modified surface was then introduced into a solution of excess PDITC (10 mM) in pyridine/DMF 1:9 (% v/v) and left to react for 2 h. After this time, unreacted PDITC and solvent was removed through stringent washing with ethanol followed by baking the surface at 100 °C for 10 min. The amine modified oligonucleotide solution, (NH_2 -probe, 50 μ M, 2 μ L) was then manually spotted onto the PDITC modified surface and left to react for 90 min at 40 °C in a humid environment. Unreacted NH_2 -probe was removed by rinsing the surface with ultra-pure water followed by air drying. Unreacted PDITC on the surface was subsequently blocked by stirring with 50 mM of ethanolamine (0.1 M sodium phosphate buffer, pH 8.0) for 20 min. Excess unreacted ethanolamine was removed by rinsing the surface with ultra-pure water and drying with air prior to hybridisation experiments.

2.3.2.2 Glass substrate

Commercially available glass microscope slides (Livingstone, Australia) were cleaned with ethanol followed by briefly heating at 60 °C to remove any residual solvent prior to modification. Glass surfaces were modified based on the schematic shown in Figure 13. Initially, the cleaned glass surface was oxidised using plasma oxidation at 0.2 Torr (O_2) for 40 s at 18 W. An alternative oxidation method was also tested using a 2 h exposure to a Piranha solution (2:1 of 18 M sulphuric acid to 30 % hydrogen peroxide). After treatment using the Piranha solution, glass slides were rinsed thoroughly with water prior to silanisation.

The oxidised surfaces were immediately introduced into a solution of APTES (2 %v/v) in ethanol and allowed to react between 5-20 min (optimal reaction time 20 min). The surfaces were subsequently removed and rinsed with ethanol, air dried then baked for 20 min at 100 °C. The APTES modified surface was then introduced into a solution of excess PDITC (10 mM) in pyridine/DMF 1:9 (%v/v) and left to react between 10-90 min (optimal reaction time 10 min). After this time, unreacted PDITC and solvent was

removed through stringent washing with ethanol followed by baking the surface at 100 °C for 10 min. Amine modified oligonucleotide solution (NH₂-probe, 50 μM, 2 μL) was then manually spotted onto the PDITC modified surface and left to react between 10-140 min (optimal time 90 min) at 40 °C in a humid environment. Unreacted NH₂-probe was removed by rinsing the surface with ultra-pure water followed by air drying. Unreacted PDITC on the surface was subsequently blocked with 50 mM of ethanolamine (0.1 M sodium phosphate buffer, pH 8.0) with stirring for 20 min. Excess unreacted ethanolamine was removed by rinsing the surface with ultra-pure water and drying with air prior to hybridisation experiments.

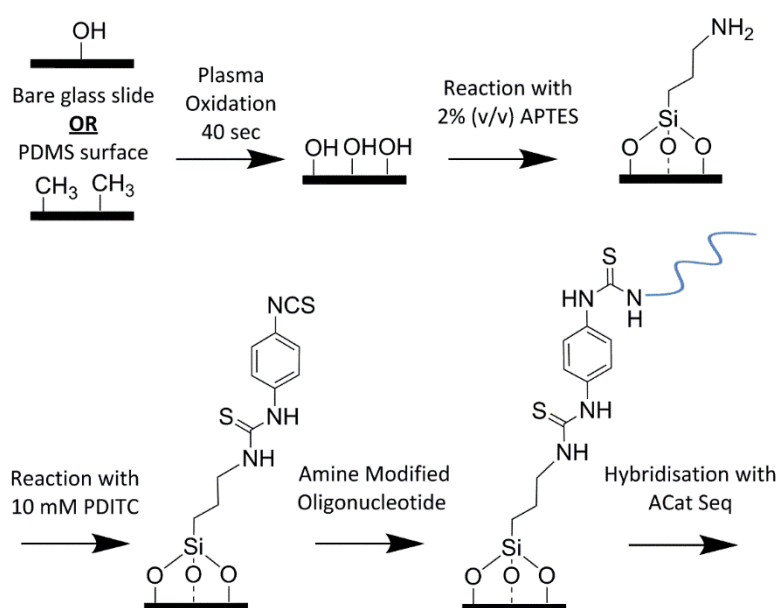


Figure 13: Reaction schematic for the APTES modification

Modification method used for both the PDMS and glass substrates using an initial APTES silanisation, attachment of a PDITC cross-linker and attachment of the amine modified oligonucleotide (NH₂-probe)

2.3.3 Surface hybridisation experiments for amine modified PDMS and glass substrates

Manual spotting hybridisation

Oligonucleotide modified glass and PDMS surfaces were subjected to model hybridisation experiments using complimentary Cy5 labelled oligonucleotide target ACat Seq (refer to Table 4 for sequence). For both surfaces, hybridisation was completed by manually spotting aqueous solutions of the complimentary Cy5 labelled target sequence (ACat Seq,

20 μM , 2 μL in 1x SSC buffer) directly over the modified NH_2 -probe area. Hybridisation followed in a humid environment at 40 $^\circ\text{C}$ for 30 min. The hybridised surfaces were then rinsed with ultra-pure water to remove any un-hybridised target material followed by air drying and analysis using fluorescence microscopy.

Analysis of hybridised surface using fluorescence microscopy

Analysis of the surface was completed using an Olympus IX-81 fluorescent microscope (Olympus, Japan) equipped with a Cy5 filter of 548-580 nm excitation and 610-660 nm emission wavelength. Signal intensities of the modified regions and background were collected for each sample using the AnalySIS software provided with the program. The intensity of the hybridised region was then used to determine the extent of hybridisation of the Cy5 labelled target at the surface during the comparison between PDMS and glass.

2.3.4 Water contact angle measurements of glass substrates modified using the APTES silanisation method

Water contact angle (WCA) measurements were recorded to track the surface modification for each strategy on glass substrates. Here, the WCA was recorded in triplicate after each step of the reaction pathway. This was completed using the sessile drop method on a Sinterface Profile Analysis Tensiometer (PAT-1, SINTERFACE technologies, Germany). The volume of ultra-pure water ranged from 5-7 μL with subsequent imaging done using a fixed objective CCD camera. WCA measurements were calculated using SINTERFACE Profile Analysis Tensiometer PAT1 version 8.01 software. These results were then compared to the PDMS WCA measurements previously reported by Khodakov *et al.* [151].

2.4 Results and Discussion

2.4.1 Surface characterisation of APTES silanisation strategies

The APTES strategy for the covalent attachment of amine modified oligonucleotides via a PDITC cross-linker was tracked using WCA measurements at each step of the modification for the glass surfaces (refer to Table 5). The WCA recorded for the modified glass surfaces was then compared to previously reported measurements for the same modification strategy optimised for PDMS surfaces by Khodakov *et al.* [151].

Silanisation of the glass substrate with 2 %v/v APTES resulted in a contact angle of $37.8 \pm 3.4^\circ$. This was significantly higher than the neat plasma oxidised glass surface ($5.2 \pm 0.4^\circ$). A further increase in WCA was observed after attachment of the PDITC cross linker, where a WCA of $65.9 \pm 1.0^\circ$ was recorded. This increase in contact angle was directly associated with the hydrophobic nature of the surface due to the phenyl functional groups within the PDITC structure. These phenyl groups restrict the amount of hydrogen bonding, thus resulting in increased hydrophobicity and an increase in WCA. Subsequent covalent attachment of the NH₂-Probe to the PDITC modified glass substrate resulted in a decrease in WCA to $47.2 \pm 5.1^\circ$, resulting from the polar properties of the attached DNA increasing the amount of hydrogen bonding sites at the surface.

A comparison between the glass substrate WCA and the previously optimised PDMS method WCA measurements [151] is shown in Table 5. The values recorded for the PDMS modification were significantly higher in all cases due to the hydrophobic properties of the PDMS substrate. Despite this difference, similar trends in WCA were observed when the APTES silanised surface was modified with the PDITC cross-linker, suggesting successful attachment was achieved. The WCA for NH₂-probe was not recorded for PDMS [151] and as such, cannot be compared.

Table 5: Step-wise WCA measurements for the APTES modified PDMS (using optimised conditions [151]) and glass substrates (n=3)

Conditions	PDMS surface WCA (reported by Khodakov <i>et al.</i> [151])	Measured glass surface WCA
APTES silanisation	$83.9 \pm 3.3^\circ$	$37.8 \pm 3.4^\circ$
PDITC modified surface	$93.5 \pm 4.0^\circ$	$65.9 \pm 1.0^\circ$
NH ₂ -probe attachment	Not reported	$47.2 \pm 5.1^\circ$

2.4.2 Oligonucleotide attachment to APTES silanised glass substrates

The strategy for the attachment of amine modified oligonucleotides (NH₂-probe) to glass surfaces was based on the method described by Khodakov *et al.* [151] for oligonucleotide attachment to PDMS substrates. As this method used a hydrophobic PDMS substrate, initial investigation into the influence of glass slide surface silanol groups on attachment chemistry was required. The variables investigated included: i) surface oxidation method, ii) APTES silanisation time, iii) PDITC exposure time, iv) attachment time for NH₂-probe and v) hybridisation time. The effect on hybridisation efficiency for each variable was evaluated by recording the average signal intensity, obtained via fluorescence microscopy, of the modified region on the surface at varying reaction times.

i) Surface oxidation method

The Khodakov *et al.* method for oligonucleotide attachment to PDMS required initial treatment of the surface using plasma oxidation to generate a layer of reactive surface silanol groups on the non-polar substrate, for subsequent silanisation [151, 152]. In contrast to PDMS, the physical structure of glass already contains reactive silanol groups at the surface [163] meaning initial treatment to provide a reactive surface may not be necessary. Despite this, oxidation of the glass surface is often completed to maximise surface silanol coverage and remove organic contaminants. As such, the fluorescence intensities of the Cy5 labelled ACat Seq hybridised surfaces prepared from i) untreated glass, ii) glass treated with plasma oxidation and iii) glass treated with Piranha oxidation [164] were compared to determine which method was able to provide the greatest quantity of reactive silanol groups. Background measurements were also collected from regions outside of the oligonucleotide modified region in order to evaluate any fluctuations in signal that may arise from batch to batch variation of the glass slides.

The results from the hybridisation experiments are shown in Figure 14. Successful hybridisation of the surface was identified by the fluorescent signal (red due to emission at 670nm) with the background shown in black surrounding the spotted region. The recorded fluorescence intensity was dependent on the level of hybridisation of complimentary Cy5 labelled ACat Seq at the oligonucleotide modified region. As such, a higher fluorescence intensity corresponds to a greater level of hybridisation at the oligonucleotide modified surface.

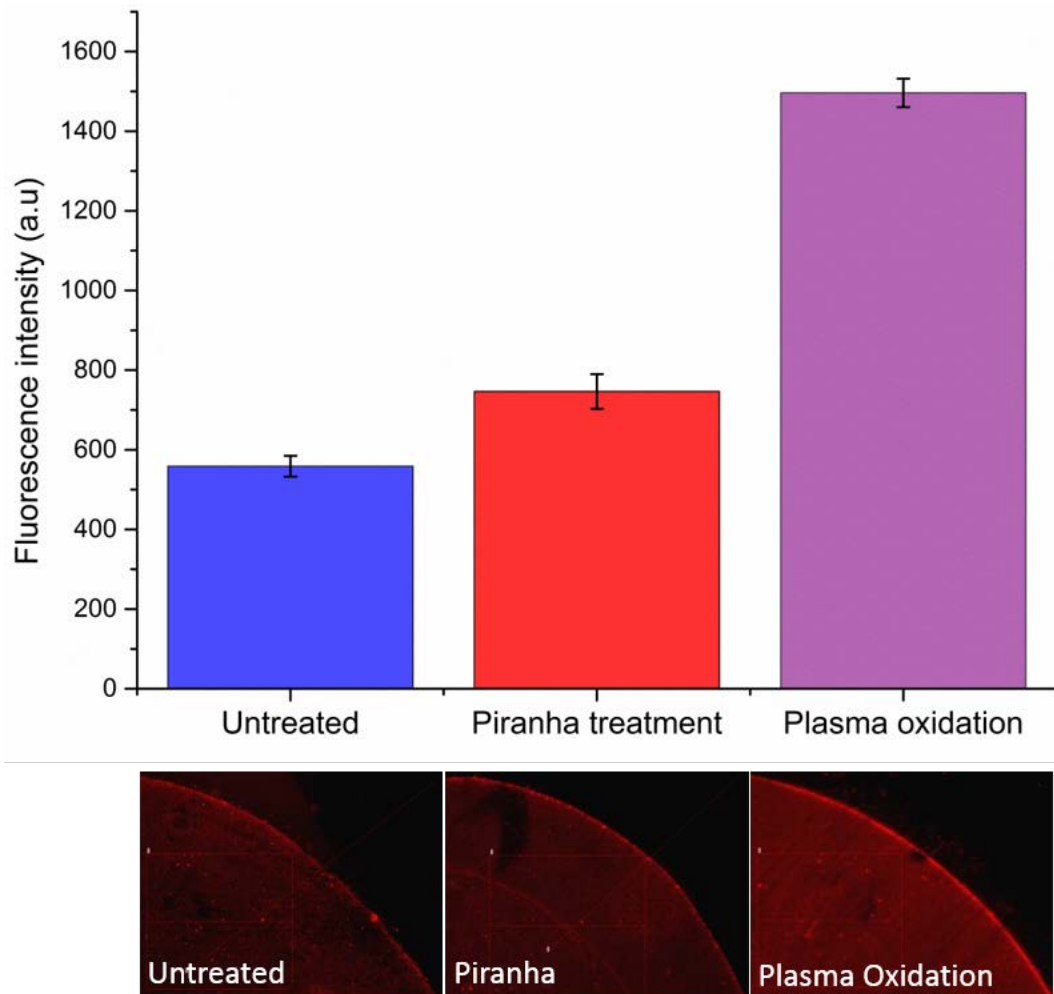


Figure 14: Effect of initial oxidation method on the final hybridisation with Cy5 labelled ACat Seq for glass surfaces

Graph of average fluorescence intensity with corresponding fluorescence microscope images for the hybridised untreated, piranha oxidised and plasma oxidised glass slides. Analysed on the Olympus IX-81 (n=3).

One interesting feature of some hybridised regions was the presence of a higher fluorescence intensity around the outer rim of the spotted region, as seen in the fluorescence microscope images shown in Figure 14. This phenomenon was associated with the “coffee-spot effect” where a distinctive ring like pattern is formed along the perimeter of a drop during evaporation or drying [165]. This effect has been reported for DNA microarrays [166, 167]. During the drop deposition, a pinned contact line is formed around the edge of a droplet. As evaporation occurs, a capillary flow action draws the solute to the edge of this contact angle leading to a ring-shaped deposition on the outer rim of the droplet [168]. In this research, this solute transport during evaporation leads

to a higher concentrated region of Cy5 labelled ACat Seq at the outer rim of the droplet, which in turn exhibits higher signal intensity around the perimeter of the modified region.

When observing the resulting average signal intensities, the untreated glass surface produced a relatively non-homogenous, low fluorescence signal (559 ± 26 a.u, Figure 14). This signal intensity was also considerably lower than the other pre-treatment methods suggesting initial treatment was essential to expose the maximum level of reactive silanol groups for silanisation. The Piranha treated slide resulted in a uniform fluorescence across the oligonucleotide modified region with an average fluorescence intensity of 746 ± 20 a.u. This was a significant improvement to the untreated glass slide suggesting the 2 h Piranha treatment successfully increased the number of available silanol groups. Both signal intensity and homogeneity was further improved when using the 40 s plasma oxidation method, the same method used for the pre-treatment of the PDMS [151] resulting in a signal intensity of 1113 ± 31 a.u. Plasma oxidation was determined to be the most effective method for cleaning the glass and exposing the maximum number of reactive silanol groups on the surface than the Piranha treatment. Additionally, plasma oxidation was only a 40 sec treatment unlike the Piranha treatment which required 2 h and required the use of harsh chemicals.

ii) APTES silanisation time

Silanisation of the oxidised glass surface was achieved via a condensation reaction with the silanol groups on the oxidised glass slide surface with the APTES (Figure 15). It was hypothesised that longer reactions with APTES would result in a greater level of amine functionalisation for increased oligonucleotide attachment. If this was the case, a greater level of hybridisation, and thus higher fluorescence intensity, will be obtained at higher reaction times. An APTES silanisation time of 20 min has been reported previously for the modification of PDMS surfaces [151]. As glass already contains reactive silanol groups at the surface, an investigation into APTES silanisation was required to determine if surface structure influences the time required for maximum silanisation. Plasma oxidised glass surfaces were exposed to APTES (2 %v/v) for times ranging from 5 to 20 min. The resulting fluorescence intensity was measured to determine the level of hybridised Cy5 labelled ACat Seq on the final oligonucleotide modified glass surface.

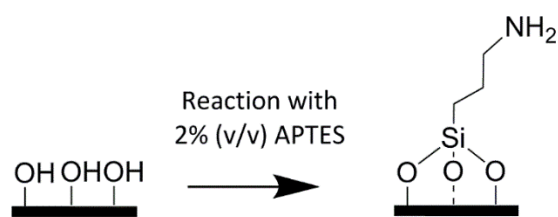


Figure 15: Modification of oxidised glass surface to amine functionalised surface using 2 % (v/v) APTES

A steady increase in fluorescence intensity was observed as the silanisation time was incrementally increased (Figure 16). The highest signal intensity was obtained after a 20 min exposure (1113 ± 31 a.u) with a uniform level of fluorescence over the entire modified region. Only a 11 % increase in fluorescence intensity was observed between 15 min (984 ± 28 a.u) and 20 min silanisation times. As such, a compromise between time and signal intensity was made and reaction times beyond 20 min were not investigated. In all further experiments, a silanisation time of 20 min was used for the glass surfaces.

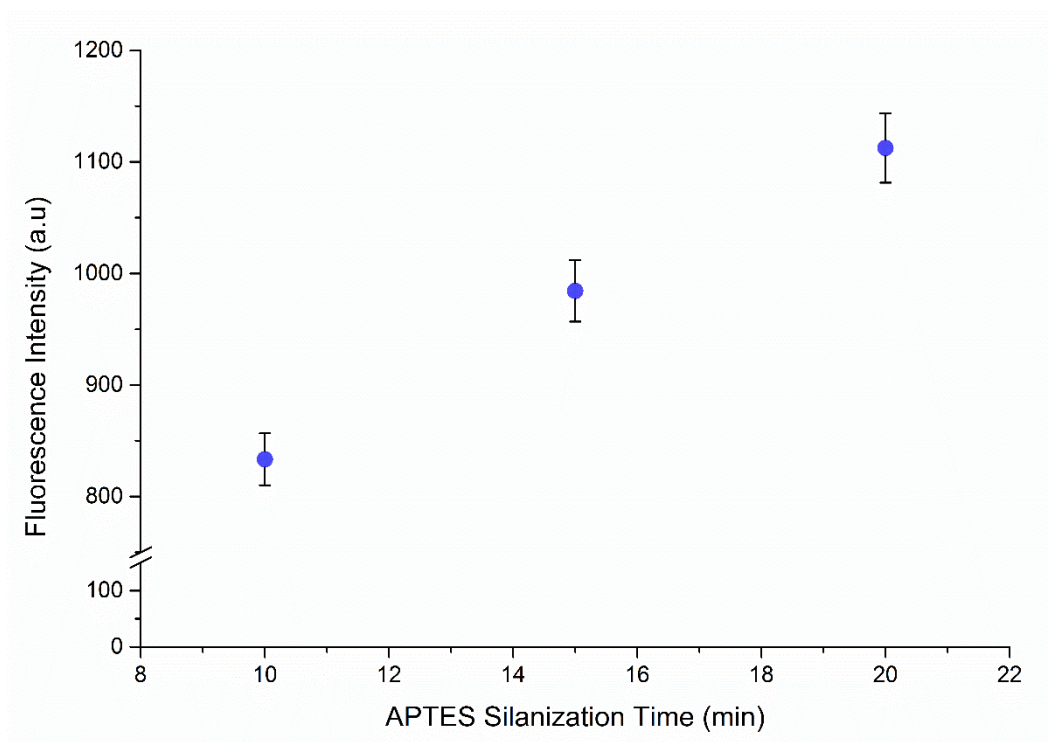


Figure 16: Effect of APTES silanisation time on the final hybridisation efficiency of the modified glass surface

Graph of average fluorescence intensity analysed on the Olympus IX-81 (n= 3, ± standard deviation).

iii) PDITC exposure time

PDITC cross-linker attachment to amine functionalised surfaces was achieved through the formation of a thioether bond between the thiocyanate of PDITC and the amine functionalised glass slide (Figure 17). Addition of this cross-linker increases the distance of the oligonucleotide from the surface resulting in improved hybridisation efficiency due to minimised steric interference compared to those positioned close to the surface [146]. PDITC attachment time is dependent on the number of available amine groups present based on the initial APTES silanization. Maximum attachment of PDITC to amine modified PDMS substrates has been reported at 120 min [151]. In order to examine the time required for optimal attachment of PDITC to the alternative glass surface, reaction times ranging from 10 to 120 min were examined.

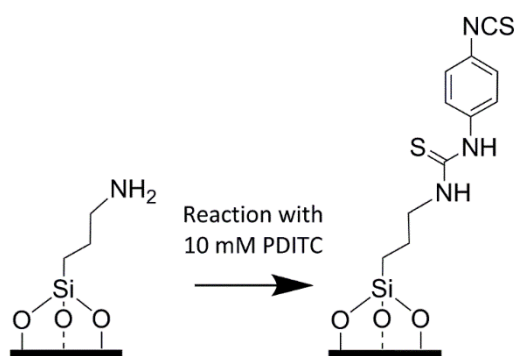


Figure 17: Modification of APTES silanised glass with 10 mM PDITC cross-linker

The resulting fluorescence intensity of hybridised Cy5 labelled ACat Seq on the surface was analysed as before with the APTES silanisation time experiments. As shown in Figure 18, fluorescence intensities obtained from the hybridised glass surfaces remained relatively stable (ranging from 752 ± 42 to 803 ± 45 a.u) up until the slide exposed to the PDITC solution for 120 min (Figure 18). The slide exposed to the PDITC solution for 120 min resulted in a decreased signal intensity of only 650 ± 36 a.u. This loss in fluorescence intensity can be visualised in Figure 18 upon comparison of the 10 min and 120 min PDITC exposure time fluorescence microscope images.

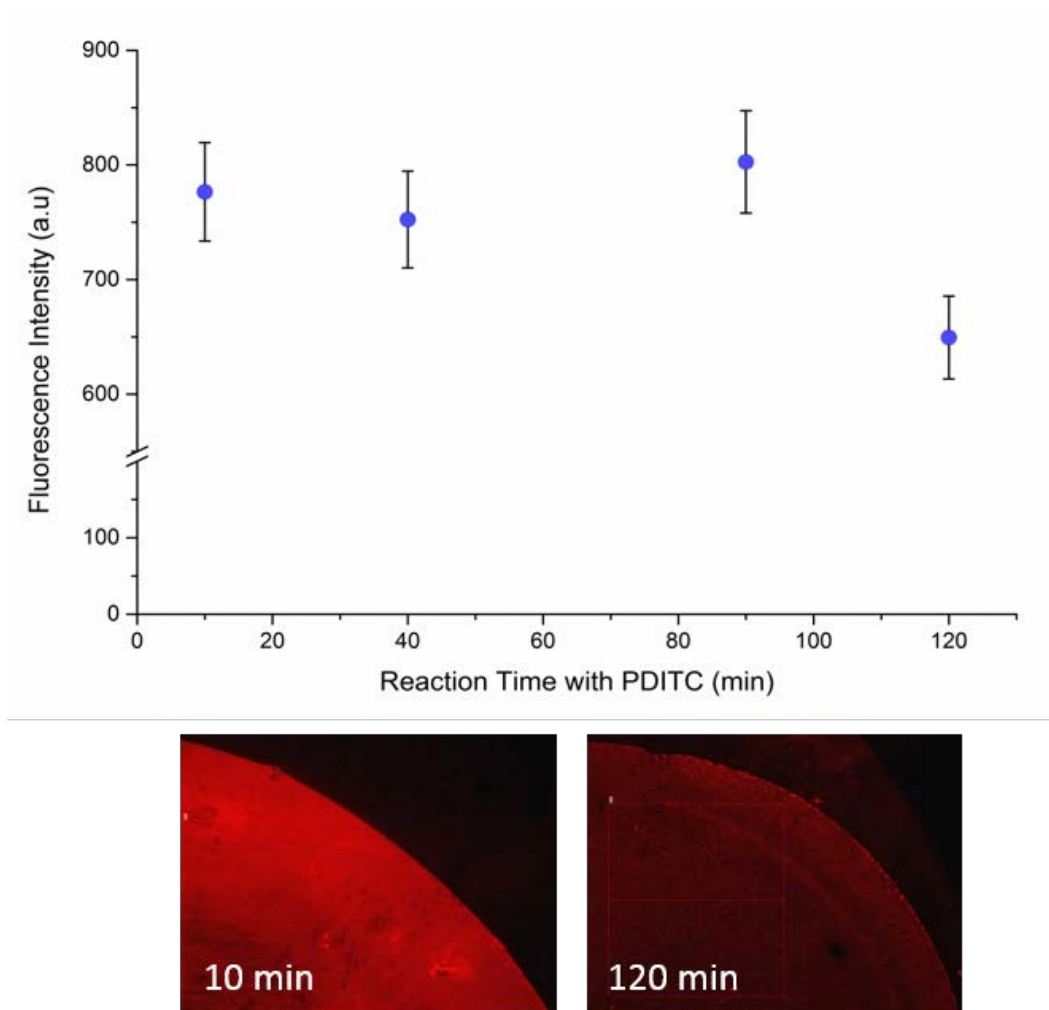


Figure 18: Effect of PDITC reaction time on the final hybridisation efficiency of the modified glass surface

Graph of average fluorescence intensity with corresponding fluorescence microscope images after 10 min and 120 min reaction times with PDITC. Analysed on the Olympus IX-81 ($n=3$, \pm standard deviation).

This decrease suggests that longer reaction times with PDITC hinders hybridisation at the surface. It was hypothesised that the observed decrease in fluorescence intensity at longer exposure times was due to high density attachment of NH_2 -probe oligonucleotides at the surface. This high density packing hinders hybridisation due to steric influences as discussed previously [150]. If the target sequence was unable to hybridise due to these steric effects, a loss of signal would be expected as observed in Figure 18. Due to the stable fluorescence intensities observed from 10 min to 90 min, the exposure time to PDITC was reduced to 10 min for all subsequent experiments.

iv) Attachment time for NH_2 -probe

Amine modified oligonucleotides are attached to the PDITC cross-linker on the surface via a thiourea bond (Figure 19). The time required for oligonucleotide attachment is dependent on the thiocyanate surface coverage achieved in the previous modification step. As such, the time required for oligonucleotide attachment was investigated. The ideal attachment time for amine modified oligonucleotides to PDITC modified PDMS has been reported at 120 min [151]. In order to maximise the attachment of oligonucleotides to the alternative glass surface, attachment times ranging from 10 to 140 min were investigated (Figure 20).

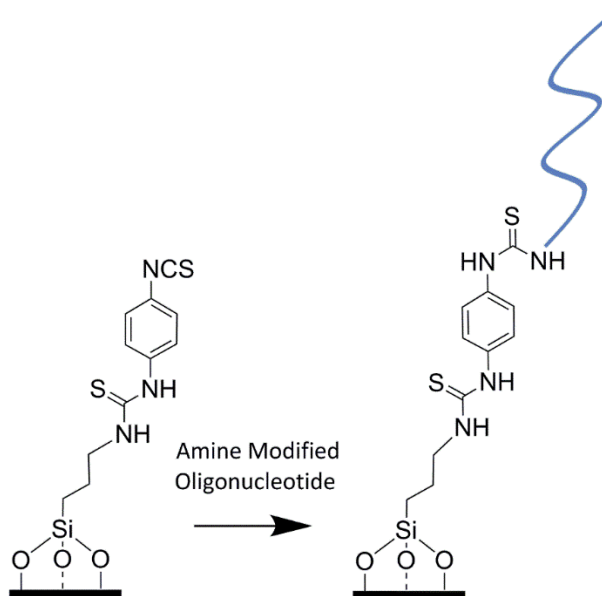


Figure 19: Attachment of the amine modified oligonucleotide (NH_2 -Probe) to the PDITC modified glass slide

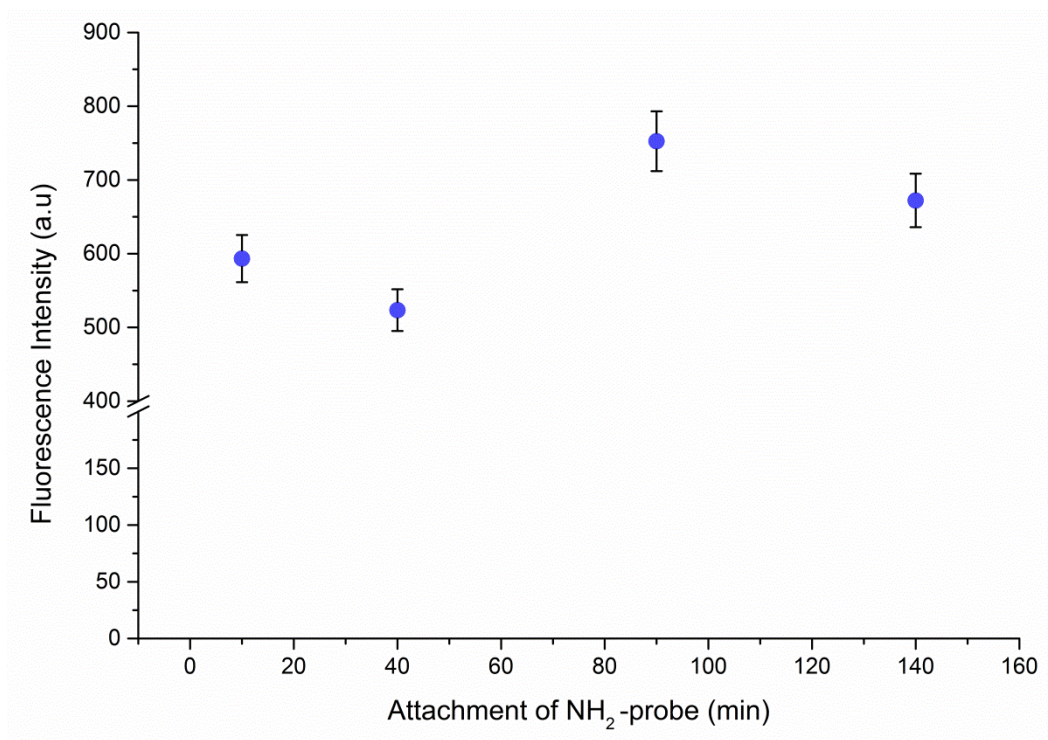


Figure 20: Effect of NH₂-probe attachment time on the final hybridisation efficiency of the modified glass surface

Graph of average fluorescence intensity analysed on the Olympus IX-81 (n= 3, ± standard deviation).

Here, a 90 min attachment time resulted in the highest level fluorescence intensity (753 ± 41 a.u) suggesting that after this time, an optimal surface attachment density was attained. The longer attachment time of 140 min resulted in a slight decrease in signal intensity (672 ± 36 a.u). This decrease in signal intensity was associated with evaporation of the spotted NH₂-probe solvent during attachment at 40 °C, hindering oligonucleotide attachment. As a result, the level of Cy5 labelled target sequence successfully hybridised at the surface also decreases, reducing the recorded fluorescence intensity. Lower signal intensities observed for 10 min (593 ± 32 a.u) and 40 min (523 ± 28 a.u) probe attachment times were associated to specific reaction kinetics between the amine modified oligonucleotide and the PDITC modified glass surface. When compared to previous methods, amine oligonucleotide probe attachment time has been reported at times ranging from 1 h to 2 h demonstrating that reaction kinetics are slow [110, 169].

v) *Hybridisation time*

Hybridisation of complimentary target oligonucleotides can be achieved when using oligonucleotides covalently attached to the surface as shown in Figure 21. For successful hybridisation at the surface, attached oligonucleotides must be distanced from the surface and available for binding. Time required for maximum hybridisation of the complimentary ACat Seq is dependent on the attachment density of the amine modified oligonucleotides from the previous step in attachment. As such, the time required for hybridisation on the glass substrate was investigated with hybridisation times with Cy5 labelled ACat Seq between 10 and 30 min being evaluated. The time required for maximum hybridisation of fluorescently labelled target sequence has previously been reported as 30 min for oligonucleotide modified PDMS microchannel surfaces [151].

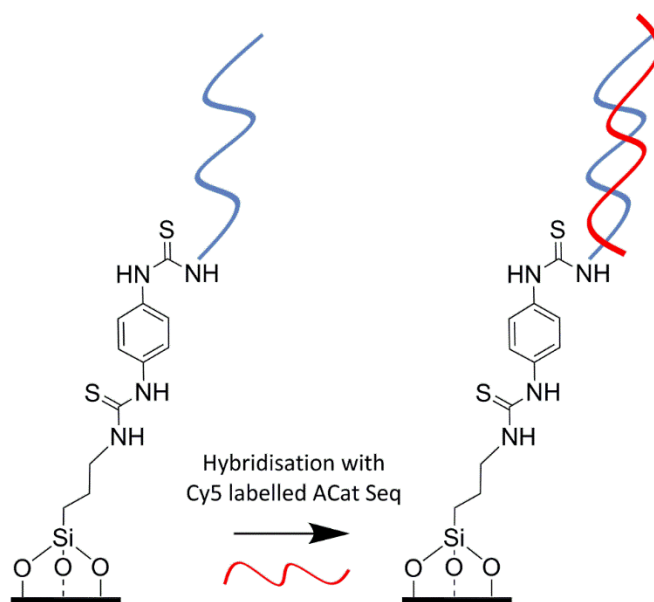


Figure 21: Hybridisation of the oligonucleotide (blue) modified glass slide with Cy5 labelled ACat Seq (red)

The recorded fluorescence intensities over the range of hybridisation times can be seen in Figure 22. After a 30 min hybridisation a maximum fluorescence intensity of 1315 ± 34 a.u. was recorded. Hybridisation times greater than 30 min were also investigated, with the extended exposure at 40 °C leading to evaporation of the solution containing the target sequence. This evaporation hindered the level of hybridisation of Cy5 labelled target at the surface. Evaporation of the spotted ACat Seq solution was also observed in the fluorescence microscope images with greater signal intensities at the rim of the spotted region. This was due to the “coffee-spot effect” discussed previously

whereby capillary actions draw the solution of a droplet to the outer edge during evaporation. This was visible for the 10 min and 20 min hybridisation times as shown in the fluorescence microscope images in Figure 22. A 30 min hybridisation time was found to provide the greatest fluorescence intensity, whilst minimising the level of spotted target sequence evaporation, and was used for all further experiments.

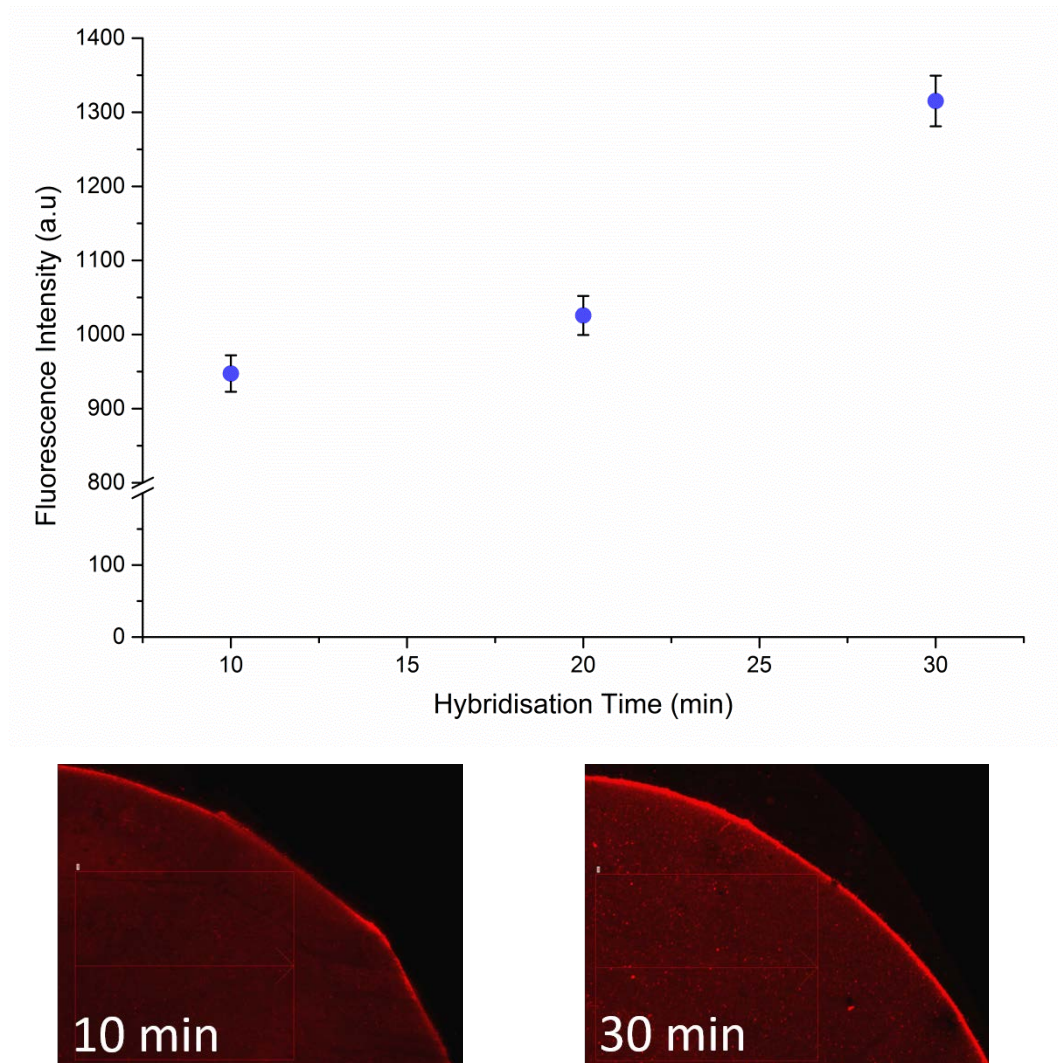


Figure 22: Effect of hybridisation time on the final hybridisation efficiency of the modified glass surface

Graph of average fluorescence intensity with corresponding fluorescence microscope images after 10 min and 30 min hybridisation with Cy5 labelled ACat Seq. Analysed on the Olympus IX-81 (n=3, \pm standard deviation).

The final conditions for both substrates are summarised in Table 6, with the PDMS values based on those reported previously by Khodakov *et al.* [151]. Both the PDMS and glass surface modification conditions reported in Table 6 were used in all subsequent experiments herein. Use of the glass slide surface resulted in an overall decrease in time required for complete oligonucleotide attachment and subsequent hybridisation. This was most likely due to the higher number of available silanol groups at the surface unlike the hydrophobic PDMS alternative.

Table 6: Final conditions of the APTES modified PDMS and glass substrates

Conditions	Reaction Time for PDMS (min) *	Reaction Time for Glass (min)
APTES silanisation	20	20
PDITC treatment	120	10
Oligonucleotide attachment	120	90
Hybridisation	30	30

* Reaction conditions as described by Khodakov *et al.* [151]

2.4.3 Hybridisation performance - A direct comparison of APTES modified glass and PDMS

A comparison in sensitivity between the oligonucleotide modified PDMS and glass slide surface was completed to determine if one substrate outperforms the other using model hybridisation experiments. Each surface was treated using the optimised conditions given in Table 6 with the fluorescence intensities being compared.

As shown in Figure 23, a significantly higher average fluorescence intensity was obtained for the glass surface compared to the PDMS. A slight increase in background for the glass surface was also observed. To overcome variations due to this background signal, signal: background fluorescence intensity ratios were calculated for both substrates. Resulting signal: background ratios of 4.15 and 1.79 were calculated for glass and PDMS surfaces respectively. The 2-fold increase in signal intensity demonstrated by the glass surface suggests that oligonucleotide modified substrates produced using this material may provide greater sensitivities than the PDMS alternative.

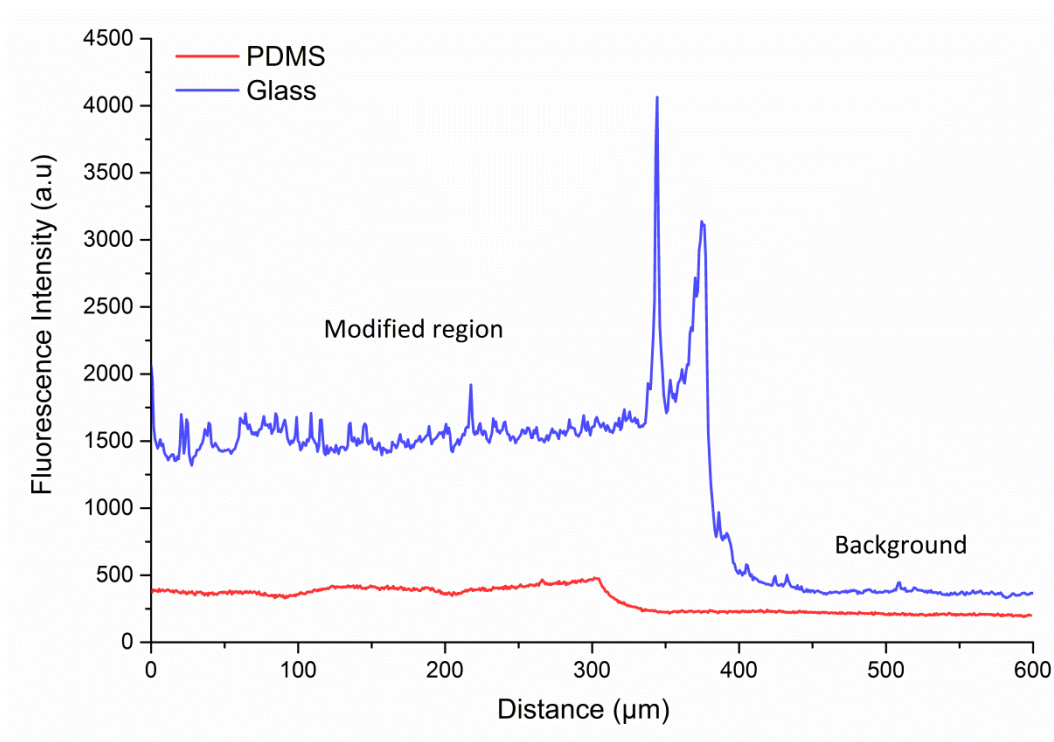


Figure 23: Obtainable fluorescence intensities using the PDMS and glass substrates

Graph of fluorescence intensity and background fluorescence intensity for both oligonucleotide modified PDMS and glass substrates. Analysed on the Olympus IX-81.

2.4.4 APTES modified PDMS and glass surface stability

The stability of a modified surface is an important feature for re-usable devices, creating a more cost effective and time efficient platform for detection. Previous research has discussed the hydrophobic recovery exhibited by PDMS when used for thermodynamically unfavourable surface modifications [153]. This effect can negatively impact oligonucleotide modified surfaces prepared using this substrate. As such, an investigation into surface stability of both the oligonucleotide modified PDMS and glass surfaces was completed to determine if the PDMS undergoes hydrophobic recovery over time and if the glass surface can provide greater chemical stability.

Initially, oligonucleotide modified PDMS and glass surfaces were stored in the dark, at room temperature, for a period of up to 9 days. On subsequent days, the glass slides were removed from storage and hybridised with Cy5 labelled ACat Seq and the fluorescence intensities recorded. Figure 24 shows that after only 1 day of storage the oligonucleotide modified PDMS surface demonstrated a 50 % loss in fluorescence intensity when

compared to the initial intensity (day 0, 667 ± 25 a.u). After 5 days of storage the fluorescence intensity had decreased by a further 50% and stability trials for oligonucleotide modified PDMS were ceased after this time period. Alternatively, the glass surface fluorescence intensity remained stable for the entire 9 day storage period (ranging from 1072 ± 30 to 1001 ± 30 a.u).

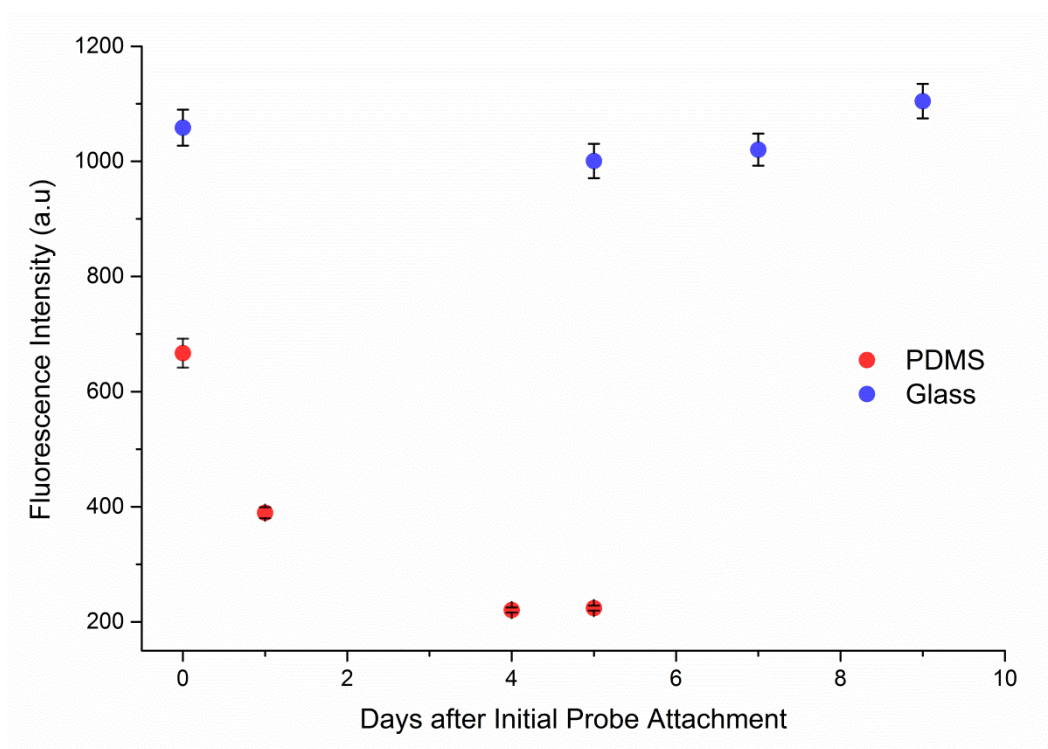


Figure 24: Comparison of PDMS and glass surface stability after initial oligonucleotide attachment

Graph of recorded fluorescence intensities after consecutive days in storage for oligonucleotide (NH_2 -probe) modified PDMS (red) and glass (blue) substrates. Analysed on the Olympus IX-81 ($n=3$, \pm standard deviation).

Hydrophobic recovery of the PDMS substrate during storage was the most viable reason for the loss in surface reactivity after only one day. Polar modifications of PDMS using silanization agents such as APTES creates a thermodynamically unstable surface, resulting in a conversion to the more stable hydrophobic structure over time [153]. Spotting the Cy5 labelled ACat Seq and hybridising on the now rearranged highly hydrophobic surface results in a decrease in available sites for hybridisation, reducing the fluorescent signal.

Over time, PDMS has also been reported to undergo “cracking” of the silanol layer due to the differences in elasticity between this and the lower PDMS substrate [170]. These cracks have been found to range between 0.3 to 0.5 μm which is enough to promote rapid hydrophobic recovery through the formed cracks, once again leading to less reactive sites [170]. Alternatively, the glass surface is stable and already contains the reactive silanol moieties. This makes the glass surface more thermodynamically stable in the hydrophilic form and hence, less likely to lose the reactivity of the surface molecules as shown in this investigation [171].

Stability of the two surfaces post-hybridisation was also investigated to determine if the surfaces can be hybridised on site and stored prior to analysis without loss of fluorescence intensity. This would be useful for field based sampling whereby the surface was exposed to the target HAB nucleic material at site and then transported to the laboratory for analysis. It would also allow for the storage of reference samples for later comparative analysis, especially when tracking bloom formations. Hybridised PDMS and glass surfaces were stored and analysed on subsequent days, with the fluorescence intensity recorded for 9 days. A significant loss in fluorescence intensity was observed for both the glass and PDMS surfaces, each loss in signal following a similar trend (refer to Figure 25). This similarity suggests that the loss in signal was most likely associated with instability of the Cy5 dye on the ACat Seq target rather than instability of the surface.

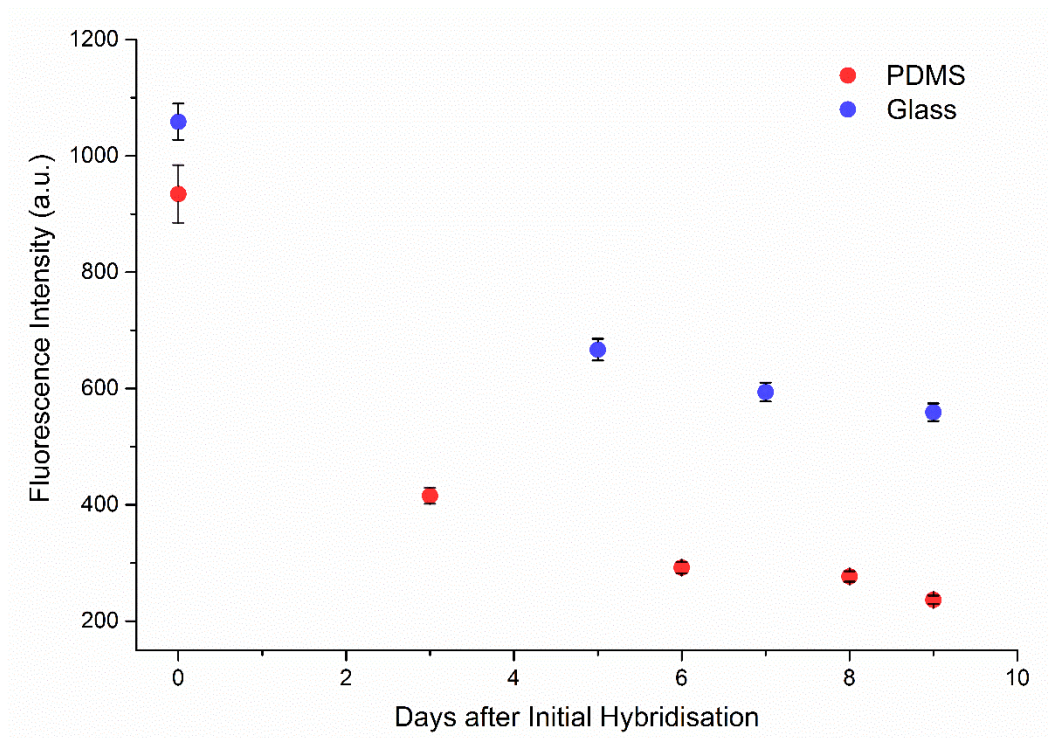


Figure 25: Comparison of PDMS and glass surface stability after hybridisation of the attached oligonucleotides

Graph of average fluorescence intensity over a 9 day storage period. Analysed on the Olympus IX-81 (n= 3, ± standard deviation).

Studies have found that Cy5 is relatively unstable with effects such as photobleaching occurring when the dye is exposed to light [172]. This effect has been observed on repetitive analysis samples, with a 2-4 % decrease in signal reported between each scan using a Microplate reader [173]. In this study, degradation occurred at a rapid rate during initial stages of analysis with a loss of 56 % recorded for PDMS and 37 % for glass after one consecutive analysis. Over the 9 day period PDMS was analysed a total of 5 times, and glass only 4 times with a 75 % and 37 % loss in signal intensity respectively. Exposure to ozone is another factor that can affect Cy5 labelled microarrays with concentrations as low as 5-10 ppm and exposure times of only 10-30 s resulting in a loss of signal [174]. Methods to improve signal stability have been discussed in literature with the most common being storage in a dark cold environment to prevent degradation of the Cy5 label [175].

Storage conditions were briefly investigated to determine if methods to improve signal stability could be implemented. Storage conditions investigated included storage in a -20 °C freezer, storage in a desiccator at room temperature and in a dark environment at

room temperature. Storage under each condition still resulted in a loss of fluorescence intensity over time (Appendix, Figure 57). Storage in a dark environment resulted in a slightly lower level of degradation of the fluorescence intensity with a 39 % loss in signal after 6 days compared with a 41 % loss recorded using the previous conditions (based on an average signal between day 5 and 7). This suggested that photobleaching of the Cy5 dye was promoting Cy5 degradation, as suggested in previous studies [175]. Due to there still being a relatively high loss in signal intensity using these storage conditions, same-day analysis was used for all subsequent experiments to minimise errors associated with photobleaching.

2.5 Conclusions

In this chapter, glass and PDMS substrates were compared for their optimised performance in model hybridisation experiments. Here, the glass substrate proved to be superior to the alternative PDMS substrate as a platform for oligonucleotide attachment and subsequent model hybridisation. A higher signal intensity was obtained in all comparative experiments between the glass and the PDMS with a signal: background fluorescence intensity ratio of 4.15 for glass compared to 1.79 for PDMS.

Investigation into stability of the two oligonucleotide modified substrates resulted in a stable signal for glass over a 9 day period. PDMS however resulted in a significant loss of fluorescence intensity after only one day storage. This demonstrates that the substrate chemistry heavily influences the stability of the attachment, with glass providing greater stability than PDMS. Post-hybridisation reactivity was also investigated with a loss in signal being recorded at similar rates over the duration of storage for both PDMS and glass surfaces. To overcome this issue, same day analysis was required to eliminate the loss of signal observed from photobleaching.

Based on the higher sensitivity and improved stability of the glass slides compared to PDMS surfaces, glass was identified as the most suitable surface for oligonucleotide attachment for future use as a stable, sensitive HAB detection platform.

3

An investigation into covalent strategies for the immobilisation of oligonucleotides to glass substrates

This chapter compares the suitability of APTES and VTES modified glass surfaces for the covalent attachment of oligonucleotides and hybridisation performance with target sequences for potential use in sensitive HAB detection platforms. Results discussed include:

- *An evaluation of VTES silanisation chemistry for the immobilisation of oligonucleotides to glass surfaces*
- *An assessment of sensitivity of the modified surfaces produced using both the APTES and VTES silanisation methods for the capture of target sequences*
- *Examination of the selectivity of the modified surfaces generated from APTES and VTES silanisation methods for binding complimentary and non-complimentary target oligonucleotide sequences*
- *Investigation into the regeneration capabilities of modified surfaces for the development of re-usable substrates for target oligonucleotide capture and detection*

3.1 Introduction

An evaluation into substrate performance for the detection of Cy5 labelled ACat Seq in Chapter 2 demonstrated that modified glass slides outperformed PDMS substrates. Consequently, glass surfaces were selected as an ideal substrate for oligonucleotide immobilisation using APTES/PDITC modification chemistry. Although this modification approach results in the successful attachment of oligonucleotides, it also gives rise to increased levels of non-specific adsorption [106, 112, 115]. This adsorption results from electrostatic interactions between the positive charge of amine modified substrates under neutral and acidic conditions and the negatively charged phosphate groups within DNA (and oligonucleotides) [176, 177]. In order to minimise non-specific adsorption, stringent blocking procedures are implemented prior to hybridisation [178].

Alternatively, different modification chemistry can be employed to minimise non-specific adsorption. For example, hydrophobic modifications can be used to minimise adsorption interactions at the surface as electrostatic interactions cannot occur between the surface and oligonucleotides [113]. Two methods that can achieve this are attachment by i) a dithiol linkage between a thiol modified surface and thiol modified oligonucleotide [112], or ii) a thiol-ene click chemistry approach, where a vinyl modified surface is reacted with a thiol modified oligonucleotide (Figure 26). In both cases, rather than using an amine terminated silanisation agent such as APTES, silanisation of the substrate is achieved using MPTS [112] (to generate a thiol surface) or VTMS [113] (to generate the vinyl functionalised surface).

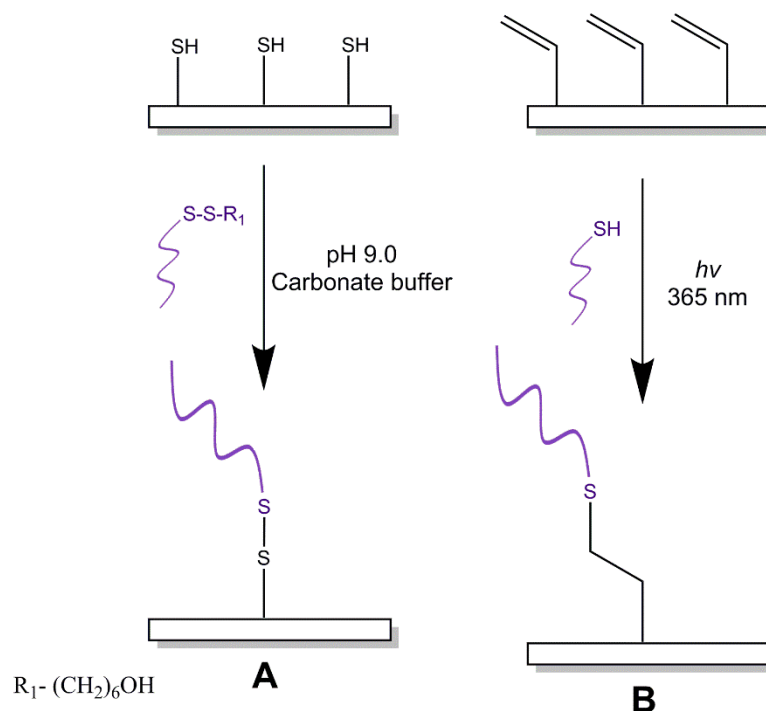
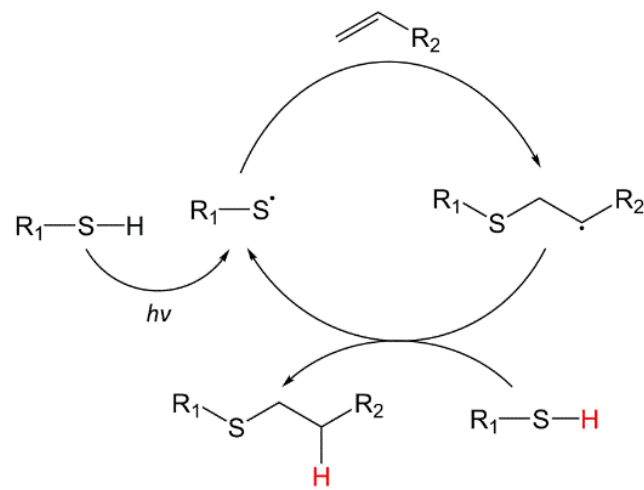


Figure 26: Thiol modified oligonucleotide attachment strategies

Achieved through A) the formation of a dithiol linkage and B) photoinitiated thiolene click-chemistry

The dithiol attachment strategy, although simple and practical, has a number of drawbacks. Firstly the dithiol bond is susceptible to reductive cleavage, effectively breaking the bond and reducing the number of available oligonucleotides bound to the surface [106]. Secondly, under certain reaction conditions (such as strong irradiation) the thiol modified surface is vulnerable to side reactions that convert reactive thiols into the sulfonate form, ultimately hindering oligonucleotide attachment [106, 179].

The thiol-ene click chemistry approach overcomes these issues, as the resulting thioether bond is not susceptible to the same reductive cleavage. Furthermore, the vinyl functionalised surface is relatively unreactive making it less susceptible to side reactions. Here, the attachment of oligonucleotides is achieved using a photoinitiated reaction between surface and oligonucleotide (mechanism shown in Figure 27) [113]. Photoinitiation (using wavelengths between 365-406 nm) generates a free radical at the reactive thiol on the oligonucleotide which then reacts further with the vinyl functionalised surface to generate the stable thioether bond [123]. Oligonucleotide attachment using this method has been reported to result in an attachment densities of 1.8 pmol.cm^{-2} [113].



R₁ = SH-probe oligonucleotide sequence
 R₂ = Glass slide surface

Figure 27: General overview of a photoinitiated thiol-ene reaction

A single thiol reacts with a single vinyl group to produce the thioether bond. Adapted from [180]

3.2 Scope of study

In Chapter 2, glass slide surfaces were found to perform significantly better than PDMS for the attachment and hybridisation of oligonucleotides. As such, glass slides were used for oligonucleotide attachment experiments discussed in this chapter. Initially, the effect of the selected surface modification chemistry on hybridisation performance was investigated. Here, the previously optimised APTES/PDITC method was compared to an alternative thiol-ene attachment whereby thiol modified oligonucleotides were attached to vinyl functionalised glass surfaces [113]. Thiol-ene attachment reaction conditions were investigated to maximise hybridisation at the surface using a univariate approach similar to the APTES method described in Chapter 2. Ultimately, hybridisation performance of the APTES and vinyltriethoxysilane (VTES) attachment chemistries were evaluated for sensitivity, selectivity and regeneration of the surface for re-use.

3.3 Experimental

3.3.1 Materials

All chemicals and reagents were of analytical grade and used as supplied. APTES, VTES, PDITC, sodium dodecyl sulfate (SDS) and tris(2-carboxyethyl) phosphine hydrochloride solution (TCEP) were purchased from Sigma-Aldrich, Australia. Ethanol (96 %), pyridine, toluene and DMF were purchased from Chem-Supply, Australia.

Livingstone Premium Microscope pathology grade glass slides (76.2 mm x 12.7 mm, Australia) were used for the tethering of the oligonucleotide capture probes. Oligonucleotides used in this study were purchased from Integrated DNA Technologies (USA) with the sequences shown in Table 7. Unless otherwise specified, a 0.1 M phosphate buffer (pH 8.0) was used to dilute the NH₂-probe prior to attachment. Ultra-pure water 18 MΩ.cm⁻¹ was used to dilute the thiol modified probe (SH-probe) prior to attachment. A 1x SSC buffer (150 mM sodium chloride, 15 mM trisodium citrate, pH 7.0) was used for all hybridisation experiments for both the APTES and VTES modification strategies.

Table 7: Oligonucleotide sequences used for attachment to APTES and VTES functionalised glass slides

Including the 5' amine and thiol for covalent attachment at the surface and Cy5 modifications for subsequent detection

Oligonucleotide Name	5' Modification	Sequence (5'-3')
NH ₂ -Probe	Amine	GCACTTGCAGCCAAAACCCA
SH-Probe	Thiol	GCACTTGCAGCCAAAACCCA
ACat Seq.	Cy5	TGGGTTTTGGCTGCAAGTGC
Non-complimentary	Cy5	CTGGGATATCTGCACCAGC

3.3.2 APTES covalent modification strategy for glass slides

The covalent attachment of oligonucleotides using the APTES method was as described in Section 2.4.1.1 (Figure 28, Strategy A). Briefly, glass microscope slides were pre-treated with a 40 s plasma oxidation treatment at 0.2 Torr (O₂), 18 W. The slides were then immediately placed in APTES (2 %v/v in ethanol) and allowed to react for 20 min. APTES

reacted slides were washed with ethanol, air dried and heated at 100 °C for 10 min. The APTES treated slides were then placed in a solution of PDITC (10 mM in pyridine: DMF 1:9 %v/v) and left to react for 120 min. Once reacted, stringent washing followed with ethanol and heated at 100 °C for 10 min to remove any unreacted PDITC and residual solvent.

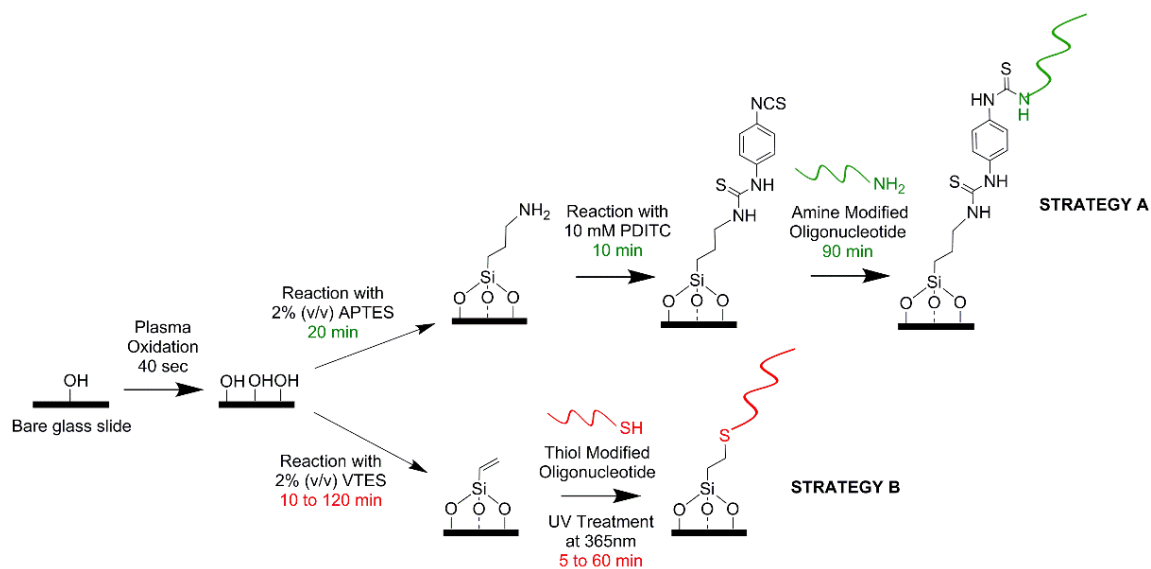


Figure 28: Schematic and optimised conditions for the attachment of oligonucleotide probes to glass substrates

Surfaces were prepared by silanisation with either APTES (Strategy A) or VTES (Strategy B)

An amine modified oligonucleotide probe solution, (NH₂-probe, 50 μM, 2 μL) was then manually spotted onto the PDITC modified glass slide and left to react at 40 °C in a humid environment for 90 min. Unreacted NH₂-probe was removed by rinsing with ultra-pure water and air drying. Unreacted surface PDITC was subsequently blocked using ethanolamine (50 mM, 0.1 M sodium phosphate buffer, pH 8.0) with stirring for 20 min. Excess unreacted ethanolamine was removed by rinsing the slide with ultra-pure water followed by air drying in preparation for subsequent hybridisation experiments.

3.3.3 VTES covalent modification strategy for glass slides

The synthetic strategy for the attachment of oligonucleotides to VTES modified glass slide surfaces is shown in Figure 28 (Strategy B). As with Strategy A, glass microscope slides were initially pre-treated with a 40 s plasma oxidation treatment at 0.2 Torr (O₂), 18 W.

After treatment the slides were immediately immersed in a solution of VTES (2 %v/v in toluene) and allowed to react for 30 to 120 min (optimal silanisation time 120 min). The slides were then removed and rinsed with toluene followed by heating at 40 °C for 10 min to remove residual solvent.

The disulfide modified oligonucleotide probe (as received) was converted to the reactive SH-probe by overnight reduction with excess TCEP (0.01 M, aqueous). The SH-probe solution (50 µM, 2 µL) was manually spotted onto the VTES modified glass slide and irradiated at 365 nm (\approx 3 cm distance from lamp) between 10 to 60 min (optimal irradiation time 60 min) for attachment. Unreacted SH-probe was removed by washing with ultra-pure water for 30 min at 40 °C with stirring followed by air drying in preparation for subsequent hybridisation experiments.

3.3.4 Hybridisation experiments for amine and vinyl modified substrates

Manual spotting hybridisation

The modified surfaces produced using both strategies followed the same hybridisation procedure. Briefly, Cy5 labelled ACat Seq target (2 µL, 20 µM in 1x SSC buffer) was manually spotted over the modified region of the glass slide. The glass slides were then left in a humid environment at 40 °C, with the APTES modified surface left to hybridise for 30 min and the VTES modified surface between 10 to 60 min (maximum hybridisation after 40 min). The hybridised surfaces were rinsed with ultra-pure water and air dried. A two-step washing procedure followed in order to minimise the level of non-specific adsorption. To do this, slides were initially immersed in 2x SSC (with 1 % SDS) for 20 min followed by rinsing with ultra-pure water. For the second wash glass slides were immersed in 0.2x SSC (with 0.1 % SDS) for 20 min, rinsed with water then air dried ready for analysis by fluorescence microscopy.

Bulk solution hybridisation

Due to issues surrounding poor spot homogeneity and variability in recorded fluorescent intensities of the modified regions an alternative hybridisation strategy was also implemented. Here, hybridisation from a bulk solution was used to minimise evaporation of the spotted target sequence. Oligonucleotide modified glass slides were immersed in 10 mL of 1x SSC buffer (pH 7.0) containing Cy5 ACat Seq (final concentrations ranging from 0.16 to 4.00 nM). Slides were left overnight at 40 °C with stirring to allow for

complete hybridisation. Stringent washing followed to minimise non-specific adsorption of the target sequence to the surface. This was accomplished by immersing the slides in 2x SSC (with 1 % SDS) for 20 min with stirring, subsequent rinsing with ultra-pure water, then immersion in 0.2x SSC (with 0.1 % SDS) for a further 20 min with stirring. The surfaces were finally rinsed with ultra-pure water and air dried ready for fluorescence microscopy analysis.

Analysis of hybridised surface using fluorescence microscopy

Hybridised glass slide surfaces were analysed using an Olympus IX-71 fluorescent microscope (Olympus, Japan) equipped with a CoolLED PE-2 system with a 635 nm excitation and 665-740 nm emission wavelength. This instrument was used in place of the Olympus IX-81 used in Chapter 2, as the IX-81 was no longer performing to the same sensitivity. Further instrument failure (due to flood damage) resulted in some experiments being analysed on an Olympus IX-73 fluorescent microscope (Olympus, Japan) replacement model instead of the IX-71. The Olympus IX-73 was equipped with a CoolLED 300 white system with a 635 nm excitation and 665-740 nm emission wavelength. The specific instruments used for each experiment are included in the figure captions for reference. Images taken using both microscopes were analysed using ImageJ 1.47t software. Here, average signal intensities and background fluorescence of the images of the hybridised regions on the glass slide were recorded and fluorescence intensity signal: background ratios calculated using Equation 1:

Signal: background ratio

$$= \frac{\text{Average fluorescence intensity of modified region (a.u)}}{\text{Average fluorescence intensity of background (a.u)}}$$

Equation 1: Calculation of the signal: background ratio for the fluorescence microscope images

3.3.5 Surface regeneration

To test the regeneration capabilities of both the APTES and VTES modification strategies, a hybridisation- de-hybridisation- re-hybridisation cycle was used. Initial hybridisation was completed as stated in 3.3.4 using hybridisation in a bulk 10 mL solution with a final concentration of 4 nM of the target ACat Seq. The stringent two step washing procedure was implemented followed by analysis using fluorescence microscopy.

De-hybridisation of the hybridised slides was done by immersing the hybridised surfaces in 20 mL of water at 80 °C for 2 h. An extended de-hybridisation was used to ensure the complete removal of the Cy5 labelled ACat Seq. Washing followed using 2x SSC (with 1 % SDS) for 20 min, subsequent rinsing with ultra-pure water, then immersion in 0.2x SSC (with 0.1 % SDS) for a further 20 min. The surfaces were rinsed with ultra-pure water and air dried followed by analysis using fluorescence microscopy.

After analysis, the de-hybridised slides underwent re-hybridisation by immersion of the glass slides in 10 mL of 1x SSC buffer (pH 7.0) containing Cy5 labelled ACat Seq (final concentration of 4 nM) and leaving to hybridise overnight at 40 °C with stirring. The same two step washing method was implemented with immersion of the slides in 2x SSC (with 1 % SDS) for 20 min, subsequent rinsing with ultra-pure water, then immersion in 0.2x SSC (with 0.1 % SDS) for 20 min. The surfaces were then rinsed with ultra-pure water and air dried ready for fluorescence microscopy analysis

Modified glass slides were analysed at each step of the regeneration cycle to determine if the complete removal of ACat Seq after de-hybridisation was possible and to evaluate the change in signal intensity upon re-hybridisation. Analysis of the surface was completed using the Olympus IX-71 and IX-73 fluorescent microscopes (Olympus, Japan) as discussed in Section 3.3.4. The specific instruments used for each experiment are included in the figure captions for reference.

3.3.6 Water contact angle measurements of glass substrates modified using the VTES silanisation method

Water contact angles (WCA) measurements were recorded to track the surface modification for both the APTES and VTES silanisation strategy. Here, the WCA was recorded in triplicate during each step of the reaction. WCA determinations were completed using the sessile drop method on a Sinterface Profile Analysis Tensiometer (PAT-1, SINTERFACE technologies, Germany). The volume of ultra-pure water ranged from 5-7 μ L and subsequent images were collected using a fixed objective CCD camera. WCA measurements were calculated using SINTERFACE Profile Analysis Tensiometer PAT1 version 8.01 software.

3.4 Results and Discussion

3.4.1 Surface characterisation of VTES silanisation strategies

WCA measurements were used to track surface changes resulting from the VTES modification of glass for the thiolene attachment of thiol modified oligonucleotides. The resulting values are shown in Table 8. The measured WCA increased from $5.2 \pm 0.4^\circ$ for the plasma oxidised glass surface to $70.2 \pm 1.6^\circ$ after treatment with VTES. This was expected as the VTES modified surface contains exposed vinyl groups that are more hydrophobic than the polar silanol groups found on the surface after plasma oxidation, thus resulting in an increased WCA. Treatment of the VTES surface with the SH-probe resulted in a decrease in the WCA to $62.4 \pm 2.2^\circ$ which can be attributed to the polar nature of the attached oligonucleotides increasing the level of hydrogen bonding, subsequently decreasing the WCA.

When compared to the resulting WCA for the APTES silanised glass slides ($37.8 \pm 3.4^\circ$) reported in Chapter 2, the VTES silanised glass slide WCA was significantly higher ($70.2 \pm 1.6^\circ$). This was due to the greater hydrophobic properties exhibited by the exposed vinyl group at the surface. In contrast, the amine modified surface in Strategy A has the ability to hydrogen bond with water leading to a more polar surface and lower WCA. It was proposed that this increase in hydrophobicity, exhibited by the VTES silanised surface, should result in a significant reduction in non-specific adsorption of oligonucleotides.

Table 8: Resulting step-wise WCA measurements for the VTES modified glass substrates (n= 3, \pm standard deviation)

Reaction Step	WCA measurement
Plasma oxidised surface	$5.2 \pm 0.4^\circ$
VTES silanisation	$70.2 \pm 1.6^\circ$
SH-Probe attachment	$62.4 \pm 2.2^\circ$

Comparison of the oligonucleotide modified surfaces prepared using the APTES surface ($47.2 \pm 5.1^\circ$, Chapter 2) and the VTES surface ($62.4 \pm 2.2^\circ$) also shows a significant variation in resulting WCA. Here, the APTES method resulted in a lower WCA. This was attributed to the surrounding polar amine groups available for hydrogen bonding. Increased oligonucleotide attachment could also reduce WCA values as well as

oligonucleotide orientation at the surface. As hypothesised in Figure 29, oligonucleotides lying flat on the surface (amine surface) versus end-to-end (vinyl surface) would result in a higher WCA, due to the greater surface coverage. The polar APTES modification strategy can promote the flat orientation of oligonucleotides at the surface, leading to a greater surface coverage and subsequent decrease in WCA. This would be due to electrostatic interactions between the modified substrates and the negatively charged phosphate groups of the attached oligonucleotides [176, 177]. The vinyl modification strategy however promotes end-to-end attachment due to the repulsion between the hydrophobic surface and polar oligonucleotides. This decrease in surface coverage would lead to the higher recorded WCA. This end-to-end attachment should theoretically increase hybridisation at the surface due to the higher number of available probes for hybridisation.

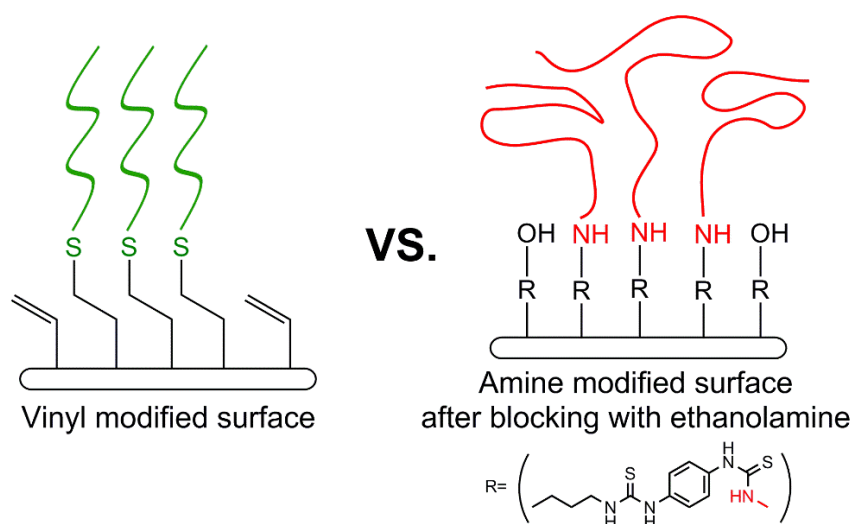


Figure 29: Hypothesised interactions between the oligonucleotides and two silanised glass substrates

Promotion of end-to-end orientation due to the hydrophobic vinyl modified surface (left) compared to the hindered ethanolamine blocked hydrophilic amine modified surface (right)

3.4.2 Oligonucleotide attachment to VTES silanised glass substrates

Having established that the VTES modification strategy was possible as an attachment method for oligonucleotides, a univariate optimisation of reaction variables was completed to maximise hybridisation at the vinyl modified surface. The variables investigated included i) VTES silanisation time, ii) SH-probe irradiation time and iii) hybridisation time.

In order to evaluate the effect of different reaction conditions on final hybridisation, the fluorescence intensity of the final hybridised surfaces was monitored at each condition. Previous research by Escorihuela *et al.* used WCA measurements to evaluate the time required for maximum VTES silanisation of the glass surface [113]. In this research the fluorescence intensity of the hybridised glass surfaces was monitored to give a more accurate representation of how silanisation time influences the final hybridisation of the surface. Furthermore, probe attachment optimisation completed by Escorihuela *et al.* used the attachment of fluorescently labelled oligonucleotide probes to evaluate optimal attachment conditions [113]. Using this method, the initial level of oligonucleotide probe attachment was not indicative of final hybridisation efficiency. Therefore, in this study the final hybridised surface was evaluated directly for all experiments.

i) VTES silanisation time

To determine optimal silanisation time with VTES, reaction times ranging from 10 to 120 min were investigated. Figure 30 shows that after a 30 min silanisation with VTES, the signal: background ratio plateaus. Shorter silanisation times resulted in a high level of variation between the triplicate oligonucleotide modified spotted regions as evidenced in Figure 30. The greatest reproducibility was observed using a 120 min silanisation with VTES. As the overall aim of this work was to create an analytical device for the quantification of HAB microalgae, the 120 min silanisation time was selected in order to provide a reliable detection platform with optimum reproducibility. This also correlated with the 120 min silanisation time calculated using WCA measurements as reported by Escorihuela *et al.* [113].

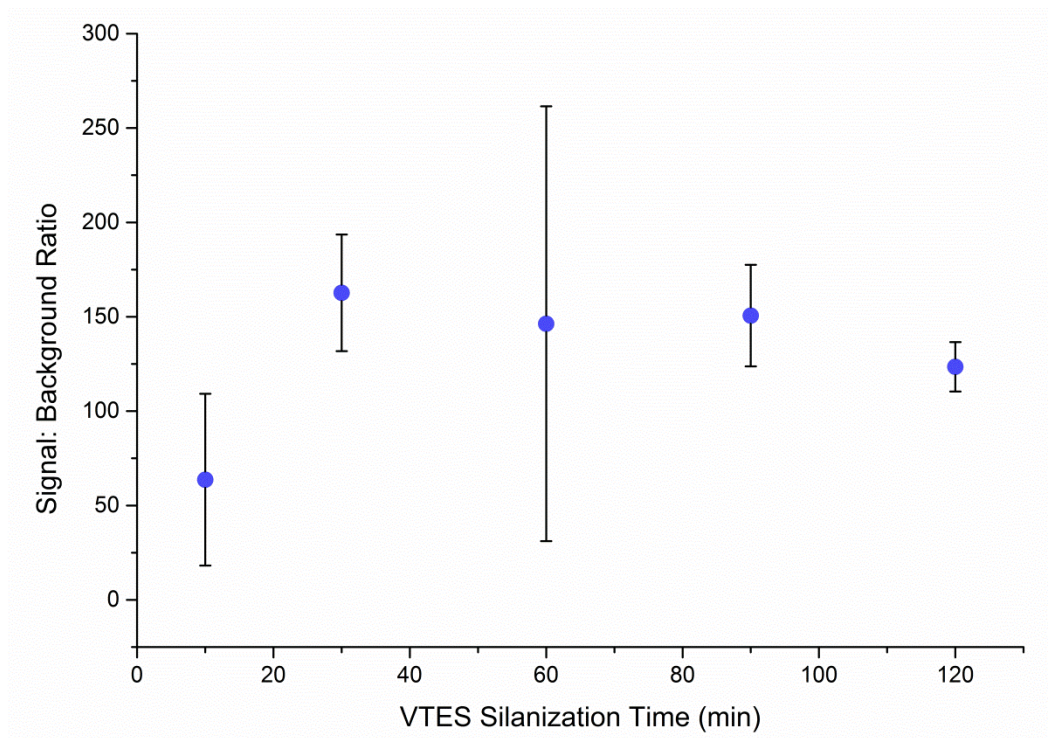


Figure 30: Effect of VTES silanisation time on the final hybridisation efficiency of the modified glass surface

Average signal: background ratios analysed on the Olympus IX-73 (n= 3, ± standard deviation)

ii) *SH-Probe irradiation time*

Escorihuela *et al.* reported that a 20 min irradiation time was required for optimal immobilization of the thiol oligonucleotide to the surface using a thiol-ene click chemistry approach [113]. It was important to note that there are some experimental differences between the Escorihuela *et al.* method [113] and the one reported herein. Spot size of the oligonucleotide probe deposited by Escorihuela *et al.* was significantly smaller, with 40 nL being spotted on the slide using a non-contact printing system. In this work 2 μ L of manually spotted SH-probe was used. Manual pipetting of such small volumes can result in reduced reproducibility, compared to automated spotting methods [181], however an automated microarray printer was not available for this research. Additionally, the distance from the UV lamp also varied. Escorihuela *et al.* reported a distance of ≈ 0.5 cm (light intensity 6 $\text{mW}\cdot\text{cm}^{-2}$), whereas the distance used in this work was ≈ 3 cm (light intensity 0.35 $\text{mW}\cdot\text{cm}^{-2}$ at 15 cm). This greater distance from the light source to the surface results in divergence of the UV light, reducing the intensity reaching the surface based on the optical inverse square law [182]. Thus, the greater distance used in this experimental procedure would result in a lower intensity of light than the method

described by Escorihuela *et al.* Therefore, it was expected that longer irradiation times would be required for optimal SH-probe attachment in this study. As such, an optimisation using the conditions specified in Section 3.3.3 of the irradiation time between 5 to 60 min at 365 nm was investigated.

Preliminary experiments demonstrated that the positioning of the glass surface under the UV lamp heavily influenced the rate of evaporation of the solvent from spotted SH-probe solution. The drying of the oligonucleotide solution on the surface hinders movement of the oligonucleotide towards the vinyl surface, influencing the rate and final density of the attached oligonucleotides. To prevent this, the distance of the surface from the UV lamp was kept at ≈ 3 cm for all experiments.

As shown in Figure 31, increasing the irradiation time resulted in an increase in both the magnitude and variation of the recorded signal: background ratios. The increase in signal: background ratios was consistent with an increased level of oligonucleotide probe attachment. The increase in variation was attributed to uneven solvent evaporation, also observed in previous optimisation experiments for the APTES modified glass in Chapter 2 (Section 2.4.2). A longer irradiation time resulted in evaporation of the spotted SH-probe regions, limiting attachment to the surface. As such, longer irradiation times were not investigated, as the drying effect would only further hinder attachment of the probe to the vinyl terminated surface. As shown in the Figure 31 fluorescence microscope images for the 60 min irradiation time ($n=3$), the “coffee-spot” effect was present, where a higher fluorescent signal was observed at the outer rim of the circle compared to the centre of the circle. This was further evidence of evaporation during attachment, with a capillary flow action drawing the solute to the edge of this contact angle leading to a ring-shaped deposition on the outer rim of the droplet [168]. Use of a uniform UV light source could eliminate the variable evaporation observed due to uneven drying and result in improved probe attachment at the surface. A 30 min irradiation time was selected for maximum attachment of thiol modified oligonucleotides to the vinyl terminated surface as this resulted in minimal evaporation.

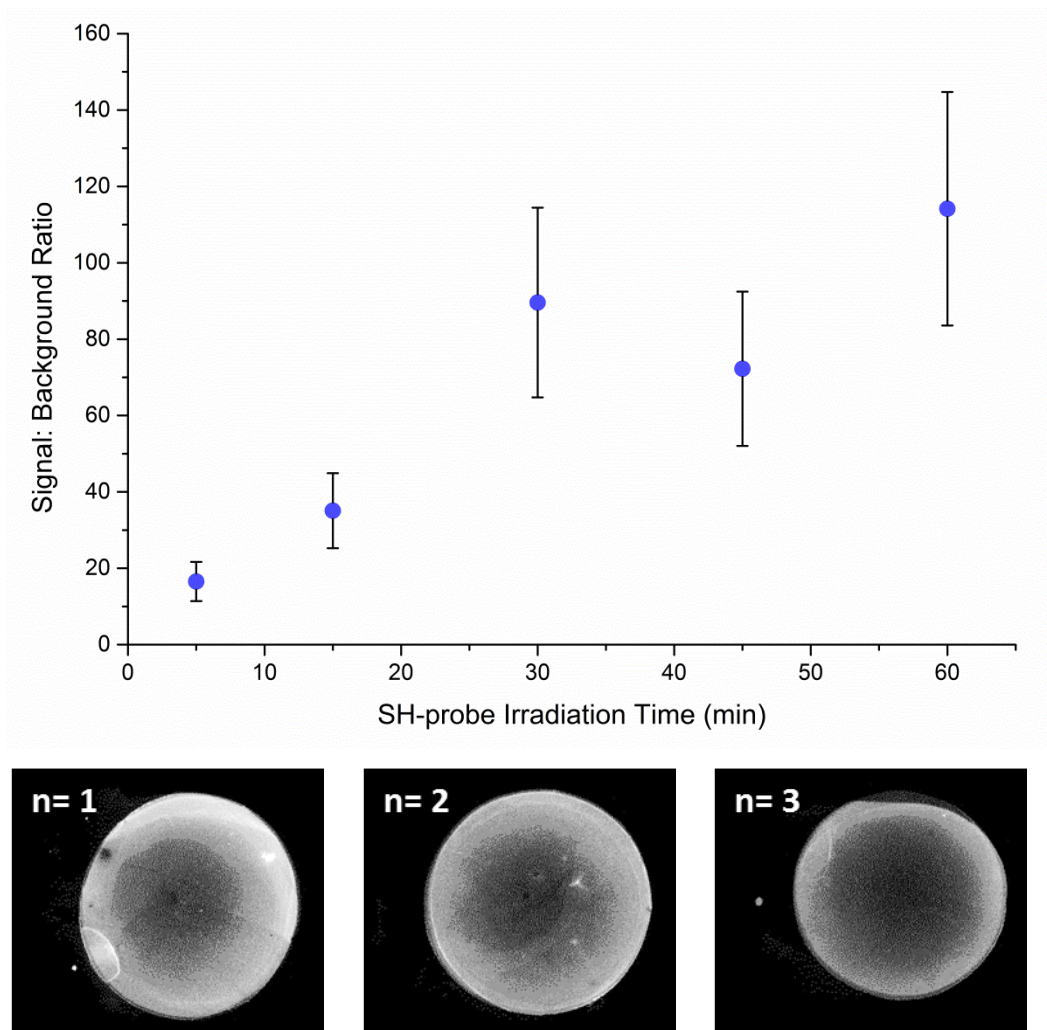


Figure 31: Effect of irradiation time on SH-probe thiolene attachment to vinyl modified glass slide surfaces

Average signal: background ratios analysed on the Olympus IX-73 (n= 3, \pm standard deviation) with corresponding fluorescence microscope images of the 60 min irradiation time samples (n= 3). Image brightness increased 80% for visualisation.

iii) Hybridisation time

Maximising the hybridisation of target sequences with the modified surface is important for achieving the low detection limits required for HAB detection. Consequently, an optimisation of hybridisation times for the complimentary Cy5 labelled ACat Seq was required for optimal performance and sensitivity of the oligonucleotide modified substrate. Hybridisation times between 10 to 80 min were investigated.

Escorihuela *et al.* reported an optimal hybridisation of 45 min at 37 °C when detecting PCR products of *Escherichia coli*. [113]. This hybridisation method used 50 µL of fluorescently labelled target, spread across the oligonucleotide modified surface using a coverslip. During preliminary experiments, this same method for hybridisation was trialled on the modified surfaces prepared in this study. Although thought to minimise evaporation of spotted sequence observed in previous experiments, the hybridisation method resulted in a significant increase in background fluorescence intensity. Due to this, the coverslip hybridisation approach was not investigated further and instead the manual spotting of ACat Seq was employed.

As shown in Figure 32, the maximum fluorescence intensity was obtained after a 60 min hybridisation followed by a slight decrease at the longer hybridisation time of 80 min. A high level of variation was also observed for both the 60 min and 80 min hybridisation times between the triplicate spots analysed on the same slide. Similar to previous results, the high level of variability for the 60 and 80 min hybridisations was associated with drying of the spotted ACat Seq region during longer exposure times at 40 °C. Consequently, longer hybridisation times were not investigated to improve signal: background ratios. A hybridisation time of 40 min was selected for all subsequent experiments as it provided a good compromise between signal intensity and reproducibility.

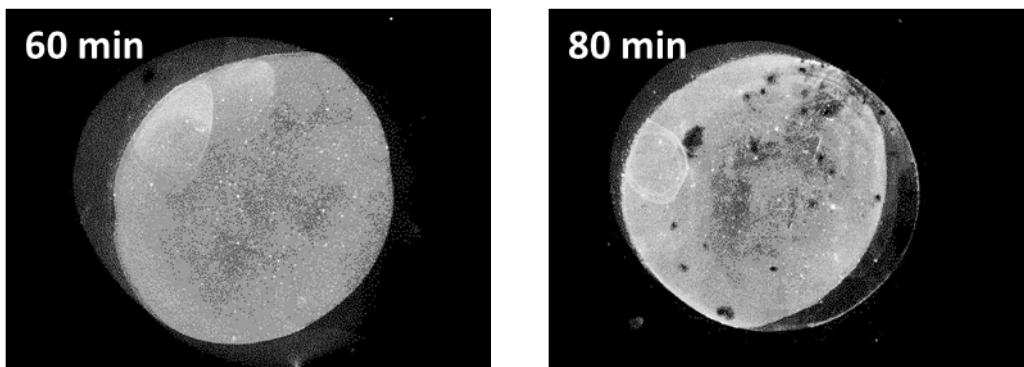
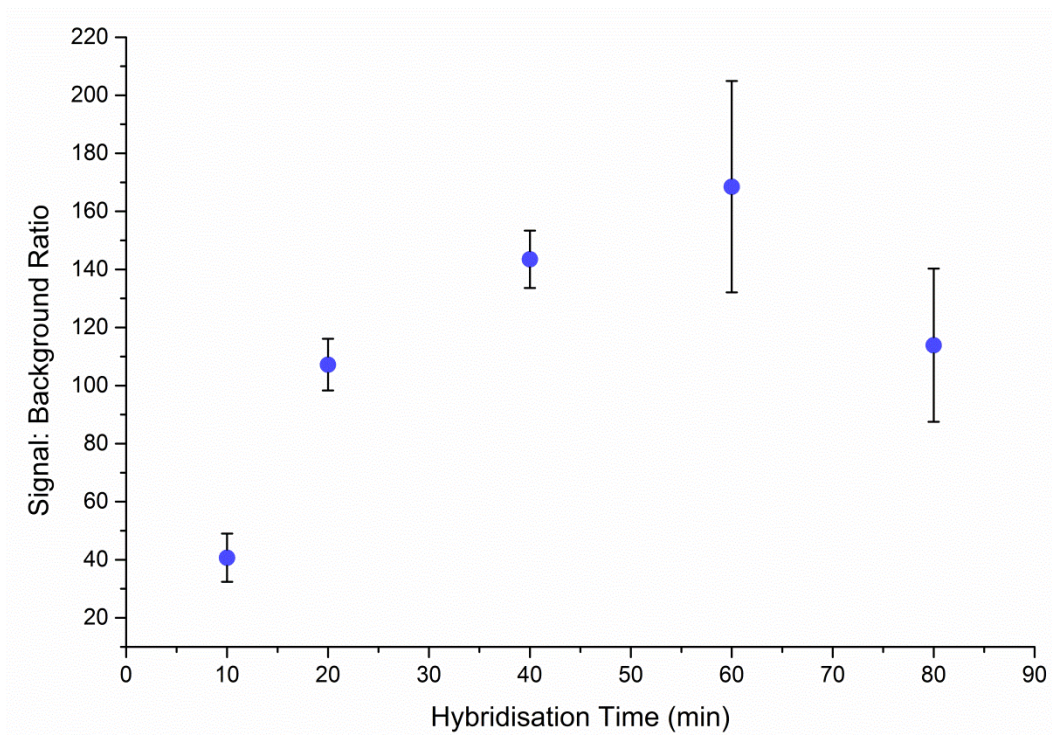


Figure 32: Effect of hybridisation time on the final signal: background ratio of the VTES modified region

Average signal: background ratios analysed on the Olympus IX-73 (n= 3, \pm standard deviation) with corresponding fluorescence microscope images of the 60 min and 80 min hybridisation demonstrating coffee-ring effect from evaporation. Image brightness increased 80% for visualisation.

The final conditions used for the modification of glass slides using the VTES silanisation strategy can be seen in Table 9. When compared to the conditions discussed in Chapter 2, the total modification time using APTES was significantly less than the discussed VTES modification (Table 9). The APTES strategy required an oligonucleotide attachment and hybridisation time of 150 min with the alternative VTES method taking 190 min. Despite

this, the VTES method provided a much simpler modification that requires no blocking of the surface prior to hybridisation. This was due to the hydrophobic surface reducing electrostatic interactions involved in non-specific adsorption. The VTES method also has the advantage of not using toxic reagents, such as the PDITC, used in the APTES modification strategy. When comparing the optimised method in this study with that reported by Escorihuela *et al.* [113] there are some differences in reaction times. The silanisation time with VTES was the same and the hybridisation time only differed by 5 min. However, the time required for maximum SH-probe attachment varied the most with this method taking 60 min and the method described by Escorihuela *et al.* only taking 20 min [113]. This was expected due to the experimental differences between each method influencing the overall attachment chemistry as discussed previously. Distance of the surface from the UV light source was the most likely cause for the greater attachment time required using this method. When compared to the method described by Escorihuela *et al.* [113] our method distanced the surface \approx 3 cm from the UV light source, at a 6 times greater distance than described by Escorihuela *et al.* The extended distance in this study was used to minimise evaporation, however increasing the distance also resulted in a decrease in UV intensity based on the optical inverse square law [182]. Furthermore, the lamp used by Escorihuela *et al.* was a high power mercury capillary lamp, which would result in variations of attachment efficiency. One way to overcome these variations in SH-probe attachment time would be to use a high powered mercury capillary lamp for oligonucleotide attachment. Alternative light sources for UV photoinitiated attachment were not available for this study and thus could not be investigated.

Table 9: Final reaction conditions for the APTES and VTES modification compared to the Escorihuela *et al.* conditions [113]

Conditions	Optimised APTES method (min)	Optimised VTES method (min)	Escorihuela <i>et al.</i> [113] VTES method (min)
Silanisation	20	120	120
Probe attachment	100 *	30	20
Hybridisation	30	40	45

* Probe attachment time includes attachment of PDITC cross-linker

3.4.3 Selectivity comparison between VTES and APTES modified glass substrates

In order to obtain discriminative information on the microalgae species present in a natural seawater sample, the selectivity of oligonucleotide modified surfaces is very important. In order to compare the selectivity of the two surfaces, both the optimised VTES and APTES modified glass slides were subjected to a hybridisation with complimentary Cy5 labelled ACat Seq and a non-complimentary Cy5 labelled sequence (5'- CTGGGATATCTGCACCAGC-3'). The resulting fluorescence intensities were recorded to determine if there was any cross-reactivity with the non-complimentary oligonucleotide sequence. The resulting signal: background ratios are shown in Figure 33.

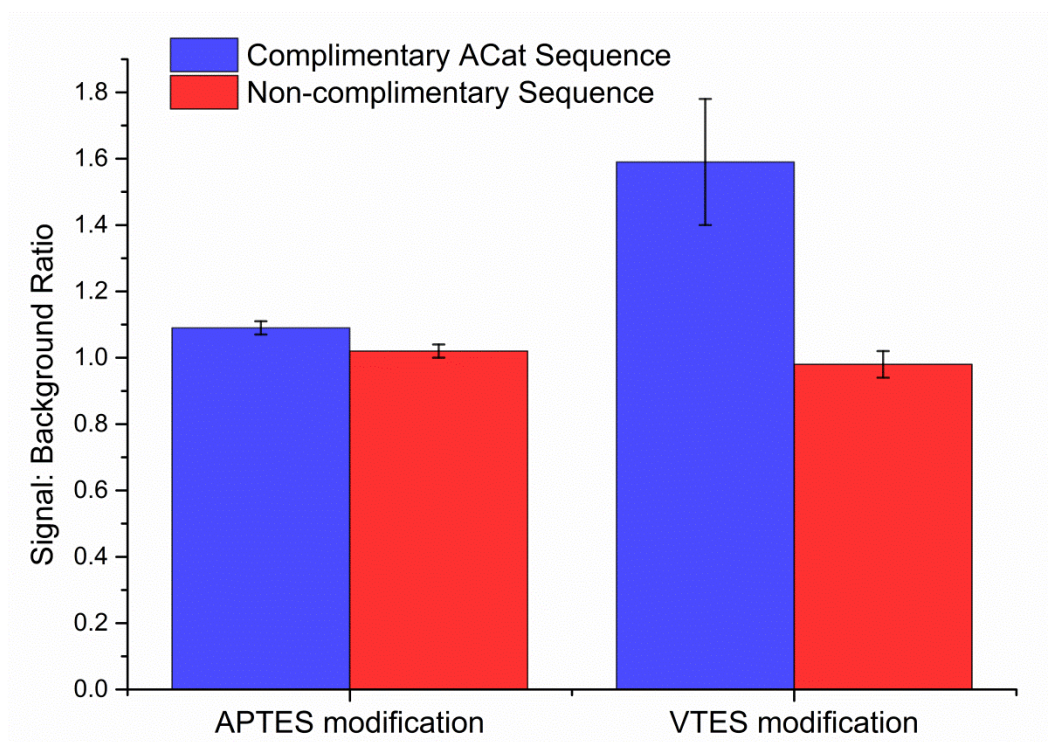


Figure 33: Selectivity of the APTES and VTES modified glass surfaces for complimentary and non-complimentary target sequences

Average signal: background ratios analysed on the Olympus IX-71 (n= 3, \pm standard deviation) using a bulk solution hybridisation.

The VTES modified surface resulted in a higher signal:background ratio for the complimentary oligonucleotide (1.59 ± 0.19) compared to the non-complimentary oligonucleotide (0.98 ± 0.04) which was close to background (1.00). This difference in signal: background ratios makes it easier to discriminate between the complimentary and non-complimentary sequences. The APTES modified surface exhibited a signal: background ratio that was similar between the complimentary oligonucleotide

(1.09 ± 0.02) and the non-complimentary oligonucleotide (1.02 ± 0.02), both being close to background. As such, there was limited evidence on the selectivity of the APTES modified surface as the signal was close to the LOD for the fluorescence microscope.

A greater level of discrimination between the complimentary and non-complimentary target sequences was exhibited by the greater sensitivity VTES modified surfaces. The signal: background ratio for the non-complimentary oligonucleotide was close to background when using both the APTES and VTES modification strategies suggesting the signal produced by hybridisation was below the limits of detection.

3.4.4 Direct comparison of APTES and VTES modified glass hybridisation performance

In order to evaluate the performance of the APTES and VTES silanised glass slides, both optimised modifications were compared for sensitivity (VTES and APTES optimised conditions in Table 9). A standard curve was produced using both surfaces to determine if there was a correlation between signal intensity and concentration of target ACat Seq within the range of 0.16 and 1.81 nM (1.6 - 18.1 pmol in 10 mL). If quantitative, a linear response was expected, with an observed increase in fluorescence intensity as the concentration of hybridised Cy5 labelled ACat seq was increased.

Due to the variability issues observed across manually spotted oligonucleotides regions arising from evaporation, an alternative bulk solution hybridisation was implemented as described in 3.3.4. Preliminary results using this alternate hybridisation method demonstrated a significant improvement in spot homogeneity and reproducibility ($n=3$). Furthermore, a stringent two-step washing procedure was employed (details in 3.3.4) and was found to eliminate non-specific adsorption, improve spot homogeneity and increase fluorescent signal reproducibility.

Higher signal: background ratios were obtained over the concentration range when using the VTES modification when compared to the APTES modification (Figure 34). This increase in the signal: background ratio suggests that the VTES modification strategy is able to achieve lower detection limits than the APTES modification approach. The higher sensitivity exhibited by the VTES modification was attributed to the orientation of oligonucleotides at the surface as hypothesised in Chapter 3 (Figure 29, Section 3.4.1). If the oligonucleotides are attached end-to-end on the vinyl surface as hypothesised, the number of available sites for hybridisation is higher; resulting in a greater obtainable

fluorescent signal. The VTES modified surface also resulted in a linear increase ($R^2 = 0.954$) over the concentration ranges making it a viable quantitative method for the detection of the target sequence and as a potential platform for the detection of HAB causative microalgae.

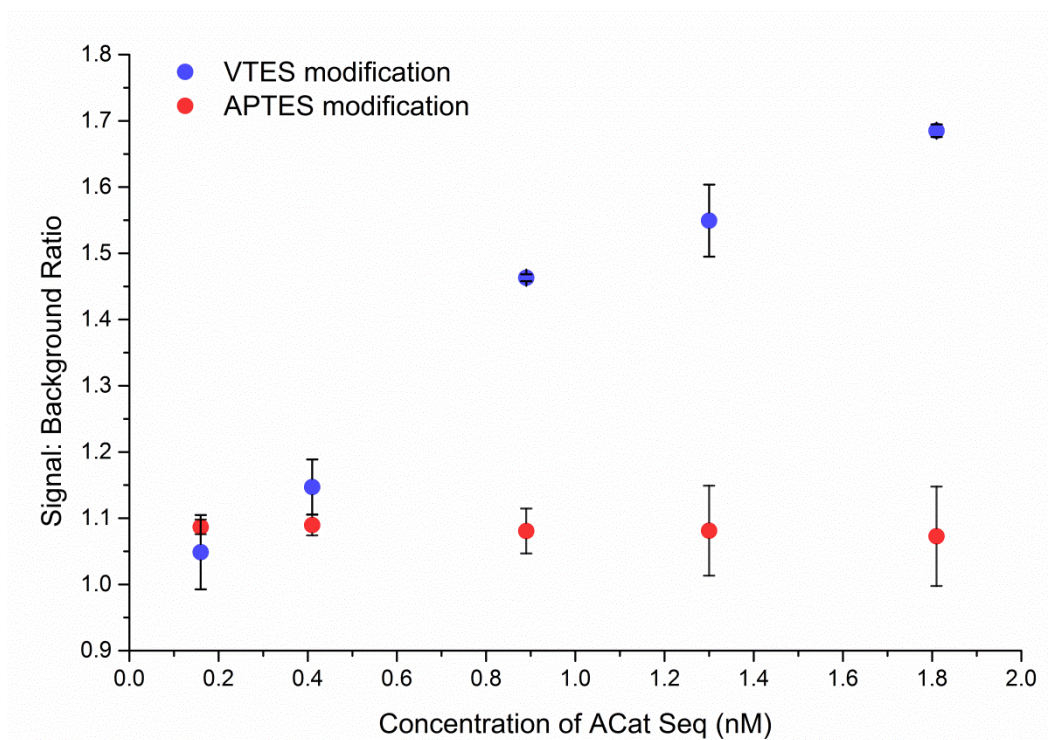


Figure 34: Standard curve for target ACat Seq generated using the APTES (red) and VTES (blue) modified glass surfaces

Average signal: background ratios analysed on the Olympus IX-71 (n= 3, \pm standard deviation) using a bulk solution hybridisation.

The standard curve prepared using the APTES modified glass surface did not exhibit a linear response as demonstrated by the VTES modified surface. Similar levels of fluorescent intensity were recorded across the concentration range investigated (signal: background between 1.07 and 1.09) making this approach unsuitable for quantification. Lower signal: background ratios were also obtained for the APTES modified surface suggesting hindrance of the hybridisation of the target sequence with the covalently attached oligonucleotides at the surface. This hindrance was hypothesised to be due to the effect discussed in Section 3.4.1 (Figure 29). In the case of the APTES modified surface, the polar surface promotes the flat orientation of oligonucleotides via electrostatic interactions with the surface, hindering hybridisation and resulting in much lower signal intensities [183].

Lower concentrations were investigated for both the VTES and APTES modified surfaces however, the signals obtained were below the instruments LOD making identification of the hybridised regions impossible. Overall, the VTES modified surface proved superior to the alternative APTES modified surface with the potential for quantitative analysis and higher obtainable signal: background ratio across a broad range of target concentrations. Therefore, the VTES modification strategy was used for all subsequent surface performance experiments.

3.4.5 Regeneration capacity of VTES modified glass substrates

When developing microarray devices, re-usability of the surface is favourable as it allows for a more cost effective and time efficient analysis as the preparation of new surfaces is not required [184, 185]. In order to evaluate the re-usability of the VTES modified surfaces a hybridisation, de-hybridisation and re-hybridisation cycle was used to evaluate the reusability of the surface and loss of fluorescent signal upon re-hybridisation.

Initial investigations into the regeneration capabilities for the VTES modified surface were completed using a single regeneration cycle (hybridisation, de-hybridisation then re-hybridisation). As shown in Figure 35, a 2 h de-hybridisation at 80 °C was found to completely remove hybridised Cy5 labelled ACat Seq (signal: background ratio \approx 1.0). At these de-hybridisation conditions, a loss of 52 % of the initial fluorescence signal was recorded upon re-hybridisation of the VTES surface. These preliminary results suggest that there was significant loss in reactivity of the surface during de-hybridisation when using these conditions, leading to poor regeneration of the surface upon re-hybridisation.

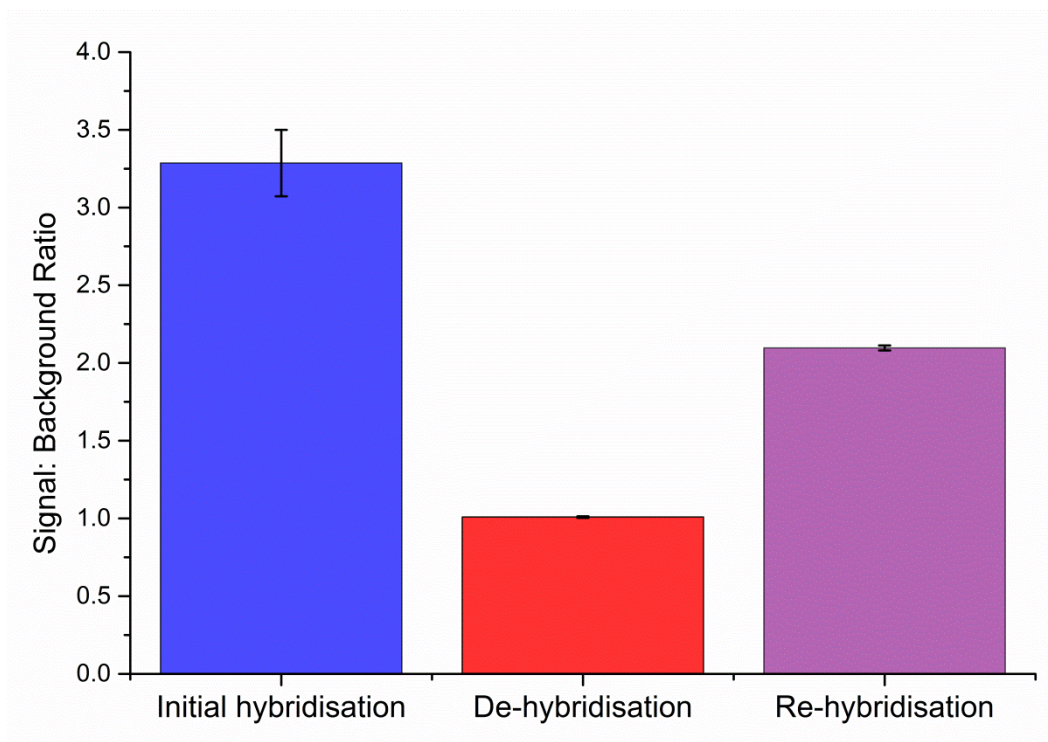


Figure 35: Regeneration capacity of the VTES modified glass surface for 120 min at 80 °C

Average signal: background ratios after one regeneration cycle analysed on the Olympus IX-71 (n= 3, ± standard deviation) using a bulk solution hybridisation.

The recorded loss in reactivity of the surface upon re-hybridisation was due to oligonucleotide degradation using the specified de-hybridisation conditions. It was hypothesised that this was either due to i) the water matrix being used for oligonucleotide de-hybridisation resulting in hydrolysis, ii) the high temperature (80 °C) or iii) extended exposure time (120 min) leading to thermal degradation. Each of these variables was investigated to try to improve the surface regeneration capabilities for the VTES modified surface.

To identify if acid hydrolysis was the cause of degradation, de-hybridisation was trialled in buffered systems (pH 7 and 8, Appendix, Figure 58 and Figure 59). Preliminary results demonstrated that moving to buffered systems did not improve the re-hybridisation of the surface compared to those in ultra-pure water confirming that acid hydrolysis was not the cause of degradation. This is consistent with previous research, which has also demonstrated that the phosphodiester linkages, such as the linkages that join DNA nucleotides, are relatively resistant to hydrolysis in water [186, 187].

3.4.5.1 Effect on de-hybridisation time on the complete removal of Cy5 labelled ACat Seq using VTES modified glass substrates

Optimisation of the time required for de-hybridisation of the VTES modified surface was tested to evaluate whether thermal degradation may be occurring from long exposure times at 80 °C. The previous extended de-hybridisation time was chosen as theoretically it should be able to completely de-hybridise ACat Seq from the surface. However, the extended exposure to high temperatures may be resulting in thermal degradation. To determine the minimum time required for de-hybridisation a range of de-hybridisation times between 10 min to 120 min at 80 °C were tested. As shown in Figure 36, the signal of the de-hybridised surface remained close to 1.0 for all slides over each time tested suggesting that the time required for de-hybridisation could be reduced from 120 min to 10 min.

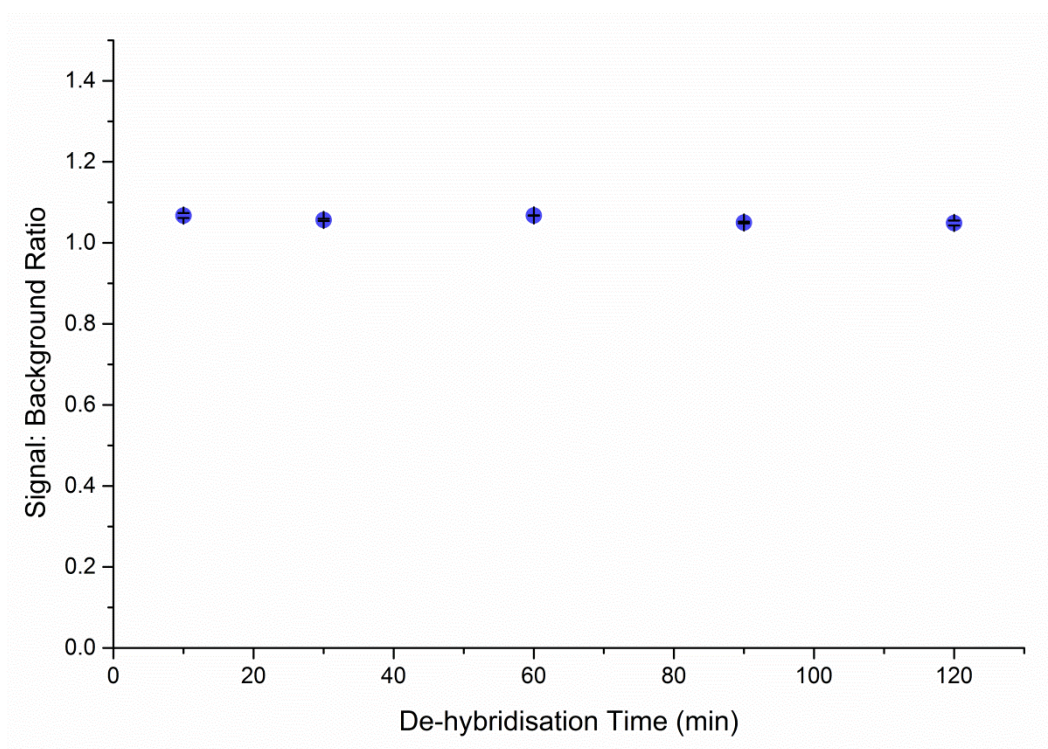


Figure 36: Effect of de-hybridisation time on the complete removal of hybridised Cy5 labelled target sequence

Average signal: background ratios for the de-hybridised surface analysed on the Olympus IX-71 (n= 3, \pm standard deviation) using a bulk solution hybridisation.

As shown in Figure 37, upon re-hybridisation of the 10 min de-hybridised surface, a 24 % reduction in signal was recorded when compared to the initial hybridised surface signal: background ratio. Compared to the 120 min de-hybridisation, which resulted in a 52 % loss in signal: background ratio upon re-hybridisation, a significant improvement in regeneration of the surface was achieved by decreasing the de-hybridisation time to 10 min.

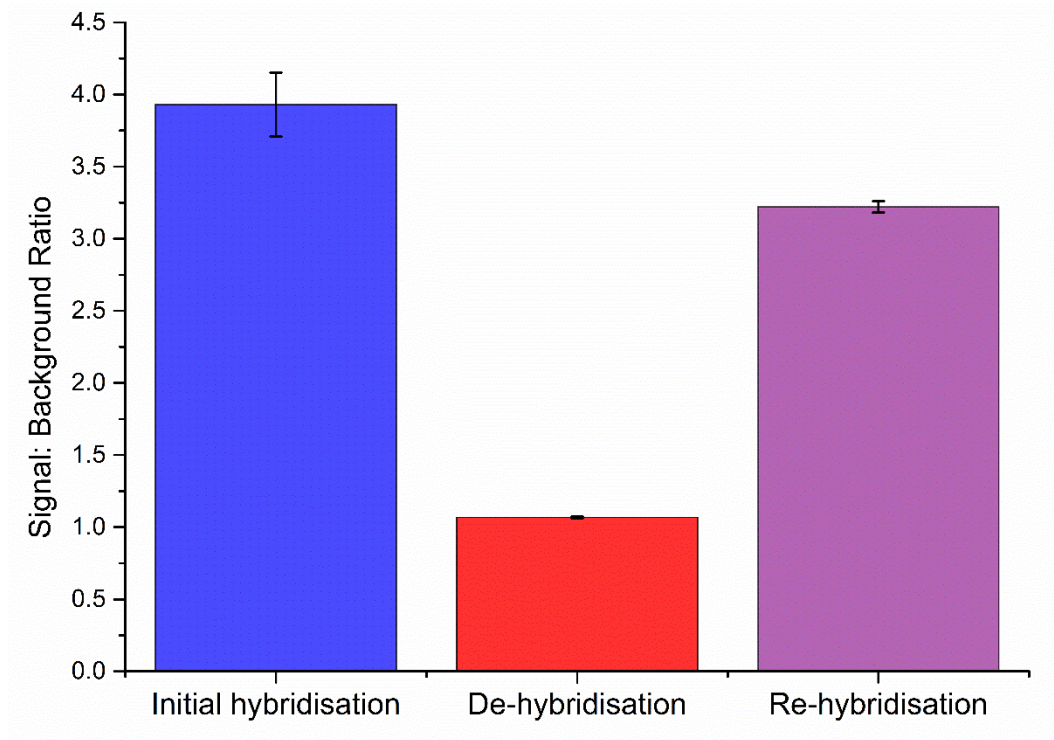


Figure 37: Regeneration capacity of the VTES modified glass surface after de-hybridisation for 10 min at 80 °C

Average signal: background ratios after one regeneration cycle analysed on the Olympus IX-71 (n= 3, ± standard deviation) using a bulk solution hybridisation.

3.4.5.2 Effect on de-hybridisation temperature on the complete removal of Cy5 labelled ACat Seq using VTES modified glass substrates

Due to the improved regeneration of the signal observed when reducing the time required for de-hybridisation, an optimisation of temperature was also tested. The reduction in exposure time of the glass slide significantly improved the regeneration capabilities of the surface and as such, temperature may be influencing the degradation of probe on the surface. The melting temperature (T_m) of the SH-ACat probe used in this

study was 59.4 °C, suggesting that at lower temperatures than the 80 °C, de-hybridisation could still be achieved. Temperatures for de-hybridisation were tested at 60, 70 and 80 °C to evaluate if thermal degradation at 80 °C is the cause of the regeneration issues. The signals of the slides after de-hybridisation at the different temperatures are shown in Figure 38. Here a relatively similar signal: background ratio was obtained over the three different temperatures. As such, it was decided that the de-hybridisation temperature could be decreased to 60 °C for the complete removal of previously hybridised ACat Seq.

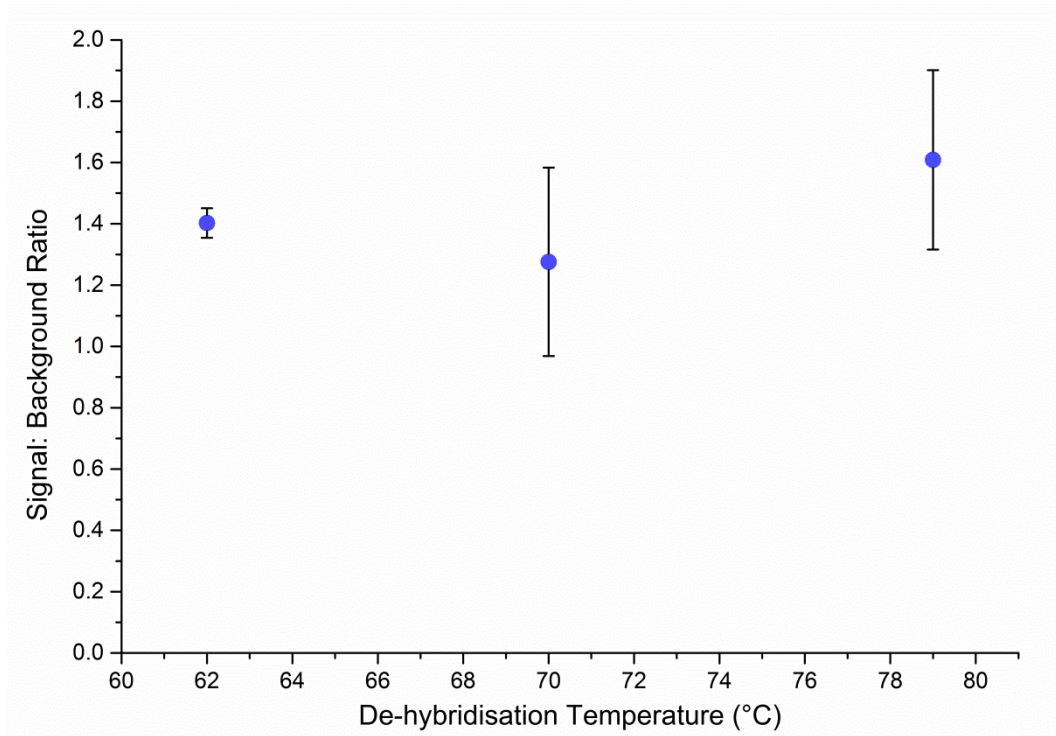


Figure 38: Effect of de-hybridisation temperature (°C) on the complete removal of hybridised Cy5 labelled target sequence

Average signal: background ratios for the de-hybridised surface analysed on the Olympus IX-73 (n= 3, ± standard deviation) using a bulk solution hybridisation.

As shown in Figure 39, regeneration of the surface using a 60 °C de-hybridisation for 10 min and subsequent re-hybridisation only resulted in a loss of signal of 0.7 %, well within the error margin. This was a significant improvement to the previous methods demonstrating that the excessive de-hybridisation time and temperature heavily influenced the stability of attached oligonucleotides on the surface. This data suggests that the high temperatures used for de-hybridisation resulted in damage of the attached oligonucleotides. This would effectively decrease the number of available sites for

hybridisation causing a subsequent loss in fluorescent signal intensity upon re-hybridisation. Overall, the VTES modified surface was found to be effectively be re-used, with minimal loss in reactivity, over one regeneration cycle when using a 60 °C de-hybridisation for 10 min.

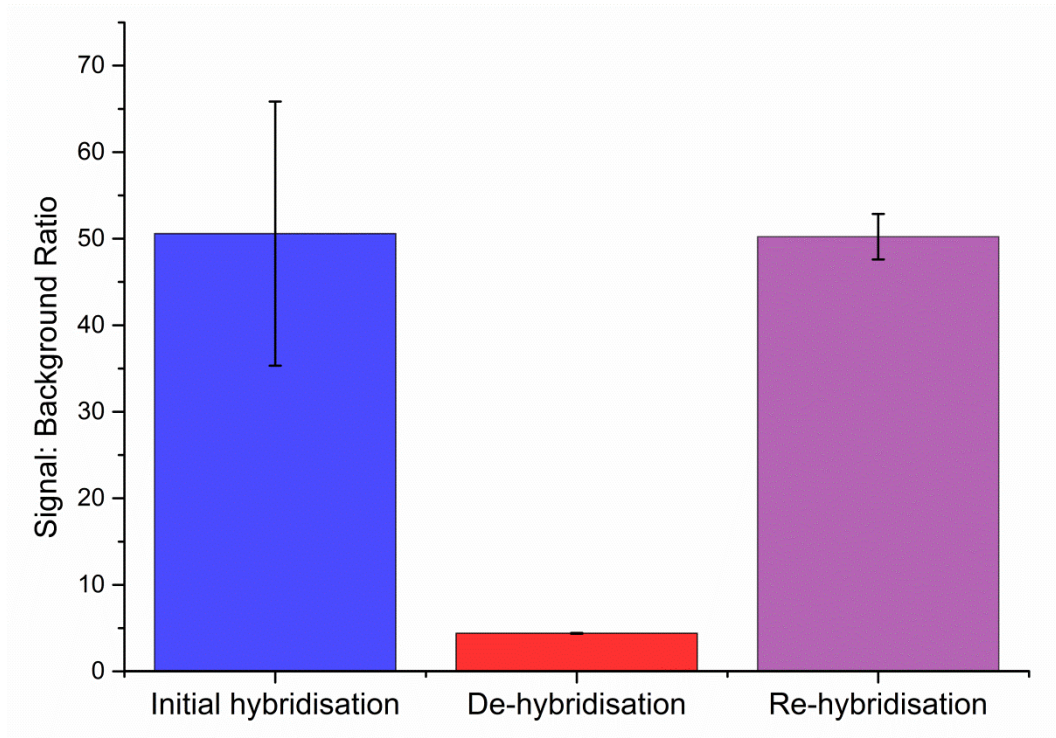


Figure 39: Regeneration capacity of the VTES modified glass surface after de-hybridisation for 10 min at 60 °C

Average signal: background ratios after one regeneration cycle analysed on the Olympus IX-73 (n= 3, ± standard deviation) using a bulk solution hybridisation.

3.5 Conclusions

In this chapter, the APTES modification (Chapter 2) and a VTES modification chemistry for oligonucleotide attachment were investigated to ascertain how reaction chemistry influences hybridisation performance of the surfaces. When preparing surfaces for the detection of HAB causative microalgae, both sensitivity and selectivity need to be investigated. Quantitative analysis is also beneficial as it allows for tracking of a bloom formation over time. These variables were investigated using model hybridisation experiments on both the APTES and VTES modified surfaces.

The optimised VTES modification performed better in a number of aspects when compared to the APTES modification. The attachment using the VTES can be achieved in a simple two-step reaction with no need for blocking of the surface prior to hybridisation or the use of toxic cross-linkers such as PDITC. The VTES modification reported also resulted in a linear relationship between concentration of target sequence (ACat Seq) and the recorded signal: background ratio, demonstrating its suitability for quantitative analysis of HAB causative microalgae. The VTES oligonucleotide modification approach also resulted in a much higher signal: background ratio demonstrating this method provides a greater level of sensitivity compared to the APTES oligonucleotide modification. Selectivity studies using complimentary and non-complimentary Cy5 labelled target oligonucleotides showed that the VTES strategy resulted in a high level of selectivity with non-complimentary signals being close to background (1.0).

Regeneration capabilities of both the APTES and VTES modified glass substrates was investigated using a single hybridisation, de-hybridisation, re-hybridisation cycle. The APTES strategy sensitivity was too low to discriminate between the hybridised and de-hybridised surface and so was not used for further studies. The VTES modified surface however was regenerated with minimal loss (0.7 %) in signal intensity upon re-hybridisation when using a 10 min de-hybridisation at 60 °C. This suggests that the VTES modified surface can be regenerated for further use which was an important feature when developing sensor detection systems [116].

Overall, it was demonstrated that the VTES modification for glass provided the greatest sensitivity, selectivity and regeneration capabilities when compared to the APTES modification strategy optimised in Chapter 2 making it a viable modification option for the sensitive and selective detection of HAB causative microalgae in the future

4

Covalent attachment of oligonucleotides to vinyl terminated silica nanoparticles

This chapter describes an adaptation of the VTES attachment strategy for glass surfaces discussed in Chapter 3 for use on higher surface area nanoparticles. Results discussed include:

- *The synthesis and characterization of vinyl terminated silica nanoparticles*
- *Model attachments of 1-dodecanethiol to vinyl terminated silica nanoparticles to ascertain whether thiolene attachment is feasible on this high surface area platform and attainable attachment densities*
- *Trial attachment of thiol modified oligonucleotides to vinyl terminated nanoparticles as a proof of concept*

4.1 Introduction

Covalent methods for the attachment of oligonucleotides to planar surfaces, such as glass, have been vastly researched [109, 110, 112, 113, 115, 156, 188]. More recently, covalent attachment chemistries have been shifted towards using high surface area platforms such as nanoparticles [124]. Use of these surfaces as a solid support is hypothesised to increase loading capacities of the attached oligonucleotide probe resulting in improved sensitivity of detection. As discussed in Chapter 3, glass was found to be an effective substrate for the covalent attachment of oligonucleotides. As such, this research focuses on the use of silica nanoparticles as they share similar chemical characteristics to silica glass surfaces.

Thiol modified oligonucleotides have been attached to thiol terminated nanoparticles previously via a dithiol attachment mechanism [143]. Synthesis of these thiol terminated nanoparticles required a two-step reaction. First, silica nanoparticles were generated using tetraethylorthosilicate (TEOS) followed by subsequent silanisation using MPTS to create a thiol terminated surface (Figure 40). Thiol modified oligonucleotides were subsequently attached to the surface and fluorescently labelled targets (FAM) were used for hybridisation and detection [143]. This method allowed for the detection of target oligonucleotides up to 5 nM, however optimal surface performance was limited to only one day storage [143]. This same dithiol chemistry for oligonucleotide attachment was described using glass slide surfaces in Section 3.1 [112]. The resulting dithiol modification is susceptible to reductive cleavage [106] and is vulnerable to side reactions that convert reactive thiols into the sulfonate form [106, 179] hindering attachment. Both of these issues impact stability resulting in a decreased level of sensitivity.

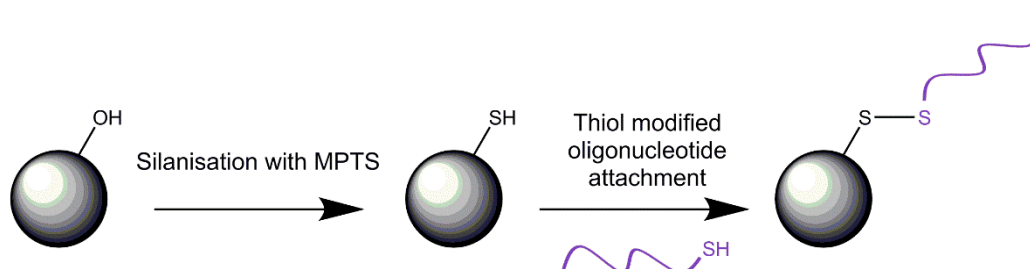


Figure 40: Dithiol attachment of thiol modified oligonucleotides to MPTS silanised silica nanoparticles

Alternatively, a thiolene attachment can overcome these issues as the thioether bond formed is less susceptible to reductive cleavage, resulting in a stable attachment at the surface. Based on the results obtained in Chapter 3, the thiolene attachment of oligonucleotides was found to provide a sensitive, selective method for target sequence hybridisation on glass slides. The use of a thiolene attachment for oligonucleotides on silica nanoparticles has so far not been reported in literature.

Model thiolene click-chemistry attachments using 11-bromo-1-undecene to thiol terminated silica nanoparticles using the thiolene mechanism described in Chapter 3 (Figure 27) have been previously reported by Mangos *et al.* [189]. Use of this model reaction allowed for the viability of attachment to be tested as well as theoretical attachment densities to be calculated. Analysis of the surface attachment densities was tracked using a non-destructive, attenuated total reflection Fourier transform infrared spectroscopy (ATR-FTIR) method. Here, ATR-FTIR absorption changes associated with attachment were monitored relative to a standard reference peak that is specific to the nanoparticle core, remaining unchanged during attachment. From this a calibration curve was generated and theoretical attachment densities of reacted nanoparticles calculated. In this study, attachment densities of 4.9 attachments.nm⁻² of the 11-bromo-1-undecene were reported after only a 60 min irradiation at 365 nm.

4.2 Scope of study

Chapter 3 demonstrated that the thiolene attachment of thiol modified oligonucleotides to vinyl terminated glass slides was able to selectively hybridise target oligonucleotides in solution. The superior performance exhibited by the vinyl functionalised surface was a significant improvement to the alternative amine modified oligonucleotide attachment mechanism.

The use of an alternative, high surface area platform is hypothesised to further improve detection sensitivity to that demonstrated by the glass slides, based on higher attainable attachment densities. This chapter investigates the use of vinyl terminated silica nanoparticles as an alternative, high surface area substrate for oligonucleotide attachment. Initially model attachment reactions using 1-dodecanethiol were used to demonstrate the feasibility of thiolene attachment using this approach. Furthermore, theoretical attachment densities were calculated using the same ATR-FTIR quantification method described by Mangos *et al.* [189]. After confirmation of attachment using the model 1-dodecanethiol system, a trial attachment with thiol terminated oligonucleotides followed, as a proof of concept study.

4.3 Experimental

4.3.1 Materials

VTES and TCEP were purchased from Sigma-Aldrich, Australia. Ethanol (absolute, 99 %), 1-dodecanethiol and ammonia solution (28-30 % in water) were purchased from Chem-Supply, Australia. All chemicals and reagents were of analytical grade and used as supplied.

Thiol modified oligonucleotides (SH-ACat) and Cy5 labelled ACat Seq were purchased from Integrated DNA Technologies (USA) with the sequences shown in Table 7 (Chapter 3). Ultra-pure water ($18 \text{ M}\Omega\cdot\text{cm}^{-1}$) was used to dilute SH-ACat probe prior to attachment as salt based buffers have been reported to promote nanoparticle aggregation which would inhibit oligonucleotide attachment [190].

4.3.2 Synthesis of vinyl terminated nanoparticles

Vinyl terminated silica nanoparticle suspensions were prepared using a one-pot Stöber synthesis based on the similar method described by Mangos *et al.* for the formation of thiol modified nanoparticles [189]. VTES was added drop wise ($960 \mu\text{L}$, $4.01 \times 10^{-3} \text{ mol}$) to aqueous ammonia (50 mL, 2 %v/v) on a low stir speed. The solution was left to stir slowly for a further 30 min to promote hydrolysis of the VTES. The stir speed was then increased to maximum speed with the reaction mixture left for a further 1.5 h to shift the reaction from hydrolysis to condensation promoting formation of the vinyl terminated nanoparticles (Figure 41). The resulting nanoparticle suspension was then transferred into 10 mL centrifuge tubes and centrifuged at 1700 g for 20 min to obtain a pellet. The nanoparticle pellet was then washed 3 times in ethanol using centrifugation at 1700 g for 20 min. After washing, all nanoparticles were transferred in the same centrifuge tube and made up to a 50 mL stock solution with ethanol.

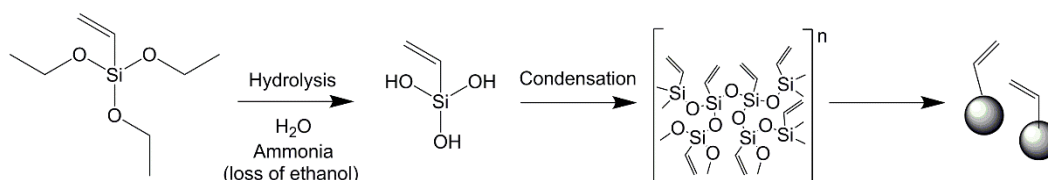


Figure 41: Simplified nanoparticle synthesis diagram for VTES

To determine the concentration of nanoparticles ($\text{mg}\cdot\text{mL}^{-1}$) in the suspension, 1 mL of the stock solution was accurately pipetted into a pre-weighed vial, left to dry to constant weight, and then weighed again. The difference measured between these weights corresponded to the mass of nanoparticles present per mL. Surface area measurements were taken using Brunauer-Emmet-Teller (BET) isotherm measurements on a micromeritics TriStar II 3030 surface area and porosity analyser. Prior to BET analysis, 280 mg of vinyl terminated nanoparticles were dried (30 mbar at 60 °C) overnight followed by treatment at 0.1 mbar at 90 °C for 3 h prior to analysis. SEM analysis of the synthesised nanoparticles was achieved using a FEI Inspect F50 system. Images were taken to calculate the diameter of the nanoparticles using ImageJ [191] and to check morphology between batches. ATR-FTIR was used to confirm nanoparticle functionality and was completed using a Nicolet Nexus 870 FT-IR, equipped with a Thermo Scientific ATR-IR 'Smart Orbit Attachment'. 64 scans were collected in absorbance mode for each reading with a resolution of 4 cm^{-1} with a range of $525\text{-}4000\text{ cm}^{-1}$.

4.3.3 Preparation of calibration samples to determine attachment density of 1-dodecanethiol

Due to the expensive nature of thiol modified oligonucleotides, model reactions using 1-dodecanethiol was used to gain an understanding of the viability of attachment and also to evaluate theoretical attachment densities. 1-dodecanethiol was selected as it was affordable, readily available and could successfully model the same thiol-ene attachment. There are some limitations to using this model reagent as the oligonucleotide structure is very different to 1-dodecanethiol. Both the size of the oligonucleotide and the polarity may influence attachment to the nanoparticle surface. Although there are variations, the 1-dodecanethiol will still be able to effectively model the thiolene attachment for preliminary experiments. Approximate attachment densities were calculated using model reactions with 1-dodecanethiol based on similar methods described by Mangos *et al.* [189]. Initially, non-reacted nanoparticles were analysed using ATR-FTIR to generate a calibration curve. Use of the generated calibration curve allowed for the molar amount of 1-dodecanethiol present on the surface to be determined in reacted samples.

For each calibration mixture, 1-dodecanethiol (ranging from $4.17\text{ }\mu\text{mol}$ to $167\text{ }\mu\text{mol}$) was added directly to 30 mg of dried, vinyl terminated nanoparticles. Mixtures were homogenised using a mortar and pestle until the 1-dodecanethiol and vinyl nanoparticles formed a homogenous sample followed by analysis using ATR-FTIR. An internal standard

reference peak was selected for each analysed sample to improve reproducibility of the analysis across sample batches. The absorbance of the $\nu(\text{C}=\text{C})$ stretch vibration at 1600 cm^{-1} was selected as the reference peak as it remained unchanged during the attachment process with 1-dodecanethiol. The absorbance of the $\nu_{\text{asymm}}(\text{CH}_2)$ stretch at 2920 cm^{-1} peak formed during the attachment, and as such was used to track the additions of 1-dodecanethiol. ATR-FTIR analysis was completed in absorbance using 64 scans and a resolution of 4 cm^{-1} across a range of 525 to 4000 cm^{-1} . Analysis of the absorbance readings for both the 1600 cm^{-1} and 2920 cm^{-1} vibrations was completed using FITYK 0.9.8 [192].

4.3.4 Covalent attachment of 1-dodecanethiol to vinyl terminated nanoparticles

Reacted samples of 1-dodecanethiol with the vinyl terminated nanoparticles were used both initially to test the viability of attachment and then later to calculate theoretical attachment densities. 13 mg of benzophenone was initially dissolved in 7 mL of ethanol in 20 mL scintillation vials. 3 mL of vinyl terminated nanoparticles (stock concentration $5\text{ mg}\cdot\text{mL}^{-1}$) were then transferred into the vial along with varying molar amounts of 1-dodecanethiol. For the preliminary test attachment of 1-dodecanethiol $210\text{ }\mu\text{mol}$ to $840\text{ }\mu\text{mol}$ was added. For the attachment density experiments 10 to 1000 molar excesses of 1-dodecanethiol were reacted with the nanoparticles. Nanoparticle suspensions were irradiated at 365 nm for 2 h, with stirring, to promote UV initiated thiolene attachment. Once reacted, suspensions were transferred to 10 mL centrifuge tubes and centrifuged at 1700 g for 20 min. The supernatant was removed and the pellet washed 3 times with ethanol and centrifugation at 1700 g for 20 min. Samples were then dried at $100\text{ }^\circ\text{C}$ followed by analysis using ATR-FTIR in absorbance mode with 64 scans and a resolution of 4 cm^{-1} across a range of 525 to 4000 cm^{-1} . The formation of vibrations at $\nu_{\text{asymm}}(\text{CH}_2)$ stretch at 2920 cm^{-1} and $\nu_{\text{symm}}(\text{CH}_2)$ stretch at 2850 cm^{-1} [193] confirmed successful attachment of the 1-dodecanethiol. Analysis of the absorbance readings for both the 1600 cm^{-1} and 2920 cm^{-1} vibrations was completed using FITYK 0.9.8 [192].

4.3.4.1 Molar excesses of 1-dodecanethiol used for attachment density calculations

In order to determine the attachment density of 1-dodecanethiol to the vinyl terminated nanoparticles, a number of molar excesses of the model reagent were investigated. These included 10, 20, 40, 100 and 1000 molar excesses of 1-dodecanethiol. Using the surface area and mass of the synthesised nanoparticles, the volumes required to meet these

excess requirements could be calculated. Initially the number of particles present in the 3 mL of 5 mg.mL⁻¹ stock solution was calculated based on the g.nanoparticle⁻¹ (refer to Equation 10):

$$\begin{aligned} & \textit{Approximate number of Nanoparticles available} \\ & = \frac{\textit{Mass of nanoparticles in 3 mL (g)}}{\textit{g.nanoparticle}^{-1}} \end{aligned}$$

Equation 2: Number of nanoparticles available for reaction (3 mL, 5 mg.mL⁻¹ stock solution)

The number of nanoparticles present in the 3 mL reaction sample was determined to be 3.34 x 10¹¹ nanoparticles (Appendix, Equation 16). Using the 502,000 nm² surface area calculated using the resulting BET isotherm (Equation 11), the total available surface area per reaction was calculated:

$$\begin{aligned} & \textit{Available surface area} = \\ & \textit{Surface area per nanoparticle (nm}^2\text{)} \times \textit{approximate number of nanoparticles} \end{aligned}$$

Equation 3: Total available surface area (nm²) per reaction

A total surface area of 1.68 x 10¹⁷ nm² was available for attachment with 1-dodecanethiol (Appendix, Equation 17). Based on the Zhuravlev model, the total number of available hydroxyl molecules on the surface of a silica nanoparticle is approximately 5 per nm² [194]. Based on this, it was assumed that the number of available vinyl groups would also be in the range of 5 per nm². This suggests that for a 1:1 stoichiometric attachment with 1-dodecanethiol, the maximum number of attachments was 5 attachments.nm⁻². From this, the number of attachments of 1-dodecanethiol for a 1:1 stoichiometry was calculated using the available surface area calculated in Equation 3:

$$\begin{aligned} & \textit{Estimated number of attachments} \\ & = 5 \textit{ attachments.nm}^{-2} \times \textit{available surface area (nm}^2\text{, Equation 3)} \end{aligned}$$

Equation 4: Number of attachments possible for 1:1 stoichiometry

For a 1:1 stoichiometric reaction between vinyl terminated nanoparticles and the 1-dodecanethiol, 8.39 x 10¹⁷ attachments was possible (Appendix, Equation 18). The correlating number of moles required to meet this requirement was determined by dividing with Avogadro's number:

$$\begin{aligned} & \text{Number of moles of 1 – dodecanethiol} \\ &= \frac{\text{Number of attachments per reaction (Equation 4)}}{\text{Avogadro's number}} \end{aligned}$$

Equation 5: Molar equivalent of 1-dodecanethiol (mol) from attachment number using 1:1 stoichiometry

For a 1:1 stoichiometric attachment of 1-dodecanethiol, 1.39×10^{-6} mol of 1-dodecanethiol must be added to the reaction mixture (Appendix, Equation 19). Using this molar amount required for 1:1 stoichiometry, molar excesses of 10:1, 20:1, 40:1, 100:1 and 1000:1 was calculated:

$$\begin{aligned} & 10:1 \text{ molar excess 1 – dodecanethiol} \\ &= 10 \times \text{number of moles required for 1:1 stoichiometry (mol)} \end{aligned}$$

Equation 6: Molar amount of 1-dodecanethiol (mol) required for a 10 molar excess attachment

The number of moles of 1-dodecanethiol was calculated as being 1.39×10^{-5} mol for the 10:1 molar excess reaction (Appendix, Equation 20). This value was then converted to the volume required for addition using the density (0.845 g.mL^{-1}) and molar mass (202.4 g.mol^{-1}) of 1-dodecanethiol:

$$\text{Volume of 1 – dodecanethiol required (mL)} = \frac{n \times M}{d}$$

Equation 7: Volume of 1-dodecanethiol (mL) required for a 10 molar excess attachment

A 10 molar excess required the addition of 3.3 μL , 20 molar excess required the addition of 6.7 μL , 40 molar excess required the addition of 13.3 μL , 100 molar excess required the addition of 33.3 μL and 1000 molar excess required the addition of 333.0 μL (Appendix, Equation 21).

4.3.5 Thermogravimetric analysis of reacted nanoparticles

Thermogravimetric analysis (TGA) of 1-dodecanethiol reacted nanoparticles was performed as a secondary method for the calculation of attachment densities. This was done using a Perkin Elmer Simultaneous Thermal Analyser (STA) 8000 using 50 mL.min^{-1}

of N₂ gas for thermal decomposition. A temperature profile of 30 to 500 °C was recorded at a temperature ramp of 10 °C.min⁻¹. The percentage mass loss was then used to determine the mass of 1-dodecanethiol present using methods described by Mangos *et al.* [189]. Calculated working for the attachment density of 1-dodecanethiol using TGA can be found in the Appendix (Equation 22 and Equation 23). The resulting decomposition curve allowed for the mass loss (%) to be calculated. Using this and the mass of the 350 nm nanoparticle (4.49 x 10⁻¹⁴ g.nanoparticle⁻¹) the mass of 1-dodecanethiol at the surface was calculated:

$$\begin{aligned} & \text{Mass of 1 – dodecanethiol} \\ & = \text{Mass of nanoparticle (g)} \times \text{Average mass loss (\%, n = 2)} \end{aligned}$$

Equation 8: Mass (g) of 1-dodecanethiol based on the TGA average mass loss (%)

The average mass of 1-dodecanethiol attached to the vinyl nanoparticles was calculated to be 4.01 x 10⁻¹⁶ g. The number of moles of 1-dodecanethiol was then calculated using the molar mass of 1-dodecanethiol (202.4 g.mol⁻¹) and used to calculate attachment density using Avogadro's number and the calculated surface area of a nanoparticle (502,000 nm²):

$$\begin{aligned} & \text{Attachment density of 1 – dodecanethiol} \\ & = \frac{\left(\text{Mass of 1 – dodecanethiol (g)} / \text{Molar mass (g.mol}^{-1}) \right) \times \text{Avogadro's number}}{\text{Surface area of a nanoparticle (nm}^2)} \end{aligned}$$

Equation 9: TGA calculated attachment density of 1-dodecanethiol (attachments.nm⁻²)

4.3.6 Attachment of SH-ACat probe to vinyl terminated nanoparticles

Once attachment was confirmed using the 1-dodecanethiol model reagent, a trial attachment of thiol modified oligonucleotides to the vinyl terminated nanoparticles was completed. 2 mL of vinyl terminated nanoparticles (stock concentration 3 mg.mL⁻¹) were transferred into the individual wells of a plastic 6-well culture plate. Solvent was removed by evaporation at 40 °C followed by re-constitution in ultra-pure water or 50 % ethanol. Ultrasonication was used to promote re-suspension of the nanoparticles in the solvent.

Prior to attachment, the disulfide modified oligonucleotide probe (as received) was reduced with excess TCEP (0.01 M, aqueous) as described in Section 3.3.3. The resulting

reduced SH-probe solution (50 μ M, 2 μ L) was then added to each well containing the vinyl terminated nanoparticles and irradiated at 365 nm with stirring for 2 h to initiate the thiolene attachment (Figure 28). Reacted nanoparticles were then transferred into 10 mL plastic centrifuge tubes and centrifuged at 1700 g for 20 min to obtain a pellet. The supernatant was removed and the sample washed 3 times in the previously used solvent (ultra-pure water or 50 % ethanol) to remove all unreacted SH-probe. After the final wash, modified nanoparticles were re-dispersed in 3 mL of the same solvent (ultra-pure water or 50 % ethanol) and transferred into 20 mL scintillation vials ready for hybridisation.

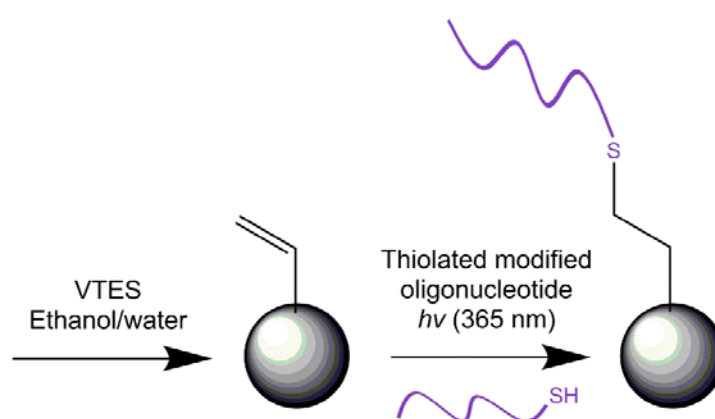


Figure 42: Schematic for the attachment of thiol-modified oligonucleotides to vinyl nanoparticles

Hybridisation of reacted nanoparticles with Cy5 labelled ACat Seq followed

4.3.7 Hybridisation experiments for VTES silica nanoparticle oligonucleotide modified substrates

For hybridisation, Cy5 labelled ACat Seq (100 μ M, 2 μ L) was added to each of the prepared 20 mL scintillation vials containing oligonucleotide reacted nanoparticles and left to hybridise overnight at 40 $^{\circ}$ C with stirring. Samples were transferred into 10 mL centrifuge tubes and washed twice with either ultra-pure water or 50 % ethanol by centrifugation at 1700 g for 20 min. The supernatant was removed and nanoparticles re-constituted in 5 mL of either ultra-pure water or 50 % ethanol. Samples were then spotted on glass microscope slides and left to dry ready for analysis. Fluorescence imaging of the hybridised nanoparticles was achieved using a Leica TCS SP5 Spectral Confocal Microscope equipped with a Cy5 filter.

4.4 Results and Discussion

4.4.1 Nanoparticle synthesis and characterization

Nanoparticles synthesised using the one-pot Stöber synthesis method described in Section 4.3.2 were subjected to SEM analysis to gain information on nanoparticle size, shape and uniformity. As shown in Figure 43, the cleaned vinyl terminated nanoparticles were homogenous and spherical across the sample. The size of the nanoparticles were calculated using ImageJ [191] with an average diameter of 350 ± 30 nm ($n= 75$ measurements, \pm standard deviation).

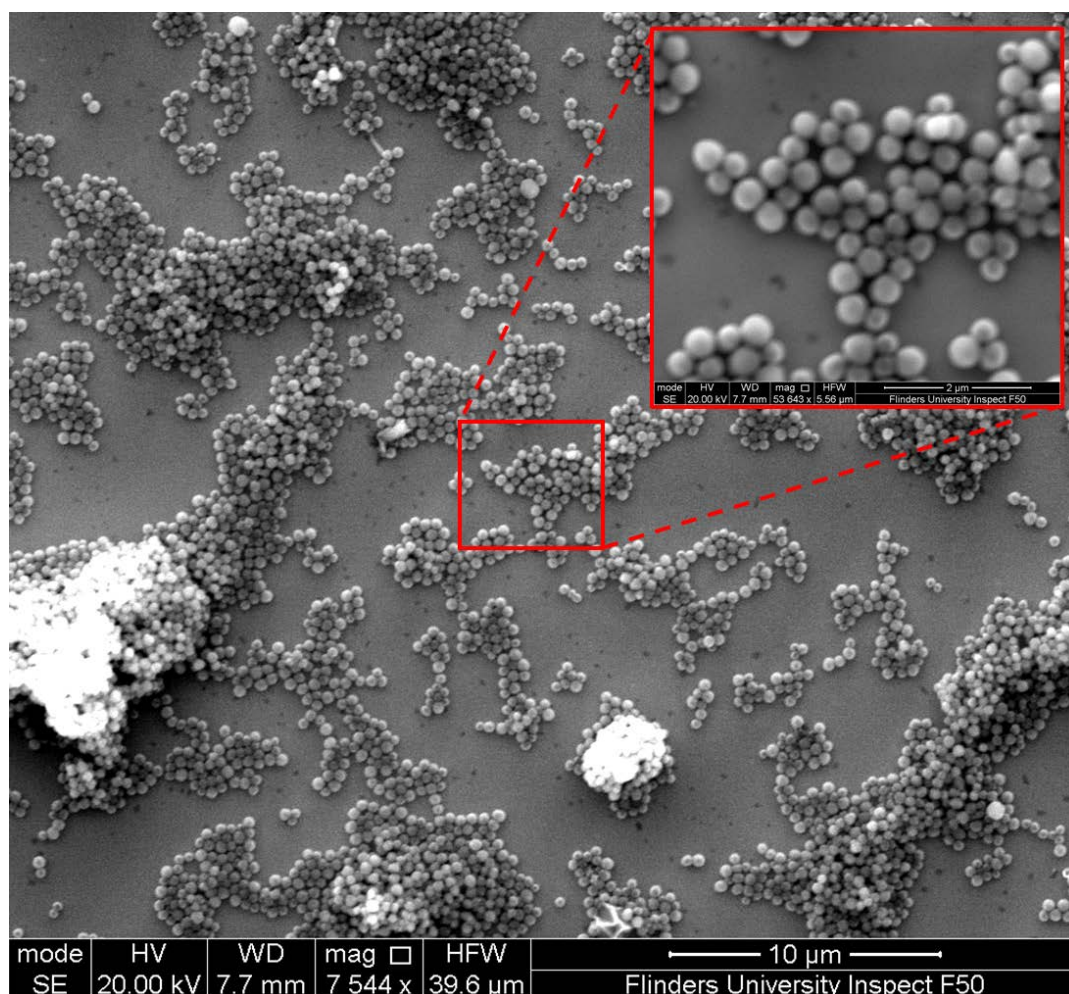


Figure 43: SEM images of synthesised vinyl terminated silica nanoparticles (average diameter 350 ± 30 nm)

The BET isotherm produced from the synthesised nanoparticles is shown in Figure 44. This isotherm has similar characteristics to a Type II classification indicating that the nanoparticles have a smooth surface with low porosity.

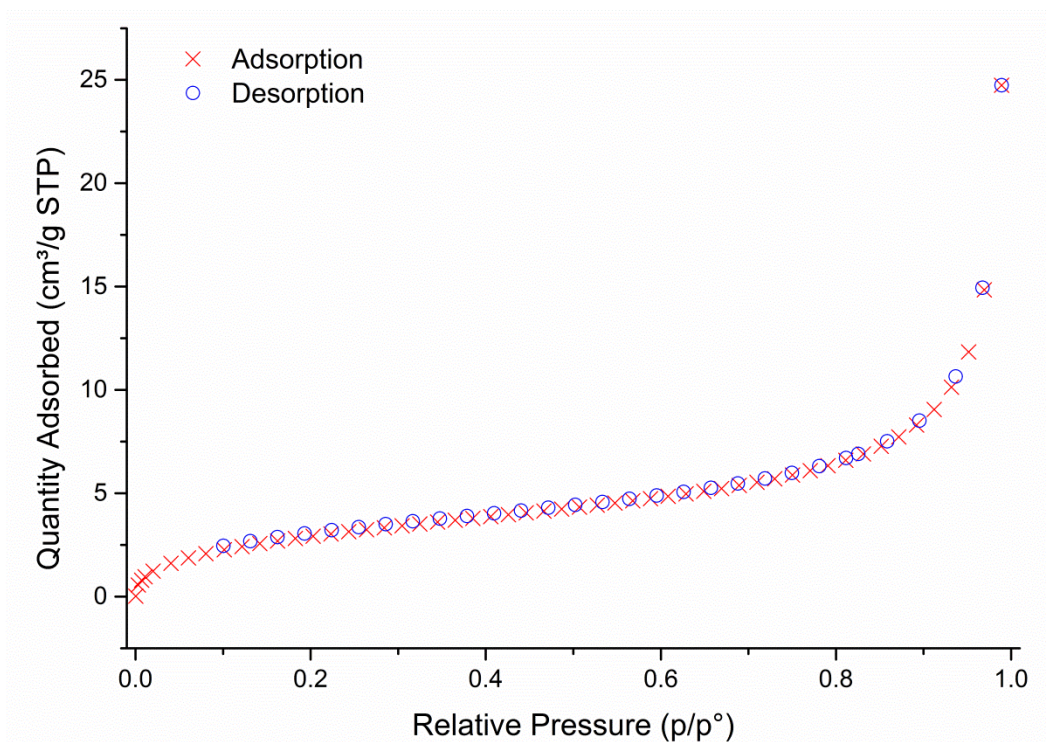


Figure 44: BET isotherm of the synthesised vinyl terminated silica nanoparticles

Prepared using 280 mg of synthesised nanoparticles. Surface area calculated as 11.18 m².g⁻¹

The resulting value for surface area recorded using the BET isotherm analysis was 11.18 m².g⁻¹. Conversion of this value to nm² per nanoparticle was required to gain an understanding on the surface area available for reaction with 1-dodecanethiol. Initially, the estimated mass of a single nanoparticle was calculated using a reported silica nanoparticle density of 2.0 g.cm³ [195-197] and a radius of 175 x 10⁻⁷ cm:

$$\begin{aligned}
 \text{Mass of nanoparticle} &= \text{density} \times \text{volume} = \text{density} \times \frac{4}{3} \pi r^3 \\
 &= 2.0 \text{ g.cm}^3 \times \frac{4}{3} \pi \times (175 \times 10^{-7} \text{ cm})^3 \\
 &= 4.49 \times 10^{-14} \text{ g.nanoparticle}^{-1}
 \end{aligned}$$

Equation 10: Mass (g) per nanoparticle

A nanoparticle mass of $4.49 \times 10^{-14} \text{ g.nanoparticle}^{-1}$ was calculated based on a density of 2.0 g.cm^3 and a diameter of $\approx 350 \text{ nm}$. By inverting this value, the number of nanoparticles per gram was calculated as $2.23 \times 10^{13} \text{ nanoparticles.g}^{-1}$. Using these values the surface area per nanoparticle was calculated using the resulting BET isotherm:

$$\begin{aligned} \text{Surface area per nanoparticle} &= \frac{\text{BET isotherm value (m}^2\cdot\text{g}^{-1}\text{)}}{\text{nanoparticles.g}^{-1}} \\ &= \frac{11.18 \text{ m}^2\cdot\text{g}^{-1}}{2.23 \times 10^{13} \text{ nanoparticles.g}^{-1}} = 5.02 \times 10^{-13} \text{ m}^2 \\ &= 502,000 \text{ nm}^2 \text{ per nanoparticle} \end{aligned}$$

Equation 11: Surface area (nm²) per nanoparticle calculated from BET isotherm

An available surface area of $502,000 \text{ nm}^2$ was calculated for a 350 nm diameter nanoparticle. This value was also compared to a theoretical calculation of surface area based on $4\pi r^2$:

$$\begin{aligned} \text{Theoretical surface area of nanoparticle} &= 4\pi r^2 = 4 \times \pi \times (175 \text{ nm})^2 = \\ &385,000 \text{ nm}^2 \end{aligned}$$

Equation 12: Theoretical surface area (nm²) based on a radius of 175 nm

This method results in a nanoparticle surface area of $385,000 \text{ nm}^2$, significantly lower than that determined using the BET isotherm. The theoretical value assumes that the nanoparticle surface is a perfect, uniform sphere of a single radius. Small changes in surface roughness, as well as size distribution would thus influence the actual surface area. This was demonstrated by the SEM shown in Figure 43 where variations in size between nanoparticles of the same batch was observed. As such, the BET isotherm reported surface area gives a more accurate representation of available surface area and was used for all future calculations.

Unreacted vinyl terminated nanoparticles were analysed using ATR-FTIR to confirm functionality prior to attachment experiments with the spectra shown in Figure 45, with the corresponding peaks assigned as outlined in Table 10.

Vibrations at 746 cm^{-1} [198, 199], 1021 cm^{-1} [199-201] and 1103 cm^{-1} [199, 200, 202] correlate to ν_{symm} (Si-O-S) and ν_{asymm} (Si-O-S) vibrations respectively, both associated with the silanol groups within the core silica nanoparticle structure. Peaks present at 1000 cm^{-1} [201, 203] and 1275 cm^{-1} [201] correlate to ν_{asymm} (Si-O-R) and ν_{asymm} (Si-O-CH₂CH₃) indicating that residual unreacted VTES was present amongst the cleaned nanoparticles. Furthermore, the vibration at 961 cm^{-1} [198, 204], correlating to ν_{asymm} (Si-OH), suggests that some hydrolysed, residual VTES is also present within the cleaned nanoparticles. Peaks located at 3062 cm^{-1} and 2959 cm^{-1} [201] are from the ν (=C-H) and ν_{asymm} (-C-H) stretch vibrations correlating to the heterogeneous vinyl residue on a siloxane backbone. The main peak of interest within the spectra is at 1602 cm^{-1} which corresponds to the ν (C=C) stretch vibration confirming that the vinyl functional group is present within the structure of the synthesised nanoparticles [201].

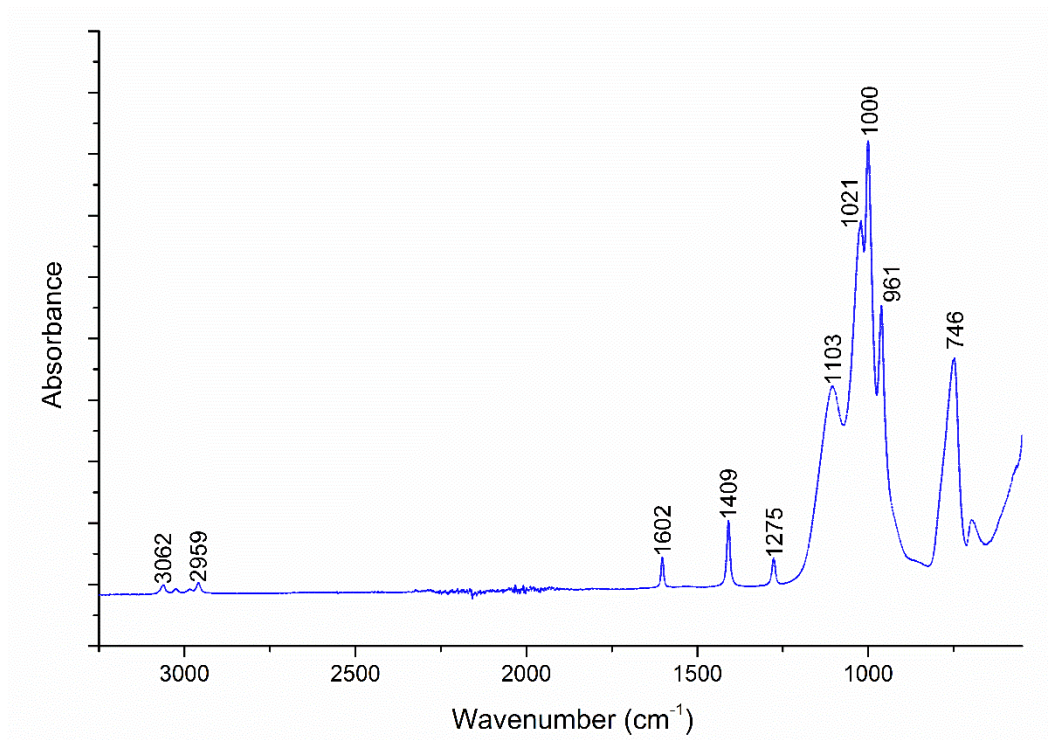
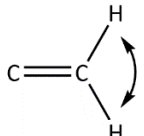


Figure 45: ATR-FTIR of neat vinyl terminated nanoparticles

Table 10: Correlation of functional groups based on spectra in Figure 45

Wavenumber (cm ⁻¹)	Functional group	Vibrational mode	Ref.
746	$\text{Si} \overset{\leftarrow}{-} \text{O} \overset{\rightarrow}{-} \text{Si}$	Symmetric stretch	[198, 199]
961	$\text{Si} \overset{\leftarrow}{-} \text{O} \overset{\leftarrow}{-} \text{H}$ (hydrolysed VTES)	Asymmetric stretch	[198, 204]
1000	$\text{Si} \overset{\leftarrow}{-} \text{O} \overset{\leftarrow}{-} \text{R}$ (unreacted VTES)	Asymmetric stretch	[201, 203]
1021	$\text{Si} \overset{\leftarrow}{-} \text{O} \overset{\leftarrow}{-} \text{Si}$	Asymmetric stretch	[199-201]
1103	$\text{Si} \overset{\leftarrow}{-} \text{O} \overset{\leftarrow}{-} \text{Si}$	Asymmetric stretch	[199, 200, 202]
1275	$\text{Si} \overset{\leftarrow}{-} \text{O} \overset{\leftarrow}{-} \text{CH}_2\text{CH}_3$ (unreacted VTES)	Asymmetric stretch	[201]
1409		Scissor	[201]
1602	C=C	Stretch	[201]
2959	$\text{R} \overset{\leftarrow}{-} \text{C} \overset{\leftarrow}{-} \text{H}$	Asymmetric stretch	[201]
3062	$\text{R} \overset{\leftarrow}{=} \text{C} \overset{\leftarrow}{-} \text{H}$	Asymmetric stretch	[201]

4.4.2 Vinyl terminated nanoparticle model experiment

Due to the expensive nature of thiol modified oligonucleotides, model reactions using 1-dodecanethiol were initially investigated. To do this 1-dodecanethiol was reacted with a solution of synthesised VTES nanoparticles to model the attachment chemistry for future use with thiol modified oligonucleotides. These model reactions allowed investigation into i) the feasibility of the thiolene attachment to vinyl terminated nanoparticles and ii) calculation of approximate attachment densities.

i) Feasibility of thiol-ene reaction on vinyl terminated nanoparticles

In order to evaluate the viability of thiolene attachment of 1-dodecanethiol to vinyl terminated nanoparticles, varying concentrations (ranging from 292 to 835 μmol) were reacted with synthesised nanoparticles. The resulting ATR-FTIR was then used to determine if attachment was possible using this method. Figure 46 shows the ATR-FTIR spectra of the reacted nanoparticles after extensive washing to remove residual unreacted 1-dodecanethiol. A notable increase in the absorbance of the $\nu_{\text{asymm}}(\text{CH}_2)$ stretch at 2926 cm^{-1} and $\nu_{\text{symm}}(\text{CH}_2)$ stretch at 2850 cm^{-1} was seen upon increasing amounts of 1-dodecanethiol with respect to the internal reference peak. This increase is attributed to the CH_2 functionality within 1-dodecanethiol as well as the thiolene reaction removing the vinyl functionality subsequently replacing the sp^2 hybridised carbons with sp^3 hybridised CH_2 groups. The formation of these vibrations for the cleaned samples indicates the successful attachment of 1-dodecanethiol.

It was expected that the thiolene attachment would reduce the intensity of the $\nu(\text{C}=\text{C})$ stretch vibration at 1602 cm^{-1} , however this was not observed. Based on the resulting BET isotherm discussed in Section 4.4.1, a Type II classification was obtained suggesting non-porous nanoparticles were synthesised. From this it can be assumed that the reaction was restricted to the surface. Given that ATR-FTIR is not a surface specific analytical technique, the change observed after attachment at the $\nu(\text{C}=\text{C})$ stretch vibration at 1602 cm^{-1} would be negligible as the surface is only a small percentage of the bulk sample. As such, the $\nu(\text{C}=\text{C})$ stretch vibration could be used as the internal reference peak. Comparison with this $\nu(\text{C}=\text{C})$ stretch vibration and core, silanol vibration $\nu(\text{Si}-\text{O}-\text{Si})$ at 1021 cm^{-1} as an alternative reference peak resulted in closely correlated ratios ($R^2 = 0.98$, Appendix, Figure 60). This indicated that use of the $\nu(\text{C}=\text{C})$ vibration as a reference provides similar results to the $\nu(\text{Si}-\text{O}-\text{Si})$ core vibrations. The use of a $\nu(\text{C}=\text{C})$ vibration minimises

difficulties surrounding the overlapping peaks ranging from 1000 to 1250 cm^{-1} , making quantification of the ν (Si-O-Si) difficult. Overall, it was demonstrated that attachment of the model reactant 1-dodecanethiol was possible using photoinitiated aqueous conditions.

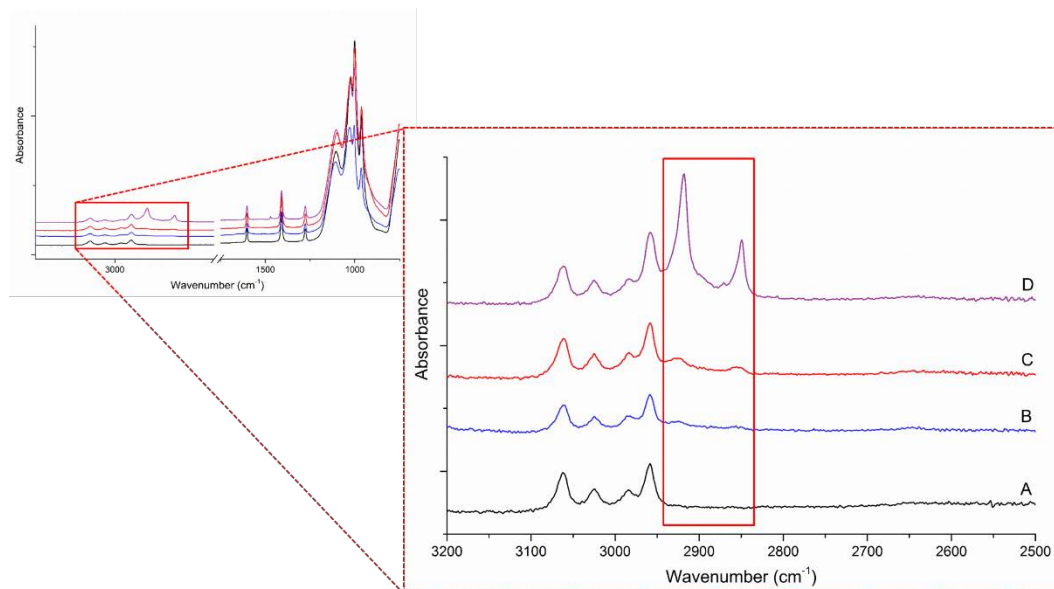


Figure 46: ATR-FTIR spectra of the trial attachment of 1-dodecanethiol with vinyl terminated nanoparticles

Bare VTES silica nanoparticles (A) and VTES silica nanoparticles reacted with (B) 2.1×10^{-4} mol, (C) 4.2×10^{-4} mol and (D) 8.4×10^{-4} mol of 1-dodecanethiol

ii) *Calculation of approximate attachment densities*

Calibration curves were generated using absorbance ratios for intensities using the $\nu_{\text{asymm}}(\text{CH}_2)$ stretch of the methylene at 2926 cm^{-1} relative to the $\nu(\text{C}=\text{C})$ stretch vibration at 1602 cm^{-1} from mixtures of unreacted 1-dodecanethiol vinyl terminated nanoparticles. Use of this reference peak was required to account for the variability in sample mass in the ATR-FTIR. Normalisation of the absorbance was achieved by calculating a ratio of $\nu_{\text{asymm}}(\text{CH}_2)$ at 2920 cm^{-1} to $\nu(\text{C}=\text{C})$ stretch vibration at 1600 cm^{-1} as shown in Equation 13:

$$\text{Normalised } \nu_{\text{asymm}}(\text{CH}_2) \text{ intensity} = \frac{\text{Absorbance at } 2920 \text{ cm}^{-1}}{\text{Absorbance at } 1600 \text{ cm}^{-1}}$$

Equation 13: Normalisation of the $\nu_{\text{asymm}}(\text{CH}_2)$ stretch at 2920 cm^{-1}

Absorbance data normalised with FITYK 0.9.8

The calibration curve generated (Figure 47) shows a linear correlation between the normalised ATR-FTIR absorbance and the amount of 1-dodecanethiol present (mol, $R^2 = 0.98$). This demonstrated that quantitative analysis was possible when using the ν (C=C) stretch vibration as an internal standard to normalise the relative absorbance changes.

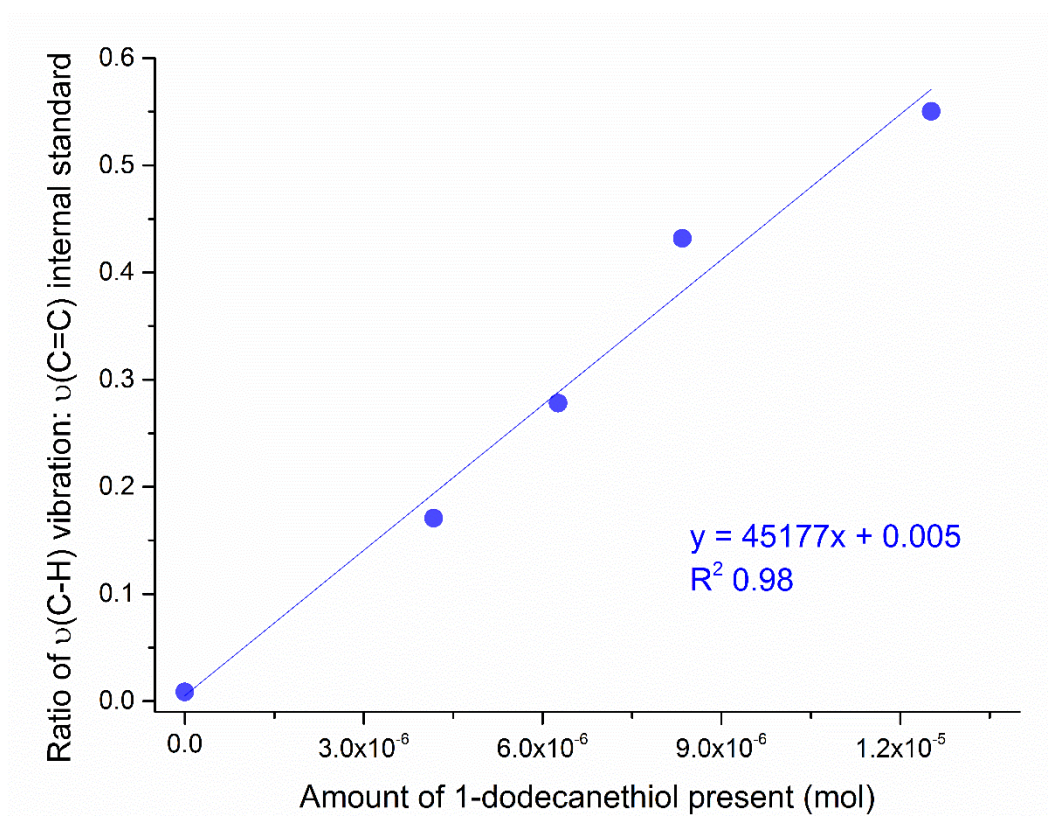


Figure 47: Calibration curve generated using the ratio of $\nu_{\text{asymm}}(\text{CH}_2)$ vibration at 2920 cm^{-1} relative to the ν (C=C) stretch vibration at 1602 cm^{-1}

LOD of 2.79×10^{17} mol of 1-dodecanethiol ($1.66 \text{ attachments.nm}^{-2}$) calculated based on 3 times the corrected ratio of the blank sample (0.01)

This calibration curve was applied to reacted nanoparticle samples to calculate theoretical attachment densities of 1-dodecanethiol using model reactions. The attachment of 1-dodecanethiol to vinyl terminated nanoparticles was evaluated at 10, 20, 40, 100 and 1000 molar excesses of 1-dodecanethiol. Attachment was tracked by monitoring the increase in absorbance for the $\nu_{\text{asymm}}(\text{CH}_2)$ stretch at 2920 cm^{-1} and $\nu_{\text{symm}}(\text{CH}_2)$ stretch at 2850 cm^{-1} as both peaks are attributed to the covalent attachment of 1-dodecanethiol. As shown in Figure 48, at lower molar excesses (10-100 fold excess)

the vibrations at 2920 cm^{-1} and 2850 cm^{-1} were not present indicating attachment was either not possible under these conditions or that the level of attachment was below the limits of detection of the ATR-FTIR. Addition of a 1000 molar excess of 1-dodecanethiol resulted in the formation of peaks at 2920 cm^{-1} and 2850 cm^{-1} indicating the successful attachment of 1-dodecanethiol using these conditions. From the resulting absorbances, attachment densities was calculated using the ATR-FTIR calibration curve in Figure 47.

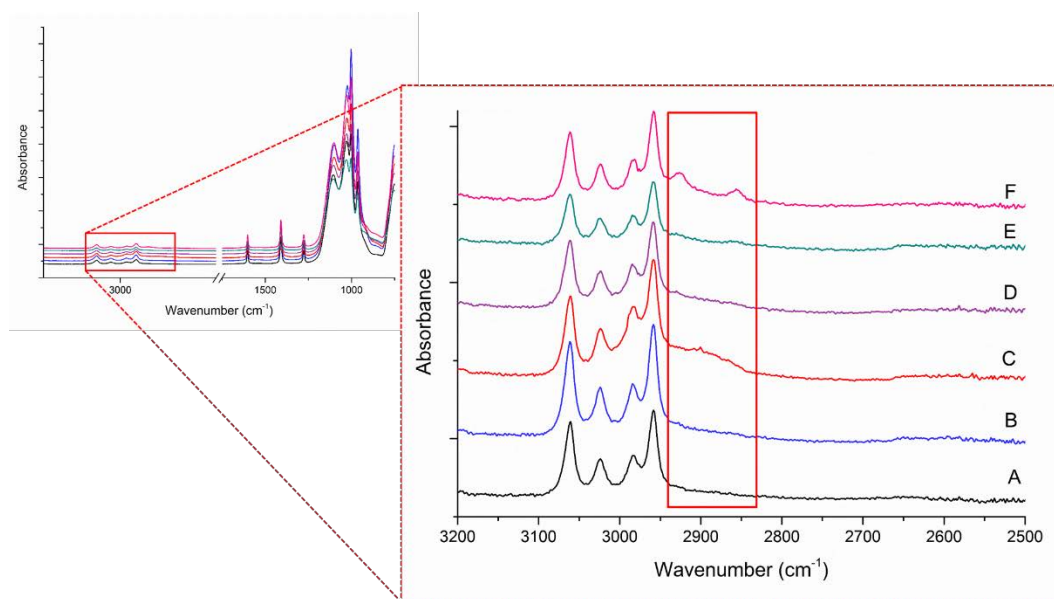


Figure 48: ATR-FTIR spectra of varying molar excesses of 1-dodecanethiol reacted with vinyl nanoparticles

Unreacted vinyl nanoparticles (A) and nanoparticles reacted with 10 (B), 20 (C), 40 (D), 100 (E) and 1000 (F) molar excesses of 1-dodecanethiol

From the resulting ATR-FTIR spectra for the 1000 molar excess sample, the absorbance at 1600 cm^{-1} and 2920 cm^{-1} were recorded using FITYK. A signal: background ratio was then calculated and used to measure the molar amount of 1-dodecanethiol present using the calibration in Figure 47:

$$y = 45177x + 0.005 \therefore 0.12 = 45177x + 0.005 \therefore 45177x = 0.115$$

$$\therefore x = 2.57 \times 10^{-6} \text{ mol of 1-dodecanethiol}$$

Equation 14: Number of moles of 1-dodecanethiol (mol) present based on the calibration curve (Figure 47)

Using the calculated number of moles of 1-dodecanethiol, attachments per nm² was calculated based on the 15 mg nanoparticle sample used in the reaction. Finally, the number of attachments per nm² was calculated based on the available surface area (1.68 x 10¹⁷ nm², Equation 3):

$$\begin{aligned}
 & \textit{Attachments per 15 mg sample} \\
 &= \textit{mol of 1 - dodecanethiol} \times \textit{Avogadro's number} \\
 &= 2.57 \times 10^{-6} \textit{ mol} \times 6.02 \times 10^{23} \\
 &= 1.55 \times 10^{18} \textit{ attachments per 15 mg sample}
 \end{aligned}$$

$$\begin{aligned}
 \textit{Attachments per nm}^2 &= \frac{\textit{Attachments per 15 mg sample}}{\textit{Surface area available in 15 mg sample (nm}^2\text{)}} \\
 &= \frac{1.55 \times 10^{18} \textit{ attachments per 15 mg}}{1.68 \times 10^{17} \textit{ nm}^2 \textit{ per 15 mg}} = 9.2 \textit{ attachments.nm}^2
 \end{aligned}$$

Equation 15: Attachments per nm² of 1-dodecanethiol attached to the vinyl terminated nanoparticles

An attachment density of 9.2 attachments.nm⁻² was calculated for the 1000 molar excess addition of 1-dodecanethiol (Equation 15). As no attachment was visualised at lower molar excesses it was hypothesised that for detectable thiolene attachment a high molar excess was required.

Previous researchers have suggested that the use of unquenched nanoparticle solutions, when compared to cleaned nanoparticles, can result in higher attachment densities [205]. The process of cleaning and centrifugation can result in irreversible agglomeration of nanoparticles in solution [131, 206], effectively minimising the attachment of 1-dodecanethiol with the surface. In order to investigate the effect of cleaning on nanoparticle agglomeration, attachment densities were calculated based on 1000 molar excess attachments prepared using both unquenched and cleaned nanoparticles. Table 11 shows that only a slightly higher level of attachment was attained for the cleaned nanoparticles (average 5.1 attachments.nm⁻²) when compared to the unquenched nanoparticles (average 3.7 attachments.nm⁻²). This suggests that in this case, the use of cleaned nanoparticles does not hinder attachment of 1-dodecanethiol by agglomeration.

Table 11: Effect of reaction solvent on 1-dodecanethiol attachment to cleaned and unquenched nanoparticles

Reaction Solvent	Ratio of Intensity at	
	2920 cm ⁻¹ : intensity at 1600 cm ⁻¹ (x10 ⁻²)	Attachments.nm ⁻²
Unquenched Blank	1.44	0.7
Unquenched replicate 1	5.56	4.0
Unquenched replicate 2	4.78	3.4
Clean Blank	1.22	0.6
Clean replicate 1	7.13	5.3
Clean replicate 2	6.60	4.8

Unquenched nanoparticles were analysed using SEM in order to evaluate the cause for the different attachment densities calculated in Table 11. Comparison between the two SEM images shows some obvious morphological differences between the unquenched nanoparticles (Figure 49) and cleaned nanoparticles (Section 4.4.1, Figure 43). The unquenched nanoparticles, whilst still consisting of spherical nanoparticles, created a film like structure over the surface. This film is most likely created due to side reactions between unreacted VTES and ammonium during storage. This film may inhibit attachment of 1-dodecanethiol at the surface resulting in the lower attachment densities observed in Table 11.

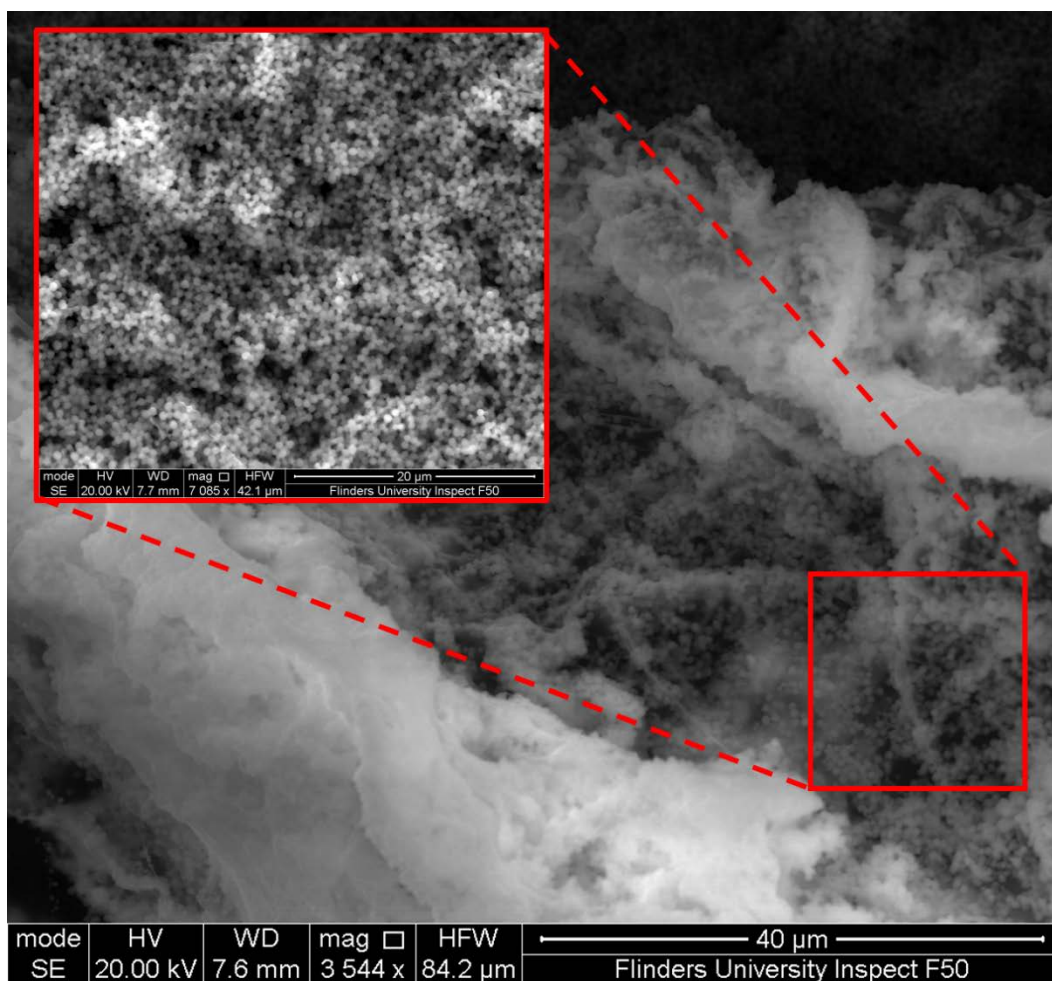


Figure 49: SEM of unquenched vinyl terminated nanoparticles showing modified structure compared to clean vinyl nanoparticles in Figure 43

In order to evaluate the reproducibility of the model thiolene attachment, 1000:1 molar excesses of 1-dodecanethiol were reacted with vinyl terminated nanoparticles and analysed over 5 replicates. As shown in Figure 50, evidence of attachment is present in all five 1000:1 molar excess samples due to the presence of the $\nu_{\text{asymm}}(\text{CH}_2)$ vibration at 2920 cm^{-1} and $\nu_{\text{symm}}(\text{CH}_2)$ vibration at 2850 cm^{-1} .

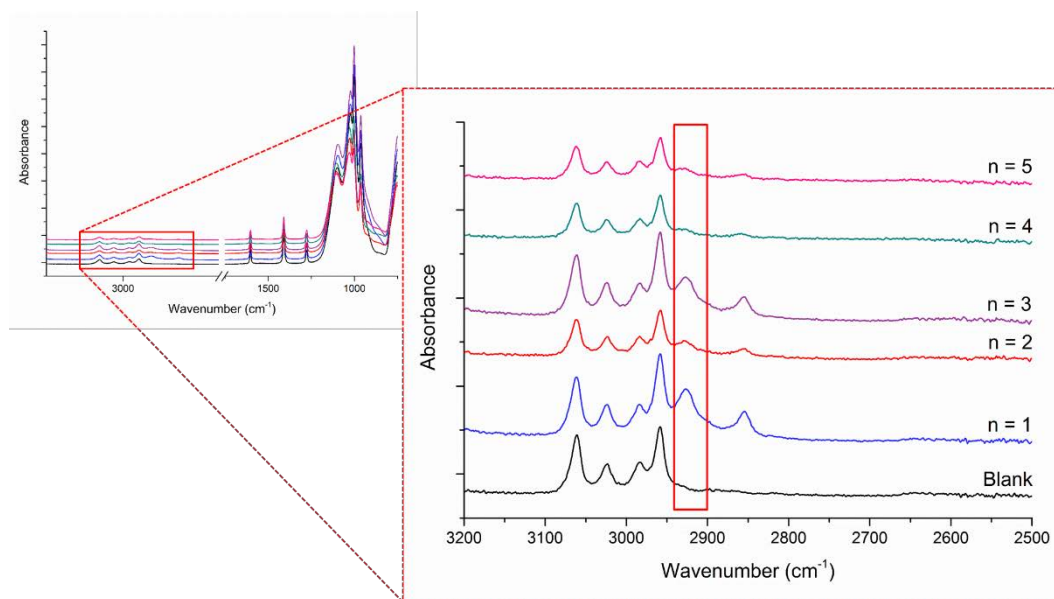


Figure 50: ATR-FTIR spectra of 1-dodecanethiol attachment replicates to vinyl nanoparticles (n=5)

Attachment densities were then calculated by FITYK normalisation of the ATR-FTIR spectra and subsequent analysis using the generated calibration curve (Equation 14 and Equation 15) with the final calculated attachment densities shown in Table 12.

Table 12: Resulting Ratio of $\nu_{\text{asymm}}(\text{CH}_2)$ to $\nu(\text{C}=\text{C})$ and subsequent attachment densities for 1000:1 molar excess (n = 5)

Analysis of absorbance completed using FITYK and baseline subtraction

Replication of 1000 molar excess 1- dodecanethiol	Ratio of $\nu_{\text{asymm}}(\text{CH}_2)$ to $\nu(\text{C}=\text{C})$ ($\times 10^{-1}$)	Attachments.nm ⁻²
Blank	0.04	Below detection limit
1	2.38	18.5
2	1.10	8.3
3	1.85	14.3
4	0.67	4.9
5	0.95	7.1

A high level of variation was observed for the reacted samples as seen in the calculated theoretical attachment densities in Table 12. In order to understand the cause for variation, reaction conditions were investigated including position under the UV lamp,

adjusted molar excesses of 1-dodecanethiol and mass of benzophenone added. The positioning of the vials under the UV light source are shown in Figure 51. Here, the positioning of each vial did not heavily influence the level of attachment as there was no correlation between location of the reaction vial under the UV light source and higher attainable attachment densities.



Figure 51: Orientation of samples under UV light source
Sample 1-5 correspond to those referred to in Table 12

Comparison between the attachment densities calculated and the adjusted molar excesses of 1-dodecanethiol (Figure 52A) and mass of benzophenone (Figure 52B) resulted in no linear correlation for each condition. This indicates that neither fluctuations in the addition of 1-dodecanethiol or benzophenone resulted in the variable attachment densities in Table 12.

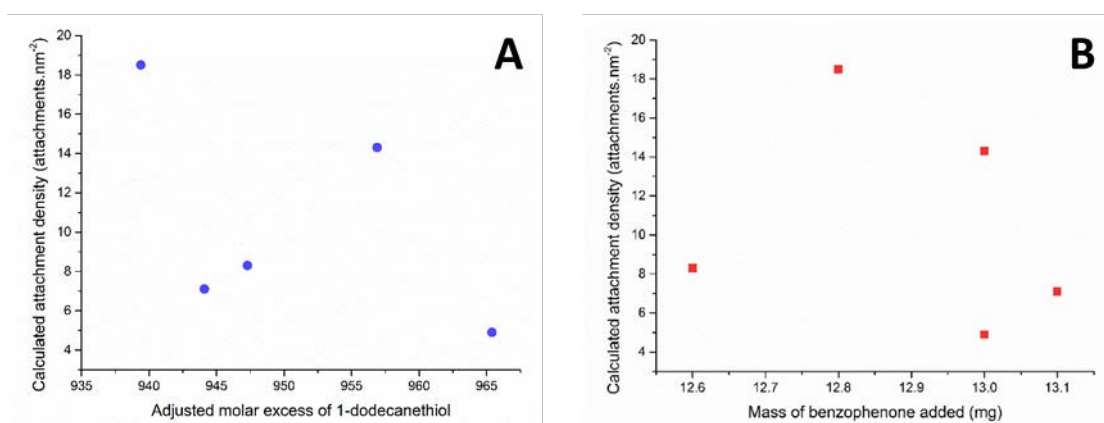


Figure 52: Effect of molar excess of 1-dodecanethiol (A) and mass of benzophenone (B) on reproducibility of calculated attachment densities

Other sources of variation could include: i) batch to batch variability, ii) the reaction chemistry is not reproducible under the conditions or ii) that the ATR-FTIR analysis is not suitable for approximating attachment density as previously reported by Mangos *et al.* [189]. Batch to batch variability is a possible cause for the different calculated attachment densities during the model attachment of 1-dodecanethiol. The Stöber synthesis conditions may be resulting in slight variations in surface structure or size, ultimately influencing the attachment densities attained. Using the ATR-FTIR technique, an average attachment density of 10.6 ± 5.6 attachments.nm⁻² was calculated with a 52 % level of variation between samples. According to the Zhuravlev model, the maximum number of attachments per nm² would be expected in the range of 5 attachments.nm⁻² [194]. Owing to this, the calculated attachment density of 10.6 attachments.nm⁻² is above the theoretical range, suggesting this analytical technique may not be optimal for quantifying attachment densities of 1-dodecanethiol on vinyl nanoparticles.

Alternatively, TGA has been reported as a method for quantifying attachment densities of molecular decorations on silica nanoparticles [189]. This method is able to characterise attachments based on decomposition curves generated upon heating reacted samples to high temperatures [207]. Carbon-based molecules, such as 1-dodecanethiol, are decomposed with the resulting mass loss recorded. This percentage mass loss can then be used to calculate the number of moles of attached molecules allowing for calculation of attachment densities. Both this TGA method and the ATR-FTIR calibration results discussed in Section 4.4.2 were compared to see if TGA was better suited for the quantification of 1-dodecanethiol attachment to vinyl terminated nanoparticles.

At 500 °C, a 2.9 % mass loss resulted for the blank unreacted vinyl nanoparticles as seen in the thermal mass trace in Figure 53. In contrast, reacted nanoparticles replicate 1 and replicate 2 resulted in a 3.7 % and 4.0 % mass loss respectively. This additional 0.7 and 1.1 % mass loss, compared to the unreacted sample, is attributed to the mass of 1-dodecanethiol present on the surface of the vinyl terminated nanoparticles.

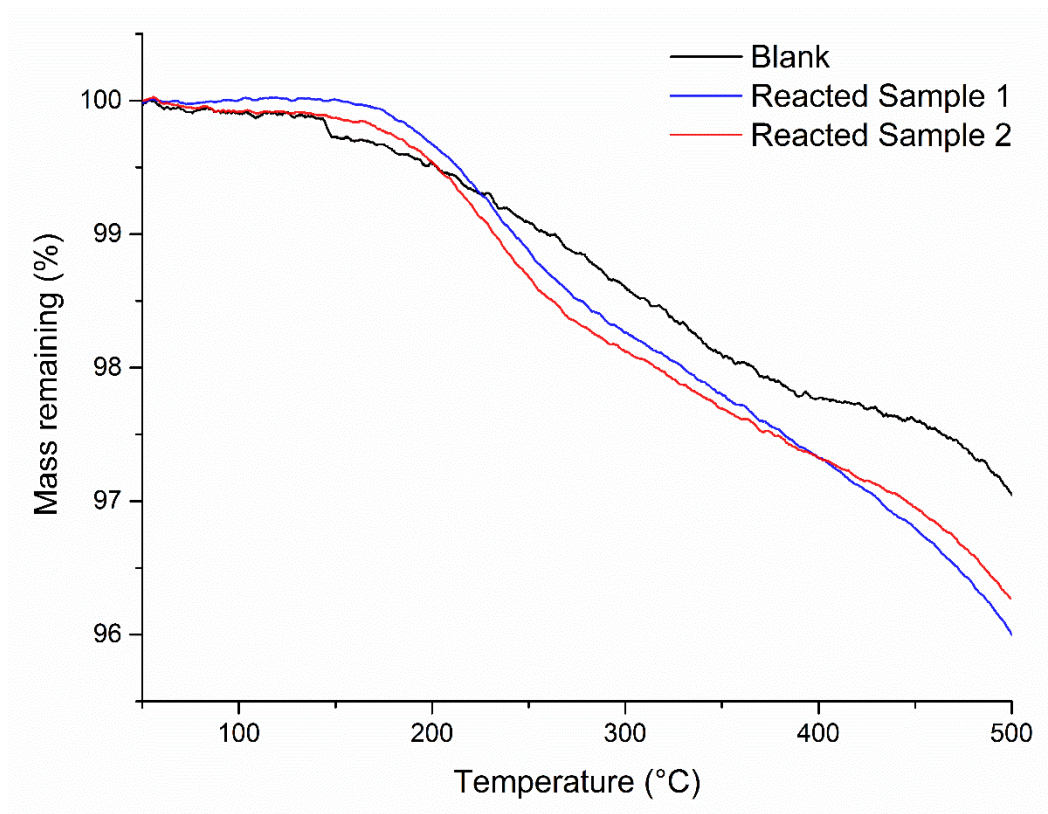


Figure 53: Resulting TGA plots of blank, unreacted vinyl nanoparticles (black) and vinyl nanoparticles reacted with 1-dodecanethiol (blue and red)

An average loss due to 1-dodecanethiol of 0.9% was recorded for the two replicates between 30 °C to 500 °C. This 0.9% average mass loss correlated to 4.01×10^{-16} g of 1-dodecanethiol being present on the surface of the nanoparticles used in the reaction (Appendix, Equation 22). Based on the recorded surface area of $502,000 \text{ nm}^2$ from the BET isotherm (Equation 11), an attachment density of $2.4 \text{ attachments.nm}^{-2}$ was calculated (Appendix, Equation 23). This average attachment density was significantly lower than that calculated using ATR-FTIR which resulted in an average attachment density of $10.6 \pm 5.6 \text{ attachments.nm}^{-2}$. Although TGA analysis resulted in a lower attachment density, the value was within the theoretical maximum of $5 \text{ attachments.nm}^{-2}$ described by the Zhuravlev model [194]. This suggests that the TGA technique provides an improved method for the approximation of attachment densities when compared to ATR-FTIR for the tracking of thiolene attachment to vinyl terminated nanoparticles.

4.4.3 Oligonucleotide attachment optimisation for vinyl nanoparticles

Attachment of thiol modified oligonucleotides to vinyl terminated nanoparticles was investigated using the same modelled thiolene attachment chemistry described in Section 4.4.2 as a proof of concept. Given the increased size of the SH-probe (MW = 6368.4 g.mol⁻¹) relative to the model reagent 1-dodecanethiol (MW = 202.4 g.mol⁻¹), a lower attachment density was expected due to steric effects. As such, the higher excesses previously observed using 1-dodecanethiol may not be required to promote attachment of the oligonucleotides.

Ethanol solutions were previously used for the model attachment of 1-dodecanethiol to vinyl terminated nanoparticles. As oligonucleotides are susceptible to precipitation in high concentrations of ethanol, the reaction matrix required an adjustment. In Chapter 3, thiolene attachment of oligonucleotides to vinyl functionalised glass slides was achieved in water. As vinyl nanoparticles are hydrophobic, dispersion in an aqueous matrix may cause agglomeration thus inhibiting oligonucleotide attachment. As such, an initial evaluation of nanoparticle stability in ultra-pure water and a 1x SSC buffer (pH 7.0) was required. Dispersing the nanoparticles in the 1x SSC buffer resulted in aggregation after only 2 h. Aggregation of nanoparticles in buffered solutions has been reported in literature, resulting from the high ionic strength of the solution creating electrostatic interactions [208, 209]. The resulting aggregation would hinder overall oligonucleotide attachment in solution as less surface is available for attachment. Ultra-pure water also resulted in vinyl terminated nanoparticle aggregation but at a slower rate. As such, initial oligonucleotide attachment and hybridisation was trialled using ultra-pure water following methods described in Section 4.3.4 and 4.3.5. Vinyl nanoparticles initially underwent a thiolene attachment with thiol modified oligonucleotides followed by subsequent hybridisation with Cy5 labelled ACat Seq. Analysis of the reacted samples by fluorescence microscopy resulted in no visible fluorescence indicating that either the thiolene attachment or hybridisation was unsuccessful when using ultra-pure water, most likely due to nanoparticle aggregation.

An investigation into the effect of pH on nanoparticle stability was also completed as this has been found previously to influence nanoparticle aggregation [210]. Unquenched nanoparticles, investigated in Section 4.4.2, provide a basic solution for oligonucleotide attachment. At this high pH, synthesised nanoparticles remained stable in solution and remained in suspension when stored for long periods of time. This stability is similar to a

previous study by Brown *et al.* who found that silica nanoparticles remained stable in high pH aqueous solutions [210]. The pH of the resulting unquenched nanoparticle suspension (in aqueous ammonia) was tested, recording a pH value of 12. Although this pH results in promoted nanoparticle suspension, it would negatively impact oligonucleotide hybridisation in solution. This high pH would result in the denaturation of double stranded DNA, thus inhibiting hybridisation at the nanoparticle surface [211, 212]. As such, use of the unquenched nanoparticles was not investigated further for oligonucleotide attachment and subsequent hybridisation.

Alternatively, varying concentrations of ethanol were investigated in order to find a compromise between nanoparticle stability and oligonucleotide solubility in solution. Nanoparticle aggregation was observed in ethanol concentrations ranging from 25 %, 50 %, 75 %, and 100 % compared to ultra-pure water. As shown in Figure 54, the ultra-pure water resulted in the rapid aggregation of nanoparticles, due to repulsion between the hydrophilic water and hydrophobic vinyl terminated surface. Nanoparticle aggregation was also observed for the 25 % ethanol sample where nanoparticles accumulated on the walls of the plastic well-plate. Above 25 % ethanol, nanoparticles remained stable in solution with minimal aggregation.

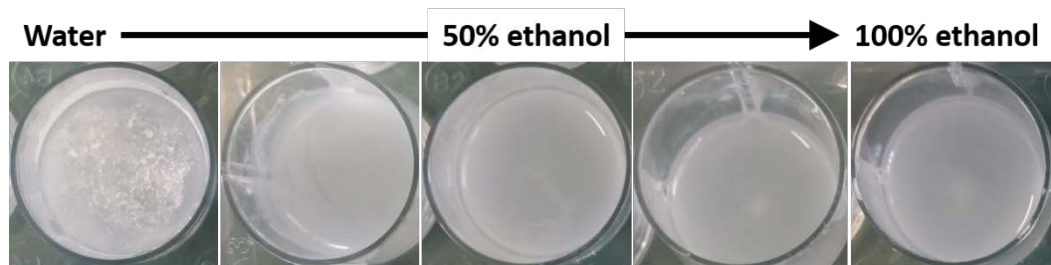


Figure 54: Nanoparticle interactions in different percentage compositions of ethanol

Comparison between water, 25 %, 50 %, 75 % and 100 % ethanol

Oligonucleotide precipitation for biological extractions is achieved using 70-100 % ethanol [208]. Based on this, it was assumed that ethanol percentages below 70 % would minimise the precipitation of oligonucleotides in solution during attachment and hybridisation with vinyl terminated nanoparticles. As shown in Figure 54, the 50 % ethanol solution resulted in minimal aggregation of nanoparticles in solution, as well as keeping oligonucleotides solubilised. As such, 50 % ethanol was tested for the thiolene attachment of oligonucleotides to vinyl terminated silica nanoparticles. Reacted samples were subsequently hybridised with Cy5 labelled ACat Seq and analysed using confocal

microscopy. Both the blank sample (Figure 55A) and the reacted sample hybridised with the Cy5 labelled ACat Seq (Figure 55B) generated a fluorescence response outlined in the white squares. This suggested that the observed signal was not caused by hybridised Cy5 labelled ACat Seq but resulted from a false positive signal. Fluorescent regions were concentrated around nanoparticle agglomerates formed upon drying on the glass slides prior to analysis. This agglomeration is the most likely cause for the false fluorescence response.

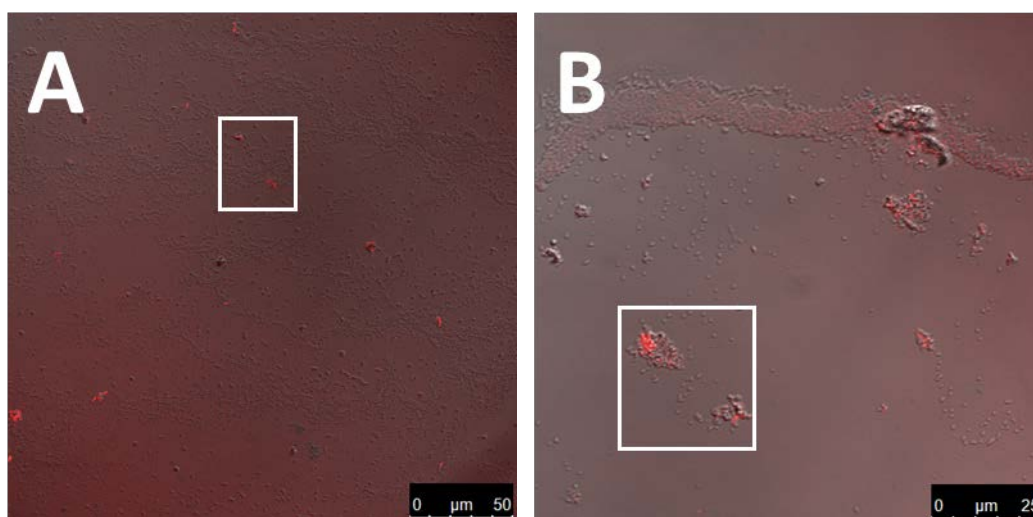


Figure 55: Confocal microscope imaging of blank vinyl terminated nanoparticles (A) and Cy5 ACat Seq hybridised nanoparticles (B)

In order to evaluate whether hybridisation was successful, but potentially below limits of detection, intercalating dye YO-PRO-1 (Life Technologies, USA) was introduced to the reacted, hybridised nanoparticle sample. Approximately 5 μL of 25 μM diluted YO-PRO-1 (in water) was added directly to the dried nanoparticle spot and covered with a coverslip. YO-PRO-1 has an excitation/emission wavelength (491/509 nm) which is different compared to the Cy5 dye (650/670 nm) allowing for discrimination between aggregation fluorescence and fluorescence resulting from intercalation. The confocal microscope image shown in Figure 56 shows regions of fluorescence specific to the YO-PRO-1 dye. The resulting fluorescent regions however do not correspond to the nanoparticles, further demonstrating that the successful attachment and hybridisation of oligonucleotides using these conditions was not possible.

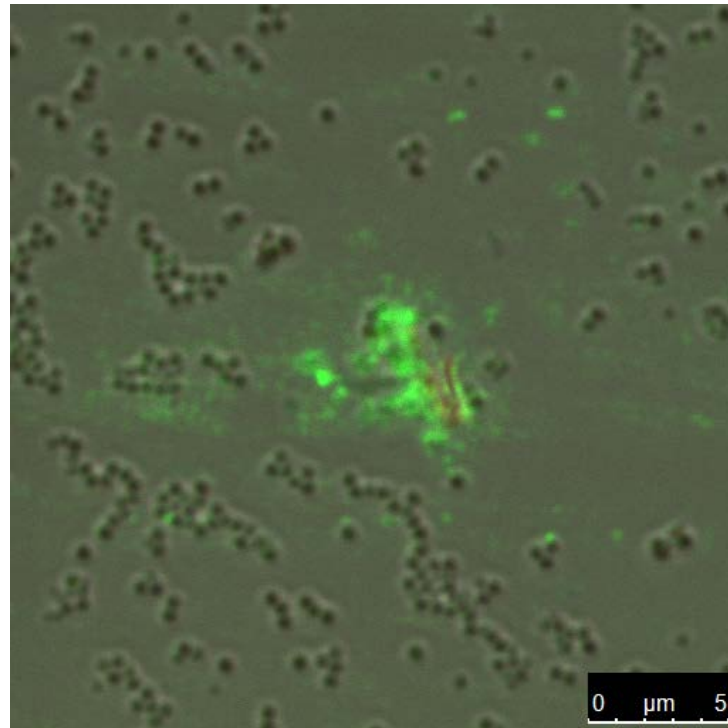


Figure 56: Confocal image of YO-PRO-1 treated hybridised nanoparticles

The resulting fluorescence observed by the YO-PRO-1 dye was due to either glass slide contamination or the carry over of unreacted oligonucleotides. Organic contamination was observed on the glass slide prior to confocal microscopy analysis, which could result in the false positive signal. Alternatively, unreacted oligonucleotides that were not removed during washing may have hybridised in solution and subsequently transferred to the glass slide resulting in the recorded fluorescent signal.

Overall, oligonucleotide attachment was found to be unsuccessful using these reaction conditions. In the future, evaluation into whether the hindrance is associated with oligonucleotide attachment at the surface or the subsequent hybridisation will be required. To do this, fluorescently labelled probes can be attached directly to the nanoparticle surface to specifically identify whether probe attachment was possible using these conditions.

4.5 Conclusions

In this chapter, the thiolene attachment chemistry developed in Chapter 3 for glass slide surfaces was adapted to silica nanoparticles. Use of this high surface area substrate was hypothesised to increase loading of attached oligonucleotides allowing for further improvement in sensitivity, beneficial for the detection of HAB causative microalgae in the future.

Due to the expensive nature of thiol modified oligonucleotides, model thiolene reactions using 1-dodecanethiol were initially used to mimic oligonucleotide attachment. Attachment densities calculated based on the generation of an ATR-FTIR calibration curve were recorded as 10.6 ± 5.6 attachments.nm⁻² based on a nanoparticle diameter of 350 nm and a measured BET surface area of 502,000 nm² per nanoparticle. A 1000 molar excess of 1-dodecanethiol was required for detectable attachment, however the resulting attachment densities suffered from poor reproducibility. Attachment densities were also calculated using an alternative TGA approach which resulted in a recorded attachment density of 2.4 attachments per nm² for 1-dodecanethiol. This value, whilst significantly lower than that calculated using the ATR-FTIR calibration, is more reasonable as it is below the theoretical attachment density of 5 attachments.nm⁻² based on the Zhuravlev model [194].

Although attachment reproducibility was poor, a trial attachment using thiol modified oligonucleotides to vinyl terminated nanoparticles was completed. Here, a compromise between the stability of the suspension of vinyl nanoparticles and also oligonucleotide solubility was required when selecting the reaction solvent. A 50 % ethanol solution was found to meet these requirements, promoting vinyl terminated nanoparticle suspension whilst keeping oligonucleotides solubilised. Analysis of oligonucleotide reacted nanoparticles resulted in fluorescent responses being recorded for both the blank vinyl nanoparticles and the Cy5 ACat Seq hybridised nanoparticles. This indicated that either the attachment of oligonucleotides or subsequent hybridisation was unsuccessful. During drying, the nanoparticles formed aggregates resulting in fluorescent signals upon analysis. Use of the YO-PRO-1 intercalating dye further concluded that the signal present from the aggregates was not caused by hybridised Cy5 labelled ACat Seq as there was no correlation between the nanoparticles and resulting signal. As such, further investigation into the attachment of oligonucleotides to nanoparticle substrates was required before application for the sensitive detection of HAB causative microalgae.

5

Conclusions and Future Work

5.1 Conclusions

This research outlines a covalent attachment approach towards the development of oligonucleotide surfaces for the sensitive and selective detection of HAB causative microalgae. Chapter 2 described the attachment of amine modified oligonucleotides via an APTES functionalised surface and PDITC cross-linker. Using this method, both PDMS and glass were evaluated as substrates for oligonucleotide attachment. The glass slide surface attachment resulted in a significantly higher sensitivity for hybridisation with complimentary Cy5 labelled ACat Seq compared to the PDMS. Use of oligonucleotide modified glass slides also demonstrated superior stability over a 9 day storage period whereas PDMS resulted in a loss of reactivity after only one day storage, caused by hydrophobic recovery. Loss of signal from photobleaching was observed for both the hybridised PDMS and glass surfaces after only one day storage, thus use of the surfaces was restricted to same day analysis.

The use of amine functionalised surfaces for oligonucleotide attachment can promote non-specific adsorption via electrostatic interactions. To overcome this extensive blocking of the modified surface prior to hybridisation was required. As such, an alternative VTES functionalised surface was also evaluated (Chapter 3). This VTES functionalised surface was hypothesised to minimise non-specific adsorption of oligonucleotides due to the hydrophobic nature of the surface, eliminating the need for blocking reactions. Evaluation of reaction times resulted in maximum hybridisation performance when using a VTES silanisation time of 120 min, SH-probe irradiation time of 60 min and an overnight hybridisation in bulk solution. Comparison of the VTES and APTES modification strategy resulted in a higher signal: background ratio for the VTES strategy. Furthermore, a linear relationship between the signal: background ratio and concentration of target ACat Seq was attained for the VTES surface ($R^2 = 0.954$), but not the APTES surface. This suggests that quantitative analysis using the VTES surface for the detection of HABs is possible in the future. Regeneration of the VTES surface was possible with only a 0.7 % loss in signal upon regeneration (re-hybridisation) using a de-hybridisation of 60 °C for 10 min.

Following the significant improvement in performance of oligonucleotide modified glass surfaces prepared using a VTES functionalisation, an adaptation of this thiolene attachment chemistry to nanoparticle surfaces was trialled (Chapter 4). Model reactions with 1-dodecanethiol were used to track theoretical attachment densities using ATR-FTIR, with a calculated value of 10.6 ± 5.6 attachments.nm⁻². The high level of variation was

attributed to batch-to-batch variability of the nanoparticles and possible reproducibility problems with the ATR-FTIR analysis. Alternatively, TGA was used to calculate the 1-dodecanethiol attachment densities resulting in a calculated value of 2.4 attachments.nm⁻². Compared to the ATR-FTIR attachment, this TGA value seemed more accurate as it was below the theoretical attachment of 5 attachments.nm⁻² as based on the Zhuravlev model [194]. Thus, TGA was selected as an optimal method for calculating the thiolene attachment density of 1-dodecanethiol to vinyl terminated surfaces when compared to ATR-FTIR.

Although there were difficulties associated with the reproducibility of attachment using 1-dodecanethiol to vinyl nanoparticles, oligonucleotide attachment was still assessed as a proof of concept. Moving to an aqueous solvent for oligonucleotide attachment resulted in nanoparticle aggregation which ultimately hindered attachment to the surface. Use of a 50 % ethanol solution provided a compromise between nanoparticle stability in solution and oligonucleotides remaining solubilised for attachment. Analysis of oligonucleotide reacted vinyl nanoparticles using confocal microscopy demonstrated a resulting fluorescent signal for the blank and hybridised samples. This suggested that the resulting fluorescence was not from hybridised Cy5 ACat Seq but instead from an interaction of aggregated nanoparticles at 650 nm. To confirm that hybridisation of the ACat Seq was not achieved, intercalating dye YO-PRO-1 was introduced to the hybridised nanoparticle sample. Although a fluorescent signal was generated upon analysis, the fluorescent regions did not correlate to the nanoparticles. This suggested that hybridisation was not successful at the surface of the nanoparticle and the signal was caused by slide contamination or residual hybridised oligonucleotides in solution. As such, further investigation into the reaction conditions would be required for the future use of nanoparticle substrates for oligonucleotide attachment.

5.2 Future work

5.2.1 Oligonucleotide attachment to glass and PDMS surfaces

Oligonucleotide modified glass slides were found to outperform PDMS based on stability and sensitivity for hybridisation with complimentary ACat Seq. PDMS is still a very promising substrate for oligonucleotide attachment however as the versatility of the polymer allows for preparation of microfluidic devices for portable, in field analysis. This would be highly beneficial for the on-site analysis of HAB samples in the future. Evaluation of the effects of hydrophobic recovery on oligonucleotide modified substrates would assist in overcoming this downfall. By understanding rates of recovery and effect of this on the final functionalised surface, different strategies could be implemented to overcome or minimise the level of hydrophobic recovery. This can be achieved by monitoring surface recovery using WCA measurements and tracking changes in functionality due to surface rearrangement using methods such as ATR-FTIR.

In Chapter 3, the difference in performance between APTES and VTES silanised glass slides was hypothesised to be due to orientation of oligonucleotides at the surface based on electrostatic interactions. To prove this theory, analytical techniques could be implemented to compare the two oligonucleotide modified surfaces. Dual polarisation interferometry (DPI) has been previously reported as a method for identifying oligonucleotide conformation at the surface [183]. This method provides information on surface thickness and refraction index based on interference patterns produced as a laser passes through a sandwiched structure [183]. This label free detection method can be used to calculate surface mass and density of oligonucleotide attachment [183]. The difference in measured thickness between the VTES and APTES oligonucleotide surface can provide information on orientation with flat oligonucleotide conformations resulting in a lower recorded thickness than those perpendicular to the surface in an end-to-end attachment.

Alternatively, if amine functionalised surfaces were to be used for oligonucleotide attachment, blocking strategies to minimise non-specific adsorption and interactions between attached oligonucleotides and the surface would need to be investigated. The use of ethanolamine blocking strategies has been found to not completely eliminate adsorption of oligonucleotides for amine functionalised surfaces [183]. Other methods for blocking substrates that could be trialled include the use of succinic anhydride (SA) or

bovine serum albumin (BSA) [178]. Use of these alternative blocking agents may also promote end-to-end conformation of oligonucleotides at the surface making them more readily available for hybridisation with target ACat Seq.

5.2.2 Oligonucleotide attachment to nanoparticles

Based on the evidence of successful thiolene attachment using 1-dodecanethiol model reactions on vinyl nanoparticles, attachment of oligonucleotides using thiolene chemistry should be possible. The most probable cause for hindered attachment is the formation of nanoparticle aggregations in aqueous systems. Use of non-ionic surfactants, such as Triton X-100, may be able to improve stability of the nanoparticle suspension in water, promoting oligonucleotide attachment at the surface. Oligonucleotide interactions with the surfactant would need to be examined to determine if use of surfactant interferes with oligonucleotide attachment.

The attachment of oligonucleotides to vinyl terminated nanoparticles can be investigated by attaching fluorescently labelled oligonucleotide probes to the surface. This method would also allow for optimisation of attachment for improved sensitivity if successful. Alternatively, the dithiol attachment of oligonucleotides to thiol terminated nanoparticles has been reported in buffered systems by Hilliard *et al.* [143]. This suggests that the use of alternative thiol terminated nanoparticles would allow for a shift to an aqueous or buffered reaction matrix. Reversing the thiolene attachment with the use of alkene modified oligonucleotides may overcome issues surrounding hydrophobic nanoparticle aggregation whilst still incorporating the stable thiolene attachment. If attachment using this reversed method was successful it would indicate that oligonucleotide attachment to vinyl nanoparticles was unsuccessful due to hydrophobic aggregation in aqueous systems.

To further improve nanoparticle stability in aqueous suspensions, alternative polar functionalised nanoparticles can be investigated for oligonucleotide attachment. Preliminary investigations using amine terminated nanoparticles for oligonucleotide attachment via a PDITC cross-linker was completed as a part of this study. Excessive non-specific adsorption of Cy5 labelled ACat Seq was observed on the surface of bare amine terminated nanoparticles (Appendix, Figure 61). This demonstrated that blocking strategies would need to be implemented to overcome this adsorption prior to use. If a suitable blocking strategy could be developed, oligonucleotide attachment to amine terminated nanoparticles could be achieved in aqueous systems.

5.2.3 Application of surfaces for the selective detection of *A. catenella*

The overall aim of this project was to develop oligonucleotide modified surfaces for the sensitive and selective detection of HAB species. To achieve this, the introduction of the developed oligonucleotide modified glass surfaces to extracted HAB RNA would be required. During the initial stages of this study, *A. catenella* (Strain ACAD01) cultures were grown in the laboratory. A growth curve was established comparing both f/2 medium and GSe medium (Appendix, Figure 62) for optimal growth, with f/2 being selected for future culturing experiments. Unfortunately, culture crash due to fluctuations in salinity levels used in the preparation of culture mediums meant that research into the application of these surfaces was unable to be completed as planned.

In the future, the developed oligonucleotide modified surfaces would be applied to crude lysates for a range of HAB species to investigate surface sensitivity and selectivity to the variable nucleic acid regions described in Chapter 1. As molecular identification of HABs has risen in popularity, a large number of species specific probe sequences have already been reported in literature which can be applied to the developed surfaces. A shift towards label-free detection would also be advantageous for the detection of HAB causative microalgae using these surfaces. This could be achieved using electrochemical methods [94], dual polarisation interferometry [183] or through the use of sensitive quartz crystal microbalances [213].

6

Appendix

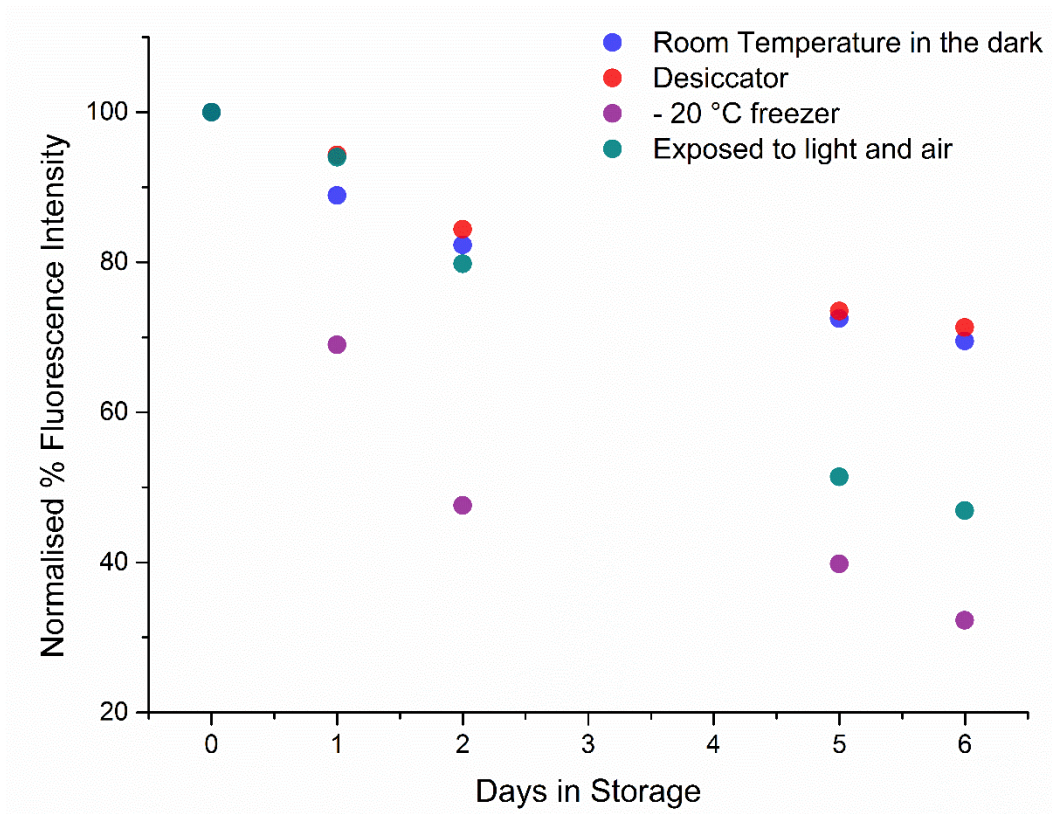


Figure 57: Effect of fluorescence intensity degradation under different storage conditions

Graph of recorded fluorescence intensities after consecutive days in storage. Analysed on the Olympus IX-81 (n= 1).

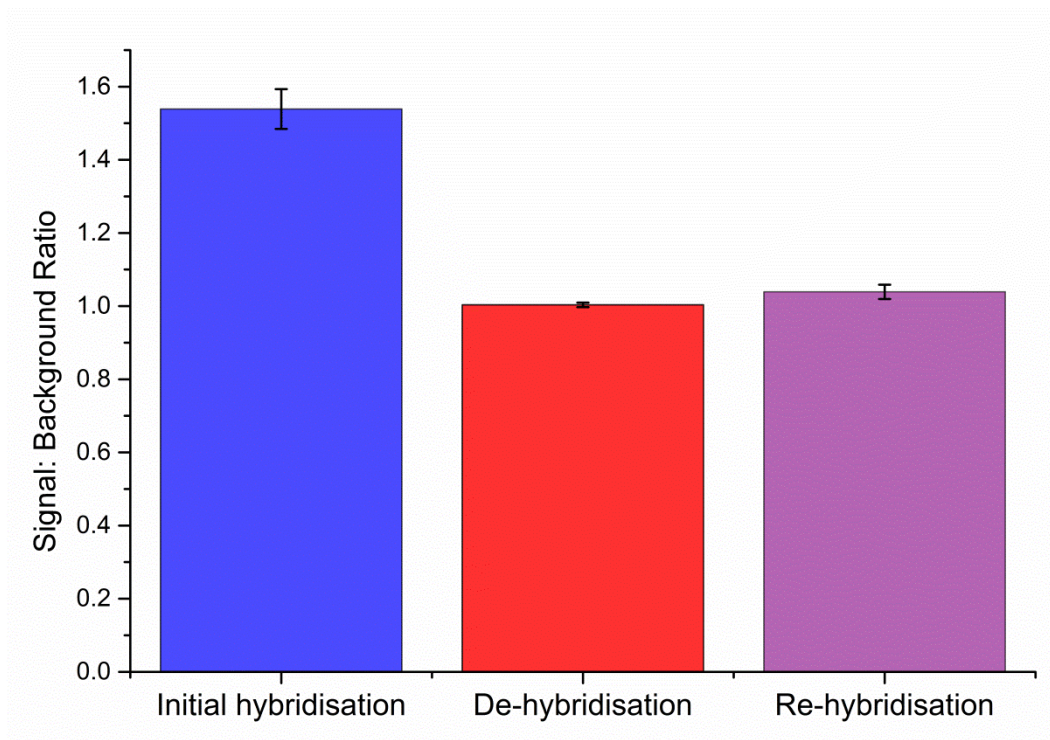


Figure 58: Use of 0.1 M sodium phosphate buffer (pH 8.0) for the de-hybridisation of Cy5 labelled target sequence

Average signal:background fluorescence intensity ratios after one regeneration cycle analysed on the Olympus IX-71 (n= 3, \pm standard deviation) using a bulk solution hybridisation.

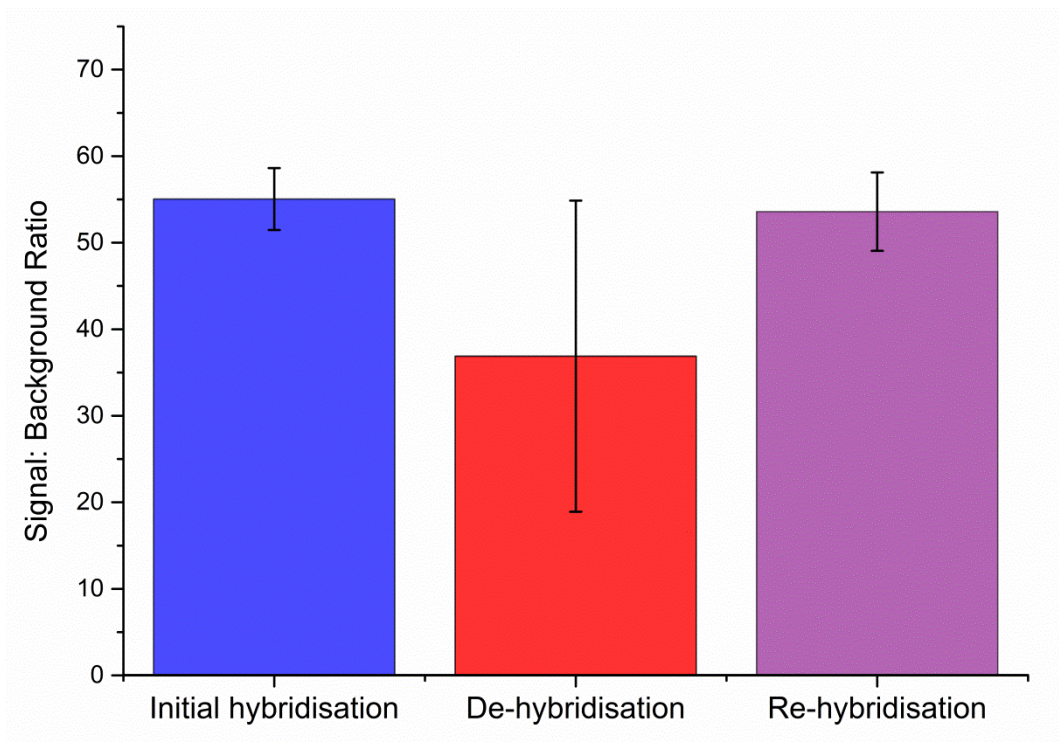


Figure 59: Use of 1x SSC buffer (pH 7.0) for the de-hybridisation of Cy5 labelled target sequence

Average signal:background fluorescence intensity ratios after one regeneration cycle analysed on the Olympus IX-73 (n= 3, \pm standard deviation) using a bulk solution hybridisation.

Calculation of 1-dodecanethiol excesses with working

The calculation of volumes of 1-dodecanethiol required for the molar excesses are shown below with each individual step fully worked out:

1. Initially the number of nanoparticles present in a 3 mL sample of vinyl terminated nanoparticles ($5 \text{ mg}\cdot\text{mL}^{-1}$) was calculated using the $4.49 \times 10^{-14} \text{ g}\cdot\text{particle}^{-1}$ calculated in (Section 4.4.1, Equation 10):

$$\begin{aligned} \text{Nanoparticles available} &= \frac{\text{Mass of nanoparticles in 3 mL (g)}}{\text{g}\cdot\text{particle}^{-1}} = \\ &= \frac{15 \times 10^{-3} \text{ g}}{4.49 \times 10^{-14} \text{ g}\cdot\text{particle}^{-1}} = 3.34 \times 10^{11} \text{ nanoparticles available per reaction} \end{aligned}$$

Equation 16: Calculated working for the number of nanoparticles available for reaction

2. Using the 3.34×10^{11} nanoparticles available for reaction, the total available surface area can be calculated using the $502,000 \text{ nm}^2$ surface area determined from the BET analysis (Section 4.4.1, Equation 11):

$$\begin{aligned} \text{Available surface area} &= \text{Surface area per nanoparticle} \times \text{total number of nanoparticles} \\ &= 502,000 \text{ nm}^2 \cdot \text{particle}^{-1} \times 3.34 \times 10^{11} \text{ particles} = 1.68 \times 10^{17} \text{ nm}^2 \text{ available} \end{aligned}$$

Equation 17: Calculated working for the total available surface area (nm^2) per reaction

3. Based on the Zhuralev model [194] where approximately 5 hydroxyl molecules are available for reaction on silica nanoparticles per nm^2 it was assumed that there will be 5 available vinyl groups. nm^2 available for attachment of 1-dodecanethiol. From this the number of attachments can be determined:

$$\begin{aligned} \text{Number of attachments} &= 5 \text{ attachments}\cdot\text{nm}^2 \times \text{available surface area (nm}^2\text{)} \\ &= 5 \text{ attachments}\cdot\text{nm}^2 \times (1.68 \times 10^{17} \text{ nm}^2) \\ &= 8.39 \times 10^{17} \text{ attachments for 1:1 stoichiometry with model reactant} \end{aligned}$$

Equation 18: Calculated working for the number of attachments possible for 1:1 stoichiometry

4. Next, based on the number of theoretical attachments possible for 1:1 stoichiometry, the number of moles of 1-dodecanethiol can be calculated using Avogadro's number:

$$\begin{aligned} \text{Number of moles of 1-dodecanethiol} &= \frac{\text{Number of attachments per reaction}}{\text{Avogadro's number}} \\ &= \frac{8.39 \times 10^{17} \text{ attachments}}{6.02 \times 10^{23}} = 1.39 \times 10^{-6} \text{ mol} \end{aligned}$$

Equation 19: Calculated working for the molar equivalent of 1-dodecanethiol (mol) from attachment number using 1:1 stoichiometry

5. Using the number of moles of 1-dodecanethiol, the number of moles required for 10, 20, 40, 100 and 1000 molar excesses can then be calculated using the equation below:

$$\begin{aligned} \text{10:1 molar excess 1-dodecanethiol} & \\ &= 10 \times \text{number of moles required for 1:1 stoichiometry (mol)} \\ &= (1.39 \times 10^{-6}) \text{ mol} = 1.39 \times 10^{-5} \text{ mol required for 10:1 ratio} \end{aligned}$$

Equation 20: Calculated working for the molar amount of 1-dodecanethiol (mol) required for a 10 molar excess attachment

6. Finally, the number of moles can be converted to a measurable volume to be added to the reaction using the molar mass (202.4 g.mol⁻¹) and density (0.845 g.mL⁻¹) of 1-dodecanethiol:

$$\begin{aligned} \text{Volume of 1-dodecanethiol required (mL)} &= \frac{n \times M}{d} \\ &= \frac{(1.39 \times 10^{-5} \text{ mol}) \times 202.4 \text{ g.mol}^{-1}}{0.846 \text{ g.mL}^{-1}} = 3.33 \times 10^{-3} \text{ mL} = 3.33 \mu\text{L} \end{aligned}$$

Equation 21: Calculated working for the volume of 1-dodecanethiol (mL) required for a 10 molar excess attachment

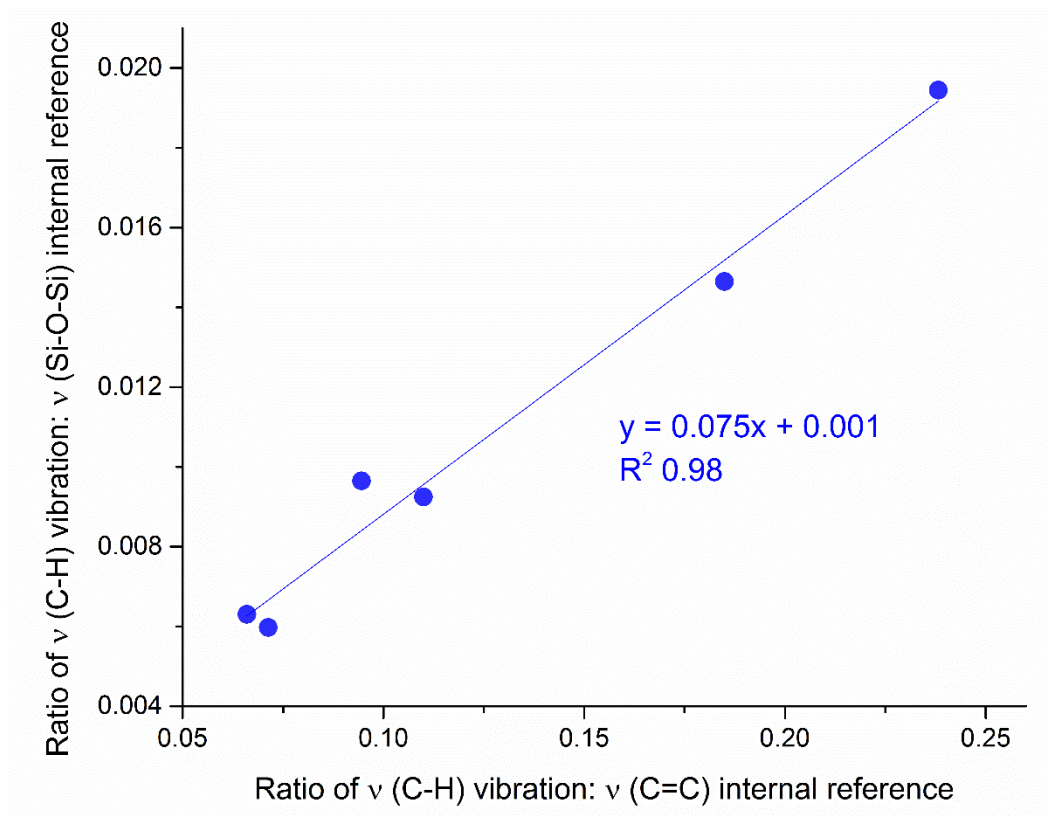


Figure 60: Comparison between the use of ν (C=C) and ν (Si-O-Si) as an internal standard reference peak for determining attachment density of 1-dodecanethiol

TGA calculation of attachment density with working:

Calculation of attachment density was also achieved using TGA analysis results and the following working based on a recorded mass loss of 0.9 % between the two replicates (averaged from 2.2 % for Sample 1 and 1.7 % for Sample 2) and the mass of a nanoparticle being $4.49 \times 10^{-14} \text{ g.nanoparticle}^{-1}$:

$$\begin{aligned} & \text{Mass of 1 – dodecanethiol} \\ &= \text{Mass of nanoparticle (g)} \times \text{Average mass loss (\%, n = 2)} \\ &= (4.49 \times 10^{-14} \text{ g.particle}^{-1}) \times 0.9\% \\ &= 4.01 \times 10^{-16} \text{ g of 1 – dodecanethiol} \end{aligned}$$

Equation 22: Calculated working for the mass (g) of 1-dodecanethiol based on the TGA average mass loss (%)

Calculation of attachment density using the recorded mass of 1-dodecanethiol was achieved using the molar mass of 1-dodecanethiol (202.4 g.mol^{-1}), Avogadro's number and the surface area of a 350 nm nanoparticle ($502,000 \text{ nm}^2$):

$$\begin{aligned} & \text{Attachment density of 1 – dodecanethiol} \\ &= \frac{\left(\text{Mass of 1 – dodecanethiol (g)} / \text{Molar mass (g.mol}^{-1}) \right) \times \text{Avogadro's number}}{\text{Surface area of a nanoparticle (nm}^2)} \\ &= \frac{\left(4.01 \times 10^{-16} \text{ g} / 202.4 \text{ g.mol}^{-1} \right) \times 6.02 \times 10^{23}}{502,000 \text{ nm}^2} = 2.4 \text{ attachments.nm}^{-2} \end{aligned}$$

Equation 23: Calculated working for the TGA calculated attachment density of 1-dodecanethiol (attachments.nm⁻²)

Thus, an attachment density of $2.4 \text{ attachments.nm}^{-2}$ of 1-dodecanethiol was calculated using TGA analysis.

Amine functionalised nanoparticles for oligonucleotide attachment and hybridisation



Figure 61: Cy5 labelled target sequence adsorbed to cleaned, bare amine functionalised nanoparticles shown as blue

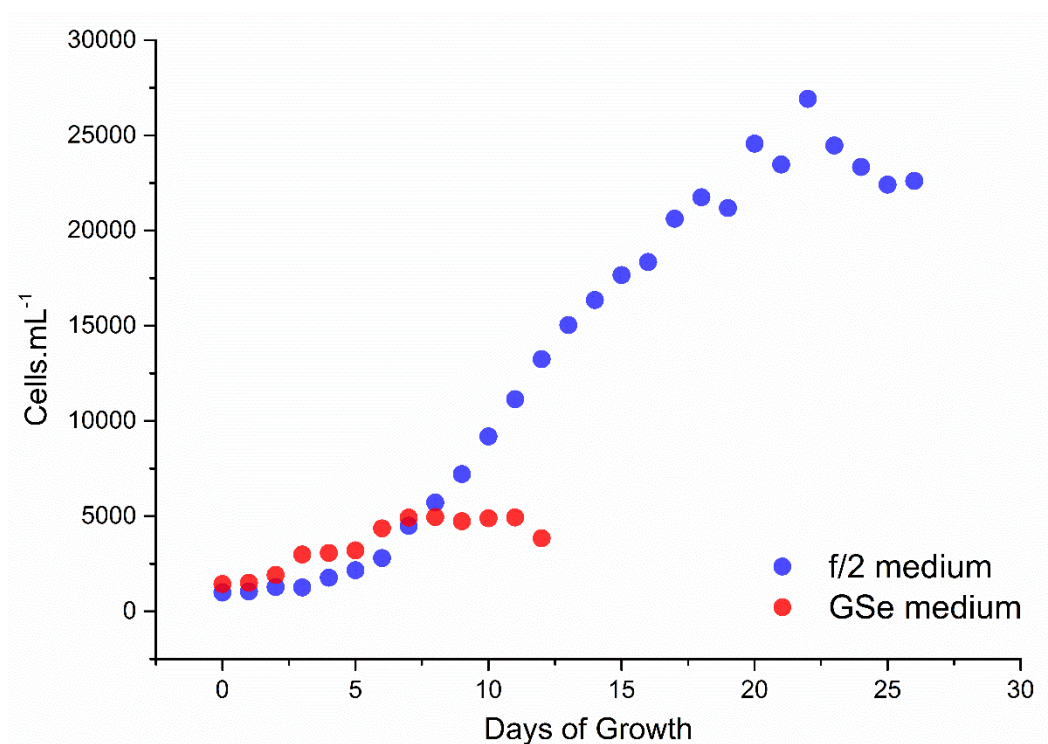


Figure 62: Growth curve for *A. catenella* cultured in f/2 medium (blue) and GSe medium (red)

7

References

1. Anderson, D.M., *Approaches to monitoring, control and management of harmful algal blooms (HABs)*. Ocean Coast Manage, 2009. **52**(7): p. 342-347.
2. Sellner, K.G., Doucette, G.J., and Kirkpatrick, G.J., *Harmful algal blooms: causes, impacts and detection*. J Ind Microbiol Biot, 2003. **30**(7): p. 383-406.
3. Quilliam, M.A., *The role of chromatography in the hunt for red tide toxins*. J Chromatogr A, 2003. **1000**(1–2): p. 527-548.
4. Christian, B. and Luckas, B., *Determination of marine biotoxins relevant for regulations: from the mouse bioassay to coupled LC-MS methods*. Anal Bioanal Chem, 2008. **391**(1): p. 117-134.
5. Gago-Martínez, A. and Rodríguez-Vázquez, J.A., *Marine Toxins: Chromatography*. Encyclopedia of Separation Science, ed. D.W. Ian. 2000, Oxford: Academic Press. 3269-3277.
6. Okamoto, K. and Fleming, L.E., *Algae*, in *Encyclopedia of Toxicology (Second Edition)*, W. Editor-in-Chief: Philip, Editor. 2005, Elsevier: New York. p. 68-76.
7. Masó, M. and Garcés, E., *Harmful microalgae blooms (HAB); problematic and conditions that induce them*. Marine Pollution Bulletin, 2006. **53**(10–12): p. 620-630.
8. Heisler, J., Glibert, P.M., Burkholder, J.M., Anderson, D.M., Cochlan, W., Dennison, W.C., Dortch, Q., Gobler, C.J., Heil, C.A., Humphries, E., Lewitus, A., Magnien, R., Marshall, H.G., Sellner, K., Stockwell, D.A., Stoecker, D.K., and Suddleson, M., *Eutrophication and harmful algal blooms: A scientific consensus*. Harmful Algae, 2008. **8**(1): p. 3-13.
9. Glibert, P.M. and Burkholder, J.M., *The Complex Relationships Between Increases in Fertilization of the Earth, Coastal Eutrophication and Proliferation of Harmful Algal Blooms*, in *Ecology of Harmful Algae*, E. Granéli and J. Turner, Editors. 2006, Springer Berlin Heidelberg. p. 341-354.
10. Adam, A., Mohammad-Noor, N., Anton, A., Saleh, E., Saad, S., and Muhd Shaleh, S.R., *Temporal and spatial distribution of harmful algal bloom (HAB) species in coastal waters of Kota Kinabalu, Sabah, Malaysia*. Harmful Algae, 2011. **10**(5): p. 495-502.
11. Shen, L., Xu, H., and Guo, X., *Satellite Remote Sensing of Harmful Algal Blooms (HABs) and a Potential Synthesized Framework*. Sensors, 2012. **12**(6): p. 7778-7803.

12. Frolov, S., Kudela, R.M., and Bellingham, J.G., *Monitoring of harmful algal blooms in the era of diminishing resources: A case study of the U.S. West Coast*. Harmful Algae, 2013. **21–22**: p. 1-12.
13. Pierce, R.H. and Kirkpatrick, G.J., *Innovative techniques for harmful algal toxin analysis*. Environmental Toxicology and Chemistry, 2001. **20**(1): p. 107-114.
14. MacKenzie, L., Beuzenberg, V., Holland, P., McNabb, P., and Selwood, A., *Solid phase adsorption toxin tracking (SPATT): a new monitoring tool that simulates the biotoxin contamination of filter feeding bivalves*. Toxicon, 2004. **44**(8): p. 901-918.
15. Andersen, R.A., *Algal Culturing Techniques*. 2005, United States: Academic Press.
16. Anderson, D.M., Anderson, P., Bricelj, M.V., Cullen, J.J., and Rensel, J.J.E., *Monitoring and management strategies for harmful algal blooms in coastal waters, in Singapore and Intergovernmental Oceanographic Commission*. 2001: Paris.
17. Blondeau-Patissier, D., Gower, J.F.R., Dekker, A.G., Phinn, S.R., and Brando, V.E., *A review of ocean color remote sensing methods and statistical techniques for the detection, mapping and analysis of phytoplankton blooms in coastal and open oceans*. Progress in Oceanography, 2014. **123**: p. 123-144.
18. Moisan, T.A., Sathyendranath, S., and Bouman, H.A., *Ocean color remote sensing of phytoplankton functional types*. Remote sensing of biomass—principles and applications. Intech, Rijeka, Croatia, 2012: p. 101-122.
19. Gerssen, A., Mulder, P.P.J., McElhinney, M.A., and de Boer, J., *Liquid chromatography-tandem mass spectrometry method for the detection of marine lipophilic toxins under alkaline conditions*. J. Chromatogr., A, 2009. **1216**(9): p. 1421-1430.
20. These, A., Scholz, J., and Preiss-Weigert, A., *Sensitive method for the determination of lipophilic marine biotoxins in extracts of mussels and processed shellfish by high-performance liquid chromatography-tandem mass spectrometry based on enrichment by solid-phase extraction*. Journal of Chromatography, A, 2009. **1216**(21): p. 4529-4538.
21. These, A., Klemm, C., Nausch, I., and Uhlig, S., *Results of a European interlaboratory method validation study for the quantitative determination of lipophilic marine biotoxins in raw and cooked shellfish based on high-*

- performance liquid chromatography-tandem mass spectrometry. Part I: collaborative study. Analytical and Bioanalytical Chemistry, 2011. 399(3): p. 1245-1256.*
22. Gago-Martinez, A., Comesana-Losada, M., Leao-Martins, J.M., and Rodriguez-Vazquez, J.A., *Study on DSP and PSP toxic profile in Haliotis tuberculata. Ciencia (Maracaibo), 1996. 4(4): p. 335-342.*
 23. Garcia, C., Pruzzo, M., Rodriguez-Unda, N., Contreras, C., and Lagos, N., *First evidence of Okadaic acid acyl-derivative and dinophysistoxin-3 in mussel samples collected in Chiloe Island, Southern Chile. J. Toxicol. Sci., 2010. 35(3): p. 335-344.*
 24. Louppis, A.P., Badeka, A.V., Katikou, P., Paleologos, E.K., and Kontominas, M.G., *Determination of okadaic acid, dinophysistoxin-1 and related esters in Greek mussels using HPLC with fluorometric detection, LC-MS/MS and mouse bioassay. Toxicon, 2010. 55(4): p. 724-733.*
 25. Prassopoulou, E., Katikou, P., Georgantelis, D., and Kyritsakis, A., *Detection of okadaic acid and related esters in mussels during diarrhetic shellfish poisoning (DSP) episodes in Greece using the mouse bioassay, the PP2A inhibition assay and HPLC with fluorimetric detection. Toxicon, 2009. 53(2): p. 214-227.*
 26. Galluzzi, L., Penna, A., Bertozzini, E., Vila, M., Garcés, E., and Magnani, M., *Development of a Real-Time PCR Assay for Rapid Detection and Quantification of Alexandrium minutum (a Dinoflagellate). Applied and Environmental Microbiology, 2004. 70(2): p. 1199-1206.*
 27. Fux, E., Marcaillou, C., Mondeguer, F., Bire, R., and Hess, P., *Field and mesocosm trials on passive sampling for the study of adsorption and desorption behavior of lipophilic toxins with a focus on OA and DTX1. Harmful Algae, 2008. 7(5): p. 574-583.*
 28. Turrell, E., Stobo, L., Lacaze, J.P., Bresnan, E., and Gowland, D. *Development of an 'early warning system' for harmful algal blooms using solid-phase adsorption toxin tracking (SPATT). in OCEANS 2007 - Europe. 2007.*
 29. Rundberget, T., Gustad, E., Samdal, I.A., Sandvik, M., and Miles, C.O., *A convenient and cost-effective method for monitoring marine algal toxins with passive samplers. Toxicon, 2009. 53(5): p. 543-550.*
 30. Scholin, C.A., Buck, K.R., Britschgi, T., Cangelosi, G., and Chavez, F.P., *Identification of Pseudo-nitzschia australis (Bacillariophyceae) using rRNA-*

- targeted probes in whole cell and sandwich hybridization formats*. *Phycologia*, 1996. **35**(3): p. 190-197.
31. Ayers, K., Rhodes, L.L., Tyrrell, J., Gladstone, M., and Scholin, C., *International accreditation of sandwich hybridisation assay format DNA probes for microalgae*. *New Zealand Journal of Marine and Freshwater Research*, 2005. **39**(6): p. 1225-1231.
 32. Scholin, C.A., Villac, M.C., Buck, K.R., Krupp, J.M., Powers, D.A., Fryxell, G.A., and Chavez, F.P., *Ribosomal DNA sequences discriminate among toxic and non-toxic Pseudo-nitzschia species*. *Natural Toxins*, 1994. **2**(4): p. 152-165.
 33. Scholin, C.A., Herzog, M., Sogin, M., and Anderson, D.M., *Identification of group- and strain-specific genetic markers for globally distributed Alexandrium (Dinophyceae). II. Sequence analysis of a fragment of the LSU rRNA gene*. *Journal of Phycology*, 1994. **30**(6): p. 999-1011.
 34. Miller, P.E. and Scholin, C.A., *Identification of cultured Pseudo-nitzschia (Bacillariophyceae) using species-specific LSU rRNA-targeted fluorescent probes*. *Journal of Phycology*, 1996. **32**(4): p. 646-655.
 35. Tyrrell, J.V., Bergquist, P.R., Bergquist, P.L., and Scholin, C.A., *Detection and enumeration of Heterosigma akashiwo and Fibrocapsa japonica (Raphidophyceae) using rRNA-targeted oligonucleotide probes*. *Phycologia*, 2001. **40**(5): p. 457-467.
 36. Popels, L.C., Cary, S.C., Hutchins, D.A., Forbes, R., Pustizzi, F., Gobler, C.J., and Coyne, K.J., *The use of quantitative polymerase chain reaction for the detection and enumeration of the harmful alga Aureococcus anophagefferens in environmental samples along the United States East Coast*. *Limnology and Oceanography: Methods*, 2003. **1**: p. 92-102.
 37. Antonella, P. and Luca, G., *The quantitative real-time PCR applications in the monitoring of marine harmful algal bloom (HAB) species*. *Environmental Science and Pollution Research*, 2013. **20**(10): p. 6851-6862.
 38. Hosoi-Tanabe, S. and Sako, Y., *Species-Specific Detection and Quantification of Toxic Marine Dinoflagellates Alexandrium tamarense and A. catenella by Real-Time PCR Assay*. *Marine Biotechnology*, 2005. **7**(5): p. 506-514.
 39. Kamikawa, R., Nagai, S., Hosoi-Tanabe, S., Itakura, S., Yamaguchi, M., Uchida, Y., Baba, T., and Sako, Y., *Application of real-time PCR assay for detection and*

- quantification of Alexandrium tamarense and Alexandrium catenella cysts from marine sediments*. Harmful Algae, 2007. **6**(3): p. 413-420.
40. Galluzzi, L., Bertozzini, E., Penna, A., Perini, F., Garcés, E., and Magnani, M., *Analysis of rRNA gene content in the Mediterranean dinoflagellate Alexandrium catenella and Alexandrium taylori: implications for the quantitative real-time PCR-based monitoring methods*. Journal of Applied Phycology, 2010. **22**(1): p. 1-9.
41. Garneau, M.-È., Schnetzer, A., Countway, P.D., Jones, A.C., Seubert, E.L., and Caron, D.A., *Examination of the seasonal dynamics of the toxic dinoflagellate Alexandrium catenella at Redondo Beach, California, by quantitative PCR*. Applied and Environmental Microbiology, 2011. **77**(21): p. 7669-7680.
42. Murray, S.A., Wiese, M., Stüken, A., Brett, S., Kellmann, R., Hallegraeff, G., and Neilan, B.A., *sxtA-based quantitative molecular assay to identify saxitoxin-producing harmful algal blooms in marine waters*. Applied and Environmental Microbiology, 2011. **77**(19): p. 7050-7057.
43. Touzet, N., Keady, E., Raine, R., and Maher, M., *Evaluation of taxa-specific real-time PCR, whole-cell FISH and morphotaxonomy analyses for the detection and quantification of the toxic microalgae Alexandrium minutum (Dinophyceae), Global Clade ribotype*. FEMS Microbiology Ecology, 2009. **67**(2): p. 329-341.
44. Erdner, D.L., Percy, L., Keafer, B., Lewis, J., and Anderson, D.M., *A quantitative real-time PCR assay for the identification and enumeration of Alexandrium cysts in marine sediments*. Deep Sea Research Part II: Topical Studies in Oceanography, 2010. **57**(3-4): p. 279-287.
45. Dyhrman, S.T., Erdner, D., Du, J.L., Galac, M., and Anderson, D.M., *Molecular quantification of toxic Alexandrium fundyense in the Gulf of Maine using real-time PCR*. Harmful Algae, 2006. **5**(3): p. 242-250.
46. Kamikawa, R., Hosoi-Tanabe, S., Nagai, S., Itakura, S., and Sako, Y., *Development of a quantification assay for the cysts of the toxic dinoflagellate Alexandrium tamarense using real-time polymerase chain reaction*. Fisheries Science, 2005. **71**(5): p. 987-991.
47. Kavanagh, S., Brennan, C., O'Connor, L., Moran, S., Salas, R., Lyons, J., Silke, J., and Maher, M., *Real-time PCR detection of Dinophysis species in Irish coastal waters*. Marine Biotechnology, 2010. **12**(5): p. 534-542.

48. Fitzpatrick, E., Caron, D.A., and Schnetzer, A., *Development and environmental application of a genus-specific quantitative PCR approach for Pseudo-nitzschia species*. Marine biology, 2010. **157**(5): p. 1161-1169.
49. Andree, K.B., Fernández-Tejedor, M., Elandaloussi, L.M., Quijano-Scheggia, S., Sampedro, N., Garcés, E., Camp, J., and Diogène, J., *Quantitative PCR coupled with melt curve analysis for detection of selected Pseudo-nitzschia spp.(Bacillariophyceae) from the northwestern Mediterranean Sea*. Applied and Environmental Microbiology, 2011. **77**(5): p. 1651-1659.
50. Delaney, J.A., Ulrich, R.M., and Paul, J.H., *Detection of the toxic marine diatom Pseudo-nitzschia multiseriis using the RuBisCO small subunit (rbcS) gene in two real-time RNA amplification formats*. Harmful Algae, 2011. **11**: p. 54-64.
51. Kamikawa, R., Asai, J., Miyahara, T., Murata, K., Oyama, K., Yoshimatsu, S., Yoshida, T., and Sako, Y., *Application of a Real-time PCR Assay to a Comprehensive Method of Monitoring Harmful Algae*. Microbes and environments, 2006. **21**(3): p. 163-173.
52. Bowers, H.A., Trice, T.M., Magnien, R.E., Goshorn, D.M., Michael, B., Schaefer, E.F., Rublee, P.A., and Oldach, D.W., *Detection of Pfiesteria spp. by PCR in surface sediments collected from Chesapeake Bay tributaries (Maryland)*. Harmful Algae, 2006. **5**(4): p. 342-351.
53. Handy, S.M., Hutchins, D.A., Cary, S., and Coyne, K.J., *Simultaneous enumeration of multiple raphidophyte species by quantitative real-time PCR: capabilities and limitations*. Limnology and Oceanography: Methods, 2006. **4**: p. 193-204.
54. Galluzzi, L., Bertozzini, E., Penna, A., Perini, F., Pigalarga, A., Graneli, E., and Magnani, M., *Detection and quantification of Prymnesium parvum (Haptophyceae) by real-time PCR*. Letters in applied microbiology, 2008. **46**(2): p. 261-266.
55. Zamor, R.M., Glenn, K.L., and Hambright, K.D., *Incorporating molecular tools into routine HAB monitoring programs: Using qPCR to track invasive Prymnesium*. Harmful Algae, 2012. **15**: p. 1-7.
56. Manning, S.R. and La Claire II, J.W., *Multiplex PCR methods for the species-specific detection and quantification of Prymnesium parvum (Haptophyta)*. Journal of Applied Phycology, 2010. **22**(5): p. 587-597.

57. Martins, A. and Vasconcelos, V., *Use of qPCR for the study of hepatotoxic cyanobacteria population dynamics*. Archives of microbiology, 2011. **193**(9): p. 615-627.
58. Park, B.S., Wang, P., Kim, J.H., Kim, J.-H., Gobler, C.J., and Han, M.-S., *Resolving the intra-specific succession within *Cochlodinium polykrikoides* populations in southern Korean coastal waters via use of quantitative PCR assays*. Harmful Algae, 2014. **37**: p. 133-141.
59. Smith, K.F., de Salas, M., Adamson, J., and Rhodes, L.L., *Rapid and Accurate Identification by Real-Time PCR of Biotxin-Producing Dinoflagellates from the Family Gymnodiniaceae*. Marine drugs, 2014. **12**(3): p. 1361-1376.
60. Zhang, C.Y., Chen, G.F., Zhou, J., Wang, Y.Y., and Lu, D.D., *Development of a quantitative PCR for detection and quantification of *Prorocentrum donghaiense**. Journal of Applied Phycology, 2016. **28**(3): p. 1683-1693.
61. Smith, C.J. and Osborn, A.M., *Advantages and limitations of quantitative PCR (Q-PCR)-based approaches in microbial ecology*. FEMS Microbiology Ecology, 2009. **67**(1): p. 6-20.
62. Yung, T.K., Chan, K.A., Mok, T.S., Tong, J., To, K.-F., and Lo, Y.D., *Single-molecule detection of epidermal growth factor receptor mutations in plasma by microfluidics digital PCR in non-small cell lung cancer patients*. Clinical Cancer Research, 2009. **15**(6): p. 2076-2084.
63. Compton, J., *Nucleic acid sequence-based amplification*. Nature, 1991. **350**(6313): p. 91-92.
64. Casper, E.T., Paul, J.H., Smith, M.C., and Gray, M., *Detection and quantification of the red tide dinoflagellate *Karenia brevis* by real-time nucleic acid sequence-based amplification*. Applied and Environmental Microbiology, 2004. **70**(8): p. 4727-4732.
65. Patterson, S.S., Casper, E.T., Garcia-Rubio, L., Smith, M.C., and Paul, J.H., *Increased precision of microbial RNA quantification using NASBA with an internal control*. Journal of Microbiological Methods, 2005. **60**(3): p. 343-352.
66. Smith, M.C., Steimle, G., Ivanov, S., Holly, M., and Fries, D.P., *An integrated portable hand-held analyser for real-time isothermal nucleic acid amplification*. Analytica Chimica Acta, 2007. **598**(2): p. 286-294.
67. Ulrich, R.M., Casper, E.T., Campbell, L., Richardson, B., Heil, C.A., and Paul, J.H., *Detection and quantification of *Karenia mikimotoi* using real-time nucleic acid*

- sequence-based amplification with internal control RNA (IC-NASBA)*. Harmful Algae, 2010. **9**(1): p. 116-122.
68. Zhang, F., Ma, L., Xu, Z., Zheng, J., Shi, Y., Lu, Y., and Miao, Y., *Sensitive and rapid detection of Karenia mikimotoi (Dinophyceae) by loop-mediated isothermal amplification*. Harmful Algae, 2009. **8**(6): p. 839-842.
69. Mori, Y. and Notomi, T., *Loop-mediated isothermal amplification (LAMP): a rapid, accurate, and cost-effective diagnostic method for infectious diseases*. Journal of Infection and Chemotherapy, 2009. **15**(2): p. 62-69.
70. Notomi, T., Okayama, H., Masubuchi, H., Yonekawa, T., Watanabe, K., Amino, N., and Hase, T., *Loop-mediated isothermal amplification of DNA*. Nucleic Acids Research, 2000. **28**(12): p. e63.
71. Parida, M., Sannarangaiah, S., Dash, P.K., Rao, P.V.L., and Morita, K., *Loop mediated isothermal amplification (LAMP): a new generation of innovative gene amplification technique; perspectives in clinical diagnosis of infectious diseases*. Reviews in Medical Virology, 2008. **18**(6): p. 407-421.
72. Wang, L., Li, L., Alam, M.J., Geng, Y., Li, Z., Yamasaki, S., and Shi, L., *Loop-mediated isothermal amplification method for rapid detection of the toxic dinoflagellate Alexandrium, which causes algal blooms and poisoning of shellfish*. FEMS Microbiology Letters, 2008. **282**(1): p. 15-21.
73. Nagai, S. and Itakura, S., *Specific detection of the toxic dinoflagellates Alexandrium tamarense and Alexandrium catenella from single vegetative cells by a loop-mediated isothermal amplification method*. Marine Genomics, 2012. **7**: p. 43-49.
74. Nagai, S., Yamamoto, K., Hata, N., and Itakura, S., *Study of DNA extraction methods for use in loop-mediated isothermal amplification detection of single resting cysts in the toxic dinoflagellates Alexandrium tamarense and A. catenella*. Marine Genomics, 2012. **7**: p. 51-56.
75. Miyazono, A., Nagai, S., Kudo, I., and Tanizawa, K., *Viability of Alexandrium tamarense cysts in the sediment of Funka Bay, Hokkaido, Japan: Over a hundred year survival times for cysts*. Harmful Algae, 2012. **16**: p. 81-88.
76. Zhang, F., Shi, Y., Jiang, K., Song, W., Ma, C., Xu, Z., and Ma, L., *Rapid detection and quantification of Prorocentrum minimum by loop-mediated isothermal amplification and real-time fluorescence quantitative PCR*. Journal of Applied Phycology, 2014. **26**(3): p. 1379-1388.

77. Chen, G., Ma, C., Zhang, C., Zhou, J., Wang, Y., Wang, G., Zhang, B., Xu, Z., and Lu, D.D., *A rapid and sensitive method for field detection of Prorocentrum donghaiense using reverse transcription-coupled loop-mediated isothermal amplification*. Harmful Algae, 2013. **29**: p. 31-39.
78. Casper, E.T., Patterson, S.S., Bhanushali, P., Farmer, A., Smith, M., Fries, D.P., and Paul, J.H., *A handheld NASBA analyzer for the field detection and quantification of Karenia brevis*. Harmful Algae, 2007. **6**(1): p. 112-118.
79. Price, C.M., *Fluorescence in situ hybridization*. Blood Reviews, 1993. **7**(2): p. 127-134.
80. Liehr, T., *Fluorescence in Situ Hybridization (FISH): Application Guide*. Fluorescence in Situ Hybridization (FISH): Application Guide. 2009, Berlin: Springer Berlin Heidelberg.
81. Anderson, D., *Identification of harmful algal species using molecular probes: an emerging perspective*. Lavoisier, 1995: p. 3-13.
82. Chen, G.F., Wang, G.C., Zhang, C.Y., Zhang, B.Y., Wang, X.K., and Zhou, B.C., *Development of rRNA and rDNA-targeted probes for fluorescence in situ hybridization to detect Heterosigma akashiwo (Raphidophyceae)*. Journal of Experimental Marine Biology and Ecology, 2008. **355**(1): p. 66-75.
83. Scholin, C.A., Miller, P.E., Buck, K.R., Chavez, F.P., Harris, P., Haydock, P., Howard, J., and Cangelosi, G., *Detection and quantification of Pseudo-nitzschia australis in cultured and natural populations using LSU rRNA-targeted probes*. Limnology and Oceanography, 1997. **42**(5): p. 1265-1272.
84. Miller, P.E. and Scholin, C.A., *Identification and enumeration of cultured and wild Pseudo-nitzschis (bacillariophyceae) using species-specific LSU rRNA-targeted fluorescent probes and filter-based whole cell hybridization*. Journal of Phycology, 1998. **34**(2): p. 371-382.
85. Shibata, A., Goto, Y., Saito, H., Kikuchi, T., Toda, T., and Taguchi, S., *Comparison of SYBR Green I and SYBR Gold stains for enumerating bacteria and viruses by epifluorescence microscopy*. Aquatic microbial ecology, 2006. **43**(3): p. 223-231.
86. Miller, P.E. and Scholin, C.A., *On detection of Pseudo-nitzschia (bacillariophyceae) species using whole cell hybridization: sample fixation and stability* Journal of Phycology, 2000. **36**(1): p. 238-250.
87. Scholin, C.A., Marin, R., Miller, P.E., Doucette, G.J., Powell, C.L., Haydock, P., Howard, J., and Ray, J., *DNA probes and a Receptor-Binding Assay for detection*

- of *Pseudo-nitzschia* (Bacillariophyceae) species and domoic acid activity in Cultured and Natural Samples. *Journal of Phycology*, 1999. **35**(6): p. 1356-1367.
88. Hosoi-Tanabe, S. and Sako, Y., *Rapid detection of natural cells of Alexandrium tamarense and A. catenella (Dinophyceae) by fluorescence in situ hybridization*. *Harmful Algae*, 2005. **4**(2): p. 319-328.
89. Sako, Y., Hosoi-Tanabe, S., and Uchida, A., *Fluorescence in situ Hybridization using rRNA-targeted probes for Simple and Rapid Identification of the Toxic Dinoflagellates Alexandrium tamarense and Alexandrium catenella*. *Journal of Phycology*, 2004. **40**(3): p. 598-605.
90. Hosoi-Tanabe, S. and Sako, Y., *Development and application of fluorescence in situ hybridization (FISH) method for simple and rapid identification of the toxic dinoflagellates Alexandrium tamarense and Alexandrium catenella in cultured and natural seawater*. *Fisheries Science*, 2006. **72**(1): p. 77-82.
91. Mikulski, C.M., Morton, S.L., and Doucette, G.J., *Development and application of LSU rRNA probes for Karenia brevis in the Gulf of Mexico, USA*. *Harmful Algae*, 2005. **4**(1): p. 49-60.
92. Mikulski, C.M., Park, Y.T., Jones, K.L., Lee, C.K., Lim, W.A., Lee, Y., Scholin, C.A., and Doucette, G.J., *Development and field application of rRNA-targeted probes for the detection of Cochlodinium polykrikoides Margalef in Korean coastal waters using whole cell and sandwich hybridization formats*. *Harmful Algae*, 2008. **7**(3): p. 347-359.
93. Cai, Q., Li, R., Zhen, Y., Mi, T., and Yu, Z., *Detection of two Prorocentrum species using sandwich hybridization integrated with nuclease protection assay*. *Harmful Algae*, 2006. **5**(3): p. 300-309.
94. Metfies, K., Huljic, S., Lange, M., and Medlin, L.K., *Electrochemical detection of the toxic dinoflagellate Alexandrium ostenfeldii with a DNA-biosensor*. *Biosensors and Bioelectronics*, 2005. **20**(7): p. 1349-1357.
95. Tyrrell, J.V., Connell, L.B., and Scholin, C.A., *Monitoring for Heterosigma akashiwo using a sandwich hybridization assay*. *Harmful Algae*, 2002. **1**(2): p. 205-214.
96. O'Halloran, C., Silver, M.W., Holman, T.R., and Scholin, C.A., *Heterosigma akashiwo in central California waters*. *Harmful Algae*, 2006. **5**(2): p. 124-132.

97. Diercks, S., Medlin, L.K., and Metfies, K., *Colorimetric detection of the toxic dinoflagellate Alexandrium minutum using sandwich hybridization in a microtiter plate assay*. Harmful Algae, 2008. **7**(2): p. 137-145.
98. Zhen, Y., Mi, T., and Yu, Z., *Detection of Phaeocystis globosa using sandwich hybridization integrated with nuclease protection assay (NPA-SH)*. Journal of Environmental Sciences, 2008. **20**(12): p. 1481-1486.
99. Zhen, Y., Mi, T., and Yu, Z., *Quantification methods for Alexandrium catenella, a toxic dinoflagellate: Comparison of competitive enzyme-linked immunosorbent assay and sandwich hybridization integrated with a nuclease protection assay*. Harmful Algae, 2011. **10**(6): p. 589-597.
100. Ahn, S., Kulis, D.M., Erdner, D.L., Anderson, D.M., and Walt, D.R., *Fiber-optic microarray for simultaneous detection of multiple harmful algal bloom species*. Applied and Environmental Microbiology, 2006. **72**(9): p. 5742-5749.
101. Anderson, D.M., Kulis, D., Erdner, D., Ahn, S., and Walt, D., *Fibre optic microarrays for the detection and enumeration of harmful algal bloom species*. African Journal of Marine Science, 2006. **28**(2): p. 231-235.
102. Zhu, X., Zhen, Y., Mi, T., and Yu, Z., *Detection of Prorocentrum minimum (Pavillard) Schiller with an Electrochemiluminescence–Molecular Probe Assay*. Marine Biotechnology, 2012. **14**(4): p. 502-511.
103. Orozco, J., Villa, E., Manes, C.-L., Medlin, L.K., and Guillebault, D., *Electrochemical RNA genosensors for toxic algal species: enhancing selectivity and sensitivity*. Talanta, 2016. **161**: p. 560-566.
104. Suh, S.-S., Park, M., Hwang, J., Kil, E.-J., Lee, S., and Lee, T.-K., *Detection of the dinoflagellate, Cochlodinium polykrikoides, that forms algal blooms using sandwich hybridization integrated with nuclease protection assay*. Biotechnology Letters, 2016. **38**(1): p. 57-63.
105. Steinberg, G., Stromborg, K., Thomas, L., Barker, D., and Zhao, C., *Strategies for covalent attachment of DNA to beads*. Biopolymers. Vol. 73. 2004: Wiley Subscription Services, Inc. 597-605.
106. Chrisey, L.A., Lee, G.U., and O'Ferrall, C.E., *Covalent attachment of synthetic DNA to self-assembled monolayer films*. Nucleic Acids Research, 1996. **24**(15): p. 3031-3039.
107. Witucki, G.L., *A silane primer: chemistry and applications of alkoxy silanes*. Journal of coatings technology, 1993. **65**: p. 57.

108. Halliwell, C.M. and Cass, A.E.G., *A Factorial Analysis of Silanization Conditions for the Immobilization of Oligonucleotides on Glass Surfaces*. Analytical Chemistry, 2001. **73**(11): p. 2476-2483.
109. Joos, B., Kuster, H., and Cone, R., *Covalent Attachment of Hybridizable Oligonucleotides to Glass Supports*. Analytical Biochemistry, 1997. **247**(1): p. 96-101.
110. Guo, Z., Guilfoyle, R.A., Thiel, A.J., Wang, R., and Smith, L.M., *Direct fluorescence analysis of genetic polymorphisms by hybridization with oligonucleotide arrays on glass supports*. Nucleic Acids Research, 1994. **22**(24): p. 5456-5465.
111. Lamture, J.B., Beattie, K.L., Burke, B.E., Eggers, M.D., Ehrlich, D.J., Fowler, R., Hollis, M.A., Kosicki, B.B., Reich, R.K., and Smith, S.R., *Direct detection of nucleic acid hybridization on the surface of a charge coupled device*. Nucleic Acids Research, 1994. **22**(11): p. 2121-2125.
112. Rogers, Y.-H., Jiang-Baucom, P., Huang, Z.-J., Bogdanov, V., Anderson, S., and Boyce-Jacino, M.T., *Immobilization of Oligonucleotides onto a Glass Support via Disulfide Bonds: A Method for Preparation of DNA Microarrays*. Analytical Biochemistry, 1999. **266**(1): p. 23-30.
113. Escorihuela, J., Bañuls, M.-J., Grijalvo, S., Eritja, R., Puchades, R., and Maquieira, Á., *Direct Covalent Attachment of DNA Microarrays by Rapid Thiol–Ene “Click” Chemistry*. Bioconjugate Chemistry, 2014. **25**(3): p. 618-627.
114. Rasmussen, S.R., Larsen, M.R., and Rasmussen, S.E., *Covalent immobilization of DNA onto polystyrene microwells: The molecules are only bound at the 5' end*. Analytical Biochemistry, 1991. **198**(1): p. 138-142.
115. Beattie, W.G., Meng, L., Turner, S.L., Varma, R.S., Dao, D.D., and Beattie, K.L., *Hybridization of DNA targets to glass-tethered oligonucleotide probes*. Molecular Biotechnology. **4**(3): p. 213-225.
116. Dolan, P.L., Wu, Y., Ista, L.K., Metzberg, R.L., Nelson, M.A., and Lopez, G.P., *Robust and efficient synthetic method for forming DNA microarrays*. Nucleic Acids Research, 2001. **29**(21): p. e107.
117. Jacobs, J.W. and Fodor, S.P.A., *Combinatorial chemistry — applications of light-directed chemical synthesis*. Trends in Biotechnology, 1994. **12**(1): p. 19-26.
118. Charles, P.T., Vora, G.J., Andreadis, J.D., Fortney, A.J., Meador, C.E., Dulcey, C.S., and Stenger, D.A., *Fabrication and Surface Characterization of DNA Microarrays*

- Using Amine- and Thiol-Terminated Oligonucleotide Probes†*. Langmuir, 2003. **19**(5): p. 1586-1591.
119. Le Berre, V., Trévisiol, E., Dagkessamanskaia, A., Sokol, S., Caminade, A.M., Majoral, J.P., Meunier, B., and François, J., *Dendrimeric coating of glass slides for sensitive DNA microarrays analysis*. Nucleic Acids Research, 2003. **31**(16): p. e88.
 120. Blalock, E.M., *A Beginner's Guide to Microarrays*. 2011: Springer US.
 121. Wittmann, C., *Immobilisation of DNA on Chips: Immobilization of DNA on microarrays*. 2006: Springer.
 122. Hoyle, C.E. and Bowman, C.N., *Thiol–Ene Click Chemistry*. Angewandte Chemie International Edition, 2010. **49**(9): p. 1540-1573.
 123. Chen, Y.-X., Triola, G., and Waldmann, H., *Bioorthogonal Chemistry for Site-Specific Labeling and Surface Immobilization of Proteins*. Accounts of Chemical Research, 2011. **44**(9): p. 762-773.
 124. Rao, K.S., Rani, S.U., Charyulu, D.K., Kumar, K.N., Lee, B.-K., Lee, H.-Y., and Kawai, T., *A novel route for immobilization of oligonucleotides onto modified silica nanoparticles*. Analytica Chimica Acta, 2006. **576**(2): p. 177-183.
 125. Liberman, A., Mendez, N., Trogler, W.C., and Kummel, A.C., *Synthesis and surface functionalization of silica nanoparticles for nanomedicine*. Surface Science Reports, 2014. **69**(2–3): p. 132-158.
 126. Rahman, I.A. and Padavettan, V., *Synthesis of Silica Nanoparticles by Sol-Gel: Size-Dependent Properties, Surface Modification, and Applications in Silica-Polymer Nanocomposites; A Review*. Journal of Nanomaterials, 2012. **2012**: p. 15.
 127. Tang, L. and Cheng, J., *Nonporous Silica Nanoparticles for Nanomedicine Application*. Nano today, 2013. **8**(3): p. 290-312.
 128. Stöber, W., Fink, A., and Bohn, E., *Controlled growth of monodisperse silica spheres in the micron size range*. Journal of colloid and interface science, 1968. **26**(1): p. 62-69.
 129. Sato-Berrú, R., Saniger, J.M., Flores-Flores, J., and Sanchez-Espíndola, M., *Simple method for the controlled growth of SiO₂ spheres*. Journal of Materials Science and Engineering. A, 2013. **3**(4A): p. 237.
 130. Ibrahim, I.A., Zikry, A., and Sharaf, M.A., *Preparation of spherical silica nanoparticles: Stober silica*. J. Am. Sci, 2010. **6**(11): p. 985-989.

131. Bagwe, R.P., Hilliard, L.R., and Tan, W., *Surface Modification of Silica Nanoparticles to Reduce Aggregation and Nonspecific Binding*. Langmuir, 2006. **22**(9): p. 4357-4362.
132. Yoo, H. and Pak, J., *Synthesis of highly fluorescent silica nanoparticles in a reverse microemulsion through double-layered doping of organic fluorophores*. Journal of Nanoparticle Research, 2013. **15**(5): p. 1-10.
133. Cichos, J. and Karbowski, M., *A general and versatile procedure for coating of hydrophobic nanocrystals with a thin silica layer enabling facile biofunctionalization and dye incorporation*. Journal of Materials Chemistry B, 2014. **2**(5): p. 556-568.
134. Hartlen, K.D., Athanasopoulos, A.P.T., and Kitaev, V., *Facile Preparation of Highly Monodisperse Small Silica Spheres (15 to >200 nm) Suitable for Colloidal Templating and Formation of Ordered Arrays*. Langmuir, 2008. **24**(5): p. 1714-1720.
135. Liberman, A., Mendez, N., Trogler, W.C., and Kummel, A.C., *Synthesis and surface functionalization of silica nanoparticles for nanomedicine*. Surface science reports, 2014. **69**(2-3): p. 132-158.
136. Rahman, I.A., Jafarzadeh, M., and Sipaut, C.S., *Synthesis of organo-functionalized nanosilica via a co-condensation modification using γ -aminopropyltriethoxysilane (APTES)*. Ceramics International, 2009. **35**(5): p. 1883-1888.
137. Veronese, F.M. and Pasut, G., *PEGylation, successful approach to drug delivery*. Drug Discovery Today, 2005. **10**(21): p. 1451-1458.
138. Gomes, M.C., Cunha, Â., Trindade, T., and Tomé, J.P.C., *The role of surface functionalization of silica nanoparticles for bioimaging*. Journal of Innovative Optical Health Sciences, 2016. **09**(04): p. 1630005.
139. Slowing, I.I., Trewyn, B.G., Giri, S., and Lin, V.S.Y., *Mesoporous Silica Nanoparticles for Drug Delivery and Biosensing Applications*. Advanced Functional Materials, 2007. **17**(8): p. 1225-1236.
140. Shin, Y., Lee, D., Lee, K., Ahn, K.H., and Kim, B., *Surface properties of silica nanoparticles modified with polymers for polymer nanocomposite applications*. Journal of Industrial and Engineering Chemistry, 2008. **14**(4): p. 515-519.

141. Soto-Cantu, E., Cueto, R., Koch, J., and Russo, P.S., *Synthesis and Rapid Characterization of Amine-Functionalized Silica*. *Langmuir*, 2012. **28**(13): p. 5562-5569.
142. Maria Chong, A.S. and Zhao, X.S., *Functionalization of SBA-15 with APTES and Characterization of Functionalized Materials*. *The Journal of Physical Chemistry B*, 2003. **107**(46): p. 12650-12657.
143. Hilliard, L.R., Zhao, X., and Tan, W., *Immobilization of oligonucleotides onto silica nanoparticles for DNA hybridization studies*. *Analytica Chimica Acta*, 2002. **470**(1): p. 51-56.
144. Bruce, K., Leterme, S., Ellis, A., and Lenehan, C., *Approaches for the detection of harmful algal blooms using oligonucleotide interactions*. *Analytical and Bioanalytical Chemistry*, 2015. **407**(1): p. 95-116.
145. Kirkpatrick, G.J., Millie, D.F., Moline, M.A., and Schofield, O., *Optical discrimination of a phytoplankton species in natural mixed populations*. *Limnology and Oceanography*, 2000. **45**(2): p. 467-471.
146. Shchepinov, M.S., Case-Green, S.C., and Southern, E.M., *Steric Factors Influencing Hybridisation Of Nucleic Acids To Oligonucleotide Arrays*. *Nucleic Acids Research*, 1997. **25**(6): p. 1155-1161.
147. Schlapak, R., Pammer, P., Armitage, D., Zhu, R., Hinterdorfer, P., Vaupel, M., Frühwirth, T., and Howorka, S., *Glass Surfaces Grafted with High-Density Poly(ethylene glycol) as Substrates for DNA Oligonucleotide Microarrays*. *Langmuir*, 2006. **22**(1): p. 277-285.
148. Strother, T., Cai, W., Zhao, X., Hamers, R.J., and Smith, L.M., *Synthesis and Characterization of DNA-Modified Silicon (111) Surfaces*. *Journal of the American Chemical Society*, 2000. **122**(6): p. 1205-1209.
149. Strother, T., Hamers, R.J., and Smith, L.M., *Covalent attachment of oligodeoxyribonucleotides to amine-modified Si (001) surfaces*. *Nucleic Acids Research*, 2000. **28**(18): p. 3535-3541.
150. Peterson, A.W., Heaton, R.J., and Georgiadis, R.M., *The effect of surface probe density on DNA hybridization*. *Nucleic Acids Research*, 2001. **29**(24): p. 5163-5168.
151. Khodakov, D., Thredgold, L., Lenehan, C.E., Andersson, G.G., Kobus, H., and Ellis, A.V., *DNA capture-probe based separation of double-stranded polymerase chain*

- reaction amplification products in poly(dimethylsiloxane) microfluidic channels.* Biomicrofluidics, 2012. **6**(2): p. 26503-11.
152. Zhou, J., Khodakov, D.A., Ellis, A.V., and Voelcker, N.H., *Surface modification for PDMS-based microfluidic devices.* Electrophoresis, 2012. **33**(1): p. 89-104.
 153. Bodas, D. and Khan-Malek, C., *Hydrophilization and hydrophobic recovery of PDMS by oxygen plasma and chemical treatment—An SEM investigation.* Sensors and Actuators B: Chemical, 2007. **123**(1): p. 368-373.
 154. Kumar, A., Larsson, O., Parodi, D., and Liang, Z., *Silanized nucleic acids: a general platform for DNA immobilization.* Nucleic Acids Research, 2000. **28**(14): p. e71
 155. Cohen, G., Deutsch, J., Fineberg, J., and Levine, A., *Covalent attachment of DNA oligonucleotides to glass.* Nucleic Acids Research, 1997. **25**(4): p. 911-912.
 156. Beier, M. and Hoheisel, J.D., *Versatile derivatisation of solid support media for covalent bonding on DNA-microchips.* Nucleic Acids Research, 1999. **27**(9): p. 1970-1977.
 157. McGall, G., Labadie, J., Brock, P., Wallraff, G., Nguyen, T., and Hinsberg, W., *Light-directed synthesis of high-density oligonucleotide arrays using semiconductor photoresists.* Proceedings of the National Academy of Sciences, 1996. **93**(24): p. 13555-13560.
 158. Kimura, N., Oda, R., Inaki, Y., and Suzuki, O., *Attachment of oligonucleotide probes to poly carbodiimide-coated glass for microarray applications.* Nucleic Acids Research, 2004. **32**(7): p. e68.
 159. Podyminogin, M.A., Lukhtanov, E.A., and Reed, M.W., *Attachment of benzaldehyde-modified oligodeoxynucleotide probes to semicarbazide-coated glass.* Nucleic Acids Research, 2001. **29**(24): p. 5090-5098.
 160. Zammateo, N., Jeanmart, L., Hamels, S., Courtois, S., Louette, P., Hevesi, L., and Remacle, J., *Comparison between Different Strategies of Covalent Attachment of DNA to Glass Surfaces to Build DNA Microarrays.* Analytical Biochemistry, 2000. **280**(1): p. 143-150.
 161. Vaidya, A.A. and Norton, M.L., *DNA Attachment Chemistry at the Flexible Silicone Elastomer Surface: Toward Disposable Microarrays.* Langmuir, 2004. **20**(25): p. 11100-11107.
 162. Moorcroft, M.J., Meuleman, W.R.A., Latham, S.G., Nicholls, T.J., Egeland, R.D., and Southern, E.M., *In situ oligonucleotide synthesis on poly(dimethylsiloxane):*

- a flexible substrate for microarray fabrication*. Nucleic Acids Research, 2005. **33**(8): p. e75.
163. Ernsberger, F.M., *Properties of Glass Surfaces*. Annual Review of Materials Science, 1972. **2**(1): p. 529-572.
 164. Dugas, V., Depret, G., Chevalier, Y., Nesme, X., and Souteyrand, É., *Immobilization of single-stranded DNA fragments to solid surfaces and their repeatable specific hybridization: covalent binding or adsorption?* Sensors and Actuators B: Chemical, 2004. **101**(1–2): p. 112-121.
 165. Esmonde-White, K.A., Esmonde-White, F.W.L., Morris, M.D., and Roessler, B.J., *Characterization of biofluids prepared by sessile drop formation*. Analyst, 2014. **139**(11): p. 2734-2741.
 166. Blossey, R. and Bosio, A., *Contact Line Deposits on cDNA Microarrays: A “Twin-Spot Effect”*. Langmuir, 2002. **18**(7): p. 2952-2954.
 167. Dufva, M., *Fabrication of high quality microarrays*. Biomolecular Engineering, 2005. **22**(5–6): p. 173-184.
 168. Deegan, R.D., Bakajin, O., Dupont, T.F., Huber, G., Nagel, S.R., and Witten, T.A., *Contact line deposits in an evaporating drop*. Physical Review E, 2000. **62**(1): p. 756-765.
 169. Walsh, M.K., Wang, X., and Weimer, B.C., *Optimizing the immobilization of single-stranded DNA onto glass beads*. Journal of Biochemical and Biophysical Methods, 2001. **47**(3): p. 221-231.
 170. Fritz, J.L. and Owen, M.J., *Hydrophobic Recovery of Plasma-Treated Polydimethylsiloxane*. The Journal of Adhesion, 1995. **54**(1-4): p. 33-45.
 171. Makamba, H., Kim, J.H., Lim, K., Park, N., and Hahn, J.H., *Surface modification of poly(dimethylsiloxane) microchannels*. Electrophoresis, 2003. **24**(21): p. 3607-3619.
 172. Altman, R.B., Terry, D.S., Zhou, Z., Zheng, Q., Geggier, P., Kolster, R.A., Zhao, Y., Javitch, J.A., Warren, J.D., and Blanchard, S.C., *Cyanine fluorophore derivatives with enhanced photostability*. Nat Meth, 2012. **9**(1): p. 68-71.
 173. Biosciences, A., *Stability studies of dyes in microarray applications, in Microarrays*. 2003. p. 1-6.
 174. Fare, T.L., Coffey, E.M., Dai, H., He, Y.D., Kessler, D.A., Kilian, K.A., Koch, J.E., LeProust, E., Marton, M.J., Meyer, M.R., Stoughton, R.B., Tokiwa, G.Y., and

- Wang, Y., *Effects of Atmospheric Ozone on Microarray Data Quality*. Analytical Chemistry, 2003. **75**(17): p. 4672-4675.
175. Gu, Q., Sivanandam, T.M., and Kim, C.A., *Signal stability of Cy3 and Cy5 on antibody microarrays*. Proteome science, 2006. **4**(1): p. 21.
176. Bruce, I.J. and Sen, T., *Surface Modification of Magnetic Nanoparticles with Alkoxysilanes and Their Application in Magnetic Bioseparations*. Langmuir, 2005. **21**(15): p. 7029-7035.
177. Carré, A., Lacarrière, V., and Birch, W., *Molecular interactions between DNA and an aminated glass substrate*. Journal of Colloid and Interface Science, 2003. **260**(1): p. 49-55.
178. Taylor, S., Smith, S., Windle, B., and Guiseppi-Elie, A., *Impact of surface chemistry and blocking strategies on DNA microarrays*. Nucleic Acids Research, 2003. **31**(16): p. e87.
179. Bhatia, S.K., Teixeira, J.L., Anderson, M., Shriverlake, L.C., Calvert, J.M., Georger, J.H., Hickman, J.J., Dulcey, C.S., Schoen, P.E., and Ligler, F.S., *Fabrication of Surfaces Resistant to Protein Adsorption and Application to Two-Dimensional Protein Patterning*. Analytical Biochemistry, 1993. **208**(1): p. 197-205.
180. Xu, J. and Boyer, C., *Visible Light Photocatalytic Thiol–Ene Reaction: An Elegant Approach for Fast Polymer Postfunctionalization and Step-Growth Polymerization*. Macromolecules, 2015. **48**(3): p. 520-529.
181. Gerry, N.P., Witowski, N.E., Day, J., Hammer, R.P., Barany, G., and Barany, F., *Universal DNA microarray method for multiplex detection of low abundance point mutations1*. Journal of Molecular Biology, 1999. **292**(2): p. 251-262.
182. Keith, H.W., Steve, M., and Joshua, T., *High accuracy optical inverse square law experiment using inexpensive light to frequency converters*. Physics Education, 2012. **47**(2): p. 174.
183. López-Paz, J.L., González-Martínez, M.Á., Escorihuela, J., Bañuls, M.-J., Puchades, R., and Maquieira, Á., *Direct and label-free monitoring oligonucleotide immobilization, non-specific binding and DNA biorecognition*. Sensors and Actuators B: Chemical, 2014. **192**: p. 221-228.
184. Zhang, X., Xu, W., Tan, J., and Zeng, Y., *Stripping custom microRNA microarrays and the lessons learned about probe–slide interactions*. Analytical Biochemistry, 2009. **386**(2): p. 222-227.

185. Hahnke, K., Jacobsen, M., Gruetzkau, A., Gruen, J.R., Koch, M., Emoto, M., Meyer, T.F., Walduck, A., Kaufmann, S.H.E., and Mollenkopf, H.-J., *Striptease on glass: Validation of an improved stripping procedure for in situ microarrays*. *Journal of Biotechnology*, 2007. **128**(1): p. 1-13.
186. Schroeder, G.K., Lad, C., Wyman, P., Williams, N.H., and Wolfenden, R., *The time required for water attack at the phosphorus atom of simple phosphodiester and of DNA*. *Proceedings of the National Academy of Sciences of the United States of America*, 2006. **103**(11): p. 4052-4055.
187. Gates, K.S., *An Overview of Chemical Processes That Damage Cellular DNA: Spontaneous Hydrolysis, Alkylation, and Reactions with Radicals*. *Chemical Research in Toxicology*, 2009. **22**(11): p. 1747-1760.
188. Bruce, K.L., Ellis, A.V., Leterme, S.C., Khodakov, D.A., and Lenehan, C.E. *Detection of harmful algal bloom causing microalgae using covalently immobilised capture oligonucleotide probes on glass and poly(dimethylsiloxane) surfaces*. in *SPIE Micro/Nano Materials, Devices and Systems*. 2013. Melbourne, Victoria, Australia.
189. Daniel, N.M., Takashi, N., and David, A.L., *A simple method for the quantification of molecular decorations on silica particles*. *Science and Technology of Advanced Materials*, 2014. **15**(1): p. 015002.
190. Zhang, X., Servos, M.R., and Liu, J., *Ultrahigh Nanoparticle Stability against Salt, pH, and Solvent with Retained Surface Accessibility via Depletion Stabilization*. *Journal of the American Chemical Society*, 2012. **134**(24): p. 9910-9913.
191. Schneider, C.A., Rasband, W.S., and Eliceiri, K.W., *NIH Image to ImageJ: 25 years of image analysis*. *Nat Meth*, 2012. **9**(7): p. 671-675.
192. Wojdyr, M., *Fityk: a general-purpose peak fitting program*. *Journal of Applied Crystallography*, 2010. **43**(5 Part 1): p. 1126-1128.
193. Dopico, A., *Methods in Membrane Lipids*. 2007: Humana Press.
194. Zhuravlev, L.T., *The surface chemistry of amorphous silica. Zhuravlev model*. *Colloids and Surfaces A: Physicochemical and Engineering Aspects*, 2000. **173**(1-3): p. 1-38.
195. Lin, I.C., Liang, M., Liu, T.-Y., Jia, Z., Monteiro, M.J., and Toth, I., *Effect of polymer grafting density on silica nanoparticle toxicity*. *Bioorganic & Medicinal Chemistry*, 2012. **20**(23): p. 6862-6869.

196. Godin, M., Bryan, A.K., Burg, T.P., Babcock, K., and Manalis, S.R., *Measuring the mass, density, and size of particles and cells using a suspended microchannel resonator*. Applied Physics Letters, 2007. **91**(12): p. 123121.
197. Kuo, I.T., Huang, Y.-F., and Chang, H.-T., *Silica nanoparticles for separation of biologically active amines by capillary electrophoresis with laser-induced native fluorescence detection*. ELECTROPHORESIS, 2005. **26**(13): p. 2643-2651.
198. Ferreira, G., Hernandez-Martinez, A.R., Pool, H., Molina, G., Cruz-Soto, M., Luna-Barcenas, G., and Estevez, M., *Synthesis and functionalization of silica-based nanoparticles with fluorescent biocompounds extracted from Eysenhardtia polystachya for biological applications*. Materials Science and Engineering: C, 2015. **57**: p. 49-57.
199. Lippincott, E.R., Van Valkenburg, A., Weir, C.E., and Bunting, E.N., *Infrared studies on polymorphs of silicon dioxide and germanium dioxide*. Journal of Research of the National Bureau of Standards, 1958. **61**(1): p. 61-70.
200. Pryce Lewis, H.G., Edell, D.J., and Gleason, K.K., *Pulsed-PECVD Films from Hexamethylcyclotrisiloxane for Use as Insulating Biomaterials*. Chemistry of Materials, 2000. **12**(11): p. 3488-3494.
201. Silverstein, R.M., Webster, F.X., Kiemle, D.J., and Bryce, D.L., *Spectrometric Identification of Organic Compounds*. 2014: Wiley.
202. Somasundaran, P., *Encyclopedia of Surface and Colloid Science*. 2006: Taylor & Francis.
203. Colthup, N., *Introduction to Infrared and Raman Spectroscopy*. 2012: Elsevier Science.
204. Feifel, S.C. and Lisdat, F., *Silica nanoparticles for the layer-by-layer assembly of fully electro-active cytochrome c multilayers*. Journal of Nanobiotechnology, 2011. **9**(1): p. 1-12.
205. Mangos, D.N., Personal Communication, 2016.
206. Li, D. and Kaner, R.B., *How nucleation affects the aggregation of nanoparticles*. Journal of Materials Chemistry, 2007. **17**(22): p. 2279-2282.
207. Mansfield, E., Tyner, K.M., Poling, C.M., and Blacklock, J.L., *Determination of Nanoparticle Surface Coatings and Nanoparticle Purity Using Microscale Thermogravimetric Analysis*. Analytical Chemistry, 2014. **86**(3): p. 1478-1484.
208. Tan, S.C. and Yiap, B.C., *DNA, RNA, and Protein Extraction: The Past and The Present*. Journal of Biomedicine and Biotechnology, 2009. **2009**.

209. Izak-Nau, E., Voetz, M., Eiden, S., Duschl, A., and Puentes, V.F., *Altered characteristics of silica nanoparticles in bovine and human serum: the importance of nanomaterial characterization prior to its toxicological evaluation*. *Particle and Fibre Toxicology*, 2013. **10**: p. 56.
210. Brown, M.A., Arrigoni, M., Héroguel, F., Beloqui Redondo, A., Giordano, L., van Bokhoven, J.A., and Pacchioni, G., *pH Dependent Electronic and Geometric Structures at the Water–Silica Nanoparticle Interface*. *The Journal of Physical Chemistry C*, 2014. **118**(50): p. 29007-29016.
211. Ageno, M., Dore, E., and Frontali, C., *The Alkaline Denaturation of DNA*. *Biophysical Journal*, 1969. **9**(11): p. 1281-1311.
212. Zhang, H., Mitrovski, S.M., and Nuzzo, R.G., *Microfluidic Device for the Discrimination of Single-Nucleotide Polymorphisms in DNA Oligomers Using Electrochemically Actuated Alkaline Dehybridization*. *Analytical Chemistry*, 2007. **79**(23): p. 9014-9021.
213. Lazerges, M., Perrot, H., Rabehagaso, N., and Compère, C., *Thiol- and Biotin-Labeled Probes for Oligonucleotide Quartz Crystal Microbalance Biosensors of Microalga *Alexandrium Minutum**. *Biosensors*, 2012. **2**(3): p. 245-254.